Functional Analysis of the LIM kinase 1 and its role in Cell Cycle progression

Inauguraldissertation

zur

Erlangung der Würde eines Doktors der Philosophie

vorgelegt der

Philosophisch-Naturwissenschaftlichen Fakultät

der Universität Basel

von

Ayça Sayı

aus Istanbul (Türkei)

Zürich 2008

Genehmigt von der Philosophisch- Naturwissenschaftlichen Fakultät auf Antrag von Prof. Dr. Wilhelm Krek, Prof.Dr. Matthias Peter und Prof. Dr. Denis Monard.

Basel, den 20. Juni 2006

Prof. Dr. Hans- Jakob Wirz
Dekan

Abstract

LIMK1 (LIM-kinase 1) is a member of the LIMKs family of serine/threonine kinases, comprised of LIMK1, LIMK2 and testicular specific kinases, TESK1 and TESK2. These enzymes catalyze phosphorylation of an actin depolymerizing factor cofilin, thereby inactivate its depolymerizing activity, that leads to actin stabilization as filamentous actin (F-actin). As a consequence, LIMK1 plays a key role in actin cytoskeleton remodeling, notably in response to many extracellular cues that trigger the activation of the small Rho GTPases Rho, Rac and Cdc42, these latter being able to activate LIMK1 through their downstream effectors ROCK, PAK1 and PAK4 respectively. Moreover, on a pathological point of view, dysregulation of LIMK1 has being associated to several diseases: indeed, partial loss of LIMK1 is associated to a neurological disorder called William's syndrome, whereas LIMK1 upregulation and/or hyperactivation is linked to cancer metastasis.

The introduction chapter of this thesis details the current knowledge about LIMK1 and its function in cell migration, cell cycle, neuronal differentiation, and phagocytosis. Additionally, the contribution of LIMK1 dysregulation in pathological circumstances, notably in WilliamÕs syndrome and in cancer metastasis is discussed.

The results chapter summarizes the work undertaken as partial fulfilment of this doctoral study. In the first part of the results, the endogenous localization of LIMK1 is described in cell lines and tissues. We showed that, in different cell lines, LIMK1 and LIMK2 localize mainly to cytoplasm with enrichment in cell membrane in the direction of movement. Moreover, we observed that

active LIMK1 and LIMK2 localize to membrane ruffles. Interstingly, a more detailed analysis of LIMK1 by immunostaining and fractionation shows that LIMK1 localizes to mitochondria, suggesting a possible new function or regulation of LIMK1 in this compartment. In contrast to cell lines, LIMK1 is shown to localize to both nucleus and cytoplasm in kidney and prostate tissues. However, in mouse kidney and prostate cancer models, we observed that LIMK1 relocalized to cytoplasm. Altogether, these suggest that, in exponentially growing cells (cultured cells), LIMK1 localizes to cytoplasm, whereas in differentiated cells (in tissues), its localization is both nuclear and cytoplasmic. Moreover, during cancer development, LIMK1 is thought to relocalize mainly to the cytoplasm, which might represent a new marker of cancer, proliferating cells.

In the second part of results, functional inactivation studies of LIMK1 by knockout mice and RNA interference (siRNA and lentivector-mediated shRNA) are described. For knockout mice part, the identification of embryonic stem (ES) cells with one allele of total deleted or floxed LIMK1 gene has been completed. In RNA interference part, the characterization of a LIMK1 siRNA, which efficiently targets endogenous LIMK1, has been performed. This siRNA has been later on used for downregulation experiments aiming at exploring the effect of LIMK1 in cell cycle regulation. Additionally, the generation of a powerful drug- inducible lentivector-based LIMK1 shRNA, is explained.

The third part of results outlines, the accumulation of LIMK1 protein upon loss of the tumor suppressor Von Hippel- Lindau (VHL) protein. It is demonstrated at the molecular level that the increase in LIMK1 expression is due to the transcriptional activation of its gene. Interestingly, preliminary data suggest that, this might be a HIF- independent mechanism. Thus, these observations suggest that LIMK1 might be a novel downstream effector of VHL, which might participate in tumor progression or metastasis upon VHL loss.

Finally, the fourth part of results focused on LIMK1-dependent cell cycle regulation. Especially, we demonstrated a premature exit from M phase upon LIMK1 depletion is described.

Eventhough no timing difference is detected in the first part of mitosis (nuclear envelope breakdown to anaphase onset), a 20 % increase in spindle misorientation is observed in LIMK1 depleted cells by using time-lapse microscopy. It is suggested that the premature M phase exit may be due to alterations of later stages of mitosis.

Altogether, this doctoral study provides new insights regarding endogenous LIMK1 localization in normal versus cancer cells and tissues, and highlights a novel role of LIMK1 in proper mitosis progression, which requires additional work to understand the precise molecular mechanisms underlying this phenotype. These data open new perspectives for a better understanding of LIMK1 contribution to cancer progression and metastasis, notably in terms of mislocalization of LIMK1 in cancer cells, but also, as LIMK1 has been identified as a novel effector of VHL, concerning the contribution of LIMK-dependent processes upregulation to VHL-associated tumors growth and metastasis.

Acknowledgements

First of all, I would like to express my gratitute to my thesis supervisor Prof. Dr. Wilhelm Krek, for his helpful discussions, support and patience throughout my doctoral work.

I would like to address my very special thanks to Armelle Yart, for her friendship, and additionally for critical reading, input and continued support throughout the thesis. Also, I would like to thank to all the past and present members of the laboratory for scientific discussions and helping in different ways, in particular to Dimitris Anastasiou, Pia Ballschmieter, Robert Barry, and Sreya Basu for their friendship and support.

Sincere gratitute is expressed to Prof. Dr. Denis Monard as Fakult*ä*tsverantwortlicher, and to Prof. Dr. Matthias Peter for their time and effort in processing this doctoral thesis and defense.

I would also like to thank to all my friends for extending a helping hand when I was desperate. As I am fearing that someone would be forgotten, I have chosen not to name people. Thank you all.

Finally, my very special thanks goes to my parents, sister and family who endured this long process with me, always offering support, love and care.

Contents

List of Figures

List of Tables

Chapter 1

Introduction

1.1 LIM- kinases

The LIM motif containing protein kinase (LIMK) family of proteins are comprised of two members, LIMK1 and LIMK2. Human LIMK1 was initially identified in a screen of HepG2 (human hepatoma) cell cDNA library for a novel member of the c-met/HGF receptor tyrosine kinase family [Mizuno et al., 1994]. On the other hand, mouse homologue of LIMK1(Kiz-1) was identified by polymerase chain reaction of immortalized olfactory epithelial cells [Bernard et al., 1994]. One year later, a second member of LIMK family, LIM kinase 2 (LIMK2), was identified by the same group [Okano et al., 1995]. LIMK1 and LIMK2, with characteristic structural features composed of two LIM domains, a PDZ domain at the N-terminus, and a protein kinase domain at the C-terminus, have been identified in various vertebrates, including human, mouse, rat, chick, and *Xenopus*, additionally identified in invertebrates such as *C.elegans* and *Drosophila* [Mizuno et al., 1994, Okano et al., 1995, Takahashi et al., 1997, Ohashi et al., 2000a]. There is 53 % overall identity between LIMK1 and LIMK2, with 50%, 46% and 70% amino acid identity in the LIM, PDZ and kinase domains, respectively. LIMK2 has three functional isoforms, LIMK2a, LIMK2b, and testis-specific LIMK2 isoform (tLIMK2), with different N-terminal se-

quences generated by alternative splicing (figure 1.1) [Smolich et al., 1997, Koshimizu et al., 1997, Ikebe et al., 1998, Takahashi et al., 1998]. LIMK2b lacks the first zinc-finger of the first LIM domain. Both LIM-kinases are dual specificity protein kinases which phosphorylate both serine/threonine and tyrosine residues. There are two LIMK-related protein kinases, TESK1 and TESK2 (testicular-specific kinase 1 and 2), which are also dual specificity kinases and have a 50% identity in kinase domain of LIMK1, although their overall domain structures are totally different [Toshima et al., 1995]. TESKs have an N-terminal kinase domain and a C-terminal proline-rich domain (figure 1.1). There is 64% amino acid identity between TESK1 and TESK2 [Toshima et al., 2001]. TESK1 and TESK2 were named after its high expression levels in testis [Toshima et al., 1995, Rosok et al., 1999]. Phylogenetic analysis revealed that LIM- kinases and TES- kinases constitute a novel subfamily of kinases [Toshima et al., 1995, Toshima et al., 1998].

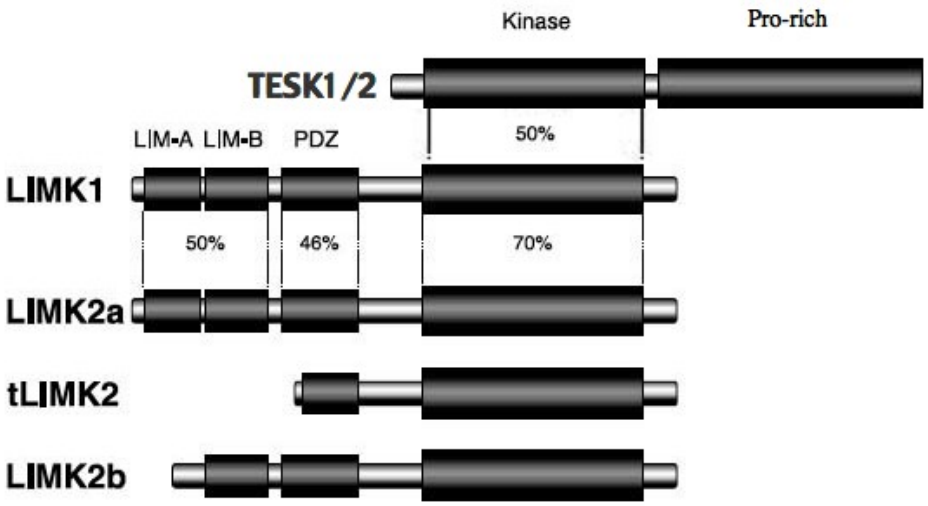

Fig. 1.1: Schematic representation of amino acid sequences of human LIMK1/2 and TESK1/2, adapted from Takahashi et al., 2003

1.1.1 LIMK gene

Analysis of the chromosomal localization of LIMK1 indicates that it lies on human chromosome 7 in the region q11.23 and on mouse Chromosome 5, band G2 by fluorescence in situ hybridization (FISH) (figure 1.2, A) [Bernard et al., 1996]. LIMK1 is comprised of 16 exons (figure 1.2, B). The first 5 exons encodes the LIM domains, the second half of exon 5 to exon 7 encodes Ser/Pro rich domain, and exon 8-16 encodes the kinase domain (figure 1.2, C).

On the other hand, LIMK2 localises to chromosome 22q12.2 in human and chromosome 1 band D in mouse by FISH [Koshimizu et al., 1997, Nomoto et al., 1999]. It also consist of 16 exons with alternative spliced forms.

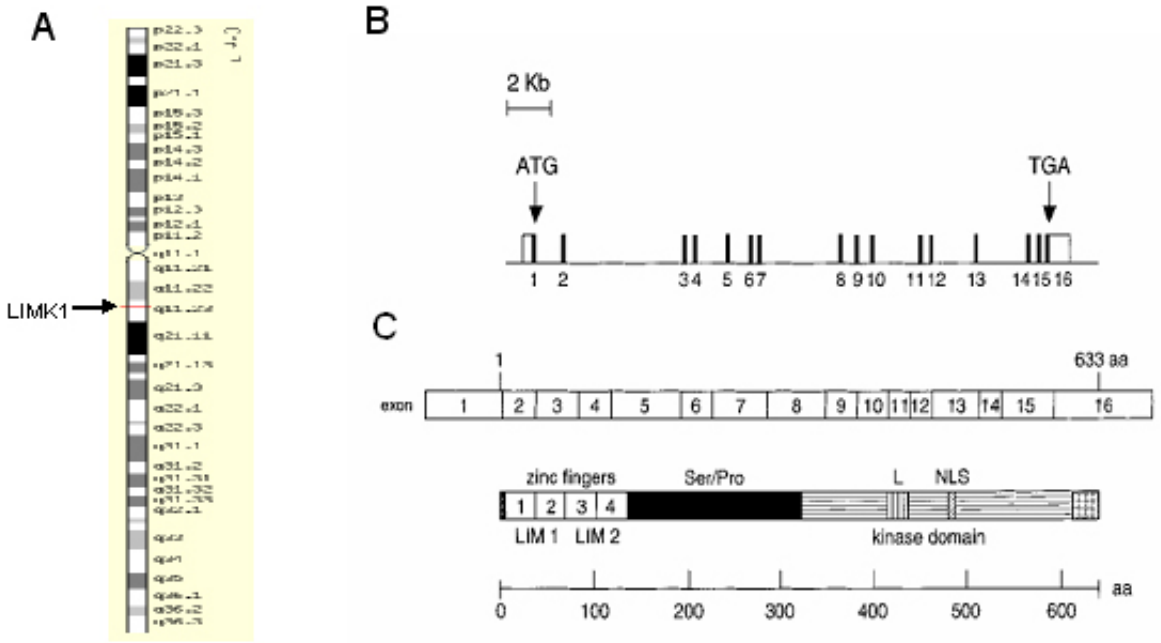

Fig. 1.2: Schematic representation of LIMK1 gene locus and the structure of the gene, A. LIMK1 localization in chromosome 7q11.3 is shown by an arrow, B. LIMK1 gene structure with 16 exons and locations of start and stop codons, C. Each box represents the protein sequence encoded by a single exon, numbered inside. Abbreviations, Ser/Pro: the region rich in serine and proline redisdues, L: region encoded by exon 11, which is alternatively spliced in the short form, NLS: nuclear localization signal adapted from Bernard et al.,1996

1.1.2 Domain structure of LIM-kinases

LIMK family of proteins feature two tandemly arranged LIM double zinc finger domains (LIM1 and LIM2) followed by one PDZ (PSD-95,Dlg,ZO-1) domain and C-terminal kinase catalytic domain (figure 1.3). LIM domain, named after three homeodomain-containing proteins, LIN-11, IsL-1, and Mec-3, is composed of around 50-60 amino acid residues with conserved cysteine and histidine residue . These domains are known to be inter- and intra-molecular interaction domains. LIM domain has been found as a single domain or in multiple copies in proteins with various functions. Dependent on the sequence relationship and overall structural similarities LIM domain containing proteins are comprised of three different groups: Group 1 proteins (LIM-homeodomain proteins) are nuclear transcriptional regulators and cell lineage determinants, whereas group 2 (cysteine-rich proteins) and group 3 proteins (zyxin, paxillin) are cytoplasmic actin cytoskeleton regulators [Khurana et al., 2002].

PDZ domain is an 80-100 amino acid residues protein-protein recognition domain which is known to function in clustering of ion channels and receptors by binding of the PDZ domain to the C-terminal S/TXV tripeptide motif. It specifically recognize the C-terminal peptide motifs or internal sequence of a protein which mimic a terminus. Many PDZ-domain containing proteins play an important role in transport and localisation [Takahashi et al., 2003, Harris and Lim, 2001].

The PDZ domain of LIMK1 contains two leucine-rich nuclear export signals, which support preferentially cytoplasmic localisation of LIMK1 [Yang et al., 1998a, Yang and Mizuno, 1999]. The N-terminal LIM domains and PDZ domain of LIMKs were shown to regulate negatively the kinase activity through direct interaction to C-terminal kinase domain [Nagata et al., 1999]. The proline-serine-rich (P/S) region separates the PDZ domain from C-terminal kinase domain (figure 1.3). The kinase domain contains a nuclear localisation sequence [Yang and Mizuno, 1999].

In LIMK1, alternative splicing of exon 11 yields a shorter isoform, LIMK(-), (L in figure1.3)

represents the sequence encoded by exon 11 that is spliced out in LIMK(-)). No detailed analysis was performed for LIMK1 (-) apart from knowing that it is catalytically inactive (figure 1.3)[Stanyon and Bernard, 1999].

LIMK2 splice variants show different localisation in cells. Although LIMK2a is distributed both in nucleus and cytoplasm, LIMK2b is found mainly in the cytoplasm and scarcely translocates to the nucleus [Osada et al., 1996]. TESKs also localise differently in the cell, though TESK1 localises mainly in the cytoplasm, TESK2 localises mainly in the nucleus, supporting the idea that they might have different cellular functions. TESK2 kinase-dead mutant localises to the cytoplasm indicating that nuclear localisation of TESK2 depends on its kinase activity [Toshima et al., 2001].

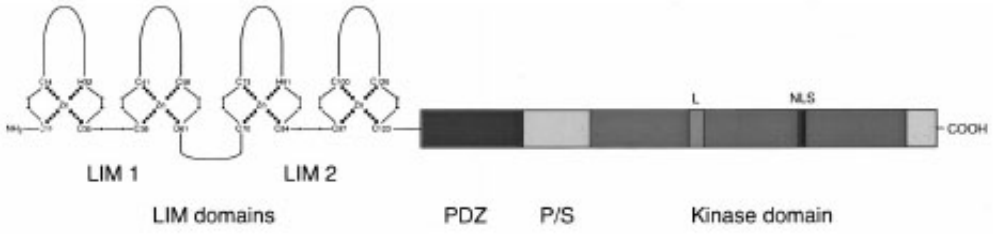

Fig. 1.3: LIMK protein structure, adapted from Stanyon et al., 1999

1.1.3 Expression profile of LIM-kinases

The highest levels of LIMK1 was found by using Northern Blot (NB) and *in situ* hybridisation (ISH) data in fetal and neural tissues, such as brain, spinal cord and various sensory organs [Takahashi et al., 2003]. Despite the data from NB and ISH, indicating the LIMK1 expression mainly in the brain, it has been reported recently by western blot analysis of mouse tissues that LIMK1 protein is expressed in various mouse tissues with different levels and different prevalance of isoforms (higher isoform (75kDa) in kidney, liver and lung, and lower isoform (45kDa) in stomach) [Foletta et al., 2004].

Human and mouse LIMK2 isoforms, LIMK2a, LIMK2b and tLIMK2 are differentially expressed in tissues. LIMK2a is ubiquitously expressed in a variety of tissues, although LIMK2b is expressed mainly in brain, and tLIMK2 is specifically expressed in differentiated, meiotic stages of spermatogenic cells [Takahashi et al., 2003]. Recently, LIMK2 protein levels were reported in various tissue extracts. Indeed, the expression was found in most of the tissue extracts that were tested with high levels in thymus and very low levels in kidney [K et al., 2006].

LIM-kinase related kinases TESK1/2 are expressed highly in testis, although TESK1 is also expressed in various tissues and cell lines at low levels [Toshima et al., 1999, Toshima et al., 2001]. TESK1 is predominantly expressed in testicular germ cells, whereas TESK2 expression is limited to nongerminal Sertoli cells, which suggests different functions of TESKs [Toshima et al., 2001].

1.2 LIMK1 and interacting partners

The LIM domains and PDZ domain in N-terminal part of LIMK1 are known to mediate protein-protein interaction. The first protein that was shown to interact with LIM domain of LIMK1 was protein kinase C (PKC) [Kuroda et al., 1996]. It only interacts with the LIM B domain. The result of this interaction should be still elucidated. Additionally, proteins interacting with LIM domain have been found in the last 3-4 years namely a cyclin-dependent kinase inhibitor p57KIP2, a tumor suppressor LATS1, which regulates cell cycle progression and apoptosis, and BMP type II receptor, which has a role in dendritogenesis (figure1.4) [Yokoo et al., 2003, Denicourt and Dowdy, 2004, Yang et al., 2004b, Lee-Hoeflich et al., 2004] (for detailed information page 36 [p57], page 48[LATS1], page 60 [BMP type II receptor]) .

In addition to that, 14-3-3 ζ is shown to interact with LIMK1, an interaction that requires LIMK1's PDZ and kinase domains [Birkenfeld et al., 2003].14-3-3 family have been involved in various physiological processes, and are thought to function as adaptors in various signal transduction

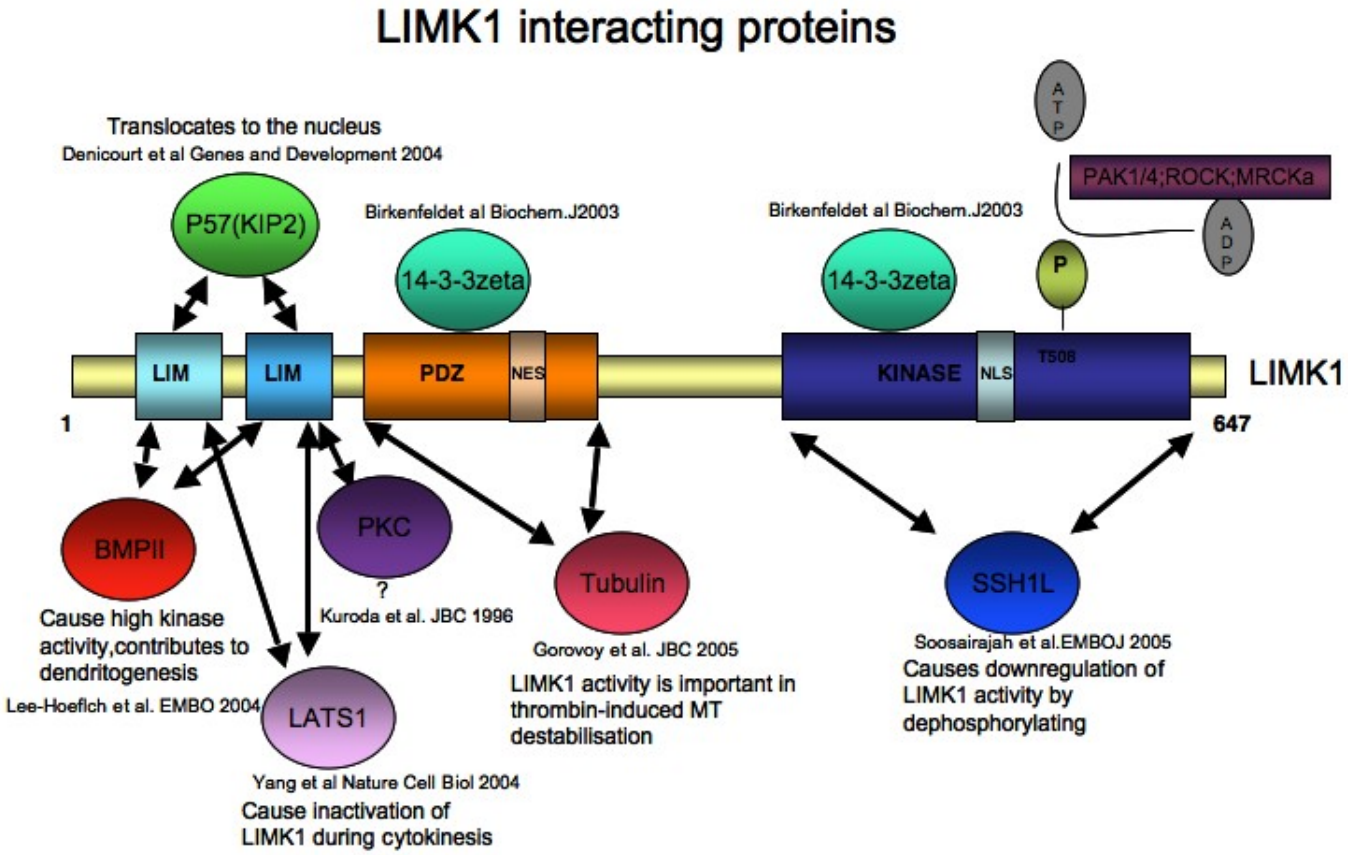

Fig. 1.4: Interacting partners of LIMK1and functional consequences reviewed from Yokoo et al., 2003, Denicourt et al., 2004, Yang et al., 2004, Lee-Hoeflich et al., 2004, Birkenfeld et al., 2003, Gohla et al., 2002, Soosairajah et al., 2005

pathways. 14-3-3 ζ is also shown to bind phosphorylated form of cofilin, and stabilizes it so that inhibits its binding and depolymerizing activity of actin [Gohla and Bokoch, 2002a]. Finally, it has been recently shown that tubulin interacts with LIMK1 through its PDZ domain (figure1.4) (for detailed information page 20).

A phosphatase for cofilin, slingshot 1L (SSH-1L), is shown to interact with kinase domain of LIMK1 and causes downregulation of its activity (figure1.4) [Soosairajah et al., 2005](for detailed information page 30).

1.3 Functions of LIM-kinase 1

LIMK functions in different cellular processes such as cell migration, cell cycle, neuronal differentiation, phagocytosis. Moreover as a pathophysiological point of view, its overexpression is found in cancer cell invasion and metastasis and hemizygosity is found in a neurodevelopmental disorder William's syndrome with the 28 other genes.
The role of LIMK1 in cell migration, cell cycle, neuronal differentiation, and phagocytosis are discussed in coming sections:

1.4 LIM-kinase 1 and cell migration

Cell migration is a vital multistep process which takes place in all multicellular organisms. It is important during development and afterwards in wound healing and immune surveillance in adults and involves dynamic changes in cytoskeleton, cell to substrate adhesion, and the extracellular matrix. Many different cell types migrate individually, such as fibroblasts, while, some cell types, e.g. epithelial and endothelial cells, migrate as sheets or groups [Yamazaki et al., 2005]. Cell migration is directed by extracellular cues either as attractants (chemotactic factors) or repellants. The cell responds in large variety to extracellular cues, by having changes in actin and microtubule cytoskeletons, in vesicular transport pathways and in gene transcription. During the migration, cell becomes polarized with a distinct leading and rear edges. This is a common feature of both fibroblastic and amoeboid motility. The major driving force of migration is extension of leading edge protrusion (lamellipodium), the establisment of new adhesion sites at the front, cell body contraction, and detachment of cell rear. All these steps involve the assembly and disassembly of the actin cytoskeleton, and each must be coordinated to achieve the net forward movement (figure 1.9) [Raftopoulou and Hall, 2004].

LIMK1 is required for cell migration by stimulating lamellipodia in the initial stages of cell re-

sponse through polymerizing actin by phosphorylation and inactivation of actin depolymerising factor cofilin at serine-3 [Arber et al., 1998, Nishita et al., 2005]. LIMK-cofilin signaling pathway for regulating actin filament dynamics is evolutionarily conserved between Drosophila and mammals [Ohashi et al., 2000a]. Overexpression of LIMK1 in variety of cell types causes the actin stabilisation and subsequent aggregation of F-actin [Yang et al., 1998b, Arber et al., 1998]. Additionally, LIMK1 interacts to F-actin through its C- terminal region [Yang et al., 1998b]. These findings indicate that LIMK1 has a role in cell migration by regulating actin cytoskeleton dynamics.

1.4.1 Actin Cytoskeleton

Actin cytoskeleton is comprised of actin filaments (microfilaments) which are solid rods made of actin. Actin exists in two forms. The monomeric form, which is called globular actin (G-actin), polymerizes to generate the filamentous form (F-actin). The rapidly growing end of F-actin is called "barbed end" or "plus (+) end" whereas the slowly growing end is called "pointed end" or "minus (-) end" (figure 1.5). Extension of actin filaments occur when ATP bound G-actin monomers are added to the free barbed end. As the actin filament ages, ATP is hydrolysed, phosphate is released and ADP-actin filaments are disassembled through loss of ADP-actin monomers from the pointed end. ADP-actin monomers can then undergo nucleotide change to ATP-actin by profilin, which is a monomeric actin binding protein, to be ready for the next round of polymerization at the barbed end. This ATP-hydrolysis driven, directional actin growth is called "actin treadmilling", which is important in cell movement, morphogenetic changes and intracellular transport (figure1.6) [Pantaloni et al., 2001, Paavilainen et al., 2004, Welch and Mullins, 2002] . The actin cytoskeleton is a major component of key cellular processes such as cell motility, cell division(cytokinesis) and endocytosis. During cell movement, there is a need of rapid elongation of actin filaments. In order to accomplish this, high concentrations of actin monomers should be available so that actin polymerization can initiate from free monomers (actin nucle-

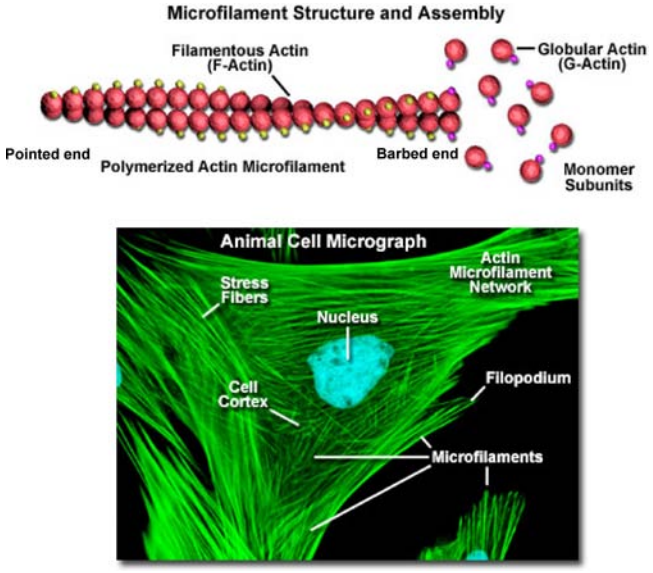

Fig. 1.5: Actin filaments (microfilaments): the upper scheme represents molecular structure of actin filaments. The lower picture represents the actin microfilament network in a mammalian cell, visualized after staining of actin

ation). Actin related protein (Arp) 2/3 complex is used as a template for nucleation. It is a conserved complex of seven polypeptides, that is found in filament networks at Y-branches [Condeelis, 2001]. To maintain the actin monomer pool, there are a group of proteins called actin-monomer-sequestering proteins that regulate the availability, subcellular localization and nuclear status of the monomers(ADP-G-actin or ATP-G-actin). One of these proteins is actin depolymerising factor (ADF) /cofilin, which is a small protein which can bind to both G-actin and F-actin. It promotes the dissociation of G-actin in the pointed end of F-actin that causes subsequent nucleation of G-actin. ADF/ cofilin display higher affinity for the ADP-actin subunits than ATP-actin subunits. By binding to F-actin, ADF/cofilin stabilizes a twisted form of actin filament [McGough et al., 1997, Galkin et al., 2001], initiates the fragmentation (severing) and increases the rate of subunit loss from the filament pointed end (figure1.6, 1.12) [Bamburg and Wiggan, 2002, Paavilainen et al., 2004].

The signals responsible for cell migration include extracellular cues (diffusible factors, signals

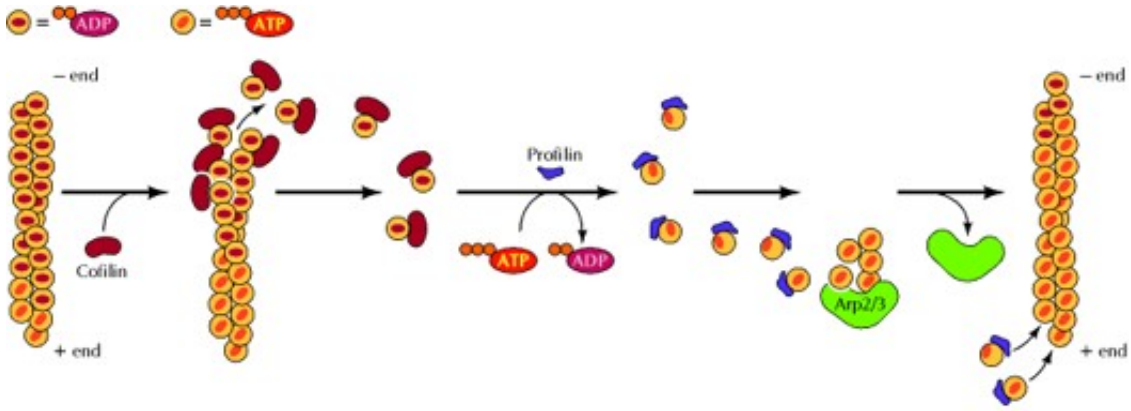

Fig. 1.6: The steps of actin treadmilling adapted from Cooper , 2000

on neighbouring cells, and/ or signals from extracellular matrix) or endogeneous events such as sponteneous oscillatory exchange of GDP for GTP on small Rho GTPases. The crucial role of Rho GTPases in cell migration is based on the formation of actin-containing structures [Ridley, 2001, Raftopoulou and Hall, 2004].

1.4.2 Rho GTPases and cell migration

The family of Rho GTPases have 20 members in mammals, 7 in flies and 5 in worms. These ubiquitously expressed proteins act on cell migration, cell-substrate adhesion, cell-cell adhesion, protein secretion, vesicle trafficking, G1 cell cycle progression and transcription. Additionally, they influence cell polarity and microtubule dynamics [Etienne-Manneville and Hall, 2002]. From Rho family GTPases, Rho A, Rac1, and Cdc42 are the ones that were studied mostly about their role in regulating actin cytoskeleton dynamics by cycling between inactive GDP-bound "off-state" and active GTP-bound "on-state" (figure1.7) [Hall, 1998].

1.4.2.1 Regulation of Rho GTPases

The Rho GTPase cycle is tightly regulated by three group of proteins. Guanine nucleotide exchange factors (GEFs) promote the exchange of GDP for GTP to activate the GTPases, GTPase-

activating proteins (GAPs) enhance the intrinsic GTPase activities of Rho GTPases and guanine nucleotide dissociation inhibitors (GDIs) block the GTPase cycle by sequestering and solubilizing the GDP-bound form and it also prevents the interaction of Rho GTPases and plasma membrane (figure1.7) [Raftopoulou and Hall, 2004] .

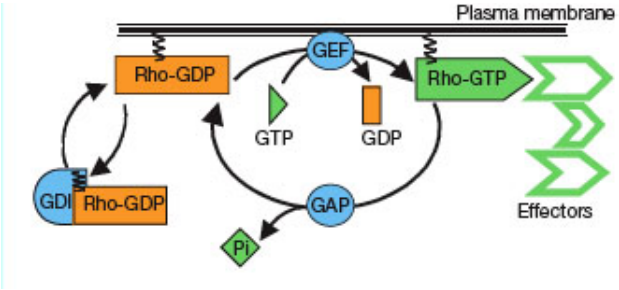

Fig. 1.7: The Rho GTPase cycle, adapted from Etienne-Manneville and Hall , 2002

1.4.2.2 The environmental signals activate Rho GTPases

Rho GTPases are activated in response to specific environmental signals and turn to the "on-state" till GTP hydrolysis returns the switch to "off-state". Each on-state GTPase induces specific changes in actin cytoskeleton: Rho induces assembly of stress fibres (contractile actin:myosin filaments) and focal adhesions; Rac induces peripheral actin accumulation and membrane ruffling (lamellipodia); CDC42 induces the formation of actin-rich finger-like membrane extensions (actin microspikes/filopodia); and in addition to that both Rac and CDC42 assemble focal complexes [Mackay and Hall, 1998] (figure1.8). These effects were shown by microinjection of Rho, Rac or CDC42 into serum-starved Swiss 3T3 cells. Apart from this, all three GTPases promote the assembly of integrin-based, matrix adhesion complexes. These distinct changes involve different upstream signals that trigger the activity of each Rho GTPase, and many downstream effectors that are stimulated by them [Aspenstrom, 1999].

In Swiss 3T3 cells, while serum stimulation or addition of lysophosphatidic acid (LPA) induces

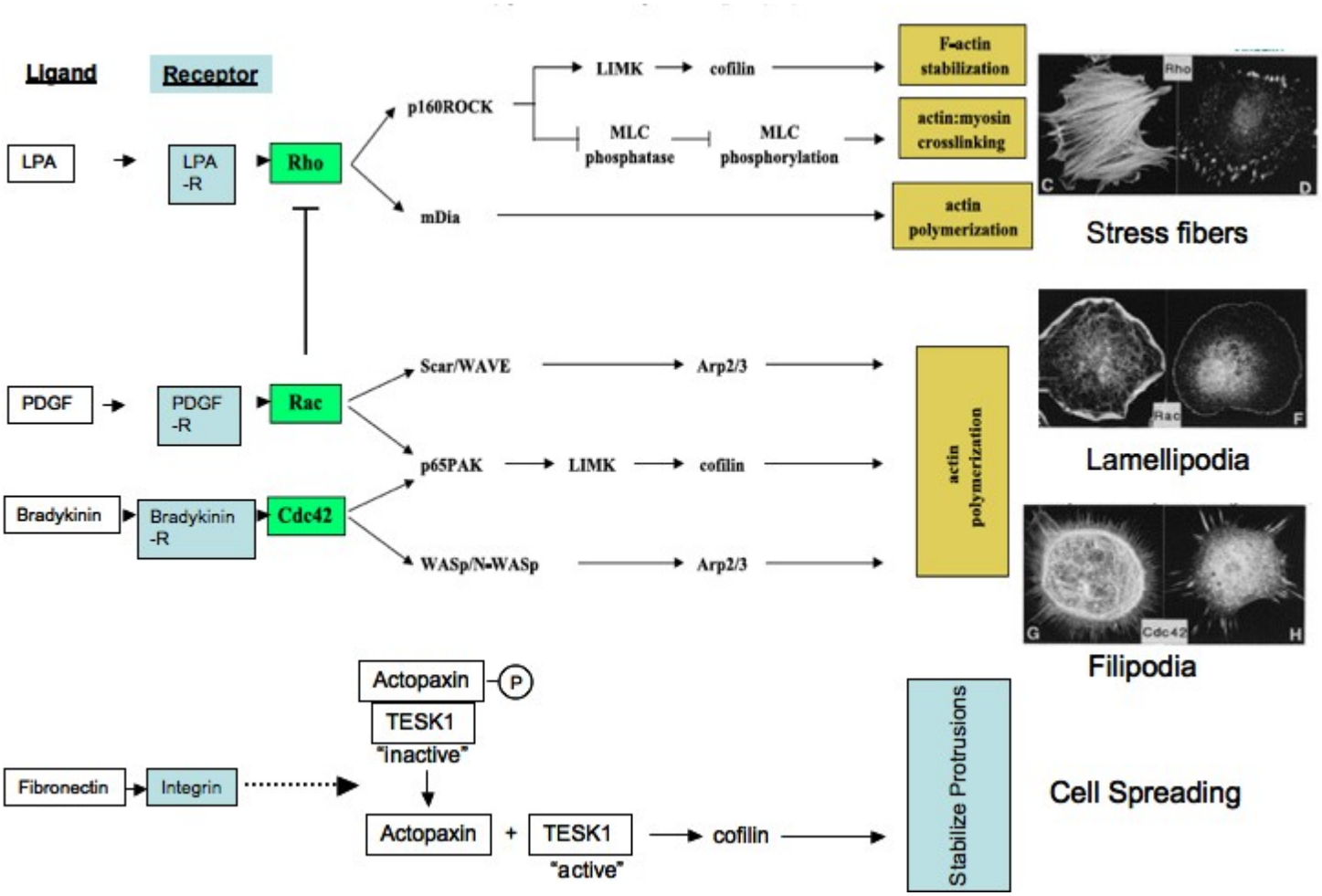

Fig. 1.8: Small Rho GTPases control the assembly and organisation of actin cytoskeleton, through downstream effectors modified from Hall, 1998, Raftopoulou and Hall, 2004

rho-mediated stress fiber formation [Ridley and Hall, 1992], addition of platelet-derived growth factor (PDGF) or insulin, induces rac-mediated lamellipodia formation [Ridley et al., 1992] and addition of bradykinin promotes Cdc42-mediated filipodia formation (figure1.8) [Kozma et al., 1995, Nobes and Hall, 1995] .

1.4.2.3 The role of Rho GTPases in cell migration through regulating actin cytoskeleton

There are pivotal roles of Rho GTPases in reorganising actin cytoskeleton in migrating cells. The four steps of cell migration are achieved by the Rho GTPase activity. The first step is **protrusion**,which is lamellipodia and filopodia formation when cells are polarized by extracellular stimuli. This step involves actin polymerization at the leading edge by Rac and Cdc42 signaling. This localised polymerization of actin in leading edge pushes the membrane forward in lamellipodia and filipodia which generates the locomotive force of migrating cells (figure 1.9). Besides this, Cdc42 also localizes to the Golgi apparatus to regulate cell polarity. The second step is the **formation of a new adhesion**. Rac contributes to the formation of adhesions by focal complex formation in lamellipodia and by inducing focal complex turnover both directly and through activation of downstream effector PAK. The other two steps are **cell body contraction(translocation)** and **tail detachment (retraction)**. Rho activity is associated with focal adhesion assembly and cell contractility (by actomyosin) and is responsible for cell body contraction and rear end retraction. Tail detachment can be the rate-limiting step of the migration. In slowly moving cells detachment depends on a protease called calpain, which degrades the focal adhesion complexes in the rear end. Although there is not a direct effect of Rho to tail detachment, the effect of it to actomyosin contractility may effect the tail detachment (figure1.9)[Ridley, 2001, Yamazaki et al., 2005].

Active forms of RhoGTPases exert these functions by interaction with their downstream effectors. Both LIMK1 and LIMK2 are known to regulate actin cytoskeletal reorganization under the control of Rho family GTPases: RhoA acting through Rho-associated coiled-coil-containing ki-

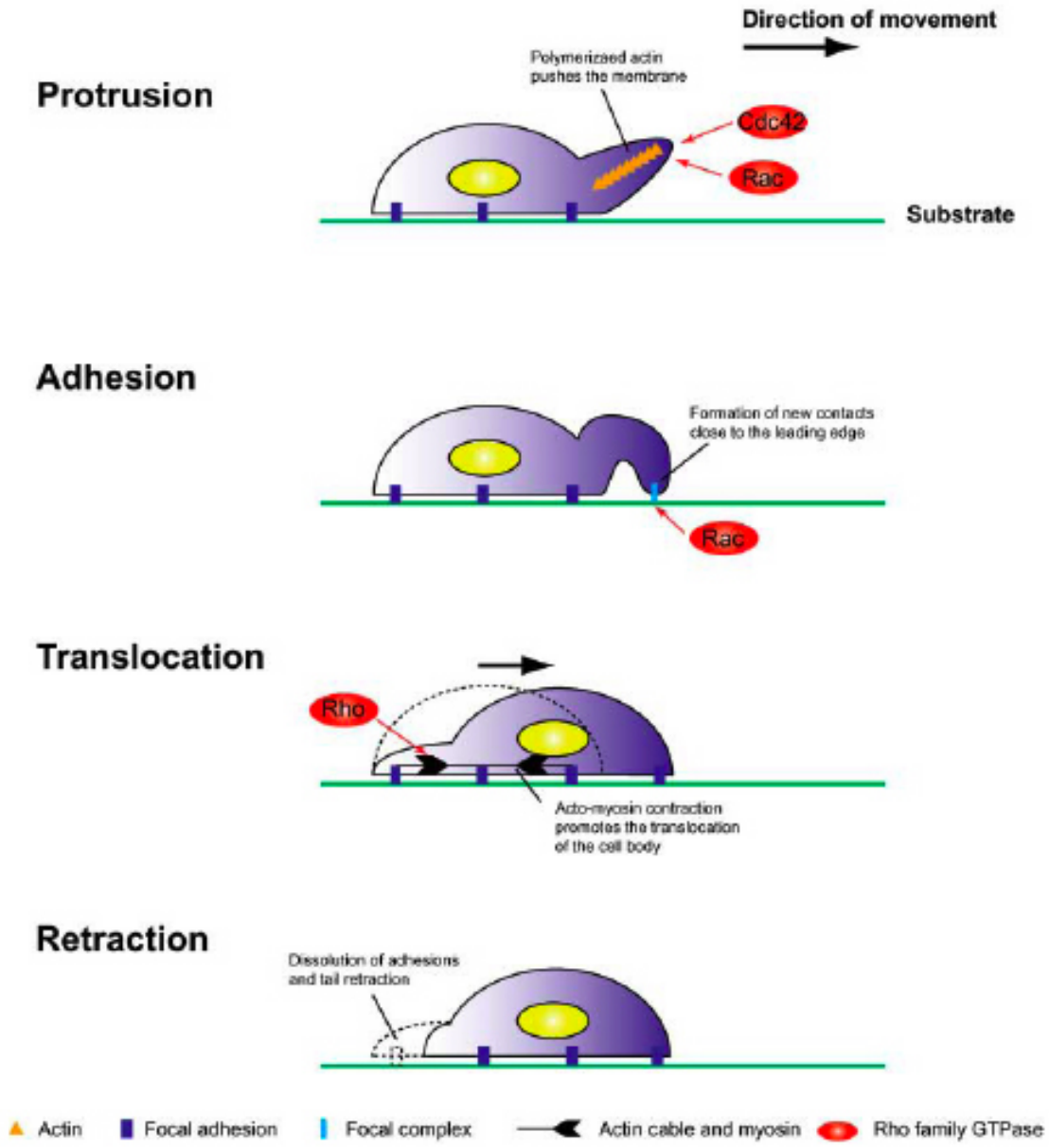

Fig. 1.9: Rho GTPases in directional cell migration adapted from Yamazaki et al., 2005

nase (ROCK) [Ohashi et al., 2000b], Rac/Cdc42 acting through p21-activated kinase (PAK)1 and PAK4 [Edwards et al., 1999, Dan et al., 2001] and Cdc42 acting through myotonic-dystrophy-related cdc42-binding kinase (MRCK), causes the phosphorylation of LIMKs (figure1.8). The activation of LIMKs occurs by phosphorylation of T508 site of LIMK1 and T505 site of LIMK2, which is followed by autophosphorylation of serines; therefore LIMKs activities are positively correlated with their level of phosphorylation [Sumi et al., 2001]. LIMK-mediated actin cytoskeletal rearrangement is mediated by the phosphorylation of cofilin and actin-depolymerizing factor at Ser 3 [Arber et al., 1998, Yang et al., 1998b, Sumi et al., 1999]. Phosphorylation of cofilin causes the inactivation of the protein and subsequently the stabilisation of actin. Although TESKs also phosphorylate and regulate cofilin, they are not stimulated by either ROCK or PAK but can be stimulated by plating cells on a fibronectin-coated surface which contributes to cell spreading. These suggest that TESKs function downstream of integrins and plays a role in integrin-mediated actin reorganisation [Toshima et al., 2001] (figure 1.8).

1.4.2.4 Downstream effectors of Rho GTPases

Apart from the LIMKs, the actin rearrangement caused by Rho, Rac and Cdc42 is through different downstream effectors. Rac and Cdc42 activates SCAR/WAVE (WASP family verproline homologous) and WASp (Wiskott-Aldrich syndrome protein) family members, respectively. The activation of SCAR/WAVE and WASp stimulates Arp2/3 complex, which can initiate the actin polymerisation either de novo or at the barbed end or sides of preexisting filaments. These leads the lamellipodial or filopodial morphology of actin, dependent on whether it is activated through Rac or Cdc42 [Weaver et al., 2003]. Although, the activation of Scar/WAVE by Rac is indirect and involves Nck-adaptor complex, the activation of WASP and N-WASP is directly mediated by Cdc42 [Rohatgi et al., 1999, Eden et al., 2002].

Rho activity is mediated through its downstream effectors ROCK(Ser/Thr kinase) and mDia

(mammalian ortholog of *Drosophilia* Diaphanous). Rho/Rock pathway is essential in rear cell detachment in single migrating cells such as leukocytes (figure1.9). In addition to the role of activating LIMKs, ROCK can also phosphorylate and subsequently inactivate the myosin light chain phosphatase (MLC phosphatase) and at the same time phosphorylate and activate myosin light chain kinase (MLC) both of which leads to increased levels of myosin phosphorylation and actin:myosin crosslinking. This promotes the movement of cell body and facilitates the detachment of cell rear. Rac inhibits Rho in leading edge since Rho activity in front side is incompatible with membrane protrusion. It is not clear how this inhibition occurs [Raftopoulou and Hall, 2004]. In addition tho that, activation of mDia through Rho causes the actin polymerisation via *de novo* F-actin assembly. It also contributes to stress fiber formation by the cooperation with ROCK [Burridge and Wennerberg, 2004]. Another effector of Rho, namely citron kinase effects actin cytoskeleton through stimulation of MLC phosphorylation and subsequently activation of myosin similar to ROCK, although it appears to function primarily following mitosis in the cleavage furrow of dividing cells (figure1.8).

Additionally, a direct link has been reported between the Rho-dependent control of actin polymerisation and the ability to regulate transcriptional activation with the serum response factor (SRF). Activation of SRF upon serum or mitogen is shown to be Rho-dependent and it can be inhibited by blokade of actin polymerisation. [Miralles et al., 2003, Settleman, 2003]. Induction of SRF-dependent transcription requires the ability of SRF to sense the reduction in G-actin levels in response to Rho signaling through ROCK/LIMK and mDia [Sotiropoulos et al., 1999]. Recently, it has been shown that a G-actin binding protein MAL (or MKL1) functions as a SRF-coactivator, and its translocation from cytoplasm to nucleus upon serum stimulation depends on its dissociation from G-actin upon Rho signaling [Miralles et al., 2003].

1.4.2.5 The role of Rho GTPases in cell migration through regulating microtubules

The pivotal role of Rho GTPases in regard to migration is not only through regulation of actin cytoskeleton, but also through regulation of microtubules. Microtubules are biopolymers composed of subunits made from an abundant globular cytoplasmic protein known as tubulin. Each subunit of tubulin is composed of a α and β tubulin which forms a heterodimer [Bryan and Wilson, 1971]. In a microtubule, the subunits are organized in a way that all of them point the same direction to form 13 parallel protofilaments [Tilney et al., 1973]. With this, the α tubulins facing one end and β tubulin the other, thereby creating a polarity. The end of polarized filament that grows and shrinks the fastest is known as the plus end and the opposing end is called the minus end (containing α tubulin). The minus end is located to the centriole containing centrosome, while the plus end (exposed to β tubulin) is projected out toward the cell's surface (figure1.10) [Song and Mandelkow, 1995, Hoenger and Milligan, 1996].

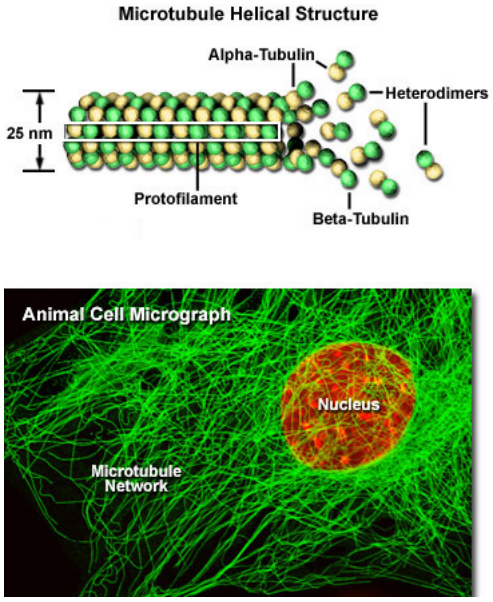

Fig. 1.10: Microtubules, the upper scheme represents molecular structure of microtubules. The lower picture represents the microtubule network in a mammalian cell, visualized after staining of tubulin

Microtubules

Microtubules are responsible for various cell movements in the cell such as beating of cilia and flagella, transport of membrane vesicles in the cytoplasm, alignment and separation of chromosomes during mitosis and meiosis. The biological functions of microtubules are regulated by two kinds of dynamics; 'dynamic instability' and 'treadmilling' [Rodionov and Borisy, 1997, Margolis and Wilson, 1998, Mitchison and Kirschner, 1984]. Dynamic instability is a process in which microtubule ends switch between phases of growth and shortening. The microtubules undergo relatively long periods of slow lengthening, short periods of rapid shortening and periods of pause [Jordan and Wilson, 2004]. Treadmilling is the net growth in one end and net shortening to balance in other end [Margolis and Wilson, 1998, Rodionov and Borisy, 1997]. These two behaviors are compatible which means that a cell can have one, the other or some mixture of both [Jordan and Wilson, 2004]. Functional diversity of microtubules is maintained through binding of various regulatory proteins for instance microtubule associated proteins (MAPs). There are many different MAPs, such as survivin, stathmin, TOG, MCAK, MAP4, EB1, dynactin 1, Rac, and FHIT [Ligon et al., 2003, Giodini et al., 2002, Cassimeris, 2002, Spittle et al., 2000].

During cell migration, selective stabilisation of plus ends of microtubules enables the microtubule-organising centre (MTOC) to reorient towards the leading edge, resulting in polarized microtubule array that facilitates the cell migration. The dynamics and organisation of microtubules are regulated by Rho GTPases during cell migration. Rho causes the accumulation of stable microtubules (termed Glu-MTs) by activating mDia which in turn interacts with adenomatous polyposis coli (APC) and EB1 and regulates the formation of Glu-MTs. PAK, which is an effector of Cdc42 and Rac, phosphorylates stathmin and causes its inactivation in the leading edge of migrating cells. This causes the decrease in microtubule catastrophe (the event by which microtubules switch from growth to shrinkage). Cdc42 regulates MTOC polarisation by activating atypical protein kinase C (aPKC) through Par6 which leads to phosphorylation and inactivation

of GSK3-β and subsequently enabling APC to stabilise microtubules at the leading edges. In addition to that, the actin binding protein IQGAP1, which is an effector of Rac and Cdc42, interacts with CLIP-170 (microtubule associated protein) and APC and captures them in leading edge and filopodia [Watanabe et al., 2005] (figure1.11).

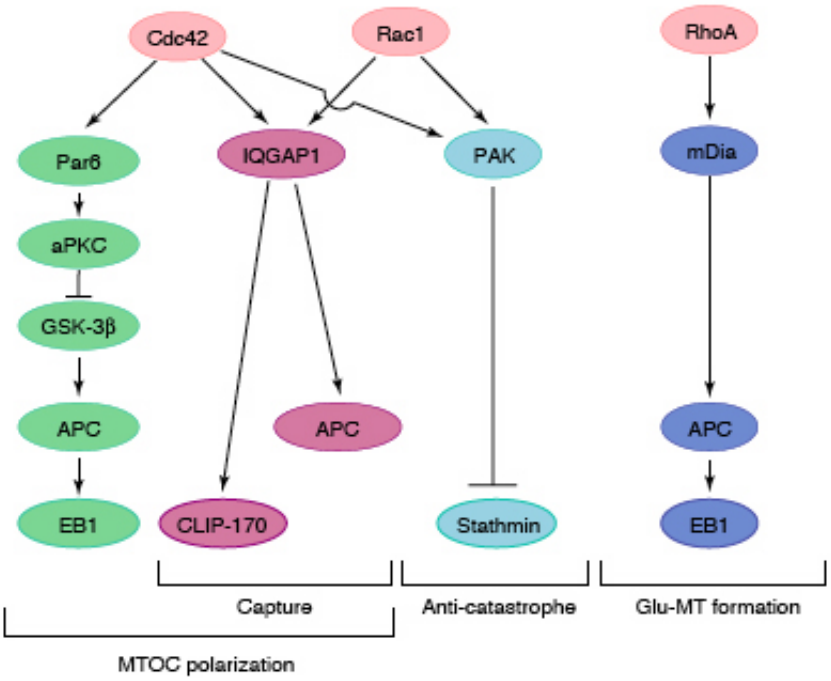

Fig. 1.11: Signaling network from Rho GTPases to microtubules adapted from Watanabe et al., 2005

1.4.2.6 The role of LIMK1 in cell migration

LIMK has an important role in cell migration by regulating actin cytoskeleton downstream of Rho GTPases. In addition to that it has been shown recently that LIMK1 interacts to microtubules (figure 1.4) through its PDZ domain and may regulate microtubules dynamics in endothelial cells, although it is not known whether this interaction effects the cell migration. In that report it was found that, thrombin or nocodazole induced microtubule destabilisation results in decreased interaction between LIMK1 and tubulin. Also, when LIMK1 is overexpressed in endothelial cells, microtubule destabisation occurs. Interestingly, when LIMK1 is activated

by Rho-ROCK, the interaction between LIMK1 and tubulin decreases while its interaction with actin increases. Upon LIMK1 depletion via small-interference RNA, or inactivation by expressing of kinase-dead LIMK1, results in release of microtubule destabization by thrombin induction. Microtubule destabilization promotes the formation of actin stress fibers and enhances the contractility of cells and there is a coordinated regulation between microtubules and actin cytoskeleton. All of this, suggests that LIMK1 may coordinate both microtubules and actin cytoskeleton [Gorovoy et al., 2005].

1.4.3 Cofilin: the substrate of LIM-kinases

Activated LIMK1 phosphorylate cofilin at Ser3, leading to its inactivation by altering the protein conformation and binding to actin. Cofilin is a 19 kDa ubiquitously expressed protein. The name "cofilin" stands for "cofilamentous protein" and reflects its filament binding activity as discovered [Nishida et al., 1984]. It is a member of actin-depolymerizing factor family (ADF/cofilin). Most vertebrates have one ADF (in human localized to chromosome 12 and 8, possible pseudogenes) and two cofilins; the latter is divided into muscle- (in human localized to chromosome14) and nonmuscle (in human localized to chromosome 11) cofilins [Ono et al., 1994]. There is 70% identitiy between ADF and cofilin. On the contrary, in unicellular organisms there is only one ADF/cofilin gene for instance *unc-60* in *Caenorhabditis elegans*, and *twinstar* in *Drosophila* [Maciver and Hussey, 2002].

The ADF/cofilin family proteins show distinct expression patterns: non-muscle cofilin is expressed mainly in most embryonic and adult mouse cells, muscle- cofilin is expressed mainly in muscle, and ADF is found mainly in epithelial and neuronal cells [Vartiainen et al., 2002]. ADF/cofilin are coexpressed in many cell types and play important roles in cytokinesis, cell motility and morphogenesis in mammals [Hotulainen et al., 2005]. Although in mammals the three members of ADF/cofilin family; ADF, cofilin, and muscle-cofilin have common properties,

ADF has a greater ability to modulate the monomer pool, whereas cofilins are more effective nucleators of assembly [Yeoh et al., 2002]. Although, ADF and cofilins are products of different genes and differ in tissue specific expression and quantitatively in their interaction with G-actin and F-actin [Vartiainen et al., 2002, Yeoh et al., 2002], they have very similar qualitative effects on actin dynamics. Additionally, they are regulated on the same site by reversible phosphorylation, and are usually co-localized in the cells. Therefore, in the literature, the two terms are used interchangeably.

1.4.3.1 Functions of Cofilin

ADF/cofilin family contains nuclear localisation signal and recently has been shown that cofilin is essential for nuclear import of actin upon stress-induced responses [Pendleton et al., 2003]. There are studies indicating the nuclear import and export of actin [Rando et al., 2000]. Although there are two leucine-rich nuclear export sequences in actin structure, there is no nuclear localization sequence indicating that there is another protein needed for the translocation of actin to the nucleus. It has been reported that the actin binding protein cofilin contains a nuclear localization sequence and translocates to nucleus together with actin after a heat shock , dimethyl sulfoxide (DMSO) treatment, latrunculin B (LB) treatment or when ATP is withdrawn. Although cofilin which is translocated to nucleus upon these stimuli is in unphosphorylated state, till which extent the state of cofilin phosphorylation determines its localization is not clear, as much of the cofilin found in cells is in unphosphorylated state and it stays cytoplasmic [Nishida et al., 1987, Iida et al., 1992, Pendleton et al., 2003]. Since most of nuclear actin does not stained with a F-actin marker (phalloidin), it is suggested that it is mainly monomeric actin that is found in nucleus. Although very little is known about the nuclear localization of actin, it has been shown that when actin translocates to nucleus there is a decrease in cell proliferation. Also, nuclear actin creates a complex with DNaseI that is stabilized by cofilin but the relevance of this interaction is not known. It is suggested that, nuclear actin may constitutes the

nuclear matrix, the non-chromatin fraction of the nucleus, enabling the reorganization of chromatin [Rando et al., 2000]. Interestingly, the localization of actin to the nucleus in two different stress-related conditions seem to be different: an actin-destabilizing reagent (LB) causes the disassembly of cortical F-actin but on the other hand, ATP-depletion is associated with an increase in F-actin.

Cofilin has some newly identified functions that are actin-independent. Cofilin is targeted to mitochondrial membranes in response to apoptotic stimuli for cytochrome c release [Chua et al., 2003]. Mitochondria are major organelles involved in signal transduction pathways and biochemical execution of apoptosis [Wang, 2001]. Many apoptotic signals induce the release of apoptotic mitochondrial proteins to the cytoplasm. Cytochrome c is one of these apoptotic mitochondrial proteins, that is released to cytoplasm and activates apoptotic caspase cascade. In staurosporine (STS)-treated apoptotic cells, the dephosphorylated cofilin translocates to mitochondria before the release of cytochrome c, and it is crucial for apoptosis to take place since the depletion of cofilin in STS- treated cells resulted in inhibition of cytochrome c release and apoptosis. Cofilin has a mitochondrial targeting signal in its N-terminal. Although the mitochondrial translocation of cofilin doesn't depend on having a functional actin-binding domain, for apoptosis-inducing ability functional actin-binding is needed [Chua et al., 2003].

Cofilin's activity which is filament severing and off-rate enhancement both causes an increase in actin turnover and also leads to nucleated filament growth from new filament ends. For that reason, the final effect of cofilin on actin cytoskeleton depends on the availability of actin subunits in the region where the process takes place (figure 1.12) [Condeelis, 2001]. Cofilin mainly localise to the leading edge of moving cells, to lamellipodia, where there is a high amounts of actin turnover [Bamburg and Bray, 1987, Yonezawa et al., 1987, Maciver and Hussey, 2002, Dawe et al., 2003].

Cells lacking cofilin have impaired locomotion [Chen et al., 2001]. Also cells which have over-expression of constitutively active LIMK1, leading high phosphorylation of cofilin, lose their polarity and in that cells single polarized lamellipodium is replaced with multiple nonpolarized lamellipodia [Dawe et al., 2003]. These findings suggest that the existence and proper regulation of cofilin is important in cell motility. The synergistic activity of Arp2/3 complex and cofilin in leading edge of migrating cells causes the generation of free barbed ends by de novo nucleation of actin and severing of F-actin, respectively, which subsequently leads the polymerization of actin, induction of protrusion and sets the direction of cell migration. It is shown that, cofilin-severed F-actin fragments act as preferred substrates from which Arp2/3 builds actin networks, which explains the polymerization of actin after cofilin severing in lamellipodia [Ichetovkin et al., 2002]). Because the spatial regulation of cofilin-dependent actin depolymerizing/severing activity is crucial for directional cell migration, as site-specific activation of caged cofilin can determine the direction of cell movement [Ghosh et al., 2004], it is important to know how cofilin is regulated.

Cofilin's activity is regulated in molecular level by the change in pH (the activity of cofilin is stimulated by an increase in pH) [Bernstein et al., 2000] ; interaction with tropomyosin (binds to actin, and prevents the binding of cofilin so that it inhibits cofilin to depolymerize actin), 14-3-3 ζ (binds to phosphorylated cofilin and prevents its dephosphorylation to maintain the cellular phospho-cofilin pool) [Gohla and Bokoch, 2002a], actin-interacting protein 1 (AIP1) (binds to cofilin and may stimulate the depolymerization activity of cofilin) [Ono, 2003], cyclase-associated protein 1 (CAP1) (it is important for proper localization and function of cofilin, it is important in recycling cofilin from actin monomers for new rounds of actin depolymerization) [Bertling et al., 2004] and phosphatidylinositol (4,5)- biphosphate(binds and inhibits the actin binding activity of cofilin) ; and phosphoregulation [DesMarais et al., 2005]. Both cofilin and ADF are regulated by same mechanisms. The only significant difference that is reported is the differential regulation in response to alterations in actin monomer pool [Minamide et al., 1997].

The phosphorylation/ dephosphorylation at Ser3 acts at a simple switch on actin assembly and

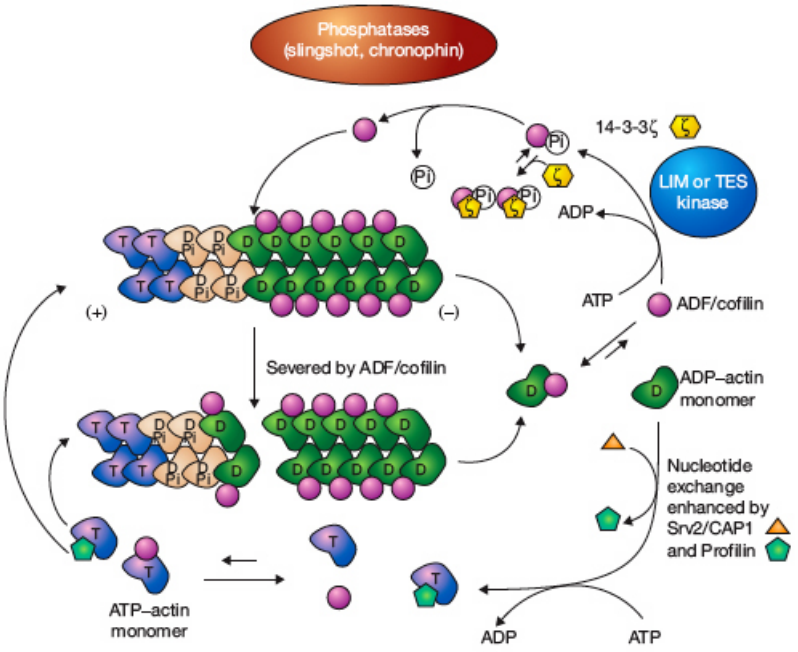

Fig. 1.12: Phosphoregulatory cycle of cofilin adapted from Wiggan et al., 2005

disassembly/severing (figure1.12) [Wiggan et al., 2005, Huang et al., 2006]. When the assembly competent-actin is high and cofilin is active, new assembly to F-actin occurs in cofilin-severed new barbed ends. However, if the actin monomer pool is low, the net effect is as actin depolymerization. In various cell lines and tissues, 14-61% of total cofilin is phosphorylated. It was shown by comparing the activity of purified phosphorylated ADF (pADF) and unphosphorylated ADF that pADF doesn't sever filaments or induce their depolymerization [Moon and Drubin, 1995]. LIMKs and TESKs are the main kinases that phosphorylate and inactivate cofilin and subsequently cause F-actin stability. Indeed their overexpression in cell lines promotes F-actin accumulation. Besides LIMKs and TESKs, another kinase called Nck-interacting kinase (NIK)-related kinase (NRK)/ NIK-like embryo-specific kinase (NESK) was recently shown to phosphorylate cofilin at Ser 3 in Cos-7 cells. NRK/NESK is a member of germinal center kinase (GCK) family. It is activated by tumor necrosis factor (TNF) α and activates the c-jun N-terminal kinase

(JNK) pathway but not the p38 kinase or ERK pathway. NRK/NESK is predominantly expressed in skeletal muscle during late stages of mouse embryogenesis. It is found that overexpressed NRK/NESK can induce actin polymerization through direct phosphorylation of cofilin in COS-7 cells [Nakano et al., 2003].

Even though, extracellular stimuli affecting actin cytoskeleton, causes a net change in phosphocofilin levels, in some cells, such as 3T3 or A431, although there is a significant increase in phosphocofilin turnover, the total phosphocofilin pool stays the same. This suggests a balance between a kinase and a phosphatase pathways to maintain the cycling of phosphate on cofilin in that cells[Meberg et al., 1998]. Despite earlier studies about having PP1, PP2A, PP2B, and PP2C as phosphatases for cofilin, as inhibitors largely fail to block dephosphorylation of cofilin, it seems that these general phosphatases may not account for the majority of phosphatase activity on cofilin in response to cellular stimuli [Huang et al., 2006]. Recently, two cofilin-selective phosphatases have been identified: the slingshot family of phosphatases (SSH), and chronophin (CIN).

1.4.3.2 Dephosphorylation of cofilin

Dephosphorylation of cofilin has been observed in response to various extracellular stimuli. Thrombin stimulated platelets causes dephosphorylation of cofilin through Ca^{2+}-dependent mechanism, which initiated either by a GTP-binding protein or Ca^{2+} [Davidson and Haslam, 1994]. On the other hand, thyrotropin-stimulated thyroid cells have dephosphorylated cofilin through thyroid stimulating hormone (TSH)-adenylate cyclase pathway (figure1.13) [Saito et al., 1994, Moon and Drubin, 1995].

It has been reported recently that neutrophils stimulated with the chemoattractant fMet-Leu-Phe (fMLP) activate phospho inositide specific phospholipase C (PI-PLC) which stimulates protein kinase C (PKC)-dependent and Ca^{2+}/ calmodulin (CaM) dependent pathways, therefore trigger-

ing dephosphorylation of cofilin via protein phosphatase 2C (PP2C) and slingshot along with translocation of this protein to the F-actin rich, ruffling membranes of these cells (figure1.13) [Zhan et al., 2003]. Recent studies have shown that calcium-dependent cofilin dephosphorylation happens through calcineurin which is a calcium/calmodulin-dependent protein phosphatase (also called protein phosphatase 2B). Calcineurin effects on cofilin through dephosphorylating and activating slingshot-1 long variant (SSH-1L) (figure 1.13) [Wang et al., 2005].

In most systems, there is evidence for calcium-independent regulatory pathways for cofilin dephosphorylation. One of these pathways is phosphatidylinositol-3-kinase (PI3K) pathway. PI3K inhibitor wortmannin has been shown to antagonize cofilin dephosphorylation upon different extracellular stimuli [Bamburg, 1999]. It was reported in MCF7 cells that insulin-induced actin reorganization occurs through PI3K and SSH, which causes subsequent dephosphorylation of cofilin. This activation of SSH can be abrogated by PI3K inhibition by PTEN (figure1.13) [Nishita et al., 2004]. Also another growth factor, platelet-derived growth factor (PDGF) causes cofilin dephosphorylation by Ras-Raf- MAPkinase/Erk-kinase (MEK) and Ras- PI3K-effector cascade [Nebl et al., 2004].

1.4.3.3 Slingshot, the phosphatase of cofilin and LIMK1

Slingshot (SSH) was initially identified as a phosphatase for cofilin in *Drosophila* by genetic studies, where its dysfunction causes disorganized epidermal cell morphogenesis, including bifurcating phenotypes of bristles and wing hair, after which '*slingshot*' was named [Niwa et al., 2002]. Although, there is a single gene coding for slingshot protein in *Drosophila* (dSSH), there are 3 genes of SSH with long (L) or short (S) variants with different tissue distribution in mouse and human. SSH is expressed in various organisms but not in *Caenorhabditis elegans, Saccharomyces cerevisae and Arabidopsis thaliana*. In mammalian cells, SSH1 long variant 1L (SSH-1L) and SSH2 long variant 2L (SSH-2L) dephosphorylate phospho-cofilin or phospho-ADF and causes

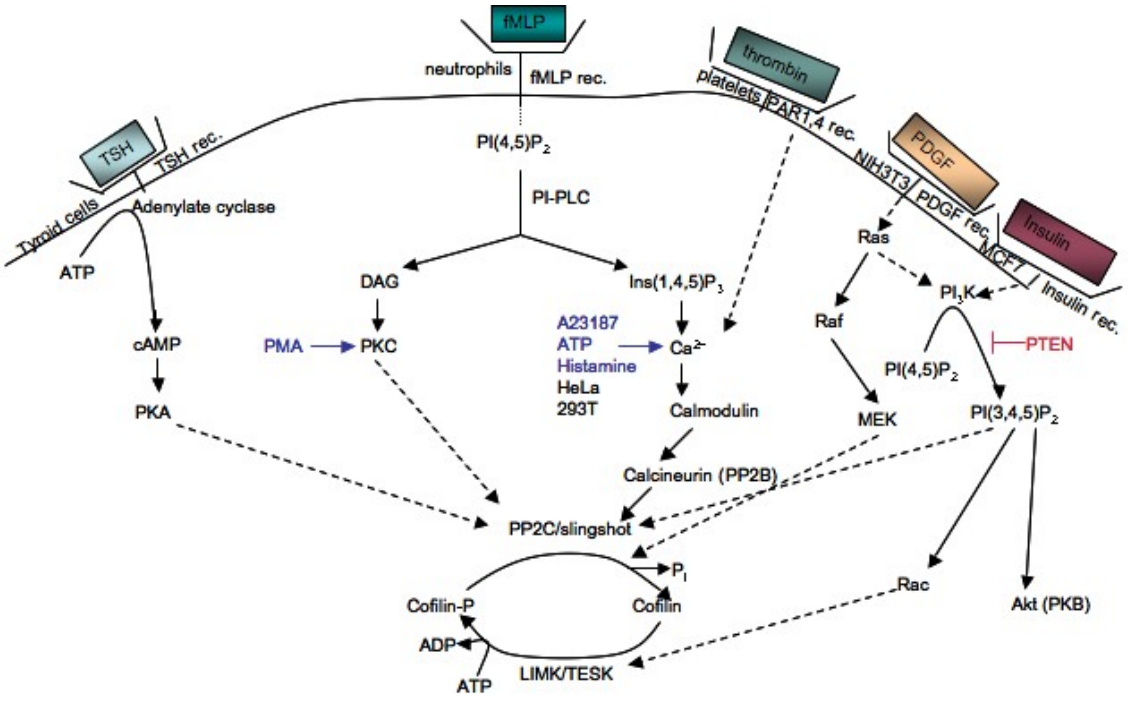

Fig. 1.13: Multiple signaling pathways that modulate stimulus-induced cofilin dephosphorylation in different cell types reviewed from Moon et al., 1995, Zhan et al., 2003, Nishita et al., 2004, Nebl et al., 2004, Wang et al., 2005

the suppression of actin assembly by LIMKs and TESKs [Niwa et al., 2002]. Using truncated mutants of SSH-1L and SSH-2L it is shown that N-terminal regions are required for their cofilin-phosphatase activity and C-terminal region has a role in F-actin binding. SSH phosphatases contain conserved A and B domains with unknown function, a protein phosphatase domain (PTP) with canonical catalytic HCxxGxxR sequence which is found in dual-specificity and protein tyrosine phosphatases, and in long variants C-terminal F-actin binding region (except SSH-3L). The third member of SSH family SSH-3L (SSH3 long variant) is less effective in dephosphorylation of cofilin and it doesn't bind to F-actin [Ohta et al., 2003]. Both SSH1L and SSH2L co-localize with actin filaments through their F-actin binding region, but they differ in F-actin binding activity, subcellular localization and tissue expression patterns. SSH1L and SSH2L accumulates on thick and thin actin fibres in the cytoplasm and on actin bundles at the cell periphery, whereas SSH3L distributes diffusely in the cytoplasm and nucleus. The tissue expression of SSH phosphatases shows differences when examined in mouse tissue sections by northern blotting. *mSsh-1*

was detected as two major mRNA species, 8.0 and 4.0 kb. 8.0 kb was found widely present in all tissues, with a higher expression in brain, thymus, heart and kidney, while 4.0 kb mRNA was present only in liver and kidney. *mSsh-2* was found also as two mRNA species, 8.0 and 4.5 kb. 8.0 kb was detected in all tissues with higher level in brain, thymus, heart and testis, while 4.0 kb was found predominantly in testis. *mSsh-3* was detected in three mRNA species, 4.4, 3.0 and 0.6 kb; the 3.0 kb was in all tissues, with higher levels in kidney and small intestine, whereas the 4.4 and 0.6 kb mRNA were only in brain and in testis, respectively.

During cell migration, cofilin plays a key role in maintaining lamellipodium extension and polarized cell shape, by stimulating actin filament dynamics in the leading edge of the cell. Cofilin activity is spatially and temporally regulated by LIMK1 and SSH-1L in directional cell migration. LIMK1 is required for cell migration by stimulating lamellipodium formation in the initial stages of cell response [Nishita et al., 2005]. The requirement of LIMK1 in initial stages of migration is indicated in the study where LIMK1 inhibition suppresses stromal cell-derived factor 1 α [SDF1α])- induced lamellipodium formation and cell migration in Jurkat human leukemic T cells and peripheral blood lymphocytes [Nishita et al., 2002]. SDF1α-induced LIMK1 activation is mediated by Rac but not by Rho or Cdc42. Although, SDF1α induces activation of LIMK1 up to 20 min, phospho-cofilin levels increased by 1-5 min and reverted to basal levels 20 min after stimulation. The decrease in phospho-cofilin levels at 20 min suggests the involvement of activation of cofilin phosphatase such as SSH-1L [Nishita et al., 2002, Nishita et al., 2005].

SSH-1L is shown to be crucial in directional cell migration by restricting membrane protrusion to one direction and locally stimulating cofilin activity in the lamellipodium. SSH-1L is found in inactive state when phosphorylated at Ser-978 and Ser-937 and bound to 14-3-3 proteins [Nagata-Ohashi et al., 2004]. It is also implicated that 14-3-3 ζ interacts with LIMK1 and phospho-cofilin and leads the stabilization of cofilin in phosphorylated state (figure 1.12) [Birkenfeld et al., 2003, Gohla and Bokoch, 2002b]. When a cell is stimulated by neuregulin-1 β,

insulin or SDF1α, although LIMK1 stays diffusely distributed in cytoplasm, SSH-1L is dephosphorylated at Ser-978, translocated to F-actin rich lamellipodium protrusion, and dephosphorylates cofilin locally [Nagata-Ohashi et al., 2004, Soosairajah et al., 2005, Nishita et al., 2005, Huang et al., 2006]. The highly activation of SSH1-L is by its association with F-actin through its Trp-458 residue.

It is proposed that upon SDF1α stimulation, there is initially activation of LIMK1 through Rac activation which transiently increases P-cofilin levels up to 5 min and induces F-actin assembly and lamellipodium extension that provides the driving force for cell migration. Afterwards, SSH-1L accumulates in F-actin rich lamellipodium and causes the dephosphorylation of cofilin. In this stage, polarized lamellipodium formation in one direction is seen, that is inhibited by excessive (in SSH-1L depleted cells) or insufficient cofilin phosphorylation. The involvement of SSH-1L is suggested since SSH-1L depleted cells retained multiple protrusion after SDF1α stimulation. In the later stages of cell response to SDF1α (after polarity is formed), both LIMK1 and SSH-1L are activated. As LIMK1 is diffusely distributed and SSH-1L is recruited to lamellipodium, it is suggested that both LIMK1 and SSH-1L are active in the front, whereas only LIMK1 is active in the rear of the cell. This restricts cofilin activity to the front of the migrating cell (figure 1.14(a)) [Nishita et al., 2005]. Also both LIMK1 and SSH-1L activation in lamellipodium could cooperatively accelerate the recycling of cofilin and actin. Additionally, SSH-1L can bind to kinase domain and downregulate LIMK1 activity by dephosphorylating T508, which enhances the cofilin activation in the front of the cell. This dephosphorylation by SSH-1L is negatively regulated by PAK4 which phosphorylates and inactivates SSH-1L (figure 1.14(b)) [Soosairajah et al., 2005, Nishita et al., 2005].

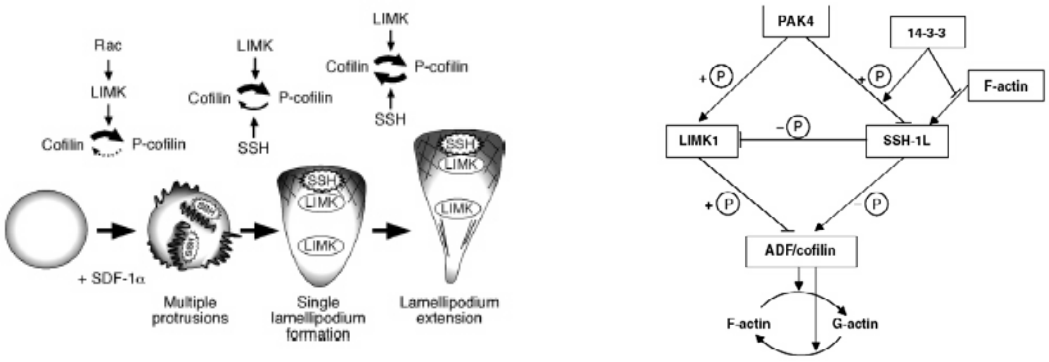

(a) (b)

Fig. 1.14: a)A model for LIMK1 and SSH-1L- mediated spatiotemporal regulation of cofilin activity during SDF1α-induced polarized F-actin assembly and cell migration adapted from Nishita et al., 2005, b) Interplay between components of LIMK1 and SSH-1L complex that regulates cofilin and subsequently actin dynamics adapted from Soosairajah et al., 2005

1.4.3.4 Chronophin

Chronophin (CIN) is found as a potential cofilin phosphatase through biochemical screen of bovine brain extracts [Gohla et al., 2005]. CIN is a member of haloacid dehalogenase (HAD) family of phosphatases which are expressed in organisms ranging from bacteria to humans. It contains a highly specific catalytic domain and 3 conserved sequence motifs characteristic of HAD hydrolases. CIN can be found in many organisms, including *Caenorhabditis elegans, Saccharomyces cerevisae and Arabidopsis thaliana* (that lacks SSH), and is widely distributed in human tissues, particularly in brain. Overexpression or reduction of CIN in mammalian cells leads to reduced or increased levels of phospho-cofilin, respectively. Interestingly CIN exhibits predicted interaction motifs potentially linking CIN to PI3K, which is suggested to be involved in signaling to cofilin dephosphorylation *in vivo*. As opposed to SSH, CIN fails to dephosphorylate LIMK1, although its overexpression leads to decrease in phospho-cofilin levels and effectively antagonizes the enhancement of cofilin phosphorylation by LIMK1. CIN localizes to actin-rich ruffles and membrane protrusions and its function is directly linked to actin dynamics at the leading edge of migrating cells [Gohla et al., 2005, Wiggan et al., 2005, Huang et al., 2006].

1.5 LIMK1 in cell cycle regulation

The cell cycle is a ubiquitous, complex process involved in the growth and proliferation of cells, organismal development, regulation of DNA damage repair, tissue hyperplasia as a response to injury, and diseases such as cancer. It can be divided into distinct phases including a synthesis (S) phase, where DNA is replicated, and a mitosis (M) phase, which include prophase, metaphase, anaphase and telophase, where cell division occurs. In animal cells, growth and synthesis of components required for these phases are regulated by extracellular growth factors and occur mainly in two gap phases, G1 (between M and S) and G2 (between S and M). The proper progression of cell cycle is achieved by cyclin-dependent kinases and their activity is controlled by phosphorylation and association with cyclins (specific regulatory subunits).

In addition to the role of LIMK1 in cell migration, a function has been reported for LIMK1 in cell cycle progression. The initial findings indicating a role of LIMK1 in cell cycle progression are taken from the involvement of XLIMK1 (*Xenopus* counterpart of mammalian LIMK1) in oocyte maturation through phosphorylation of *Xenopus* cofilin. XLIMK1-cofilin system was required for the organization of microtubule-derived precursor of the meiotic spindle [Takahashi et al., 2001]. Likewise, using LIMK2 knockout mice, it is demonstrated that LIMK2 plays an important role in the proper progression of spermatogenesis by regulation of cofilin activity in mammalian germ cells [Takahashi et al., 2002]. In subsequent section the role of LIMK1, LIMK2, and their upstream effectors Rho GTPases, in G1 phase progression and through mitosis is discussed.

1.5.1 G1 phase progression

G1 phase is the site where mitogens and cell adhesion regulates cell cycle. G1 phase progression is mediated by the activities of cyclin D-cdk4 (or cdk6) and cyclin E-cdk2. The activities of these enzymes are determined by the relative levels of their associated cyclins and cyclin-dependent kinase inhibitors and regulated by a complex interplay of signaling pathways that reflect conditions

in the extracellular environment. For instance, cyclin D1 is the rate-limiting step in the activation of cdk4/6, and is regulated by cooperative signaling by receptor tyrosine kinases (RTKs; receptors for many mitogenic growth factors), integrins (receptors for extracellular matrix proteins), and the actin cytoskeleton. At least in most fibroblasts, cyclin D1 is induced in mid-G1 phase (9 hr after mitogen stimulation of quiescent cells), and this mid-G1 phase induction requires sustained (5/6 hr) extracellular signal-regulated kinase (ERK) activity [Welsh et al., 2001]. RTKs, integrins, and actin stress fibers are jointly required to sustain the ERK signal long enough to induce cyclin D1 [Roovers et al., 1999, Roovers and Assoian, 2003, Welsh et al., 2001].

Active cyclin D-Cdk4/6 phosphorylates the carboxy-terminal domain of the retinoblastoma protein (pRb), and subsequently cause its inactivation by blocking binding of histone deacetylase [Harbour et al., 1999]. The transcriptional repressor complex includes E2F transcriptional factor, pRb, and chromatin remodelling enzymes such as histone deacetylase (HDAC) and the Swi/Snf complex (figure 1.15) [Danen and Yamada, 2001]. The progressively increasing phosphorylation and inactivation of pRb, in turn results in the expression of E2F transcriptional factor-regulated genes, including cyclin E and A [DeGregori et al., 1995]. This positive feedback loop lasts until phosphorylation of pRb is completed and cyclin A associated cdk activity starts to inhibit E2F function. After this stage, cell cycle continues to S phase without the effect of mitogens [Danen and Yamada, 2001]. Cyclin D-Cdk4/6 complex also sequester Cip/Kip family Cdk inhibitors (CDKI), $p21^{cip1}$ and $p27^{kip1}$, thereby contributing to the activation of cyclin E-Cdk2 (figure 1.15) [Sherr and Roberts, 1999, Danen and Yamada, 2001] . The other class of CDKI includes the INK4 proteins (inhibitors of CDK4), so named for their ability to specifically inhibit the catalytic subunits of CDK4 and CDK6. Four members of INK4 family $p16^{INK4a}$, $p15^{INK4b}$, $p18^{INK4c}$, and $p19^{INK4d}$ bind only to CDK4 and CDK6 but not to other CDKs or to D-type cyclins [Sherr and Roberts, 1999].

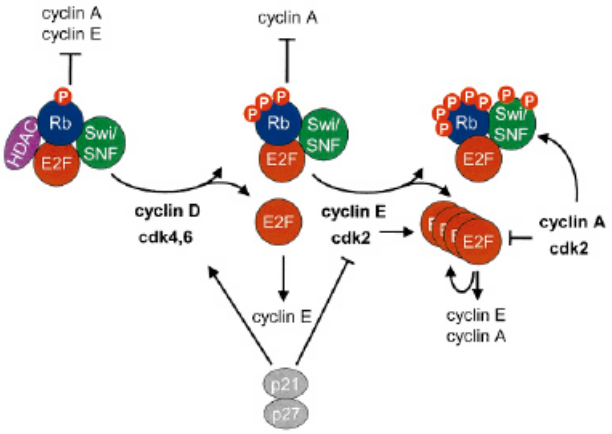

Fig. 1.15: G1 cell cycle progression adapted from Danen and Yamada, 2001

1.5.1.1 Rho GTPases in G1 phase progression

Rho family GTPases can regulate the mitogenic pathways that control G1- phase cell cycle progresion. Rac and Cdc42 stimulate cyclin D expression when ectopically expressed in various cells, and in one report it has been shown to be mediated by NFκB. Interestingly, induction of cyclin D1 by Rac and/or Cdc42 is shown to be an ERK-independent event [Westwick et al., 1997, Joyce et al., 1999, Welsh et al., 2001]. Rac/Cdc42-dependent induction of cyclin D1 requires RTK and integrin signaling, but it is independent of stress fiber formation. In fact, if cyclin D1 is induced by Rac/Cdc42, then all of G1 phase progression in fibroblasts can occur in the absence of stress fibers and the consequent imposition of cellular tension [Roovers and Assoian, 2003]. Rac/Cdc42 signaling also results in an early G1 phase induction of cyclin D1 (3 hr after mitogenic stimulation of quiescent cells), and this premature induction leads to a correspondingly early activation of cdk4 and cdk2, as well as a several hours decrease in the duration of G1 phase as cells leave quiescence. In normal cells, the function of Rac/ Cdc42 to activate Cyclin D prematurely is inhibited by Rho and additionally, Rho promotes sustained activation of ERK, both of which are crucial for correct temporal control of Cyclin D levels (figure 1.16) [Welsh et al., 2001, Roovers and Assoian, 2003]. Rho GTPases also regulate the levels of $p21^{cip1}$

and $p27^{kip1}$. There are couple of studies showing that activated Ras is unable to stimulate G1 progression in the absense of Rho since Ras promotes the accumulation of high levels of $p21^{cip1}$ and Rho causes the attenuation either by inhibition of $p21^{cip1}$ transcription or possibly protein degradation [Weber et al., 1997, Olson et al., 1998]. Rho regulation of $p27^{kip1}$ is post-transcriptional, although there are examples of it acting through protein degradation or mRNA translation (figure1.17) [Jaffe and Hall, 2005].

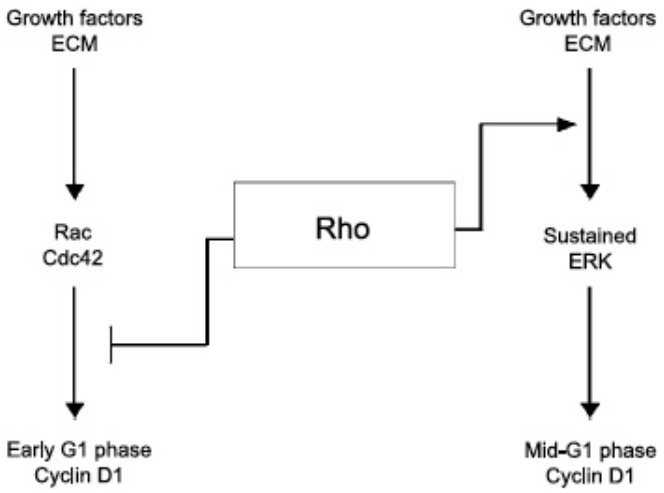

Fig. 1.16: Central role of Rho in regulating the timing of cyclin D expression during G1 phase
adapted from Welsh, 2004

1.5.1.2 The role of LIMK1 in G1 phase progression

LIMK1 is the effector of Rho, which causes sustained ERK activity and prevents early Rac/Cdc42 signaling to Cyclin D (figure1.17). Downstream effectors of Rho, ROCK, and LIMK1 as well as induction of stress fibers, maintain sustained ERK activity. Additionally, nuclear translocation of LIMK1 suppresses the Rac/Cdc42-dependent premature cyclin D activation. This function of LIMK1 is independent of its regulation role of actin polymerization [Roovers and Assoian, 2003]. Although LIMK1 has been reported to be cytoplasmic, its translocation to nucleus has been reported upon binding to $p57^{kip2}$ in cotransfection studies. Additionally, $p57^{kip2}$ inhibits the activ-

ity of LIMK1 indirectly, as coexpression of $p57^{kip2}$ and LIMK1 inhibits the formation of thick bundled actin fibers which is a phenotype in LIMK1 overexpressed cells. [Yokoo et al., 2003, Denicourt and Dowdy, 2004].

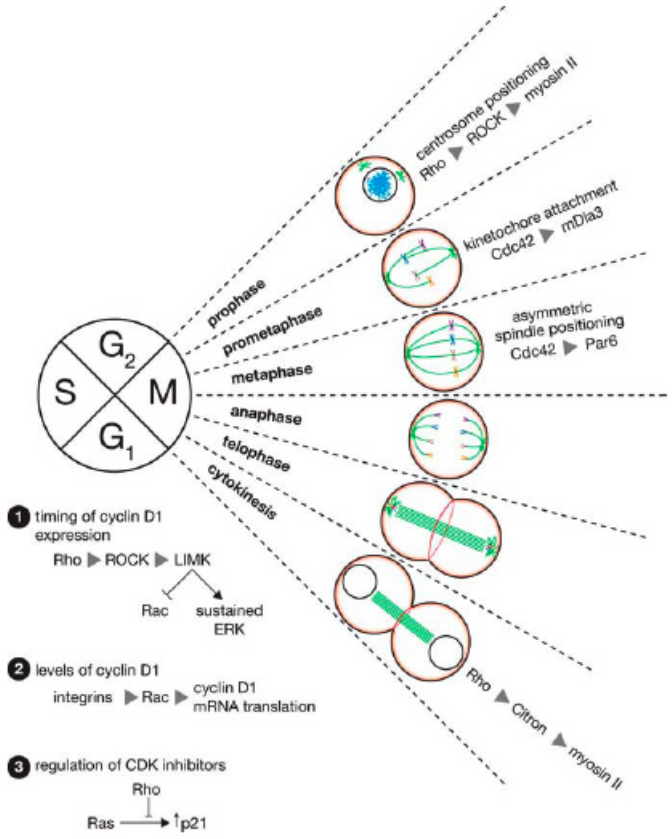

Fig. 1.17: Rho GTPases in cell cycle adapted from Jaffe and Hall, 2005

1.5.2 Mitosis

Mitosis is a eukaryotic process in which the replicated genome of a somatic cell distributed equally into two daughter cells. M phase is comprised of mitosis and cytokinesis (cytoplasmic division). Mitotic events are subdivided into five phases: prophase, prometaphase, metaphase, anaphase, and telophase. Cytokinesis (cell cleavage) occurs at the end of mitosis and its regulation is linked to mitotic progression. In most of animals and plants open mitosis occurs, in which

prophase ends with nuclear envelope breakdown, before chromosome segregation.

Mitosis is a highly integrated process which involves both assembly/disassembly of microtubules for chromosome movement by forming mitotic spindle and the dynamic reorganization of actin filaments for cell cleavage [Wittmann et al., 2001, Glotzer, 2001]. Rho GTPases influence the organization of microtubule and actin cytoskeleton during M phase (figure1.17) [Narumiya et al., 2004, Jaffe and Hall, 2005, Narumiya and Yasuda, 2006]. Additionally, LIMK1 and SSH1 cell-cycle dependent activation and inactivation,respectively, regulates cofilin activity during mitosis progression [Sumi et al., 2002, Amano et al., 2002, Kaji et al., 2003, Sumi et al., 2006]. The stages of mitosis and the functions of Rho GTPases, LIMK1 and cofilin in every stage of mitosis are as follows:

1.5.2.1 Prophase

Introduction

Prophase is the transition stage from G2 into mitosis. For cells to enter mitosis activation of cyclin B1-Cdk1 is needed. During G2 phase cyclin B1-Cdk1 is kept inactive by phosphorylation of their ATP-binding sites (threonine 14 and tyrosine 15) by the kinases Wee1 in nucleus and Myt1 in the cytoplasm, and accumulation of Cyclin B1-Cdk1 in the cytoplasm. When cells enter mitosis, before nuclear envelope breakdown, Cyclin B1-Cdk1 accumulates in the nucleus as a result of phosphorylation of the cytoplasmic retension signal of Cyclin B1 by polo-like kinase or by autophosphorylation [Toyoshima-Morimoto et al., 2001, Hagting et al., 1999]. In addition to Cyclin B1 phosphorylation Cdk1 needs to be phosphorylated by Cyclin activating kinase (CAK) on threonine 161 and its activity should be regulated by the balance between the inhibitory kinases Wee1 and Myt1 and activating phosphatase Cdc25. These enzymes are controlled by DNA structure checkpoint, which delays mitosis in the presence of unreplicated or damaged DNA

[Taylor and Stark, 2001].

Main events in prophase nuclei are chromatin condensation and nuclear envelope breakdown. Chromatin condensation reduce the length of uncondensed DNA, and it requires the combined action of multi-subunit protein complex which are composed of condensin and topoisomerase II [Swedlow and Hirano, 2003]. Two subunits of cohesin are phosphorylated by Cyclin B1- Cdk1, which in turn results in their entry into the nucleus and association with chromatin as cells enter to prophase. The onset of condensation correlates with phosphorylation of histone H1 by Cyclin B1-Cdk1 and H3 by Aurora B protein kinases. It is suggested that histone phosphorylation that leads to chromatin unfolding, permits binding of other factors such as condensin complex for condensation of chromosomes. Topoisomerase II is required for condensation as an element of the chromosome scaffold. Nuclear envelope breakdown is facilitated by phosphorylation of nuclear lamins by cyclin B1- Cdk1 which ensures at the time of transition to prometaphase. Nuclear envelope components are dispersed in the cytoplasm from prometaphase until telophase [S, 2006]. Apart from nuclear changes there are also cytoplasmic changes in prophase. Firstly, duplicated centrosomes in S phase are separated shortly before nuclear envelope breakdown. In centrosome maturation polo-like kinase plays a role. At an early stage of separation NIMA - family member Nek2 and in later stage kinesin-related motor proteins (KRPs) and cytoplasmic dynein are required for centrosome separation [Nigg, 2001].

Role of Rho GTPases in prophase

During prophase , there is a change of microtubules from extensive network throughout the cytoplasm to dense, radial arrays of short, dynamic microtubules around each of the centrosome. The microtubules that emanate from centrosomes and organize into radial arrays around it are called astral microtubules. Astral microtubules interact with cell cortex and their major role is to align the spindle along an axis perpendicular to the future cell division plane. It has been recently

shown that actin:myosin filaments, under the control of Rho downstream effector ROCK, are required at the cortex to allow positioning of the centrosome (figure 1.17) [Rosenblatt et al., 2004].

1.5.2.2 Prometaphase

Prometaphase begins with the nuclear envelope breakdown in cells having open mitosis. At this point, microtubules growing outward from the spindle pole, spindle microtubules, enter the nucleus, make contact with the chromosomes, and attach to them at specialized structures called kinetochores. Interaction between the kinetochores of paired sister chromatids (duplicated chromosomes), with the two opposite poles of the spindle results in alignment of the chromosomes in a group midway between the poles (figure1.17).

Role of Rho GTPases in prometaphase

The Rho-GTPases showed activation in different stages of mitosis: Active form of Cdc42 (GTP-bound form) has a peak in metaphase, while GTP-Rho increases in anaphase and reaches a peak during telophase. However, GTP-Rac levels doesn't change during mitosis [Rosenblatt et al., 2004].

Recently, it has been reported that Cdc42 is involved in prometaphase progression. Indeed, treatment of HeLa cells with *Clostridium difficile* toxin B., which specifically inactivates Rho GTPases, delays the progression of mitosis in prometaphase and expression of Cdc42 mutants but not those of Rac1 or RhoA mimics this phenotype. In these cells, spindle MTs fail to bind to chromosomes in the correct bipolar manner, and later on chromosomes fail to congress at the metaphase plate. These findings suggest that Cdc42 plays an important role in regulating the attachment of spindle microtubules (MT) to the kinetochore. Additionally, the role of Cdc42 includes the Cdc42 effector mDia3. mDia3 binds both to GTP-bind active form of Cdc42 and to a kinetochore protein CENP-A. Depletion of mDia3 by siRNA causes mitotic arrest similar to the treatment of toxin B. The prometaphase arrested cells, many chromosomes are clustered in ei-

ther pole in spite of apparently normal shape of the spindle (figure1.17) [Yasuda et al., 2004]. The Cdc42- positive regulator Ect2 (GEF) and negative MgcRacGAP (GAP) have been shown to control Cdc42's function in bipolar spindle assembly during prometaphase [Tatsumoto et al., 2003, Oceguera-Yanez et al., 2005].

Role of LIMK1 in prometaphase

LIMK1 shows a mitosis-specific hyperphosphorylation and activation during prometaphase and metaphase stages of mitosis and this leads to subsequent cofilin phosphorylation during these stages [Sumi et al., 2002, Amano et al., 2002]. The hyperphosphorylation is monitored in mitotic cell population after treatment of nocodazole (microtubule destabilizing agent) or with taxol (microtubule-stabilizing agent), both of which leads to block of cells in prometaphase. Although nocodazole causes the spindle assembly checkpoint activation, the phosphorylation of LIMK1 is not a result of checkpoint activation since synchronized HeLa cells in G1/S by thymidine block release causes a mitotic mobility shift after 10 hours of release (the time where most of the cells are in mitosis). Also, it is indicated that LIMK1 phosphorylation is not Rho GTPase dependent, as its phosphorylation is not affected by Rho GTPase inhibitors, while CDK inhibitor roscovitine abolishes the phosphorylation and activation of LIMK1. Additionally, in order for mitosis-dependent phosphorylation of LIMK1 to occur, N-terminal part of LIMK1 is necessary since expression of only kinase domain doesn't show the mitotic mobility shift of the protein upon nocodazole treatment. Recent study claimed that despite the localization of LIMK1 to cell-cell adhesion sites during interphase and prophase, it is concentrated to spindle poles during prometaphase and metaphase, despite no role for LIMK1 is found in these stages. Although, LIMK2 is concentrated to centrosome during prophase and prometaphase, it is localized to mitotic spindles along with spindle microtubules during metaphase and early anaphase [Sumi et al., 2006]. Interestingly, SSH1L, the phosphatase for LIMK1 and cofilin shows a decreased activation during prometaphase and metaphase when LIMK1 is highly active and shows an elevated activation in

telophase and cytokinesis when LIMK1 has a lower activity [Kaji et al., 2003].

1.5.2.3 Metaphase

Introduction

When all chromosomes bind to spindle microtubules, have attained bipolar orientation, and position midway between two spindle poles, it is called to be in metaphase. In this stage, chromosomes are grouped at the middle of the spindle to create metaphase plate. As the process to generate metaphase plate is random, it is highly regulated by a surveillance mechanism known as spindle assembly checkpoint (metaphase checkpoint), which senses the lack of attachment and/or tension at kinetochores and in response inhibits chromosome segregation by causing a delay into anaphase [Bharadwaj and Yu, 2004].

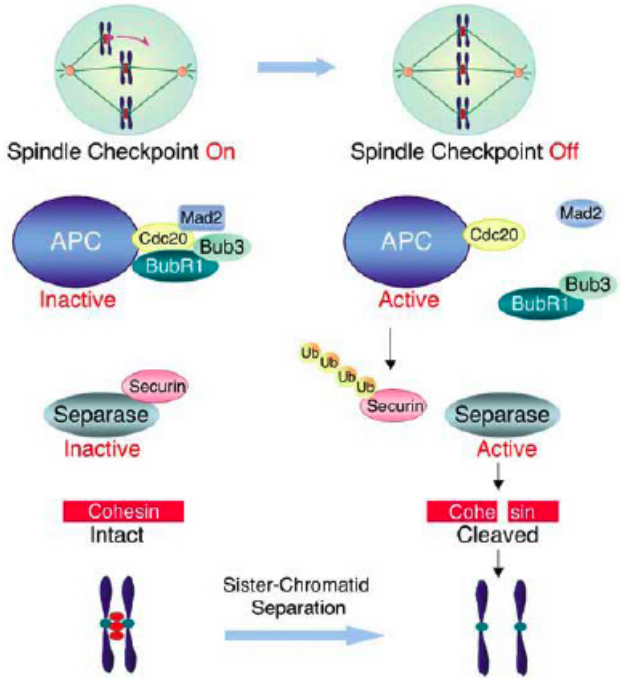

Fig. 1.18: Molecular mechanism of chromosome segregation adapted from Bharadwaj and Yu, 2004

The well characterized components of spindle assembly checkpoint kinases are Mad1, Mad2, Mad3 (BubR1), Bub1, Bub3 and Mps1. When Bub1p (budding uninhibited by benzimidazole) and BubR1 (Bub-related kinase-1) genes are mutated in yeast, cells continue to divide even when spindle is destroyed by drugs like benzimidazole or nocodazole. BubR1 is located in outer plate of the kinetochore, where it interacts with kinesin motor protein CENP-E. BubR1 kinase activity is necessary for recruitment of CENP-E to kinetochores. BUB kinases regulates Mad1 which, in turn, activates Mad2. Activated Mad2 inhibits the onset of anaphase by interacting with Cdc20, which is a substrate recognition subunit of APC/C (anaphase promoting complex/cyclosome) E3 ubiquitin-protein ligase. When the last chromosome achieved bipolar attachment to the spindle, inhibitory effect of Mad2 is extinguished and APC/C becomes active.

Before anaphase starts, sister chromatids are kept together with a protein complex called cohesin, and onset of anaphase is triggered by the proteolysis of cohesin subunit , Scc1, by a protease called separase. Normally, separase is kept inactive by an associated inhibitor securin. After attachment is properly done and APC/C becomes active, it degrades securin, which, in turn, results in activation of separase, cleavage of Scc1, chromosome cohesion, and finally the onset of anaphase (figure 1.18) [Cerutti and Simanis, 2000, Peters, 2002, Bharadwaj and Yu, 2004]. Importantly, the first wave of cohesin removal depends on phosphorylation of cohesin mainly by Cdk1 and as a second step the small amount of cohesin remaining at centromeres (a region of eukaryotic chromosome that is attached to the mitotic spindle) is removed in metaphase-anaphase transition by APC/C dependent manner [Nigg, 2001].

Role of Rho GTPases in metaphase

During metaphase, in order to have two equal daughter cells after cell division, spindles position symmetrically, except in development and in adult cases like stem cell division. For asymmetric cell division Par proteins (Par1/6) and atypical protein kinase C (aPKC) are crucial. They

distribute asymmetrically with Par6/aPKC/Par3 at the anterior and Par1/Par2 at the posterior and they determine the positioning of the spindle. Cdc42 causes a conformational change in Par6 and can activate aPKC, so that can influence the asymmetric cell division (figure1.17) [Jaffe and Hall, 2005]. Although LIMK1 is hyperphosphorylated and activated in metaphase, no mitosis specific targets of LIMK1 have been determined during this phase.

1.5.2.4 Anaphase and Telophase

Introduction

Anaphase is the stage in mitosis which begins shortly after all chromosomes have undergone proper bipolar attachment to the spindle. During anaphase, sister chromatids start to separate which results from sister chromatid cohesion. After separation of sister chromatids, chromosome movement is occured in two steps: Anaphase A, in which sister chromatids move to opposite spindle poles and Anaphase B, in which the poles move apart. Anaphase A is dependent on shortening of the kinetechore microtubules that link centromeres to spindle poles. Anaphase B involves pushing forces generated at the spindle midzone through motor proteins that cause sliding of interdigitating microtubules emanating from the opposite spindle poles. The central spindle which is highly organized interpolar microtubules between chromatids, are the elongated spindles in anaphase. The main driving force for cell cycle progression is cyclin- Cdks. The high levels of cyclin B- Cdk1 activity which is needed for mitotic progression decreases after the degradation of Cyclin B by APC/C complex in anaphase and this set the stage for mitotic exit and cytokinesis [de Gramont and Cohen-Fix, 2005]. Once the chromosomes arrive at the pole, nuclear envelope reforms around the daughter chromosomes and chromatin decondensation begins. Lamin subunits disassembled in prophase are recycled to reform the nuclear envelope at the end of mitosis [Nigg, 2001].

Role of Rho GTPases in anaphase

During anaphase, active form of Rho (GTP-Rho) levels increase and it makes a peak at telophase [Oceguera-Yanez et al., 2005]. Although LIMK1 localized to spindle poles during prometaphase and metaphase, during Anaphase B, when spindles have elongated and cells become more cylindrical, LIMK1 disappeared from these regions. Besides, LIMK2 spindle staining became weaker as cells processed through late anaphase and telophase, and LIMK2 localized to spindle midzone where it colocalized with midzone microtubules. Additionally higher activity of LIMK1 in prometaphase and metaphase returned to its basal levels in late anaphase, telophase and cytokinesis, while SSH-1L phosphatase activity is elevated in these stages [Amano et al., 2002, Sumi et al., 2006, Kaji et al., 2003].

1.5.2.5 Cytokinesis

Introduction

Cytokinesis is the process by which cell divides into two daughter cells after nuclear division. There are four morphological stages of cytokinesis: **Division site positioning or specification** in which the cell chooses the site of division ; **cleavage furrow formation and ingression** which is characterized by protein recruitment to the site of cell division; **midbody formation** which introduces membrane barriers separating the cytoplasm of the daughter cells.; and **cell separation** which seals the membrane compartments forming two new cells in the process of completion or abscission [Straight and Field, 2000, Glotzer, 2001].

In a dividing cell, after anaphase starts, an actomyosin contractile ring is formed. Contractile ring is a transient array of actin filaments attached to the plasma membrane. The interaction of these actin filaments with myosin II causes a cortical tension gradient in which the peak of tension occurs at the equator and lowest tension occurs at the cell poles which forms a cleav-

age furrow (figure 1.19). The position of the furrow is determined by the position of the mitotic spindle and its interaction with cortex during anaphase. The furrow ingression continues until it comes into contact with and compresses the microtubule bundles that make up the central spindle. Furrow ingression is often accompanied by the fusion of golgi-derived membrane vesicles with the ingressing plasma membrane. This new membrane may be required to provide the necessary surface area for the plasma membrane to surround the two daughter cells [Robinson and Spudich, 2000, Straight and Field, 2000] . For a proper furrow ingression and completion CHO1/MKLP1 class of kinesins are necessary in order to stabilize the microtubule bundles. At a late stage of cytokinesis, a narrow neck called the midbody connects the two daughter cells. Bundled microtubules derived from the central spindle are prominent component of the midbody. The midbody stage is ultimately resolved and the two cells separate; this process is also called abscission. In order for cytokinesis completion to occur, action of Aurora B kinase and its targeting factor INCENP is essential. A role for Aurora B in cytokinesis is supported by the finding that overexpression of a catalytically inactive form of Aurora-B disrupts cleavage furrow formation in mammalian cells [Terada et al., 1998].

Role of Rho GTPases in cytokinesis

Actin filament dynamics and reorganization is important in cytokinesis in animal cells. RhoA is localized to cleavage furrow and depletion of RhoA by RNAi or inhibition by Rho-specific inhibitor C3 completely blocks furrow ingression. RhoA is required both for accumulation of cortical actin during assembly and for the actomyosin contractility of the furrow. Since active RhoA is needed in furrow assembly and contractility, RhoA GEF (Pebble in *Drosophila* and ECT2 in humans) which mediate the activation of RhoA, is also required for normal cleavage furrow assembly and ingression. Upon onset of anaphase, ECT2 is dephosphorylated, which allows it to bind to the central spindle component CYK-4. This complex results in activation of RhoA and its accumulation at the furrow. Interestingly, a Rho GTPase family GAP, MgcRacGAP has also a

conserved role in cytokinesis. Disruption of MgcRacGAP causes failure of cytokinesis, leading to multinucleate cells. The phosphorylation of Mgc and its conversion to a GAP for Rho is done by association with Aurora B (figure 1.19) [Glotzer, 2001, Jaffe and Hall, 2005, Piekny et al., 2005].

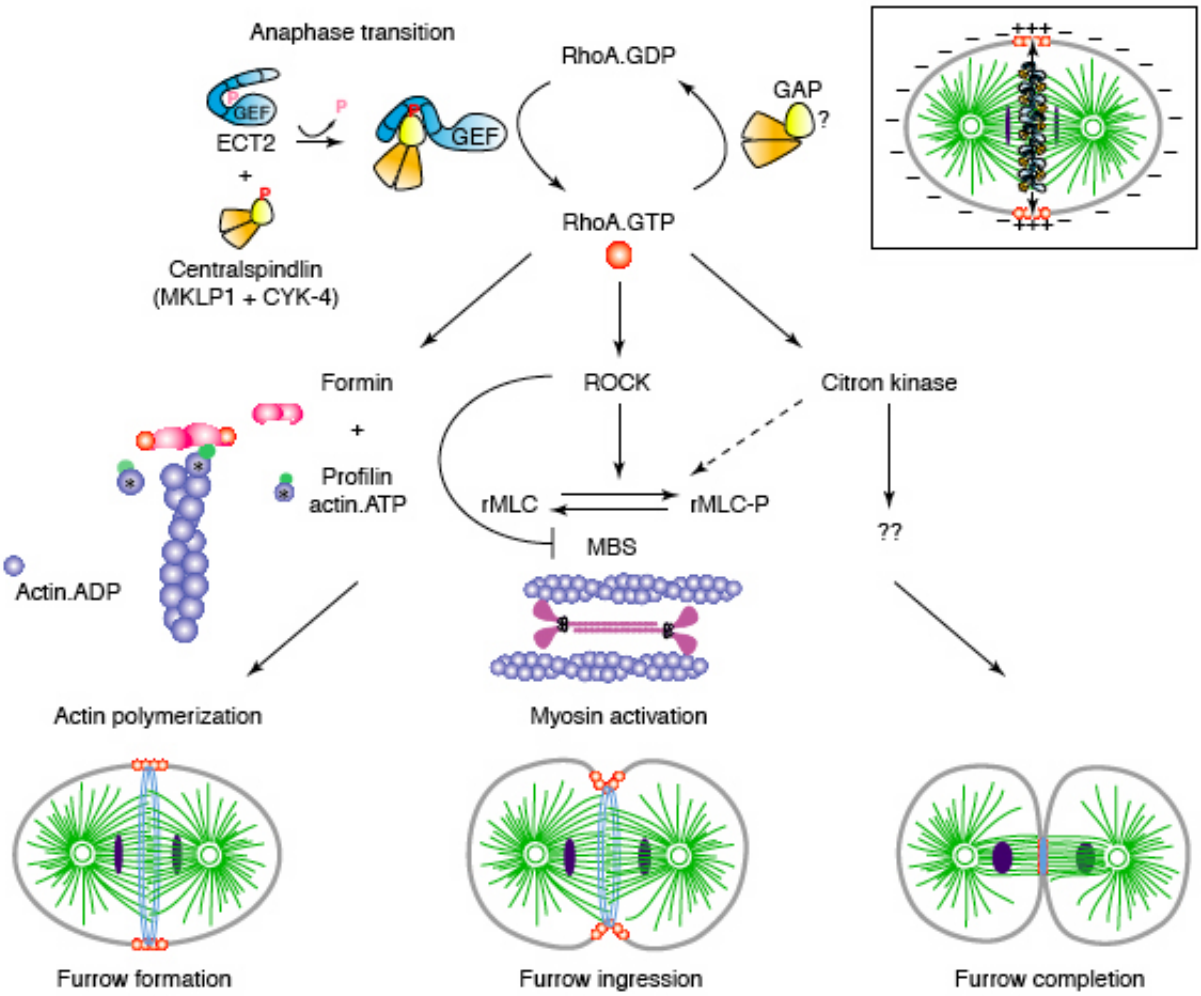

Fig. 1.19: The role of RhoA in cytokinesis adapted from Piekny et al., 2005

RhoA plays a crucial role in contractile ring function and localizes to cleavage furrow along with its effectors, ROCK, citron kinase, mDia (formin family member). Most of the actin filaments in cleavage furrow are pre-existing filaments, but since mDia is localized there, it promotes actin polymerization necessary for the formation of contractile ring. Formin binds to profilin and actin. By promoting the association of two actin monomers and creating a binding site for third

monomer, formin promote *de novo* nucleation of actin filaments. The other effectors of RhoA, citron kinase and ROCK causes the activation of myosin II by affecting its regulatory light chain (rMLC). Myosin II is a hexamer with pairs of heavy chains, essential light chains and regulatory light chains (rMLC). The activation of myosin drives the contraction of the actin filament ring. Citron kinases directly phosphorylates MLC at Thr 18 and Ser 19 sites, whereas ROCK affects Ser19 site directly and affecting both of the sites indirectly through phosphorylation and inhibition of MLC phosphatase. *C.elegans* cells depleted of ROCK activity form cleavage furrow, but their ingression is delayed or fails. Citron kinase is also required for late stages of cytokinesis. It is required for stably maintaining the ring components actin and anilin at the midbody [Piekny et al., 2005].

In addition to the function of RhoA in cytokinesis, actin depolymerizing factor cofilin is also involved during cytokinesis. Cofilin/ADF is concentrated at the cleavage furrow and at the midbody during cytokinesis of cultured mammalian cells and cleavage of *Xenopus* fertilized eggs [Nagaoka et al., 1995, Abe et al., 1996]. Decreases in cofilin expression or activity by gene mutation, RNAi, or antibody injection causes frequent failures in cytokinesis. Injection of antibody that inhibits the activity of cofilin/ADF into *Xenopus* blastomeres blocks the cleavage of blastomeres [Abe et al., 1996]. Additionally, *Drosophila twinstar* (cofilin ortholog in flies) mutants exhibit frequent failure in cytokinesis in larval neuroblasts and in testicular meiotic cells [Gunsalus et al., 1995]. Furthermore, injection of nonphosphorylatable form of cofilin blocks cytokinesis, whereas injection of wild-type cofilin with phosphorylation possibility doesn't have any effect [Nagaoka et al., 1995]. This data, suggest that cofilin should be regulated during cytokinesis.

LIMK1 and cytokinesis

Cofilin is highly phosphorylated in early stages of mitosis and it is dephosphorylated and active

during cytokinesis which is parallel to LIMK1 activity. Despite the high activity of LIMK1 during early stages, its activity decreased during cytokinesis. Ectopic overexpression of LIMK1 causes failure in cytokinesis and multinucleated cell formation [Amano et al., 2002].

Recently it has been shown that a negative regulation of LIMK1 during cytokinesis is achieved by a tumor suppressor protein called LATS1. Lats gene is first identified as a tumor suppressor in *Drosophila* as homozygous loss of lats in *Drosophila* leads to defects in morphogenesis and extensive outgrowth [Xu et al., 1995, Justice et al., 1995]. There are two mouse (Lats1 and Lats2) and two human (LATS1 and LATS2) homologues of *Drosophila* lats [Tao et al., 1999, St John et al., 1999, Yabuta et al., 2000]. Mice deficient for Lats1 develop soft-tissue sarcomas, ovarian tumours and pituitary dysfunction [St John et al., 1999]. Moreover, the human LATS1 gene is inactivated in human sarcomas and suppresses tumour growth when overexpressed in human cancer cells, suggesting that LATS1 might be a tumour suppressor in humans [Yang et al., 2001, Hisaoka et al., 2002, Xia et al., 2002]. However, how LATS1 functions as a tumour suppressor remains to be elucidated.

Human LATS1 has been shown to bind to LIM domains of LIMK1 in vitro and in vivo and colocalizes with LIMK1 at the actomyosin contractile ring during cytokinesis. LATS1 inhibits LIMK1 kinase activity towards cofilin and also LIMK1-induced cytokinesis defects. When LATS1 is inactivated by RNAi, antibody microinjection or in knockout mice, there is a failure in cytokinesis and subsequently multinucleated cells form. All these findings indicate that LATS1 is a negative regulator of LIMK1 activity during cytokinesis [Yang et al., 2004b]. The localization of LIMK1 to contractile ring suggests a role of LIMK1 during cytokinesis and maybe this activity is regulated by LATS1[Sumi et al., 2006].

On contrary to inactive LIMK1 during cytokinesis, two cofilin phosphatases Chronophin (CIN) and slingshot (SSH) are active during this stage. The effect of CIN on cell division has been

suggested as the overexpression of dominant negative forms of CIN (or downregulation by CIN siRNA treatment) causes aberrant actin assembly, frequent cleavage furrow regression, and a significant population of multinucleated cells, correlating with changes in phosphocofilin levels. Additionally, the colocalization of CIN with cofilin to the ingressing cleavage furrow and to the actomyosin contractile ring at later mitotic stages also supports the observation that CIN function is critical during cell division. Interestingly, CIN appeared to localize to membranous regions at the cell poles during telophase, and seemed to have a more cytoplasmic distribution with limited localization to the cleavage furrow at earlier stages of mitosis. This differs from SSH, which strongly localizes to the ingressing furrow at early telophase, suggesting that these two cofilin phosphatases may play distinct regulatory roles during cell division [Gohla et al., 2005].

1.6 LIMK1 and cancer metastasis

Tumor metastasis is a critical event for cancer patients because it often results in death. Invasion and metastasis are multistep processes that require the coordinated expression of a number of proteins by the tumor cells resulting in altered cell-cell and cell-substratum adhesion. During progression of tumor cells to a metastatic phenotype, they undergo a series of changes that begin with loss of contact inhibition and increased motility, which allows primary tumors to invade distant organs and induce neo-vascularization, resulting in metastasis [Chambers et al., 2002]. Many of these changes are associated with dynamic actin reorganization and activation of signaling pathways including receptor tyrosine kinases [Vivanco and Sawyers, 2002], G-protein coupled receptors [Seasholtz et al., 1999], chemokine receptors [Muller et al., 2001], and transforming growth factor- β receptor [Oft et al., 1998]. These changes are crucial for cell morphogenesis, motility, adhesion and cytokinesis.

Rho GTPases were shown to be involved in metastatic pathway, especially in breast cancer invasion[Fritz et al., 1999]. RhoA and the related RhoC are expressed at relatively high levels in metastatic tumors and their expression levels are positively correlated with the stage of tumors [Fritz et al., 1999, Clark et al., 2000]. In a tumor , RhoA is overexpressed and subsequently translocate from cytoplasm to the cell membrane where it activates actomyosin system, followed by cellular invasion *in vivo* and *in vitro* [Yoshioka et al., 1999]. The Rho effector ROCK has been shown to be involved in cancer invasion in prostate cancer where inhibition of ROCK reduced progression of this cancer. Additionally, the intraperitoneal implantation of active RhoA expressing rat hepatoma cells are highly invasive [Itoh et al., 1999, Somlyo et al., 2000]. Finally, Rac mediates prostate cancer invasion in epidermal growth factor (EGF) or neuronal growth factor (NGF) induced cells [Malliri et al., 1998]. All these reports suggests that, Rho GTPases are highly regulated in normal cells and their misregulation in cancer cells results in invasion.

Like Rho GTPases, LIMK1 level of expression, also correlates with tumor cell motility. The invasiveness of breast cancer cells with wild type LIMK1 shows high number of osteolytic lesions, which is a marker for tumor cell invasion as during osteolytic lesions, a number of cytokines are secreted and stimulate osteoclast activity and this process requires the invasion of tumor cells to bone marrow. Also, LIMK1 was shown to be expressed in high levels in different human tumors such as, melanoma, ovarian carcinoma, lung, breast, and prostate, all of which are highly invasive [Yoshioka et al., 2003]. Furthermore the upregulation of LIMK1 expression level and activity was shown in adenocarcinomatous prostatic epithelium and prostate cancer cell line, and in prostate cancer cells and tissues. The invasiveness of a tumor correlates with the degree of LIMK1 expression. When LIMK1 is partially reduced in PC3 (highly metastatic) prostate cancer cells, a G2/M arrest was seen. However, it is not clear whether reduced concentration of LIMK1 induces an increased activity of cofilin due to nonphosphorylation since no alteration in phospho-cofilin concentration was noted in these cells [Davila et al., 2003].

In addition to cytoskeleton reorganization, tumor progression requires degradation of extracellular matrix by the serine protease urokinase- type plasminogen activator (uPA). The role of uPA is to convert inactive plasminogen into plasmin and initiate the proteolytic cascade that ends with degradation of extracellular matrix [Blasi and Carmeliet, 2002]. uPA is found to be in leading edge of cancer cells which are migrating. uPA receptor (uPAR) binds to uPA and facilitates proteolytic cascade in a cell and also interacts with integrins, and initiates signaling events that alter cell adhesion, migration and proliferation [Ossowski and Aguirre-Ghiso, 2000]. Furthermore increased levels of uPA/uPAR are associated with poor prognosis [Stephens et al., 1999]. uPA system also has been implicated in the pathologic angiogenesis of a variety of tumors [Carmeliet and Jain, 2000]. LIMK1 overexpression in breast cancer cells has been shown to upregulate uPA system, to increase uPA promoter activity, to induce uPA and uPAR mRNA and protein expression, and to induce uPA secretion, which is important in invasion. When dominant-negative form of LIMK1 is expressed in same cells, these phenotypic changes are detected. Also,

inhibition of uPA or uPAR by blocking antibodies suppressed LIMK1-induced cell invasiveness.

Coordinately overexpression of LIMK1 and uPAR in breast cancer cells increased tumor growth in female atymic nude mice, promoted tumor angiogenesis and induced metastasis to lung and liver [Bagheri-Yarmand et al., 2006]. Angiogenesis is the formation of new blood capillaries from existing vessels. It is a physiological mechanism for providing oxygen and other nutrients to starved tissue and participates to development and wound healing. Also it contributes to disease progression including cancer and metastasis [Folkman and Shing, 1992]. The angiogenic growth factor VEGF enhances endothelial cell migration, proliferation and tubule formation. Actin reorganization is an important component of VEGF-induced migration. It has been found that VEGF induced LIMK1 phosphorylation and subsequently cofilin phosphorylation and inactivation, and this process is PI3K and ROCK related [Gong et al., 2004]. Later on it has been reported that activation of VEGF receptor activates MAPK kinases that activate p38 MAPK and subsequently MAPK-activated protein kinase-2 (MK2). MK2 leads to phosphorylation of two proteins: Heat shock protein 27 (Hsp27) and LIMK1. Hsp27 behaves as an actin filament cap-binding protein and, in its non-phosphorylated form inhibits actin polymerization. MK2-catalyzed phosphorylation of Hsp27 leads to its release from capped actin filaments, thereby stimulating actin polymerization and subsequent stress fiber formation. The phosphorylation of LIMK1 is directly through p38 MAPK and MK2. Although the first (p38 MAPK) doesn't cause any activation of LIMK1, the latter one (MK2) phosphorylates Ser 323 and this increases the activity of LIMK1 and VEGF-induced stress fiber formation, cell migration and tubule formation. Interestingly, LIMK1 activation is T508 independent (figure1.20) [Kobayashi et al., 2006].

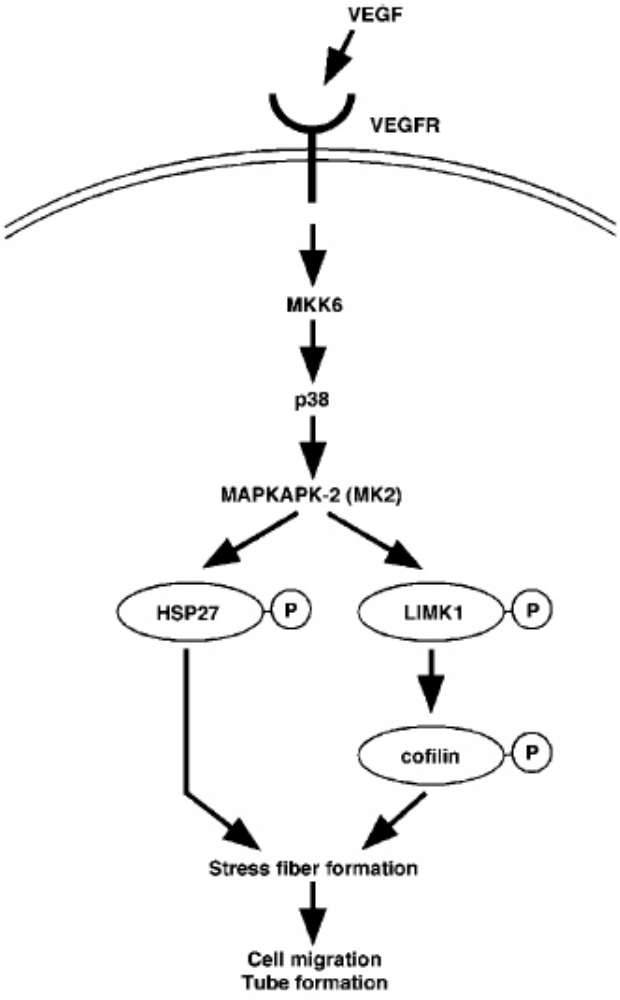

Fig. 1.20: VEGF-induced LIMK1 activation adapted from Kobayashi et al., 2006

1.7 LIMK1 and neuronal differentiation

The diverse functions of vertebrate nervous system are achieved by precise targeting of neurons to the site where they will innervate. Neurons are highly polarized cells composed of four distinct regions with differing functions: the cell body, the dendrites, the axon, and the axon terminals. The cell body contains the nucleus and is the site of synthesis of virtually all neuronal proteins and membranes. Most neurons have multiple dendrites, which extend out-ward from the cell body and are specialized to receive chemical signals from the axon termini of other neurons. Axon terminals is the part where the signal from one neuron to the other is transmitted. These interconnection between neurons are called neural circuit which are composed of synapses that are created during embryonic and postnatal development. In order for a neuron to have proper neural circuit it exhibits many morphological and functional changes. This phenomenon is named as neuronal differentiation, which consists of several processes, that is, neuritogenesis, neurite outgrowth, pathfinding, targeting and synaptogenesis. These processes are mediated by reorganization of F-actin and microtubule which are the main parts of cytoskeletal architecture [Tojima and Ito, 2004]. Neuritogenesis (figure 1.21 (A:2)), which is the neurite sprouting from the soma, occurs at the thin, actin rich protrusions surrounding the soma. The other differentiation processes; neurite outgrowth, pathfinding and targeting (figure 1.21 (A:3-4)) are driven by growth cone, which is a specialized, actin-rich, highly motile nerve-ending structure. Growth cones determine the rate and direction of neurite outgrowth. Their high motility and their ability to reorganize rapidly in response to extracellular cues enable them to guide the neuron to its final destination. Growth cone is comprised of two domains: the central domain (C-domain) contains bundled microtubules and organelles, and the peripheral domain (P-domain) consisting of actin filaments that form both a meshwork in lamellipodia and filopodia. Filipodia are essential for sensing guidance cues and steering the growth cone [Kalil and Dent, 2005, Sarmiere and Bamburg, 2004]. Exposure to repulsive cues causes the collapse of lamellipodia and retraction of filopodia, and opposite to that, extension of lamellipodia and filopodia occurs upon attractive cues. The motil-

ity of growth cones is dependent on the assembly, disassembly and retrograde flow of an organized array of F-actin at the leading edge. This three processes rely on the coupling of actin cytoskeleton to external substrates. This coupling may be achieved by the help of the cell adhesion molecules (integrins, cadherins) that provides the force for forward movement of the growth cone [Gungabissoon and Bamburg, 2003].

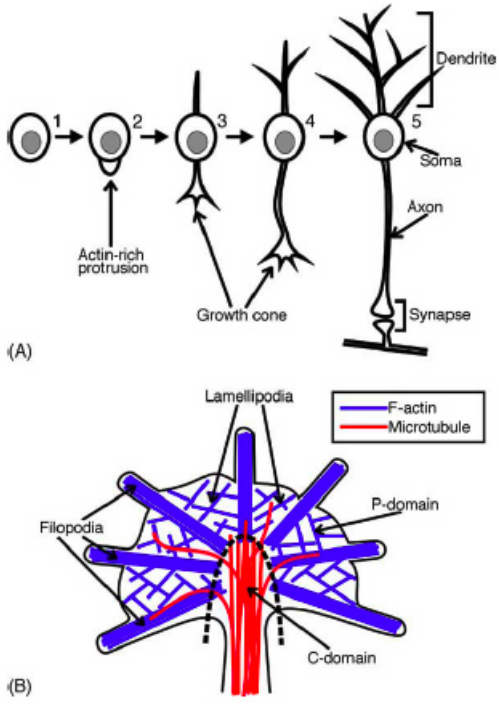

Fig. 1.21: A) Morphological changes in differentiated neurons B) Cytoskeletal structure of growth cone adapted from Tojima et al., 2004

The regulation of F-actin assembly and disassembly are regulated by actin-binding proteins that function downstream of Rho- family GTPases (RhoA, Rac1, Cdc42). Although RhoA inhibits dendritic and axonal growth, through stress fiber formation, presumably by sequestering actin for incorporation into stress fibers, Rac1 and Cdc42 are positive regulators of growth by inducing lamellipodia and filipodia formation, respectively. ADF/cofilin (A/C) family proteins are the effectors for Rho GTPase-triggered actin reorganization in neuronal and non-neuronal cells

[Gungabissoon and Bamburg, 2003]. In humans, cofilin is the prevalent member of A/C family that is found in central nervous system and concentrated mainly in soma (cell body) and growth cones of dendritic and axonal processes [Sarmiere and Bamburg, 2004]. LIMK1 is speculated to play a critical role in remodeling actin cytoskeleton in the nervous system by linking Rho GTPases to cofilin activity. It is expressed predominantly in peripheral and central nervous system and accumulates in presynaptic terminals [Arber et al., 1998, Wang et al., 2000]. LIMK1 has been implicated in determining growth cone motility and neurite extension rate by regulating cofilin activity [Tojima and Ito, 2004]. Overexpression of N-terminal domains of LIMK1, which regulates the kinase activity of the protein, leads to a decrease in neurite extension after stimulation with nerve growth factor (NGF) [Birkenfeld et al., 2001].

The initial process of neuronal differentiation (neuritogenesis) is the most critical in determining the cell fate from neuroblast to a mature neuron. The intracellular signaling cascades controls neuritogenesis by regulating the activity of A/C family. An increase in cAMP concentration by activation of adenylyl cyclase (AC) simultaneously triggers two independent cascades. The first is a slight increase in LIMK1 expression, and the second is novel expression of voltage-dependent Ca^{2+} channels (VDCCs). The expression of LIMK1 and VDCC may depend on cAMP-responsive element (CRE) binding protein (CREB), which is a central transcription factor that mediates cAMP- responsive genes by binding as a dimer to a conserved CRE motif [Yang et al., 2004a]. The increase in LIMK1 expression induces actin polymerization via inducing cofilin phosphorylation and in-

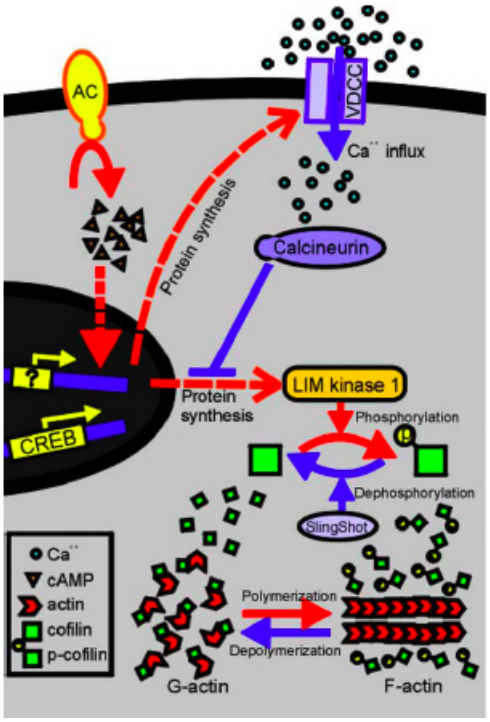

Fig. 1.22: Intracellular signal transduction cascades involved in control of actin dynamics during neuritogenesis adapted from Tojima et al., 2004

activation, which results in induction of neuritogenesis.

Novel expression of VDCCs causes an increase in intracellular Ca^{2+} levels in response to membrane depolarization, which subsequently leads to an activation of calcineurin and inhibition of LIMK1 expression. These results in, activation of cofilin and inhibition of neuritogenesis (figure1.22) [Tojima and Ito, 2004]. In addition to that, since calcineurin directly induces slingshot (SSH) activity by dephosphorylating it, it can be suggested that in addition to the role of calcineurin on activating cofilin by inhibiting LIMK1 expression, it may also cause the activation of cofilin by inducing the activity of its phosphatase slingshot (SSH) (figure1.13) [Wang et al., 2005].

Subsequent processes in neuronal differentiation (neurite outgrowth, pathfinding and targeting) are essentials for establishing highly ordered neuronal network by the precise control of axon guidance by the help of axon growth cones. Growth cones senses a variety of attractive and repulsive cues from the environment and integrate these signals into changes in their shape and motility. Actin dynamics in growth cones is the reason for the rapid changes in the shape and motility upon extracellular cues. Although attractive cues such as neurotrophins, netrins, and laminin promote actin polymerization and neurite outgrowth, repulsive cues such as semaphorins, ephrins induce actin disassembly and inhibit outgrowth [Sarmiere and Bamburg, 2004]. LIMK1 has been shown to mediate neurite outgrowth [Birkenfeld et al., 2001] and growth cone collapse in response to repulsive guidance cue Sema3A [Aizawa et al., 2001]. In COS7 cells treatment of Sema3A followed by a rapid increase of cofilin phosphorylation and afterwards a steady decrease [Aizawa et al., 2001]. Also, in cultured systems, LIMK1 overexpression causes a reduction in growth cone motility while SSH expression increases the growth cone motility which suggests a role to A/C family members in reorganizing actin filaments in response to guidance cues [Endo et al., 2003]. Axon outgrowth is regulated by a RING-finger-dependent ubiquitin ligase Rnf6, which binds, polyubiquitinates, and targets LIMK1 for proteasomal degradation in

growth cones of primary hippocampal neurons. During ubiquitin-proteosome degradation, the covalent attachment of ubiquitin to its target protein occurs in a series of enzymatic steps that are mediated by the ubiquitin-activating enzyme (E1), ubiquitin conjugating enzyme (E2), and the ubiquitin ligase (E3). The ubiquitin ligase determines the specificity of this reaction by forming proteinÐprotein interactions. The functional link between E3 ubiquitin ligase Rnf6 and LIMK1 during the development of axons has been shown, as the changes in axon outgrowth induced by up- or down-regulation of Rnf6 levels can be restored by modulation of LIMK1 expression [Tursun et al., 2005].

Most of the dendrites develop actin-rich protrusions named as spines, which form postsynaptic structures. The size, shape, and number of spines are associated with the formation and maintenance of memory and learning. Actin filaments are involved in regulating receptor complexes and in the formation of functional synapses, so that disruption of actin filament dynamics may severely effect learning, memory and development. [Sarmiere and Bamburg, 2002, Sarmiere and Bamburg, 2004]. LIMK1 accumulates highly at mature synapses. Although LIMK1-deficient mice developed quite normally, they showed aberrations in dendritic spine morphology, growth cones and actin structure [Meng et al., 2002]. Normal morphology of dendritic spine is composed of a large "head" region and a thin "neck" region extending back to the dendrite and a postsynaptic region (PSD) (figure 1.23). Within the PSD, there are scaffold proteins such as Homer, PSD-95 and Shank, as well as others, which link actin cytoskeleton to postsynaptic receptors such as AMPA and NMDA glutamate receptors. In LIMK-deficient mice, the necks of the spines are thicker, and head is reduced in size, resulting in a decrease in spine area and length of the postsynaptic density. Also they have an enhanced basal release of presynaptic vesicles suggesting a role for LIMK1 in neurotransmitter release. The reason of thicker dendritic spine neck can be due to actin rod formation, which do not stain with phalloidin and occur under condition of A/C family hyperactivation. There is a decreased F-actin staining in LIMK- null mice, suggesting disruption of actin filament formation. Despite the change in morphology of the spine, the

number of the spine is normal (figure 1.23) [Sarmiere and Bamburg, 2002, Meng et al., 2002].

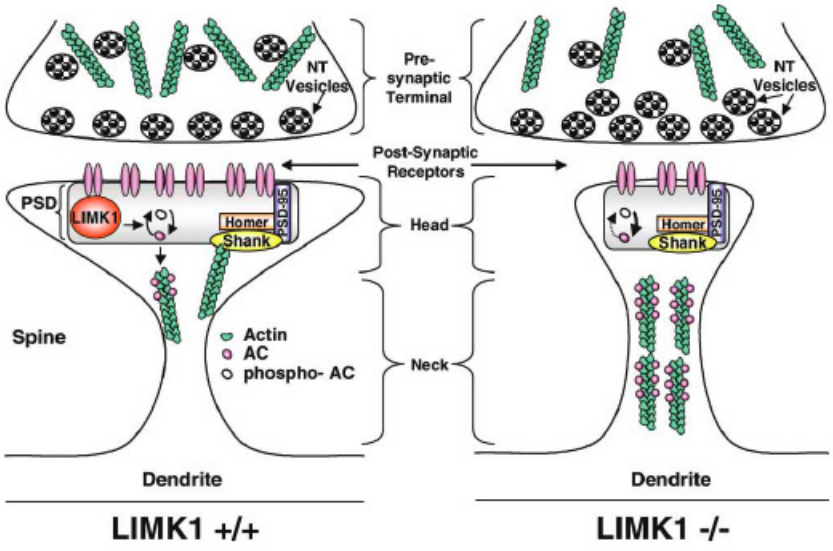

Fig. 1.23: LIMK1 influences the pre- and postsynaptic function by modulating actin filaments
adapted from Sarmiere and Bamburg, 2002

Additionally, despite the morphological changes in LIMK1-deficient mice, there was no marked phenotypic abnormalities in LIMK2-deficient mice, apart from a smaller testis size and abnormalities in spermatogenesis [Takahashi et al., 2002]. In LIMK1-deficient mice the amount of phospho- cofilin was altered approximately % 50, in LIMK2-deficient mice the amount of phospho-cofilin was not significantly altered, however in LIMK1/2 double knockout the amount of phospho-cofilin was significantly reduced. These findings suggest that although LIMK1 is the predominanty player in maintaining ADF/ cofilin (A/C) family phosphorylation in brain, LIMK2 does play a role in brain when LIMK1 is absent. In LIMK1/2 double knockout , basal synaptic response were altered significantly, which suggest a role for LIMK1 and -2 in synaptic regulation [Meng et al., 2004].

Some additional knowledge for the role of LIMK1 in synaptic regulation comes from a study in *Drosophila*. This study suggested that bone morphogenic protein (BMP) receptor- signal-

ing controls both synaptic growth and synaptic stabilization in *Drosophila* neuromuscular junction, where synaptic stabilization is LIMK1- dependent [Eaton and Davis, 2005]. It was reported previously that LIMK1's LIM domains were associated biochemically with BMP type II receptor and binding of BMP to the receptor complex leads to an increase in LIMK1 activity [Foletta et al., 2003, Lee-Hoeflich et al., 2004]. The study in flies proposed that ligand binding to BMP type II receptor counterpart in flies *wishful thinking* (*Wit*) receptor activates DLIMK1 (LIMK1 in flies) to stabilize synapses in neuromuscular junction (NMJ) and stimulates NMJ growth [Eaton and Davis, 2005]. Also another study in *Drosophila*, addresses the molecular function of DLIMK1 in neuromuscular synapse development by either knocking out or activating DLIMK1. When DLIMK1 is knocked out, there is an enlarged NMJs, and in opposite gain-of-function DLIMK1 transgene produced stunted NMJs [Ang et al., 2006].

LIMK1 is one of 28 genes that is deleted in one copy of chromosome 7q11.23 that leads to a neurodevelopmental disorder Williams syndrome (WS). WS syndrome is occurred approximately 1 in 20,000 live births and characterized by mental retardation, visual-spatial learning difficulties and skeletal abnormalities [Gray et al., 2006]. Visual-spatial learning is the ability to see and object or picture as a set of parts and then to construct a replica of the original from these parts. The impaired spatial learning and changes in fear response seen in LIMK1 knockout mice, suggest the involvement of LIMK1 in pathophysiology of WS even though the exact role of LIMK1 in cognitive profile of WS individuals has to be still defined since it is suggested that the low level of LIMK1 can only affect spatial impairment in combination with reduced levels of other proteins involved in brain function [Meng et al., 2002]. Because of the role of LIMK1 in synapse development and stabilization, the phenotypes in WS may be due to the disruption of synapse development [Eaton and Davis, 2005].

1.8 Roles of LIMK1 in phagocytosis and apoptotic response

Additional to their role in cell migration, cell cycle and neurogenesis, LIMK1 has been shown to regulate phagocytosis through regulating its ligand cofilin as its phosphocycle is important in *Listeria* induced phagocytosis [Bierne et al., 2001]. The *Listeria* induced phagocytosis process is initiated by intimate contact between bacterial invasion protein and host cell receptor and is followed by the progressive engulfment of the bacterial body into the target cell. It is shown that interaction of a invasion protein InLB with its receptor triggers actin polymerization and formation of phagocytic cup. This step involves recruitment of Arp2/3 complex which promotes actin nucleation and branching, and cofilin which stimulates actin dynamics. Inhibition of endogenous LIMK1 by expressing dominant negative mutant would lead to an excessive activity of cofilin, resulting in increased disassembly and abortion of phagocytic cup. Also overexpression of LIMK1 would increase cofilin phosphorylation leading to inhibition of actin depolymerization activity which results in inhibition of phagocytic cup closure because of thick filament network (figure 1.24) [Bierne et al., 2001].

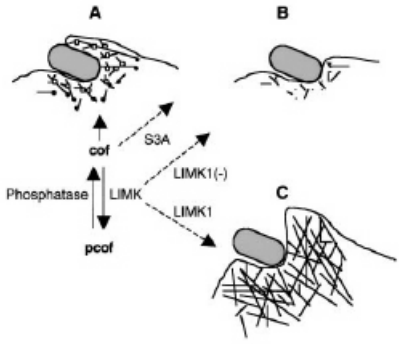

Fig. 1.24: Role of LIMK1 in phagocytosis adapted from Bierne et al., 2001

The invasion of bacterium such as *Salmonella* to non-phagocytic cells involves phosphocycle of cofilin as there is an initial dephosphorylation of cofilin followed by phosphorylation, with a role of both LIMK1 and SSH1-L as their catalytically inactive forms decreased invasion [Dai et al., 2004]. Also LIMK1 regulates the intracellular vesicle trafficking of lysosomes and endosomes such that

LIMK1 transfection to MCF breast cancer cells, abrogates the internalization of a endocytic tracer epidermal growth factor (EGF) [Nishimura et al., 2004].

Furthermore, LIMK1 has been shown to have a role in apoptotic response since its caspase mediated cleavage in N-terminal side leads to activation of the protein and apoptotic membrane blebbing. It is reported in Jurkat T cells that LIMK1 is cleaved and activated upon anti-Fas antibody induced apoptosis, and this cleavage and activation is blocked by caspase-3 inhibitors. These findings are consistent with the role of actin cytoskeleton in phase of apoptosis in cell rounding and membrane blebbing since LIMK1 is one of the regulators of actin cytoskeleton [Tomiyoshi et al., 2004]. It is also suggested that when LIMK1 is overexpressed in PC12 neuronal cells, it is more resistant to serum-withdrawal-induced cell death. Additionally, in these cells, the level of caspase 3 activation is lower than in the control cells [Yang et al., 2004a].

Aim of the project

The aim of our study was to perform the functional analysis of LIMK1 in normal and pathological proliferation. To address this question we firstly examined the endogenous localization of LIMK1 protein in cancer cell lines, normal mouse kidney tissues and prostate tissues. Additionally the localization of LIMK1 in orthotopic kidney cancer model and in PTEN depleted prostate cancer model was monitored. Secondly, to clarify the role of LIMK1, we developed different strategies to downregulate LIMK1 expression: on one side we started to create conditional knockout mice, and on the other side, we generated different RNA interference tools (siRNA and lentivector-based shRNA) to deplete LIMK1 from cell culture models. Our focus was on the role of LIMK1 in cell cycle progression and mainly M-phase progression.

Chapter 2

Materials and Methods

2.1 Materials

Tab. 2.1: **General Chemicals**

Reagent	**Supplier**
Acetic acid	Merck
Activated CH Sepharose 4B	Pharmacia
Acrylamide	Bio-Rad
Agar Gibco	BRL
Agarose	Progen
Ammonium acetate	Fluka
Ampicillin	Fisons
Aprotinin	Boehringer
Blocking Buffer	Roche
Boric acid	Fluka

Tab. 2.1 – Continued

Reagent	**Supplier**
Bromophenol blue	Ajax
BSA (bovine serum albumin)	Fluka
Centricon	Millipore
Chloroform	Fluka
Colcemid	Gibco BRL
L-cysteine	Sigma
DAPI (4Õ6Õ-diamidine-2Õ-phenylindole dihydrochloride)	Boehringer
DMEM (DulbeccoÕs Modified Eagle Medium)	Gibco BRL
DMSO (dimethylsulfoxide)	Fluka
DTT (dithiothreitol)	Promega
DNA Ladder:	
Marker II, Marker V and Marker VI	Roche
DNA polymerase:	
cloned *Pfu*	Stratagene
Pwo	Roche
Taq	Invitrogen
ECL (enhanced chemiluminescence)	Amersham
EDTA (ethylenediamine tetra-acetic acid)	Boehringer
EtOH (ethanol)	Fluka
Ethidiumbromide	Sigma
FCS (fetal calf serum)	Gibco BRL

Tab. 2.1 – Continued

Reagent	**Supplier**
Formalin (10%)	Merck
Formaldehyde	Fluka
Formamide	Merck
G418	Gibco BRL
Grace's insect medium	Boehringer
Glutathione sepharose 4B	Pharmacia
L-Glutamine	Trace
Glycerol	Fluka
Hemocyanin, keyhole limpet (KLH), Megathura Crenulata	Calbiochem
HBSS	Gibco BRL
HCL (hydrochloric acid)	Fluka
HEPES (N-2-hydroxyethylpiperazine-NÕ-2-ethanesulfonic acid)	Boehringer
H2O2 (Hydrogen peroxide)	Sigma
Isopropanol	Merck
Isoprophylthio- β- D- galactoside (IPTG)	BRL
KAc (potassium acetate)	Fluka
Kanamycin	Sigma
KCL (potassium chloride)	Sigma
Klenow enzyme	Boehringer
N-Laurylsarcosyl	Roche
Lambda protein phosphotase	New Eng. Bio.

Tab. 2.1 – Continued

Reagent	**Supplier**
β-Mercaptoethanol	Sigma
Mowiol	ICN
Methanol	BDH
MgCl2 (magnesium chloride)	Sigma
Milk powder	Migros
3-(N-Morpholino) propane- sulfonic acid (MOPS)	Sigma
NaAc (sodium acetate)	Merck
NaCl (sodium chloride)	Merck
Na2HPO4 (Sodium hydrogen phosphate)	Fluka
NaH2PO4 (Sodium dihydrogen orthophosphate)	Fluka
NaOH (sodium hydroxide)	Merck
Nitrocellulose membrane	Sclei and Schuell
Nocodazole	Sigma
Nonidet P-40	Sigma
Normal Goat Serum	Vector Lab
Oligofectamine	Invitrogen
Optimem	GibcoBRL
Paraformaldehyde	Fluka
Paraffin	Fluka
PBS (phosphate buffered saline)	Trace
Penicillin	Trace

Tab. 2.1 – Continued

Reagent	**Supplier**
Phenol	GibcoBRL
PMSF (phenyl-methyl-sulfonyl-fluoride)	Boehringer
Poly-L-Lysine solution	Sigma
Protein A/G sepharose	Pharmacia
Proteinase K	Gibco BRL
Propidium iodide	Sigma
RNase H reverse transcriptase	Gibco BRL
RNase inhibitor	Boehringer
Protease inhibitor cocktail tablet	Boehringer
SDS (sodium dodecyl sulfate)	Eurobio
Spermidine	New Eng. Bio.
Taxol (Paclitaxel)	Sigma
TEMED (N,N,NÕ,NÕ-Tetramethylethylenediamine)	Bio-Rad
Tris (Tris (hydroxymethyl) aminomethane)	Sigma
Tri- Sodium citrate	BDH
Triton X-100	Fluka
Trypsin EDTA	Gibco BRL
Tween-20	Sigma
Vectashield	Vector Lab
5-bromo-4-chloro-3-indolyl-B-D-galactopyranoside (X-Gal)	Promega

Tab. 2.2: **Antibodies**

Antibody	**Clone/ Cat no**	**Supplier**
CDK2	SC-163-G	Santa Cruz
GFP	7.1 and 13.2	Boehringer
HA. 11	MMS-101R	BabCO
HIF1 α	NB 100-123	Novus Biologicals
Lamin A/C (346)	Sc-7293	Santa Cruz
α- Mouse IgG, Cy5	715-175-150	Dianova
α- Mouse IgG, FITC	715-095-150	Dianova
α- Mouse IgG, Texas Red	715-075-150	Dianova
α- Mouse IgG, HRP	NA 931	Amersham
α- Mouse IgG, Alexa 488	A-11029	Molecular Probes
α- Mouse IgG-kappa	M7894	Sigma
rabbit α-p-cofilin		Cell Signaling
rabbit α-p21	dc-397	Santa Cruz
mouse α-p53	Ab-7	Oncogene
mouse α-PARP	C2-10/556362	BD Pharmingen
rabbit α-PTEN	9559	Cell Signaling
rabbit IgG (purified)	02-6102	Zymed
α- Rabbit IgG, Cy5	711-175-152	Dianova
α- Rabbit IgG, FITC	711-075-152	Dianova
α-Rabbit IgG, Texas Red 595	T-2767	Molecular Probes

Tab. 2.2 – Continued

Antibody	Clone/ Cat no	Supplier
α- Rabbit IgG, HRP	NA 994	Amersham
α- Rabbit IgG, Alexa 488	A-11008	Molecular Probes
mouse α-α-tubulin	MAS/YL 1/2	Harlan Sera-Lab
mouse α-γ-tubulin	MMS-258R	BabCO

2.1.1 Restriction enzymes

Restriction enzymes were purchased from Boehringer, New England Biolaboratories or Promega and used with supplied buffers according to recommended protocols.

2.1.2 Bacterial strains

Plasmid DNA was grown in the bacterial strain DH5α (Life Technologies). Alternatively HB101 was used for shRNA cloning.

2.1.3 Buffers

DIG-Buffer: was comprised of 0.1 M Maleic acid (Fluka) and 0.15 M NaCl (pH 7.5).

10x DNA Loading buffer: 250 mg bromophenol blue (Roche) was dissolved in 33 ml 150 mM Tris pH 7.6 and to that 60 ml glycerol and 7 ml H_2O is added.

HTB (for competent cells preperation): 10 mM HEPES 0.477g, 15 mM CaCl (Fluka) 0.441g

and 250 mM KCl 3.728g were dissolved in 150ml H_2O and pH adjusted to 6.7 with KOH (4M). Then MnCl2 was added and dissolved 55mM MnCl2 1.384g. Afterwards, volume was adjusted to 200ml, subsequently filter-sterilized through a 0.45?m filter and stored at 4 °C.

LB-Medium: 1% (w/v) Bacto-tryptone (BD), 0.5 % (w/v) Bacto-Yeast extract (BD) and 1% (w/v) NaCl (pH 7.0) were mixed.

LB-Agar: LB-Medium + 20 /l agar

PBS: was bought as a ready to make mix, needed only resolving in water and autoclaving.

SDS-PAGE running buffer: 10 g SDS, 30.3 g Tris and 144.1 g glycin were dissolved in 800ml H_2O and adjusted to 1 litre.

SOB (for competent cells preperation): 20 g Bacto tryptone (BD), 5 g Bacto yeast extract (BD) and 0.5 g NaCl were dissolved in 950 ml H_2O and 10ml of 250mM KCl were added. pH was adjusted to 7.0 with NaOH the final volume was 1litre. The medium was then aliquoted, autoclaved and cooled to 60ąC before adding 5ml sterile 2M $MgCl_2$

20x SSC: 3 M NaCl, 0.3M Na-citrate were mixed and pH was adjusted to 7.0.

TBE buffer: 89mM Tris, 89 mM Boric acid, and 2 mM EDTA were mixed and pH was adjusted to 8.0.

2.1.4 Oligonucleotides

Oligonucleotides for Sequencing

- T7 primer 5‘TAATACGACTCACTATAGGG 3‘
- T3 primer 5‘ATTAACCCTCACTAAAG 3‘
- SP6 primer 5‘GATTTAGGTGACACTATAG 3‘

Oligonucleotides for quantitative RT-PCR

- 18S Forward 5‘GTAACCCGTTGAACCCCATT 3‘

- 18S Reverse 5‘CCATCCAATCGGTAGTAGCG 3‘
- QPLIMK1 Forward 5‘AGGTGACACACCGTGAGACA 3‘
- QPLIMK1Reverse 5‘CCAGGCATCGCATGACCTT 3‘
- QPHIF1a Forward 5‘ATCCATGTGACCATGAGGAAATG 3‘
- QPHIF1a Reverse 5‘CTCGGCTAGTTAGGGTACACTT 3‘
- QTKIP2 Forward 5‘GCGGCGATCAAGAAGCTG 3‘
- QTKIP2 Reverse 5‘CGACGACTTAGGCGC 3‘

2.2 Methods

2.2.1 DNA and RNA Manipulation

Plasmid DNA purification from bacteria

The isolation of plasmid DNA from bacteria was performed using the NucleoBond PC Kit from Macherey-Nagel, according to manufacturerÕs instructions: A bacterial culture was set up by inoculating 50 ml of LB medium (plus antibiotic) with a single colony from a freshly streaked plate or from a glycerol stock. After overnight shaking at 37 °C, the saturated culture was centrifuged at 5.000 x g for 15 min at 4 °C. After discarding the supernatant the pellet was re-suspended in 4 ml buffer S1 (50 mM Tris-HCl, 10 mM EDTA; pH 8.0) containing 100 μg/ml RNase A. 4 ml Buffer S2 (200 mM NaOH, 1% SDS) were then added to the suspension to denature both the chromosomal and plasmid DNA. Following a short incubation of max. 5 minutes at room temperature (RT) addition of 4 ml buffer S3 (2.8 mM KAc, pH 5.1) neutralized the lysate and caused the formation of a precipitate containing chromosomal DNA and other cellular components. This incubation was carried out for 5 minutes on ice. The suspension was then filtered

through NucleoBond filters pre-wetted with sterile deionized H_2O and the cleared lysate applied onto an equilibrated column (equilibrated with 2.5 ml buffer N2 (100 mM Tris, 15% EtOH, 900 mM KCl, 0,15% Triton X-100, pH 6.3)). Following washing of the column with 10 ml buffer N3 (100 mM Tris, 15% EtOH, 1.15 M KCl, pH 6.3) the plasmid DNA bound to the anion exchange resin was eventually eluted with 5 ml buffer N5 (100 mM Tris, 15% EtOH, 1 M KCl, pH 8.5). 3.5 ml Isopropanol precipitated the eluted plasmid DNA and after 30 minutes centrifugation at 15000 g at 4 ąC the supernatant was discarded and the DNA pellet washed carefully with 70% EtOH. The pellet was then dried at room temperature and finally dissolved in 50 μl sterile deionized H_2O. If isolated plasmid DNA would be used for transfection, the dring of pellet was done under cell culture hood.

2.2.1.1 Enzymatic treatment of DNA

Restriction digest: The restriction digest was performed in a final volume of 20 ?l. The following volumes of reagents would be added to the reaction tube: 1 μg DNA, 1 μl 10x Restriction enzyme buffer, 1 μl restriction enzyme and sterile deionized H2O was used to fill up until 20 μl.

Dephosphorylation of 5ńends: In a total volume of 50 μl, 44 μl DNA were supplemented with 5 μl 10x One-Phor-All-Plus Buffer (Pharmacia) and 1 μl of a 1:20 dilution of Alkaline Phosphatase (Calf Intestine Mucosa; Pharmacia). The reaction mix was incubated at 37 °C for 30 minutes, followed by an incubation to stop the enzymatic activity at 85 °C for 20 minutes. The reaction mix was then filled up to 100 μl with sterile deionized H_2O and extracted with Phenol/Chloroform and subsequently once with chloroform. Addition of 1/10 Vol. NaAc and 2 Vol EtOH and centrifugation at 14.000 rpm for 30 minutes at 4 °C precipitated the DNA that was then resuspended in 20 μl H_2O.

Ligation: The ligation of DNA fragments was performed using the Rapid DNA Ligation Kit from Roche. The vector DNA and insert DNA was dissolved in thoroughly mixed and diluted 1x

conc. DNA Dilution Buffer to a final volume of 10 μl. 10 μl T4 DNA Ligation buffer was added to the reaction vial and mixed thoroughly. Finally 1 μl of T4 DNA-Ligase was added to the tube and after mixing the reaction was allowed to incubate for 5 minutes at RT. The ligation mix was then used directly for the transformation of competent cells.

2.2.1.2 Preparation of competent cells

A 200 ml SOB medium culture inoculated with about ten large colonies from a freshly grown plate of DH5α was left to grow at 26 $^\circ$ with vigorous shaking until reaching an OD_{600} of 0.45. The culture was then split into sterile centrifuge tubes (4x 50ml falcon tubes) and placed on ice for 10 minutes. After spinning for 15 minutes at 2500 g, the supernatant was discarded, the pellet re-suspended in 64 ml HTB (4x 16ml) and placed on ice for 10 minutes. After spinning and discarding the supernatant again the pellet was re-suspended in 16 ml HTB (each pellet in 4 ml and then pooled). 1.2 ml filter-sterilized DMSO were added slowly while gently swirling the cell suspension and the cells were then immediately aliquoted into convenient aliquots (200 μl and 500 μl) and quick frozen by throwing into liquid nitrogen. Storage of competent cells occurred at Ð80 $^\circ$ C.

2.2.1.3 Transformation of E.coli

100 μl of cold bacteria competent cells were added to the ligation mix or DNA and the whole reaction was incubated for 30 minutes on ice. After heat-shock for 2 minutes at 42 $^\circ$ C followed by 5 minutes incubation on ice, the transformed cells were spread on LB-Agar plates containing the appropriate antibiotics.

2.2.1.4 Isolation of DNA from agarose gels

DNA fragments were excised from agarose gels in a minimum volume using a scalpel, and purified using QIAquick Gel Extraction kit from Qiagen.

2.2.1.5 Polymerase chain reaction (PCR)

PCR was carried out according to the manufacturers protocol regarding the polymerase employed. Standard usage involved Taq and Pfu polymerase. Each PCR reaction amounting up to a total volume of 25 μl contained: 1 μl each of the forward and the reverse primers (both 15 pmol), 2.5 μl 10x PCR buffer (200 mM Tris-HCl (pH 8.4), 500 mM KCl), 0.5 μl 50 mM MgCl2 (final conc. 1.5 mM), 0.5 μl 10 mM dNTP mixture, 0.2 μl of 5 units/μl Taq DNA Polymerase and 18.3 μl sterile ultra-pure water to increase the reaction volume to 24 μl. 1 μl of DNA was pipetted to a PCR tube and the 19 μl mix added. After short mixing the amplification reactions were performed in a thermocycler. Negative controls in which ddH_2O replaced the DNA were included in every series of reactions as well as positive controls as a guideline for the migration of the expected bands. Thermal cycling conditions were 95 ° C for 5 minutes, 35 cycles of 95° C for 30 seconds, primer annealing for 30 seconds at the described temperatures, 72 ° C for 1 minute and a final 72 ° C incubation for 10 minutes. PCR reactions were subsequently analyzed by agarose gel electrophoresis (different agarose concentrations (depending on expected product size) containing 0.5 g/ml ethidium bromide). Inclusion of appropriate molecular weight standards DNA Markers enabled sizing of PCR products.

2.2.1.6 DNA sequencing

Samples for sequencing were sent externally to Microsynth, a company providing sequencing services

2.2.1.7 Isolation of genomic DNA from ES cell clones

Medium was aspirated from each tissue culture well of 24-well plates containing ES colonies grown to confluency. After washing once with PBS, 400 μl Lysis buffer (100 mM Tris pH 8.5, 5 mM EDTA, 0.2% SDS, 200 mM NaCl) including 50 μg/ml Proteinase K were added to each well and the plates were then incubated in a 37 ° C incubator over night. The cell-lysate of

each well was then carefully transferred into eppendorff-tubes and extracted with 400 μl of a 1:1 mixture of Phenol/Chloroform. After mixing and centrifugation at 14000 rpm for 2 minutes the upper phase was transferred into a new tube and extracted with 400 μl Chloroform. After mixing and centrifugation at 14000 rpm for 10 minutes the upper phase was again transferred into a new tube and 1 ml of 100 % EtOH was added. The DNA precipitated as a white pellet that after an additional centrifugation at 14000 rpm for 10 minutes was washed once with 70 % EtOH, centrifuged again and then left to dry for at least 5 hours to get rid of all the Ethanol. Subsequently the pellet was re-suspended in 50 μl H2O and agitated on a shaker at 30 $^\circ$ C for 24 hours to help re-dissolving. 20 μl (approximately 10 μg) of this DNA were then used for the digest.

2.2.1.8 Non-radioactive Southern blot analysis

Generation of Southern Probes by DIG labeling: For the creation of a KO 2.5‘-probe to test for homologous recombination, primers KO 2.5‘F and KO 2.5‘R were used in a PCR reaction utilizing genomic wild-type DNA as template whereas for the creation of a KO 2.3ń-probe, primers KO 2.3‘F and KO 2.3‘R were used. The bands corresponding the expected sizes were then isolated from an agarose gel and the purified DNA subjected to another PCR using the DIG labeling Kit from Roche. The 50 μl reaction contained 1x PCR buffer, 2 mM $MgCl_2$, 2 μl primer. The following program was used: denaturation at 94 $^\circ$ C for 3 minutes, 35 cycles of denaturation at 95 $^\circ$ for 20 seconds, annealing at 57 $^\circ$ for 30 seconds and elongation at 72 $^\circ$ C for 45 seconds. This was followed by incubation at 72 $^\circ$ C for 10 minutes. From the 50 μl starting volume 5 μl were loaded on an agarose gel to check for PCR efficiency and 3 μl were dissolved in 20 μl H_2O, denatured for 5 minutes in a boiling water bath and placed on ice for 5 minutes before being added to 15 ml pre-warmed Pre-hybridisation (Pre-hyb) buffer.

DNA-gel blot analysis: DNA was digested with XbaI enzyme in a reaction volume of 30 μl

containing 3 μl buffer and 1 μl enzyme. The restriction digest was allowed to take place at 37 $^\circ$ C over a period of ca. 24 hours, during which two more additions of enzyme occurred. 5 μl loading dye were then added to the reactions and the DNA was resolved on 0.8 % agarose gels, which were run overnight at 40 V. A DIG-labelled Marker II was used to enable sizing of the DNA fragments.

The gels were then incubated in an ethidium bromide ÒbathÓ (0.5 μg/ml) with gentle agitation for half an hour, washed in ddH_2O for 5-10 minutes and a picture was taken to see whether the digest had been successful. If so, the gels were incubated for 20 minutes in Denaturing buffer (1.5 M NaCl, 0.5 M NaOH) at RT and constant gentle agitation, followed by two 20 minutes-incubations in Neutralizing buffer (87.6 g NaCl, 60.8 g Tris, 33 ml 37% HCl in 1 l H2O). DNA was then capillary transferred in 20x SSC to Zeta-Probe GT positively charged nylon membranes (Bio-Rad) and fixed by UV-crosslinking.

Pre-hybridization was performed for 2 hours in 15 ml Pre-Hyb-buffer (for 30 ml: 15 ml Formamid, 7.5 ml 10x Blocking buffer (50 g powder in 500 ml DIG-Buffer), 7.5 ml 20x SSC, 300 μl 10 % N-Laurylsarcosyl, 60 μl 10 % SDS and 1 ml sonicated salmon sperm DNA (10 mg/ml)) at 42°. After addition of the denatured probe, hybridisation was performed overnight under the same conditions. The membranes were washed consecutively in 2x SSC/0.1% SDS (5 minutes, RT), in 0.5x SSC / 0.1 %SDS (20 minutes, 68 $^\circ$ C) followed by 20 minutes at 68 $^\circ$ C in 0.1x SSC / 0.1% SDS. Finally the blots were subjected to immunological detection using an anti-DIG antibody conjugated to alkaline phosphatase and the CDP-star kit from Roche Diagnostic, according to manufacturerÕs instructions.

2.2.1.9 RNA isolation

HeLa cells either treated with siRNA or hypoxia were lyzed in Buffer RLT and total RNA was extracted using of RNeasy RNA isolation kit, Qiagen. RNA content was calculated by measuring

A_{260}. First strand cDNA synthesis was performed using Superscript II reverse transcriptase kit (Invitrogen) by the standart protocol of the supplier. Random hexamers were used as primers during this protocol. The resulting cDNA was used as a template for quantitative RT- PCR.

2.2.1.10 Real-Time Quantitative Polymerase Chain Reaction(QT-PCR)

Expression levels of mRNA were measured by means of real-time fluorescence detection of SYBR Green. The real time PCR reaction was prepared as follows: 12.5 μl SYBR Green mix (2x), 0.2 μl cDNA or cDNA without reverse transcriptase (-)control, 1 μl primer pair mix (5pmol/μll each primer) and 11.3 ddH_2O were mixed and processed for QT-PCR using ABI 7900 real time PCR machine. After PCR was finished, the results were analyzed using SDS 7000 software.

2.2.2 Antibodies

Polyclonal rabbit serum against full length cofilin or Limk-1 was made by injection of the antigen GST-cofilin or MAL-LIMK-1 fusion proteins, purified from bacteria, into rabbits [J.Lisztwan, 2001]. Antisera were affinity purified using columns packed with GST-LIMK1 recombinant protein (expressed using baculovirus system) conjugated Sepharose. Affinity purification was carried out as described [Lisztwan et al., 1998]. Commercially antibodies used are listed in the Materials section of this chapter.

2.2.3 Bacterial expression and purification of GST-fused LIMK1

The GST-LIMK1 which was used in antibody competition assays was prepared as follows: E.Coli DH5 α containing expression plasmid for GST-LIMK1 protein was inoculated overnight and the next morning diluted 1/10 in LB containing 0.2mM IPTG. After 4.5 hours of incubation at 37°, bacteria were harvested by centrifugation at 5,000 rpm for 5 minutes. After resuspending

cells in TNN buffer (50mM tris pH 7.5, 250mM NaCl, 5mM EDTA, 0.5%NP-40, 50mM NaF, 1 mM Na_3VO_4, 0.5mM phenylmethanesulfonyl fluoride, 1 μg/ml aprotinin and 2.5mM dithiothreitol(DTT)), bacteria were sonicated. Cell debris was collected by centrifugation at 5,000 rpm for 5 minutes, and the supernatant transferred to a fresh tube. Meanwhile, Glutathione sepharose 4B beads were preincubated in 5 % milk for 10-15 minutes and washed 2-3 times with TNN buffer, before adding the beads to bacterial lysate. After 1-2 hours of incubation at 4°, the beads were collected by centrifugation and washed 3-4 times with TNN buffer. Protein was eluted form the beads and used for antibody competition in immunofluorescence.

2.2.4 Cell lines, Synchronisation, and Cell Cycle Analysis

Human 293 embryonic kidney cells, U2OS osteosarcoma cells, HeLa cervical cancer cells, HCT116 colon cancer cells, 786O clear cell carcinoma cells were maintained in DMEM supplemented with 10% fetal calf serum (FCS). Cells were kept at 37°C. Ts20 mouse fibroblasts were kept in DMEM (high glucose 3.5g/l)with 10% FCS at 33 °C or 39°C.

In order to synchronise cells in G1/S, cells were treated with double-thymidine block. For these experiments, an asynchronously dividing cell population was first synchronized at the G1/S boundary in the presence of excess thymidine (2mM final) for 14 hours. Cells were then incubated for 8 hours in the absence of thymidine and are then treated again with 2mM thymidine . The cells were then released from tymidine block by washing with phosphate-buffered saline (PBS) and grown for different time periods (see figures and legends).

For synchronization in prometaphase, cells were arrested using nocodazole (0,25 mM) for 15hours and released by washing several times with PBS and medium and propagated with complete medium for different points as described in legends to the figures.

For fluorescent activated cell sorting (FACS) analysis, cells were harvested by treatment with

trypsin, washed in cold PBS, and resuspended in 70% ethanol for storage at -20 °C until further analysis. Propidium iodide *( )* -stained cells were analyzed using FACS-calibur.

2.2.5 Treatment with siRNA targeting Limk-1

Cells were seeded in 6-well plates for immunofluorescence or in 10 cm plates for immunoblotting and FACS, one day before siRNA treatment. Treatment was performed for 24 and 48 h. siRNA targeting human Limk1, LIMK1 (521) siRNA and LIMK1(662) siRNA corresponding to positions 521-541, and 662-680 respectively, was synthesized by Qiagen. Control nonsilencing-siRNA was purchased from Qiagen. All siRNAs were 21 nucleotides in length and contained symmetric 3' overhangs of two deoxythymidines. Additionally, siRNA targeting human VHL was synthesized by Qiagen (characterized by Dr.Robert Barry). Transient transfection was performed using oligofectamine reagent according to manufacturer‘s instructions.
siRNA target sequences are as follows:

- Control (nonsilencing) siRNA: 5‘AAT TCT CCG AAC GTG TCA CGT 3‘
- hLimk1(521) siRNA: 5‘GCA AGC GTG GAC TTT CAG TCT 3‘
- hLimk1(662) siRNA: 5‘AAA CCG GAT CTT GGA AAT CAA 3‘
- hVHL siRNA: 5‘ACA CAG GAG CGC ATT GCA CAT 3‘

2.2.6 Lentiviral Vectors for shRNA Delivery

HIV-derived lentiviral vector (pLV-THM) for shRNA expression was described previously (Wiznerowicz*et al.* [Wiznerowicz and Trono, 2003]). pLV-THM/shRNA vector contains two expression units; the first is for shRNA expression cassette, from which a shRNA will be transcribed under the control of a H1 promoter, and the second is for a green fluorescent protein (GFP) expression unit,from which GFP gene will be transcribed from a EF1-α promoter. For shRNA

expression, the sense and antisense oligonucleotides complementary for target mRNA sequences were annealed *in vitro*, and inserted into the *Mlu1, Cla1* cloning sites downstream of the H1 promoter. The shRNA target sequence for LIMK1(1419) is GAA TGT GGT GGT GGC TGA C. Two complementary oligonucleotides, CGCGT-(target sense)-TTCAAGAGA-(target antisense)-TTTTTGGAAAT and CGATTTCCAAAAA-(target sense)-TCTCTTGAA-(target antisense)-A were synthesized for each target sequence and annealed *in vitro*. The annealed double stranded (ds) oligonucleotides with protruding ends complementary to the *Mlu1*and *Cla1* sites in the pLV-THM-GFP plasmid, were then subcloned into the pLV-THM-GFP plasmid.

2.2.6.1 Production of Lentiviral Supernatant

All lentiviruses were produced by transient transfection of 293T cells. Briefly, subconfluent 293T cells were cotransfected with 20 μg of pLV-THM/siRNA, 15μg of PAX packaging plasmid, and 5 μg of pMD2G envelope expression plasmid by calcium phosphate precipitation. After 16 h medium was changed, and recombinant lentivirus particles were harvested 24h and 48h later. The culture supernatants that was collected were used as the virus stock after concentration by ultracentrifugation.

2.2.6.2 Lentiviral transduction of cell lines

HCT116, U2-OS and HeLa cells were infected twice by lentiviral supernatant with the addition of 8μg/ml polybrene in two following days. After two days of infection, fresh medium was added and cells were harvested for Western Blot analysis or processed for FACS analysis.

2.2.7 Whole-cell extract preparation

Cell were washed twice with PBS, and resuspended in 50-200 μl of lysis buffer. Cell lysis buffer was containing 20mM HEPES, 400mM NaCl, 25% glycerol, 1mM EDTA, 15mM NaF , 0.1% Nonidet P-40, 0.5mM phenylmethanesulfonyl fluoride, 1 mM Na_3VO_4, 1 μg/ml aprotinin and

2.5mM dithiothreitol(DTT). The lysates were kept on ice for 1 h, followed by centrifugation at 14,000 rpm for 10 min to remove the insoluble materials, and kept at -80° until used. Before lysates were analysed by use of SDS-PAGE, 1 × Laemmli buffer was added and boiled for 5 min and protein concentration was assessed by Bradford assay.

2.2.8 Immunoprecipitation and Immunoblotting

100 μg of whole-cell extracts were loaded per lane on SDS- 10/15% PAGE gels. Nitrocellulose membranes were probed with primary antibodies, including hLIMK-1 diluted at 1:300 or others; P-cofilin 1:1000, total cofilin 1:1000, hVHL NT 1:500, hVHL CT 1:250, , and kept at room temperature for 2h or at 4 °C overnight. Incubation in the secondary antibody was done in 5% nonfat dry milk in Tris buffered saline with Tween 20 at 1:5,000 dilution using the HRP-conjugated secondary .... as well as the fluorescently labeled secondaries. Signals were developed using ECL kit(Amersham Biosciences) or using Odyssey system.

For immunoprecipitation(IP),cells were lysed using TNN buffer (50mM tris pH 7.5, 250mM NaCl, 5mM EDTA, 0.5%NP-40, 50mM NaF, 1 mM Na_3VO_4, 0.5mM phenylmethanesulfonyl fluoride, 1 μg/ml aprotinin and 2.5mM dithiothreitol(DTT)). Then precleared TNN lysates were immunodepleted with hLIMK-1 full length antibody overnight at 4 °C. To this antibody complex, protein A agarose beads were added for another hour and kept at 4 °C in an end-to end shaker. The beads were washed three times with lysis buffer without protease inhibitors. Finally 2 × Laemmli buffer was added to the beads, and the samples were boiled for 5 min before analysis by use of SDS-PAGE.

2.2.9 Cell Fractionation

Cell pellets were re-suspended in ice-cold grinding medium (250mM sucrose, 2mM EDTA, 10mM MOPS pH 7.4) and homogenized using Dounce homogenizer (Wheaton). The homogenate was centrifuged for 5 min at 1000 rpm, 4 °C. The pellet comprising the nuclear fraction and un-

lyzed cells, was homogenized 4-5 times using grinding medium and subsequently centrifuged. Afterwards the pellet was washed 2-3 times with grinding medium, and finally, lysed in TNN buffer, and stored on ice. The supernatant, containing the cytoplasmic fraction was centrifuged for 30 min at 10,000 rpm, 4 °C . The pellet comprising the mitochondrial fraction was washed 3-times with grinding medium followed by centrifugation for 20 min at 10,000rpm, 4 °C, lyzed in TNN buffer, and stored on ice. Supernatant was mixed 1:1 ratio with TNN buffer and stored on ice. All fractions were subsequently analyzed by immunoblotting with specific antibodies.

2.2.9.1 Protease accessibility assay

Proteinase K was added to equal amounts of mitochondrial fraction to a final concentration of 1,5,10 and 20 μg/ml. The samples were collected by centrifugation at 10,000 rpm for 10 min at 4 °C and analyzed by Western blotting.

2.2.10 Immunofluorescence

Exponentially growing cells were plated on coverslips and processed for indirect immunofluorescence microscopy 2-3 days after seeding and for protein depletion experiment with siRNA coverslips were processed after 48 hours of siRNA treatment. Cells were washed with PBS, fixed in 3% paraformaldehyde/2%sucrose in PBS at pH 7.4 for 10-15 min at 37 °C. They were then permeabilized using 0.2%Triton X-100 in PBS for 2 min at room temperature or fixed for 5 min in methanol (-20 °C) at -20 °C. All subsequent steps were carried out at room temperature. Coverslips were rinsed three times with PBS and incubated for 1 h with indicated primary antibody diluted in PBS containing 1%BSA/1% goat serum. After three 1-min washes in PBS, the appropriate secondary antibody was used. Secondary antibodies included donkey anti-rabbit fluorescein isothiocyanate (FITC) and anti mouse Cy3. DNA was counterstained with 1μg/ml 1,4,6- diamidino-2-phenylindole (DAPI, Sigma, St.Louis, MO). F-actin were stained with Texas-Red or Cy5- conjugated phalloidin (Sigma, St.Louis, MO). When anti-pMAL-LIMK1 (f.l) was

used as a primary antibody, biotinylated secondary antibody and subsequently an antibody with streptavidin-conjugated which recognized biotinylated secondary antibody was used. Coverslips were then inverted into 5 μl Vectashield medium (Vector Laboratories). Photografic images were processed using Photoshop 6.0 (Adobe Systems Inc, San Jose, CA).

2.2.11 Preparation of murine kidney tissues for immunohistochemical staining

C57BL/6J mice were obtained from Charles River Laboratoires France. Experimental procedures were designed to conform to the cantonal guidelines. Kidney from euthanized C57BL/6J mice were used for immunohistochemical studies. Tissues were fixed overnight at 4 $^\circ$ C in 10 % formalin, embedded in Paraffin and sectioned at 5-20 μm.

2.2.12 Generation of Orthotopic kidney cancer model

Balb/c female mice were implanted orthotopically with A498-luc cells (5x10^5 cells were injected in the capsule of the left kidney in each mouse). Analgesics were given to the animlas for the first three days after transplantation. For xenogen imaging, animals were anaesthetised. Luciferase substrate solution was then administered (100mg/kg, intraveneous in PBS) and imaging was performed 10 minutes later. After nephrectomy, kidneys were fixed in formalin and embedded into paraffin and processed for immunohistochemistry.

2.2.13 Immunohistochemical studies

Paraffin sections were subjected to de-paraffinization in xylene and subsequently ethanol series. After incubation in PBS (+ 0.3 % Triton X-100) for 20 minutes, sections were subjected for 10 minutes to 97 $^\circ$ C in 10 mM Citrate Buffer pH 6.0 for antigen retrieval and slides were then left to cool down by standing for at least 20 minutes at room temperature. Short incubation in PBS at RT

was followed by incubation for 30 minutes in 3% H_2O_2 / 10 % methanol to block endogenous peroxidases. After short washes in PBS sections were pre-incubated with 10 % normal goat serum (NGS; Vector Laboratories) in PBS (+ 0.3 % Triton X-100) for 30 minutes. Incubation with primary antibody was allowed over night at 4 ° C or for 2 hours at RT. For ABC stainings the anti-rat-LIMK1, anti-cofilin and anti-P-cofilin antibodies were diluted 1:50.

ABC staining: After 3 washes of 5 minutes in PBS (+ 0.3 % Triton X-100) sections were incubated with biotinylated goat ?-rabbit diluted 1:200 in 10 % NGS in PBS. Colometric detection using the ABC Elite Kit (Vector Laboratories) was performed according to manufacturerÕs instructions. Slides were counterstained with hematoxylin and finally mounted using Mowiol.

Immunofluorescent staining: Sections were washed in PBS (+ 0.3 % Triton) and incubated for 1 hour at room temperature with FITC-labeled secondary antibodies. After shortly rinsing the slides in H_2O, sections were coverslipped with Vectashield (Vector Laboratories). Propidium iodide was used as a nuclear marker.

2.3 Time-Lapse Video Microscopy

For live microscopy, cells were cultured in CO_2 independent medium (Invitrogen) into glass bottomed 2 well chambers (Millipore) and imaged at 37 ° C on a DeltaVision Deconvolution microscope in GFP- optimized filter set. Images were taken every 3 minutes , for 8-10 hours. Pictures were captured using SoftWorx software and saved as movie and analyzed using Quicktime program.

Chapter 3

Results

3.1 Endogenous LIMK1 protein levels and localization

3.1.1 Analysis of subcellular localization of LIMK1

When beginning this project, the data on the localization of LIMK1 protein in mammalian cells were limited and the information on LIMK1 has relied mainly on studies with overexpression of tagged LIMK1 protein. In that setting, the over-expressed LIMK1 was shown to be mainly cytoplasmic. Moreover, use of mutants lacking PDZ domain demonstrated that its localization depends on the nuclear export signal in the PDZ domain [Yang et al., 1998a].

Past work in our laboratory involved generation of polyclonal antibodies raised against full length human LIMK1 fused to maltose binding protein (MAL) termed as anti-pMAL-LIMK1(f.l.) and against T508-phosphopeptide of LIMK1, termed as anti-T508-P. The phosphopeptide is identical in sequence to both LIMK1 and LIMK2, meaning that, it might recognize both phosphorylated forms of LIMK1 and LIMK2. Upon affinity purification, anti-pMAL-LIMK1(f.l.) detected a single band around 72 kDa in western blotting of extracts of various human cell lines (unpublished data from former postdoc of the laboratory, Joanna Lisztwan). Even though recognition

of LIMK1 specifically by anti-pMAL-LIMK1(f.l.) in Western Blotting was characterized, the subcellular localization of LIMK1 was not tested in detail. For that reason, the detection of LIMK1 in additional human and mouse cell lines by Western blotting, and the detailed analysis of subcellular localization of LIMK1 by immunofluorescence was performed.

3.1.1.1 LIMK1 protein levels in various human and mouse cancer cell lines

The total levels of LIMK1 protein was detected by Western blotting in whole cell lysates of renal cell carcinoma cell lines (MM4, Cl4, Cl8, A498), prostate cancer cell lines (PC3, LnCAP, Du145), mouse neuroblastoma cell lines (Neuro 2A, N1E-115), and mouse NIH3T3. Anti-pMAL-LIMK1(f.l.) antibody detected both human and mouse origin LIMK1 in these cell lines. Overexpressed GFP-LIMK1 was used as a positive control (figure3.1).

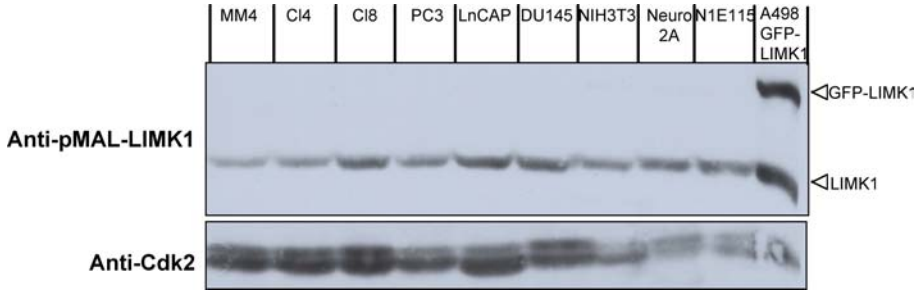

Fig. 3.1: **LIMK1 protein levels in human and mouse origin cell lines**. Whole cell lysates of renal cell carcinoma cells (MM4, Cl4, Cl8), prostate cancer cell lines (PC3, LNCaP, DU145),mouse NIH3T3 cell line, mouse neuroblastoma cell lines (Neuro 2A, N1E-115), and kidney cancer cell line A498 transfected with GFP-LIMK1 in order (lane1-10) were separated on a 10% SDS-PAGE gel and processed for Western blotting using anti-pMAL-LIMK1(f.l) antibody and Cdk2 antibody (loading control). The arrow indicated the position of LIMK1 and GFP-LIMK1. The WB shown are representative of 3 independent experiments

No difference was detected in total LIMK1 protein levels in the renal cell carcinoma cell lines with different migratory potentials (MM1high metastatic, Cl4, Cl8 low metastatic). Additionally, LIMK1 protein levels were high in tumorigenic (LNCaP) and metastatic (PC3 and DU145) cell lines as suggested before [Davila et al., 2003]. Furthermore, in mouse neuroblastoma cell lines protein level of LIMK1 was slightly higher than mouse embryonic fibroblast cell lines which is

consistent with high expression of LIMK1 in neurons [Foletta et al., 2004].

3.1.1.2 Endogenous LIMK1 localization is mainly cytoplasmic

To investigate the subcellular localization of LIMK1, indirect immunostaining experiments were performed using anti-pMAL-LIMK1(f.l.) antibody. The visualization of LIMK1 was performed in HeLa, U2OS and 7860 cells after paraformaldehyde fixation and triton permeabilization (PFA/triton). To overcome the relatively low staining with anti-pMAL-LIMK1(f.l) antibody, it was amplifed using the biotin-streptavidin system (for detailed information, see materials and methods section). The drawback of this system is that it can increase the background signal. For that reason, the specificity of the LIMK1 signal was confirmed by pre-incubation of anti-LIMK1 antibody with the 10X immunizing antigen (with an p-MAL tagged LIMK1 protein (expressed in bacteria)). The competitor removed all specific staining in all three cell lines tested (figure 3.2, 3.3, 3.4, '10X competition panels').

From the stainings, LIMK1 was found to be cytoplasmic with a stronger perinuclear signal confirming previous exogenous approaches using tagged-LIMK1 which showed that LIMK1 is mainly cytoplasmic. Even though, in the LIMK1 protein structure, there is nuclear localization signal, it is cytoplasmic due to the nuclear export signal in PDZ domain [Foletta et al., 2004]. Additionally, localization to cell membrane was observed (figure 3.2, 3.3, 3.4, 'no treatment panels').

3.1.1.3 Co-localization studies of LIMK1 using anti-pMAL-LIMK1 (f.l) antibody

In order to investigate more in detail where LIMK1 localizes in cytoplasm, co-localization experiments were performed with tubulin (anti-tubulin (Y/L1-2)), mitochondria (mitotraker) and Golgi (anti-AP1) in 7860 cells (figure 3.5). In 7860 cells a perinuclear staining in addition to membrane staining was found. Co-localization studies with tubulin, mitotraker and Golgi marker showed a

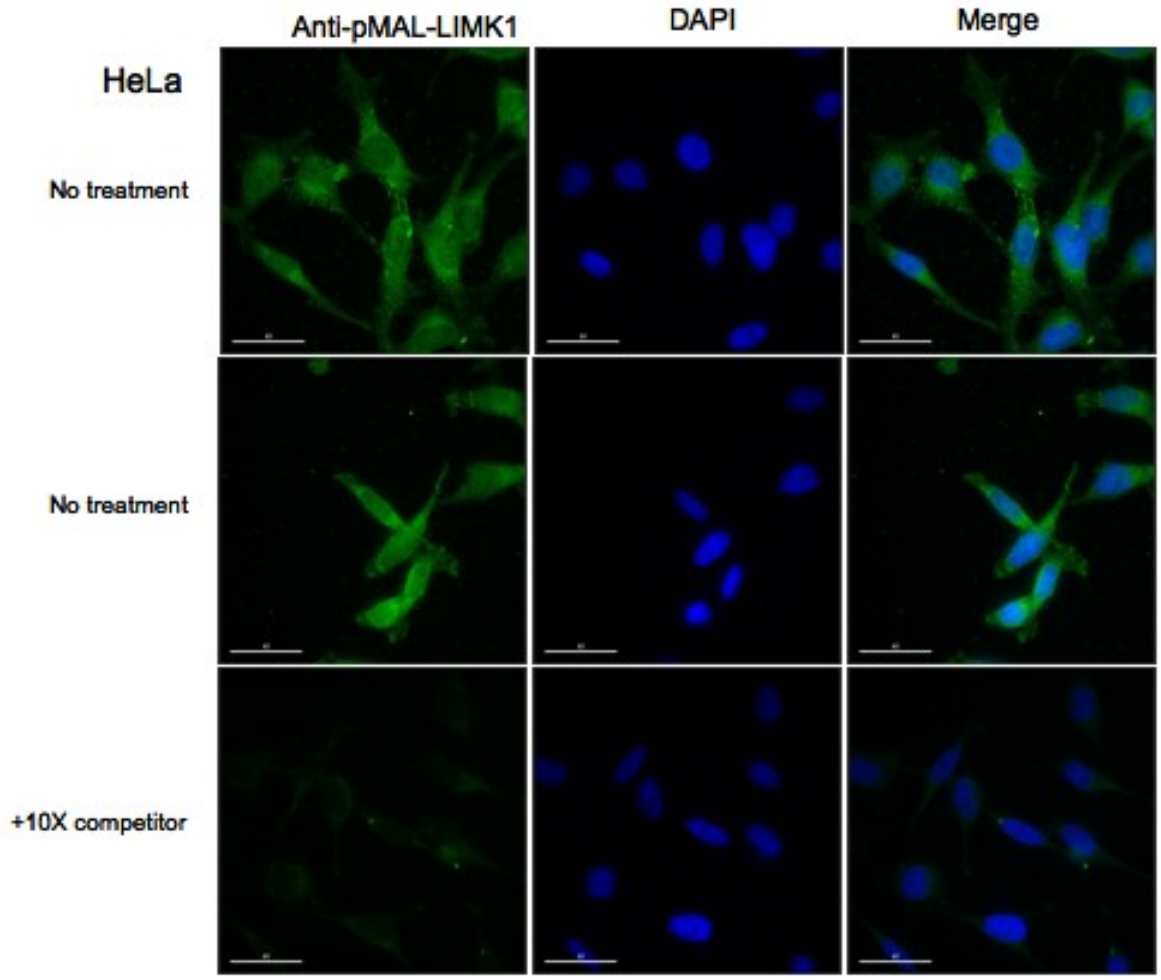

Fig. 3.2: **Subcellular localization of LIMK1 in HeLa cells**. HeLa cells were stained with anti-pMAL-LIMK1 (f.l) antibody after PFA/triton fixation. For competition experiments 10X immunizing antigen was incubated with primary antibody before applying in immunostaining. Slides were processed by Deltavision microscope. Green:anti-pMAL-LIMK1 (f.l), Blue: DAPI. Images are representative of 3 independent experiments. Scale bar 15 μm.

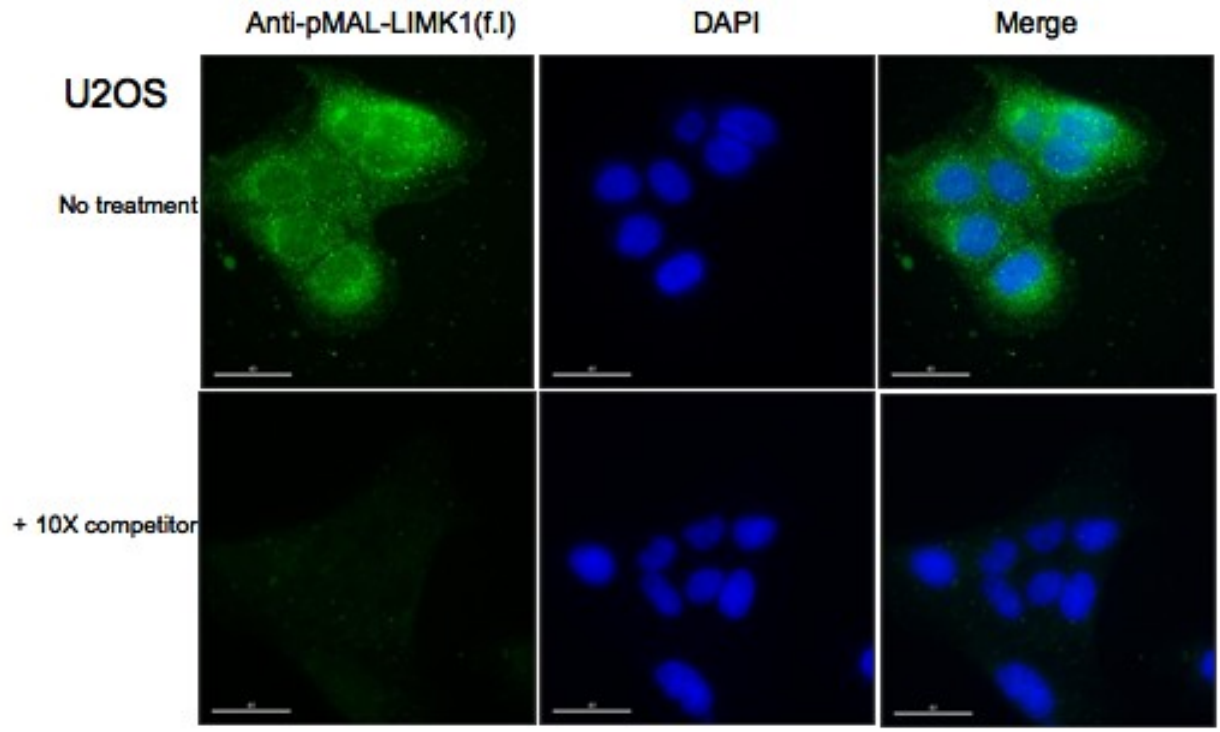

Fig. 3.3: **Subcellular localization of LIMK1 in U2OS cells**. U2OS cells were stained with anti-pMAL-LIMK1 (f.l) antibody after PFA/triton fixation. For competition experiments 10X immunizing antigen was incubated with primary antibody before applying in immunostaining. Slides were processed by Deltavision microscope. Green:anti-pMAL-LIMK1 (f.l), Blue: DAPI. Images are representative of 3 independent experiments. Scale bar 15 μm.

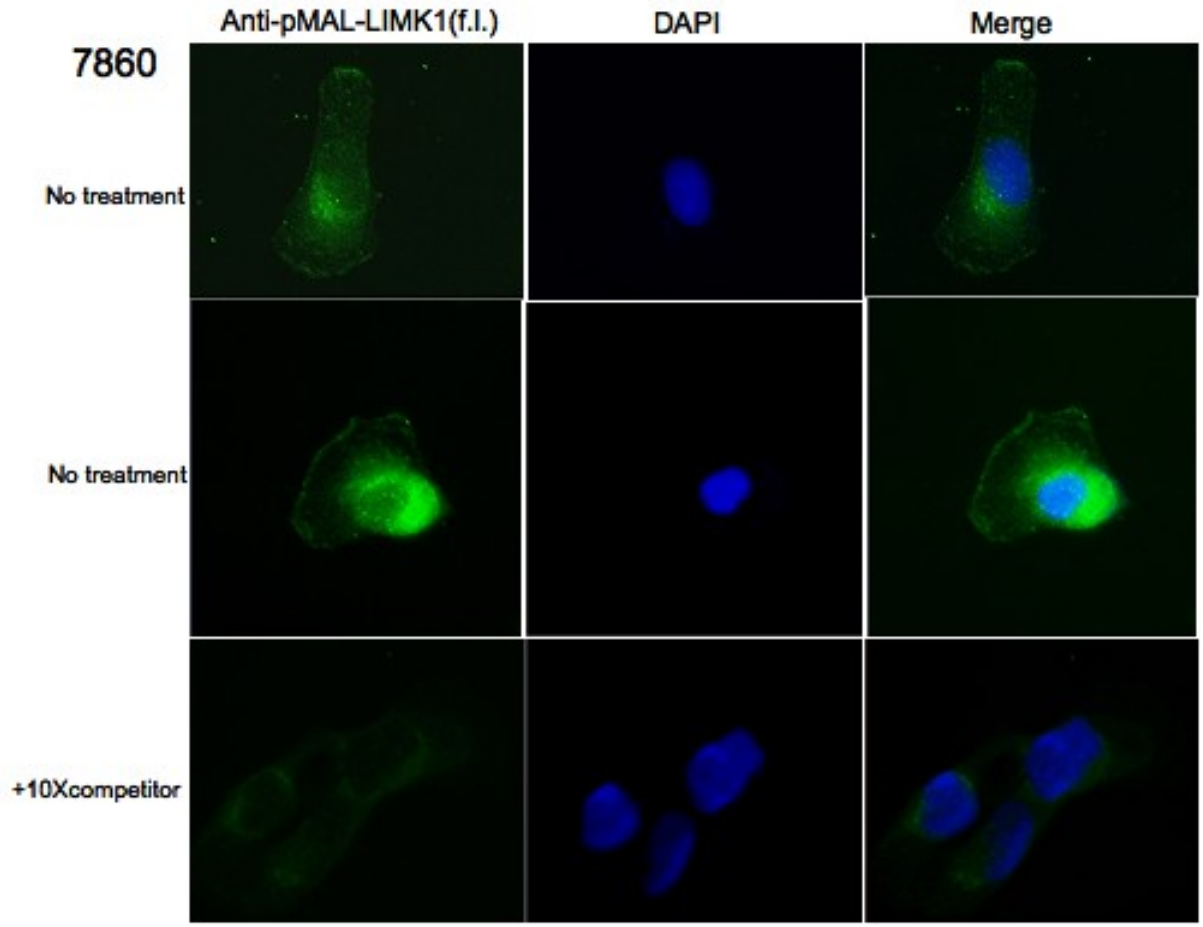

Fig. 3.4: **Subcellular localization of LIMK1 in 786O cells**. 786O cells were stained with anti-pMAL-LIMK1 (f.l) antibody after PFA/triton fixation. For competition experiments 10X immunizing antigen was incubated with primary antibody before applying in immunostaining. Slides were processed by Deltavision microscope. Green:anti-pMAL-LIMK1 (f.l), Blue: DAPI. Images are representative of 3 independent experiments.

partial but specific co-localization of them with LIMK1 suggesting that LIMK1 can localize to microtubules, mitochondria and Golgi apparatus. Interestingly, even though, there was a partial but specific co-localization with LIMK1 and tubulin in 7860 cell, no co-localization was detected in HeLa and U2OS cells. Given the fact that, LIMK1 colocalizes with tubulin in human vascular endothelial cells (HUVEC), the missing co-localization in HeLa and U2OS cells may be because of a cell-type specific co-localization [Gorovoy et al., 2005]. Limitations with the antibody did not allowed for a more detailed analysis.

3.1.1.4 LIMK1 and LIMK2 subcellular localization using anti-LIMK1(J) and anti-LIMK2 (J)antibodies

A recent collaboration with T.Nakamura, Japan, made it possible to investigate the subcellular localization of LIMK1 (anti-LIMK1(J)) more in detail, additional to using anti-pMAL-LIMK1 (f.l) in HeLa, U20S and 7860 cells [Sumi et al., 2006]. Since the stainings with these antibodies were relatively higher than anti-pMAL-LIMK1 (f.l), no biotin-streptavidin system was used.

By using anti-LIMK1(J) antibody, a similar localization of LIMK1 was observed as by anti-pMAL-LIMK1 (f.l), such that a cytoplasmic staining with perinuclear and membrane staining which was in the direction of movement (in lamellipodia). Additionally, with this antibody, some vesicles in the cytoplasm were stained in most of 7860 cells and some of HeLa and U2OS cells (figure 3.6). Also, some filamentous staining of LIMK1 was observed in 7860 cells which needs further investigation.

LIMK2 is a member of LIMK family and is activated by phosphorylation by Rho GTPases in its kinase domain (T505) and regulates the cofilin activity by phosphorylation similar to LIMK1. Even though, the similarities between LIMK1 and LIMK2, there are some differences in their localization in the cell since it was reported recently that LIMK2 localizes to mitotic spindles during early M-phase and to midbody during late M-phase, whereas LIMK1 localizes to spindle

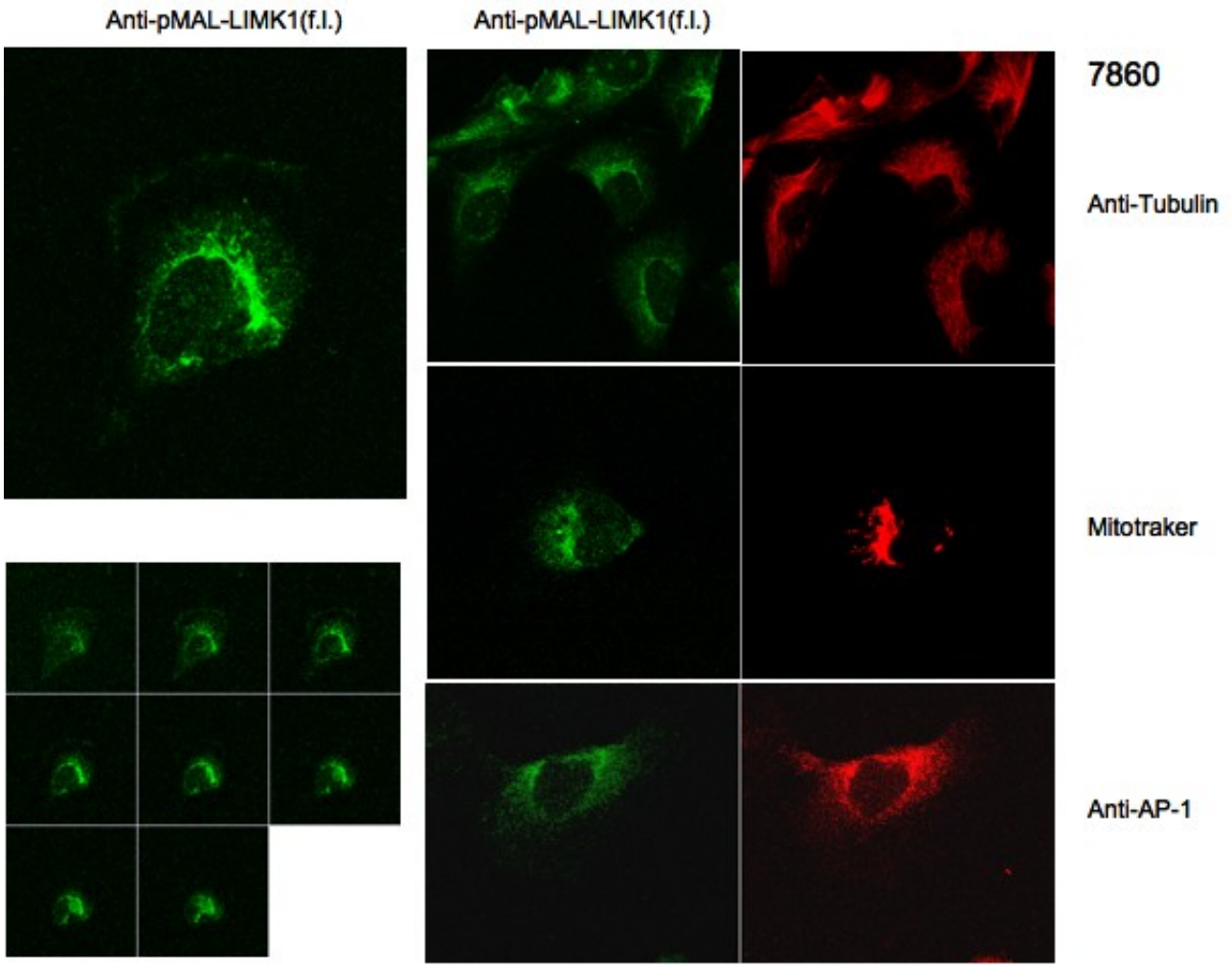

Fig. 3.5: **Co-localization experiments of LIMK1 with tubulin, mitochondria and golgi**. 7860 cells were co-stained with anti-pMAL-LIMK1 (f.l) antibody and either anti-tubulin (YL1/2), mitotracker or anti-AP1 (golgi marker) after PFA/triton fixation. Slides were processed by confocal microscopy. Green:anti-pMAL-LIMK1 (f.l), Red: Antibodies as depicted in the figure. Images are representative of 3 independent experiments.

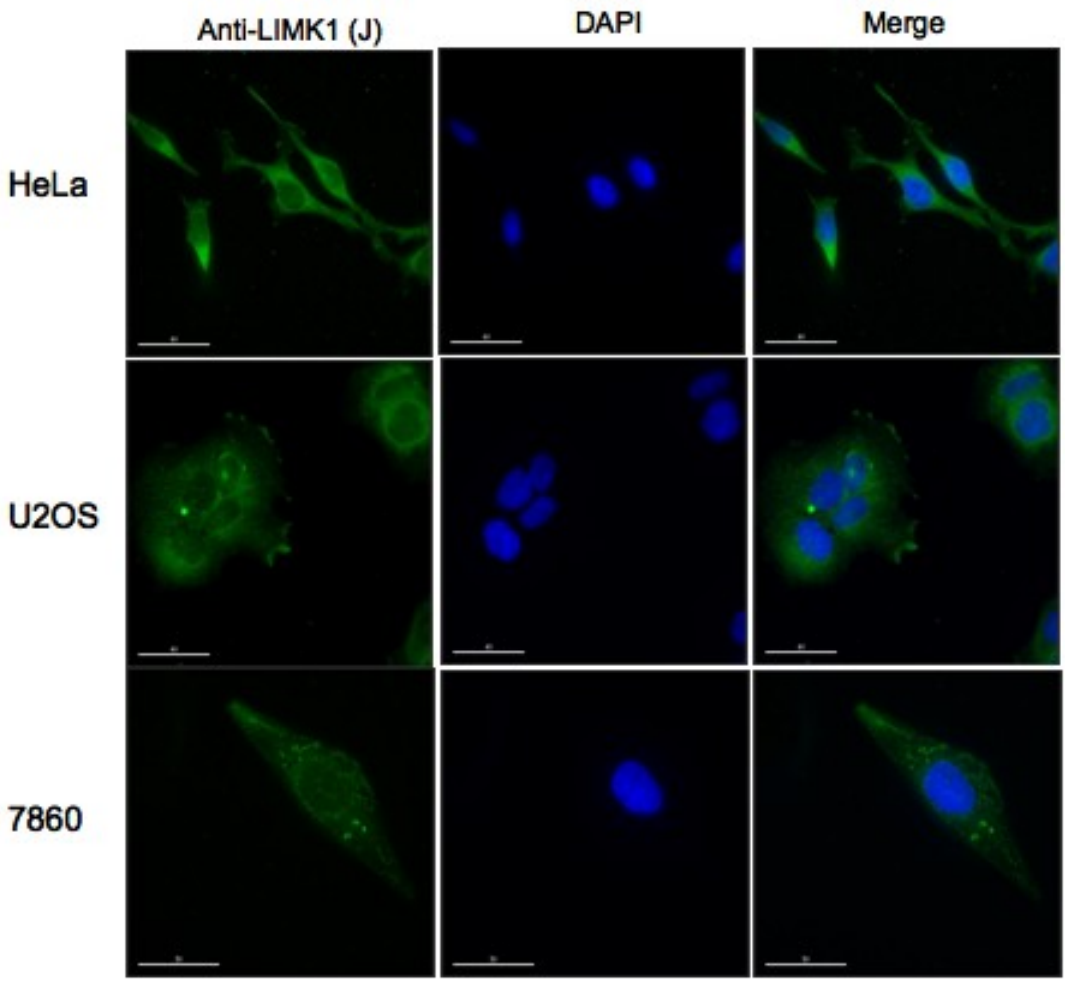

Fig. 3.6: **Subcellular localization of LIMK1 using anti-LIMK1(J)antibody in HeLa, U2OS and 7860 cells**. All three cell lines were fixed with PFA/triton and labeled using anti-LIMK1(J) antibody. Slides were processed using DeltaVision microscope. Green: anti-LIMK1(J), Blue: DAPI. Images are representative of 3 independent experiments. Scale bar 15 μm.

poles during early M-phase and to midbody during late M-phase [Sumi et al., 2006]. To elucidate the subcellular localization of LIMK2, LIMK2 (J) antibody was used. As shown in figure 3.7, localization of LIMK2 to cytoplasm and nucleus was observed in HeLa, U2OS and 7860 cells. LIMK2 also localizes to the membrane in the direction of movement. The difference between LIMK1 and LIMK2 was the localization of LIMK2 to nucleus (figure 3.7).

Altogether, by using LIMK1 and LIMK2 antibodies, subcellular localization of total proteins were investigated and cytoplasmic and membrane staining for both LIMK1 and LIMK2 with an additional nuclear staining of LIMK2 was determined.

Additional to that, in order to assess the localization of active LIMK1 and LIMK2, an antibody which recognized a common phospho-peptide in LIMK1 and LIMK2, anti-T508-P, was used for immunostainings in HeLa and U2OS cells. Similar to the findings from LIMK1 and LIMK2 stainings, with anti-T508-P antibody there was a strong staining in cell membrane, mainly in lamellipodia (figure 3.8). Until recently, the function of LIMK1 was not known in directional cell migration since the unphosphorylated active form of cofilin was found in lamellipodia and mediated lamellipodium extension and polarized cell migration, which suggested that LIMK1was inactive in leading edge of migrating cell [Dawe et al., 2003]. However, LIMK1 was shown to be needed for SDF-1 α- induced chemotaxis of T cells [Nishita et al., 2002]. This ambiguity disappeared when it was reported recently that LIMK1 activity was needed in stimulating the lamellipodium formation in the initial stages of cell response and that cofilin and LIMK1 phosphatase SSH-1L was involved in directional cell migration. Both of the functions of LIMK1 and SSH-1L was performed through cofilin phosphorylation and dephosphorylation, respectively [Nishita et al., 2005].

Our findings about phospho-LIMK1 localization in lamellipodia is consistent with the idea that LIMK1 functions for phosphorylation of cofilin in lamellipodia for directional cell migration.

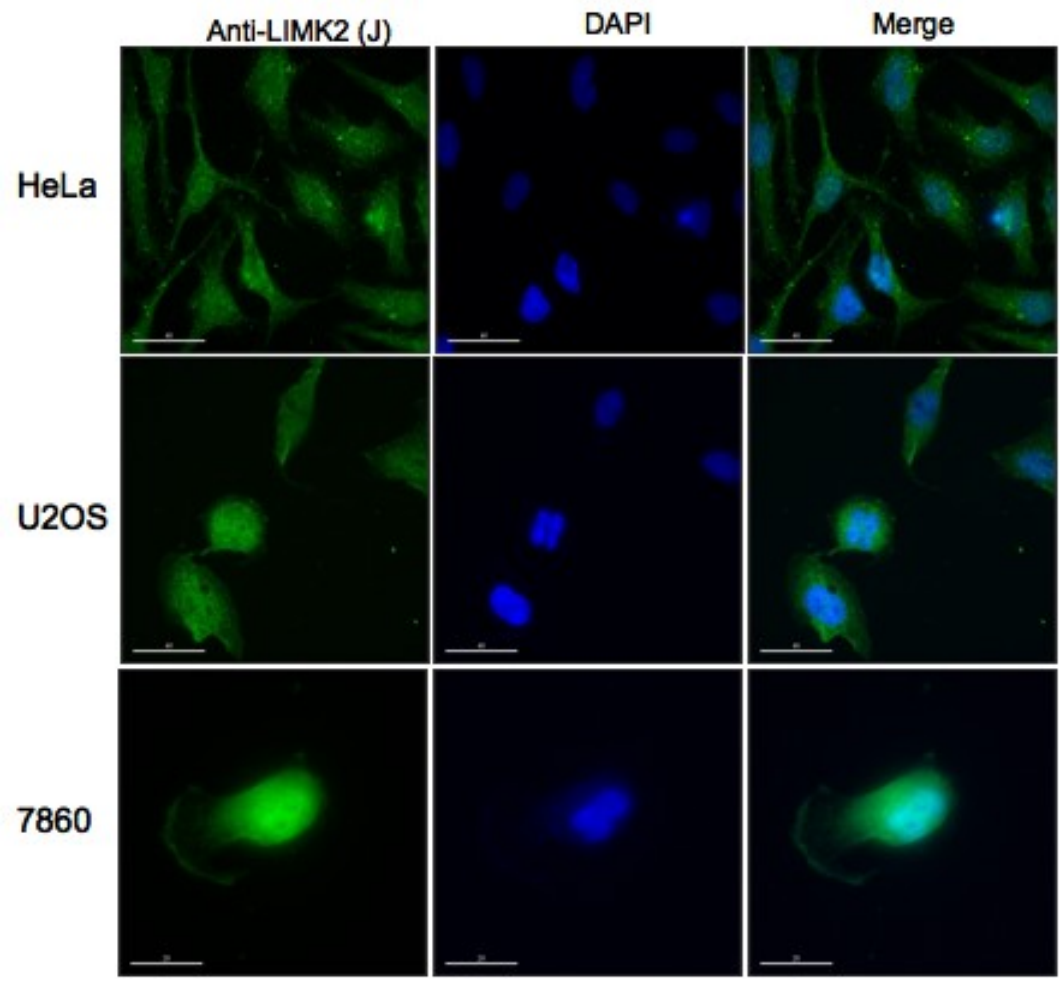

Fig. 3.7: **Subcellular localization of LIMK2 (J) using anti-LIMK2 antibody in HeLa, U2OS and 7860 cells**. All three cell lines were fixed with PFA/triton and labeled using anti-LIMK2(J) antibody. Slides were processed using DeltaVision microscope. Green: anti-LIMK2(J), Blue: DAPI. Images are representative of 3 independent experiments. Scale bar 15 μm.

Moreover, given the differential staining between anti- LIMK1, anti- LIMK2 and anti- T508- P, one can propose that only active LIMK2 is present in the nucleus. These results suggests that there is phosphorylated active form of LIMK2 in the nucleus, which may open new perspectives about a novel role of LIMK2 in nucleus.

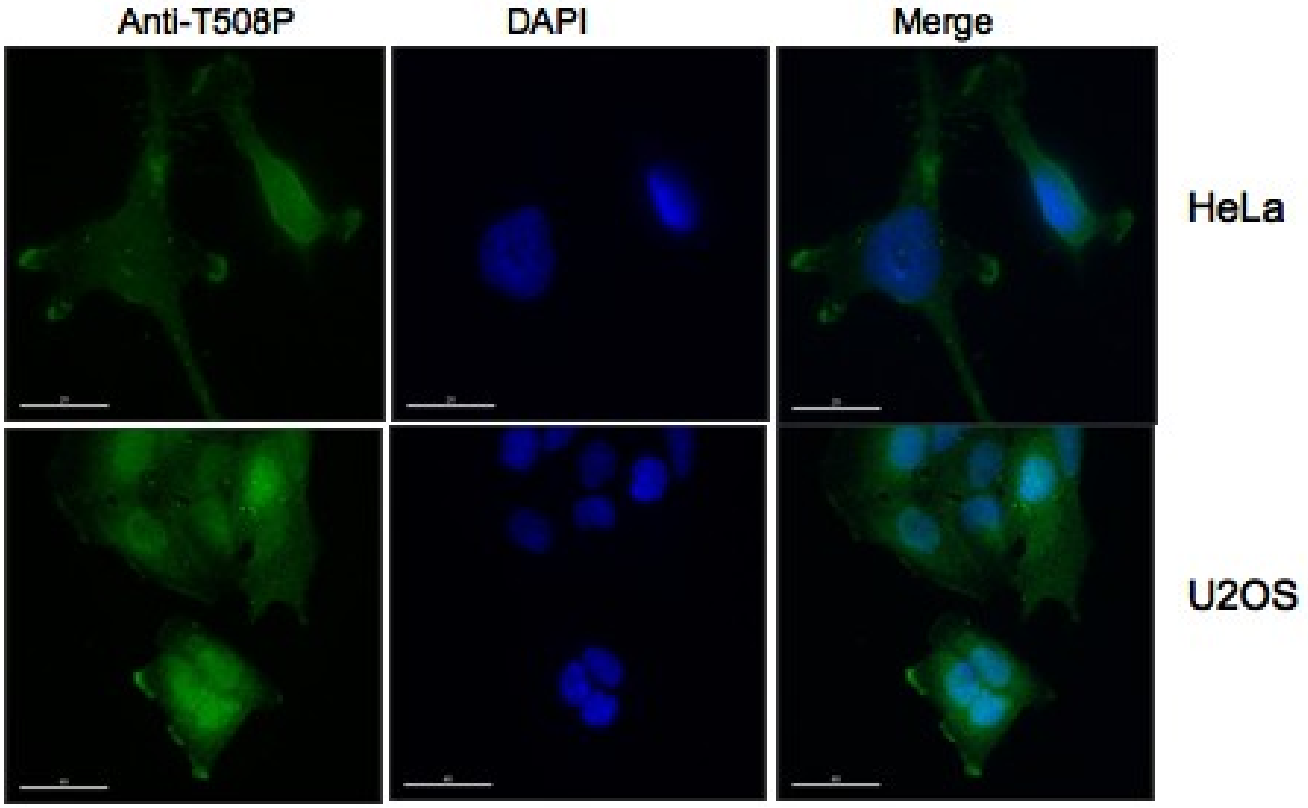

Fig. 3.8: **Subcellular localization of p-LIMK1/2 using anti-T508-P antibody in HeLa and U2OS cells**. Both of the cell lines were fixed with PFA/triton and labeled using anti-T508-P antibody. Slides were processed using DeltaVision microscope. Green: anti-T508-P, Blue: DAPI. Images are representative of 3 independent experiments. Scale bar 15 μm.

3.1.1.5 LIMK1 is found in crude mitochondrial fraction

In addition to the localization studies using immunostaining, a cellular fractionation assay was performed to elucidate the distribution of LIMK1. HeLa cells were homogenized and fractionated by differential centrifugation to nuclear, cytoplasmic and mitochondrial fractions and sub-

sequently were analyzed by Western Blotting with antibodies specific for LIMK1, and organelle marker proteins (figure 3.9(a)). The purity of fractions were confirmed using antibodies against nuclear (lamin), cytoplasmic (tubulin) and mitochondrial (prohibitin) marker proteins. LIMK1 was shown to be in cytoplasmic fraction and not detected in nuclear fraction which was consistent with the findings from microscopic studies. Additionally, it was found to be in crude mitochondrial fraction, confirming the colocalization with mitotracker.

In order to elucidate further the localization of LIMK1 in mitochondria, the crude mitochondrial fractions were subjected to proteinase K digestion. As shown in figure 3.9(b), all of LIMK1 was degraded by 5 μg/ml proteinase K treatment. Interestingly, the phosphatase of LIMK1 and cofilin; SSH1-L was also found in mitochondrial fraction and in the outer membrane as it was degraded also by 5 μg/ml proteinase K treatment. Cofilin in this fractionation was shown to be only in cytoplasmic fraction which was consistent with previous findings from Chua et al. showing that cofilin was found in cytoplasm and translocates to mitochondria upon apoptotic stimuli [Chua et al., 2003].

These results indicated that mitochondria-resided LIMK1 is mainly located in the outer membrane, but is not associated with the intermembrane space, inner membrane and matrix.Since, as low as 5 μg/ml of proteinase K was enough to degrade LIMK1 and SSH1L, this may suggest that the localization of both proteins to mitochondria are not strong. Additionally, since this is a crude mitochondrial fraction, a proportion of LIMK1 in this fraction can be contaminants from other organelles such as golgi or endoplasmic reticulum which need to be further investigated. Indeed, there are studies showing the localization of LIMK1 to golgi vesicles that supports this idea [Rosso et al., 2004]. Also, the existence of SSH-1L mainly in the crude mitochondrial fraction, suggests a role of SSH-1L in LIMK1 regulation in this fraction. Especially, one can hypothesize that LIMK1 is specifically sequestered at mitochondria and inactivated by SSH-1L, which could provide an interesting mechanism of regulation of LIMK1 function.

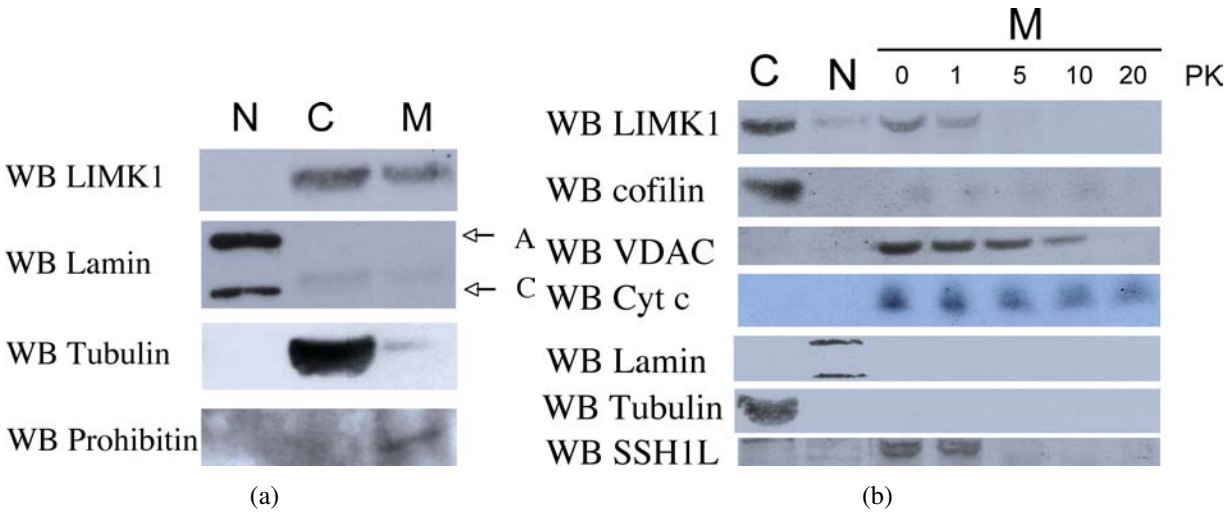

(a) (b)

Fig. 3.9: a)**LIMK1 localizes to mitochondria**; HeLa cells were fractionated into cytoplasmic, nuclear and mitochondrial portions by homogenization and subsequent centrifugation and were analyzed using Western blotting using antibodies against LIMK1, lamin, tubulin and prohibitin. Lamin, tubulin and prohibitin were used as specific marker proteins for nucleus, cytosol and mitochondria respectively. (see materials and methods for detailed information) b)**Mitochondria-resided LIMK1 is mainly located in the outer membrane** Proteinase K (PK) digestion of mitochondrial fraction with 0,1,5,10 and 20 μg/ml PK were performed and the samples were analyzed using Western blotting using antibodies against LIMK1, cofilin, VDAC, cytochrome c, Lamin, tubulin, and SSH-1L. VDAC, Cytochrome c, Lamin and tubulin were used as specific marker proteins for outer membrane, inner membrane, nucleus and cytosol, respectively. N, nuclear fraction; C, cytosolic fraction, and M mitochondrial fraction .

3.1.2 Localization of LIMK1 in mouse tissues

3.1.2.1 Immunohistochemical analysis of LIMK1 in mouse tissues

The immunostaining of LIMK1 of cultured cells indicated a cytoplasmic staining with high perinuclear and membrane stainings. To further elucidate the localization of LIMK1, stainings of LIMK1 in mouse kidney and prostate tissues were investigated using immunohistochemical staining. Moreover, given the role of LIMK1 in cancer progression, we wanted to address the question of potential misregulation of LIMK1 in cancer tumoral tissues.

Introduction: Structure of Kidney

Kidney performs the essential function of removing waste products from the blood and regulating the water fluid levels. Kidney is composed of two layers, an outer layer called cortex and a inner layer called medulla. The functional units of the kidneys, are called nephrons. In nephrons, filtering of the blood and removal of wastes in the form of urine takes place. A nephron, which extends between cortex and medulla, consists of glomerulus, a network of capillaries, where the filtration takes place, and tubules. Glomerulus is contained in a cuplike structure called Bowman's capsule, from which renal tubule extends. There are three types of renal tubules, proximal, distal and collecting tubules. The extension from glomerulus is as the proximal tubule, afterwards it makes a hairpin turn (loop of Henle), it returns to the distal tubule and drains into the collecting tubule. Figure 3.10 shows the anatomical structure and histological section of a kidney with glomerulus, distal and proximal tubules.

To investigate the localization of LIMK1 in mouse kidney, kidney from Balb/c mice, was isolated and embedded to paraffin, then sections were analyzed by immunohistochemical (IHC) analysis with anti-rat-LIMK1 antibody, and by fluorescent IHC with anti-pMAL-LIMK1 antibody (for details see materials and methods section). Initial stainings were performed with anti-pMAL-LIMK1 (f.l) antibody. Although there was low staining of LIMK1 in sections using anti-pMAL-

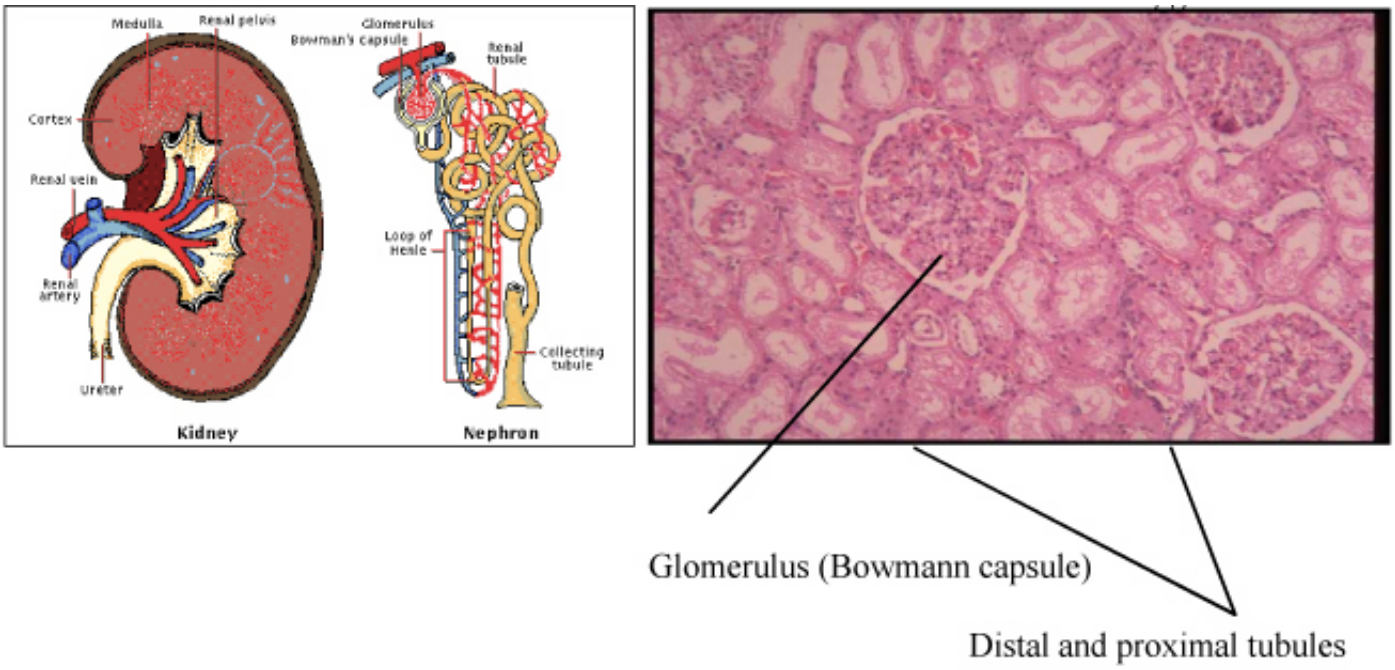

Fig. 3.10: **Anatomy and Histology of Kidney** adapted from http://encarta.msn.com

LIMK1 antibody in IHC, fluorescent IHC made it possible to monitor the LIMK1 staining in mouse kidney tissue. It was shown that , LIMK1 localized to all renal tubules with nuclear and cytoplasmic localization (figure 3.11, B). Later on, the article from Foletta et al. using anti-rat LIMK1 antibody, confirmed our staining ([Foletta et al., 2004] and figure 3.11, A). Additionally, Foletta et al. showed that LIMK1 localized both to nucleus and cytoplasm in various mouse tissues such as lung, testis, and intestine.

These findings, indicated a differential localization of LIMK1 in exponentially growing cells in cell culture, and differentiated (nondividing) cells in tissues, i.e. that LIMK1 is cytoplasmic in cultured cells and both nuclear and cytoplasmic in differentiated cells.

Additional to LIMK1 staining, in order to elucidate the localization of its substrate cofilin, both IHC and fluorescent IHC were performed using anti-cofilin, and anti-p-cofilin antibodies. Anti-cofilin antibody raised against GST-cofilin was generated in our laboratory. Cofilin staining of

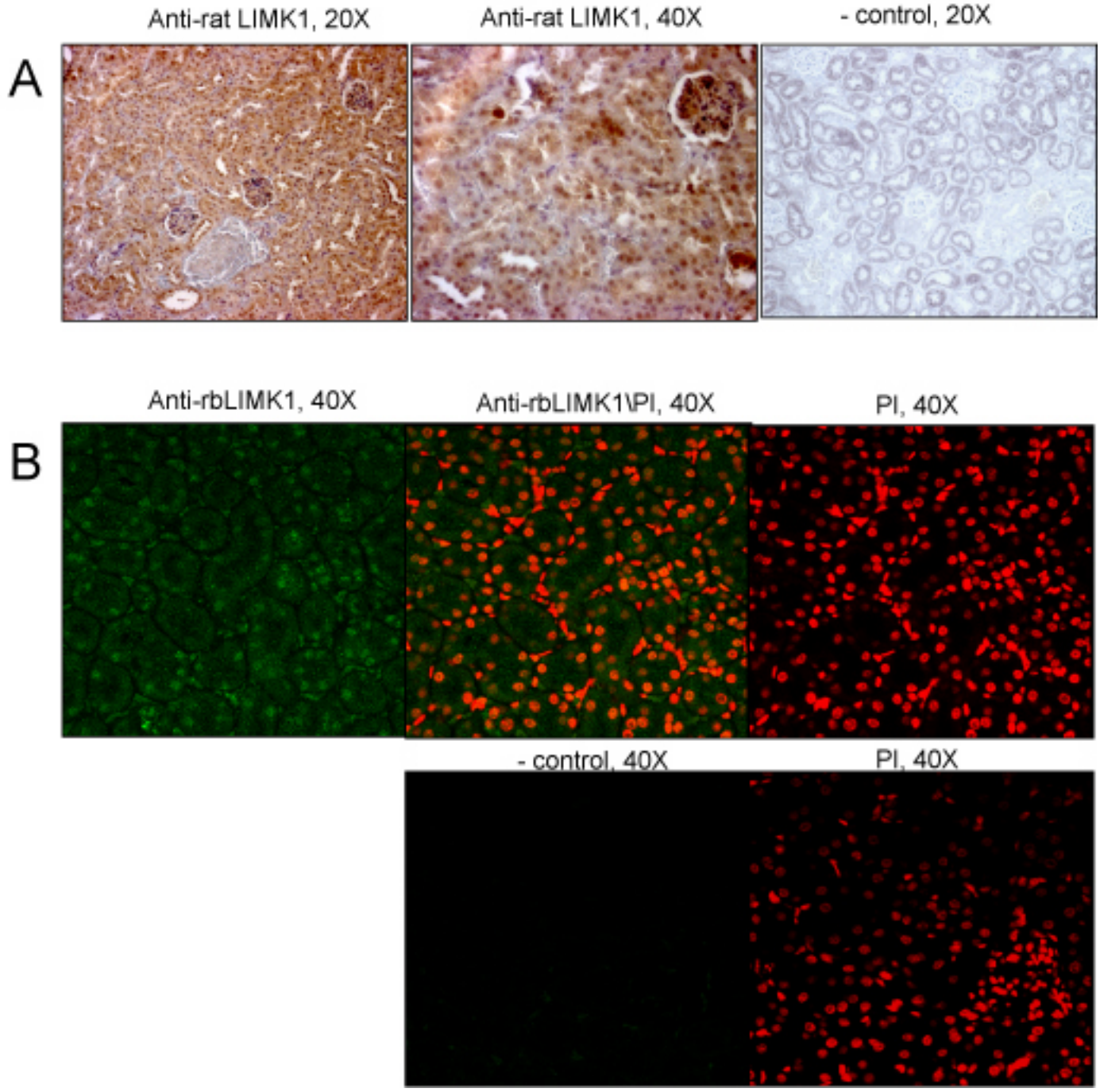

Fig. 3.11: **LIMK1 staining in renal tubules were nuclear and cytoplasmic A.** Immunohistochemical staining of LIMK1 in paraffin-embedded formalin fixed sections from mouse kidney tissues. Sections were stained with anti-rat-LIMK1 antibody. Pictures taken were in 20X and 40X magnification. **B.** The fluorescent immunohistochemical staining of LIMK1 in paraffin-embedded PFA fixed sections from mouse kidney tissues. Sections were stained using anti-pMAL-LIMK1 antibody (green). Nucleus was stained by propidium iodide (PI, red). Pictures taken were in 40X magnification. -control: staining without indicated primary antibodies. Images are representative of 3 independent experiments.

paraffin-embedded formalin fixed sections, showed a diffuse cytoplasmic localization of cofilin in all renal tubules (figure 3.12). The localization of cofilin was similar to the staining of actin-depolymerizing factor (ADF), a factor of the same family as cofilin, that displays identical functions, which was reported previously [Schwartz et al., 1999, Ashworth et al., 2001].

Although, cofilin staining was in all renal tubules, immunohistochemical and fluorescent- IHC stainings using P-cofilin antibody showed a cytoplasmic staining only in some of the tubules (figure 3.13). Because of the structure of the tubules stained, it was proposed that cofilin was mainly phosphorylated in proximal tubules. Previously, it was shown that ADF was dephosphorylated and activated upon ischemia (low oxygen and nutrients)-induced cell injury which was initiated by structural, biochemical and physiological changes in proximal tubules. It was also suggested that, upon ischemia-mediated cell injury, active cofilin relocalized from cytoplasm to apical membrane region of proximal tubule [Schwartz et al., 1999, Ashworth et al., 2001]. These findings may suggest that in proximal tubules, cofilin is found mainly in its inactive phosphorylated form and pathological conditions such as ischemia caused its activation and relocalization.

3.1.2.2 Immunohistochemical analysis of LIMK1 in orthotopic kidney cancer model

An orthotopic kidney cancer model was generated by collaboration with Novartis Oncology department. Luciferase-expressing renal cell carcinoma cell lines, A498-luc (under CMV promoter), that were used in this study, were generated by a former postdoc Dr. Peter Staller. A498 cells are VHL-deficient cell lines. These cells were used for creating this model, as loss of VHL is found in many renal cancers, and that SDF1/CXCR4 mediated activation of LIMK1 is suppressed by VHL reintroduction [Staller et al., 2003].

A498-luc cells were generated, screened for bioluminescence, and injected into kidney subcapsule of severe combined immunodeficient mice (SCID) (figure 3.14). 14, 22 and 28 days after orthotopic A498-luc injection, growth of luciferase-expressing carcinoma cells were monitored

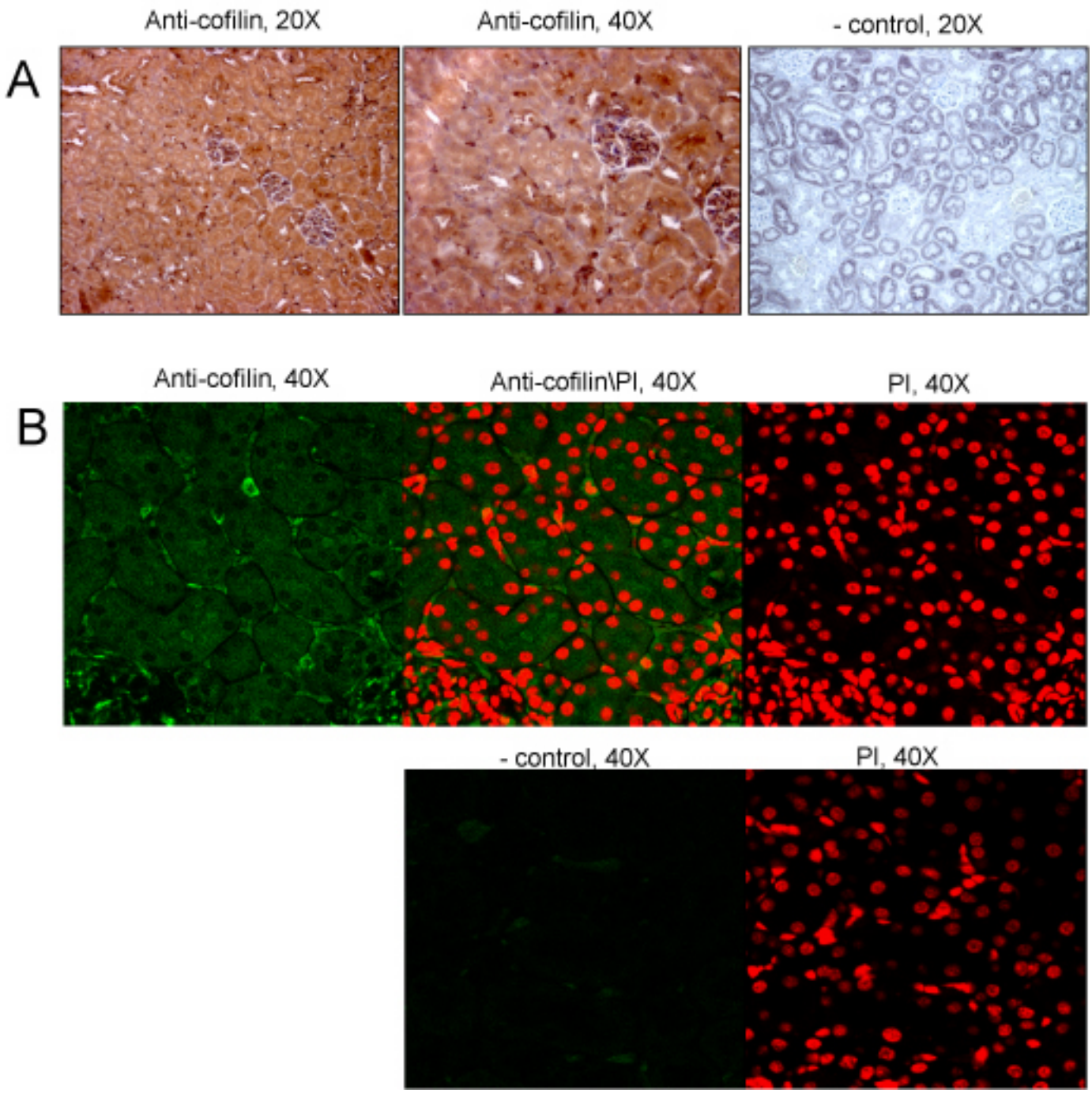

Fig. 3.12: **Cofilin localized in cytoplasm of renal tubules**. **A.** The immunohistochemical staining of cofilin in paraffin-embedded formalin fixed sections from mouse kidney tissues. Sections were stained with anti-cofilin antibody. Pictures taken were in 20X and 40X magnification. **B.** The fluorescent immunohistochemical staining of cofilin in paraffin-embedded PFA fixed sections from mouse kidney tissues. Sections were stained using anti-cofilin antibody (green). Nucleus was stained by propidium iodide(PI, red). Pictures taken were in 40X magnification. -control: staining without indicated primary antibodies. Images are representative of 3 independent experiments.

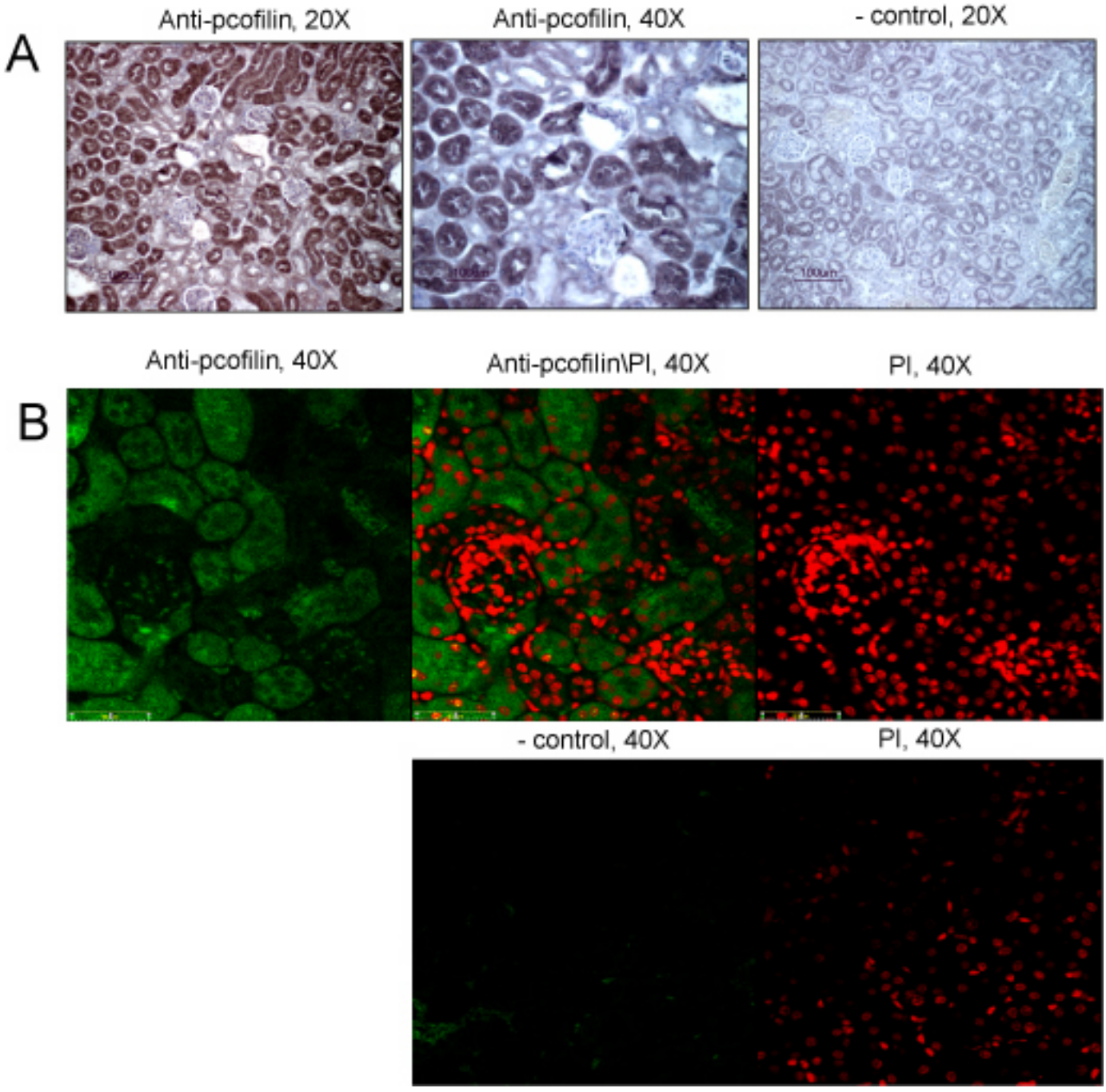

Fig. 3.13: **Phospho-cofilin localized only in cytoplasm of renal tubules**. **A.** The immunohistochemical staining of phosph-cofilin in paraffin-embedded formalin fixed sections from mouse kidney tissues. Sections were stained with anti-P-cofilin antibody. Pictures taken were in 20X and 40X magnification. **B.** The fluorescent immunohistochemical staining of phospho-cofilin in paraffin-embedded PFA fixed sections from mouse kidney tissues. Sections were stained using anti-P-cofilin antibody (green). Nucleus was stained by propidium iodide(PI, red). Pictures taken were in 40X magnification. -control: staining without indicated primary antibodies. Images are representative of 3 independent experiments.

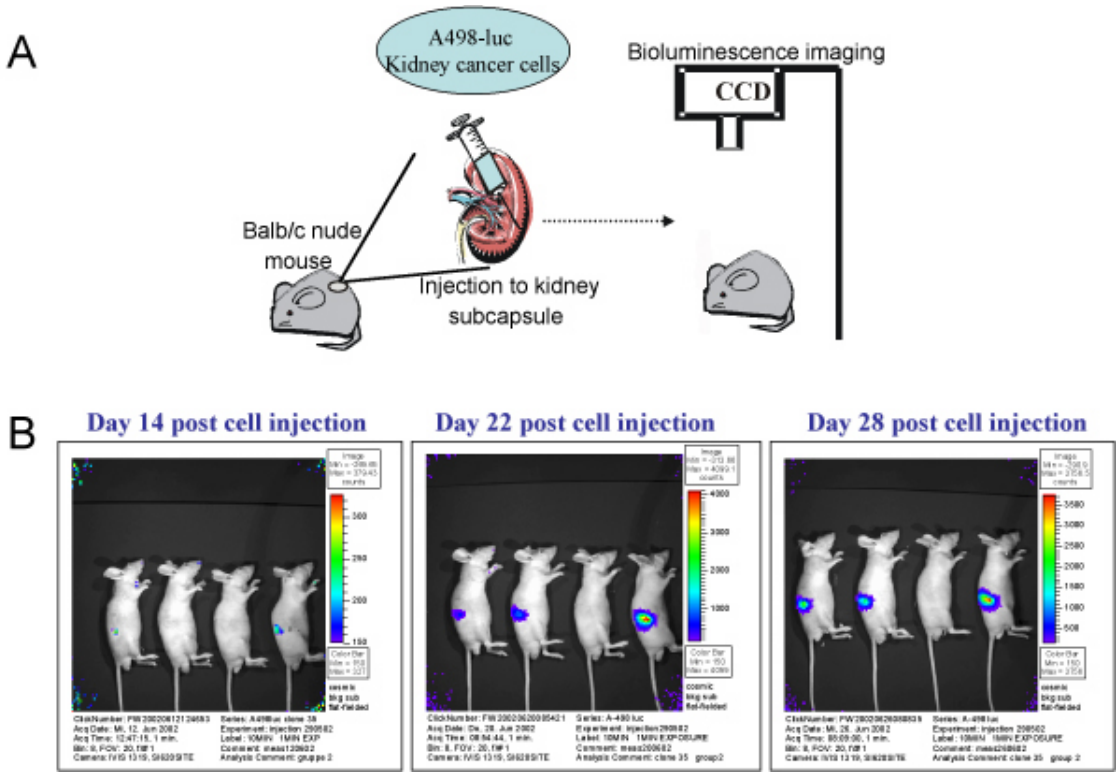

Fig. 3.14: **Generation of A498-luc orthotopic kidney cancer model**. **A.** Schematic representation of cellular orthotopic injection of cell suspension and imaging by Xenogen. **B.** Serial images of representative mice with a A498-luc kidney tumor.

using bioluminescence imaging (Xenogen). There were indications of primary tumor formation. Following that, 2 months after injection, one kidney was removed by nephrectomy, formalin fixed and paraffin embedded. Finally, 6 months after injection, mice were euthanized, the presence of metastases was examined using ex vivo imaging of organs. However no metastases were monitored (data not shown). Figure 3.14 summarize the formation of orthotopic kidney cancer model with A498-luc cells and the bioluminescence imaging of 4 mice. In total 70 animals were used for this project.

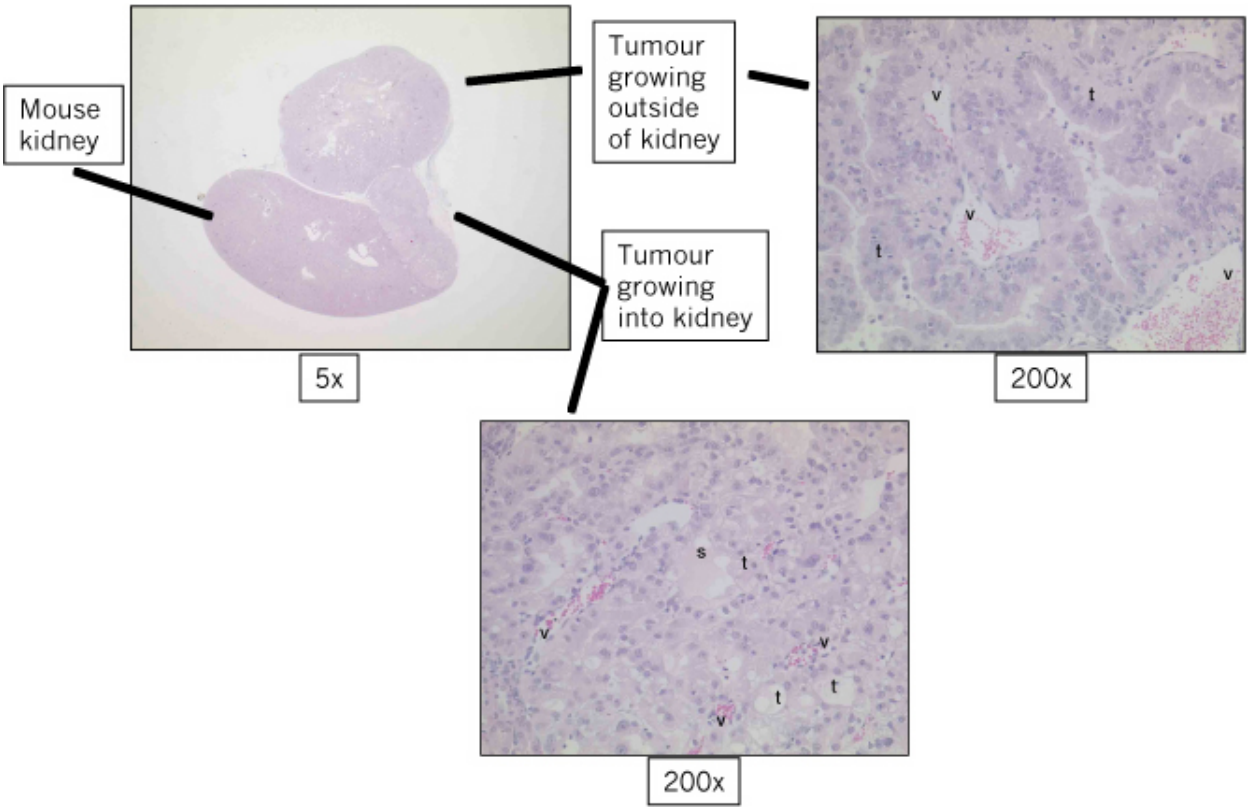

Fig. 3.15: ***Ex vivo*** **imaging of kidney tissue confirmed the primary tumor formation into and outside of mouse kidney**. Mouse kidney was sectioned, stained with hematoxylin & eosin, and photographed (5X magnification of whole kidney, 200X magnification of tumor growing into kidney (transition zone[tz]) and tumor growing outside of kidney) Abreviations: v: vessel, t,: tumor, s: secretion.

Figure 3.15 shows hematoxylin and eosin (H+E) staining of mouse kidney, with a tumor growing

into mouse kidney (transition zone between kidney and tumor) and the tumor growing outside of kidney. Hematoxylin stains the nuclear heterochromatin blue and eosin stains the cytoplasm in pink. In transition and tumor zones, tumor cells grow in lobules or tubules surrounded by a dense network of blood vessels. Some of tumors also showed secretory activity.

Since LIMK1 showed cytoplasmic staining in exponentially growing cells, and both nuclear and cytoplasmic staining in differentiated cells in kidney, it was intriguing to investigate whether there was a localization change between normal kidney and in tumor. The LIMK1 immunohistochemical staining was performed using anti-rat LIMK1 antibody of the mouse kidney with transition zone and tumor (figure 3.15). As it was indicated in the previous section, LIMK1 localized to nucleus and cytoplasm of renal tubules of mouse kidney (figure 3.16). However it was monitored that both in transition zone(TZ) and in the tumor there was mainly cytoplasmic staining. It was observed that in TZ, the staining of LIMK1 was lower than the normal kidney and in tumor, which may suggest the LIMK1 didn't have a role in initial changes. These results support the possible relocalization of LIMK1 from nucleus to cytoplasm in proliferating cancer cells.

To elucidate if there was difference in activity of LIMK1, the staining of phospho-LIMK1/2 was performed using anti-T508-P antibody (figure 3.17). Even though, few renal cells were stained with this antibody in normal kidney and TZ, there was high cytoplasmic staining in most of the tumor cells. These data showed that LIMK activity increased in kidney tumor cells. However additional analysis of LIMK2 need to be done for detailed analysis since anti-T508-P antibody recognized both LIMK1 and LIMK2.

Additionally, the cytoplasmic localization of p21 in tumor cells were tested to investigate the development of neoplasm. The reason behind using p21 as a positive cancer marker is as follows: p21 is a downstream target of p53, and it reenforced G1 and G2 arrest following genotoxic insults, to facilitate DNA repair. The nuclear localization of p21 is required for the integrity of G1

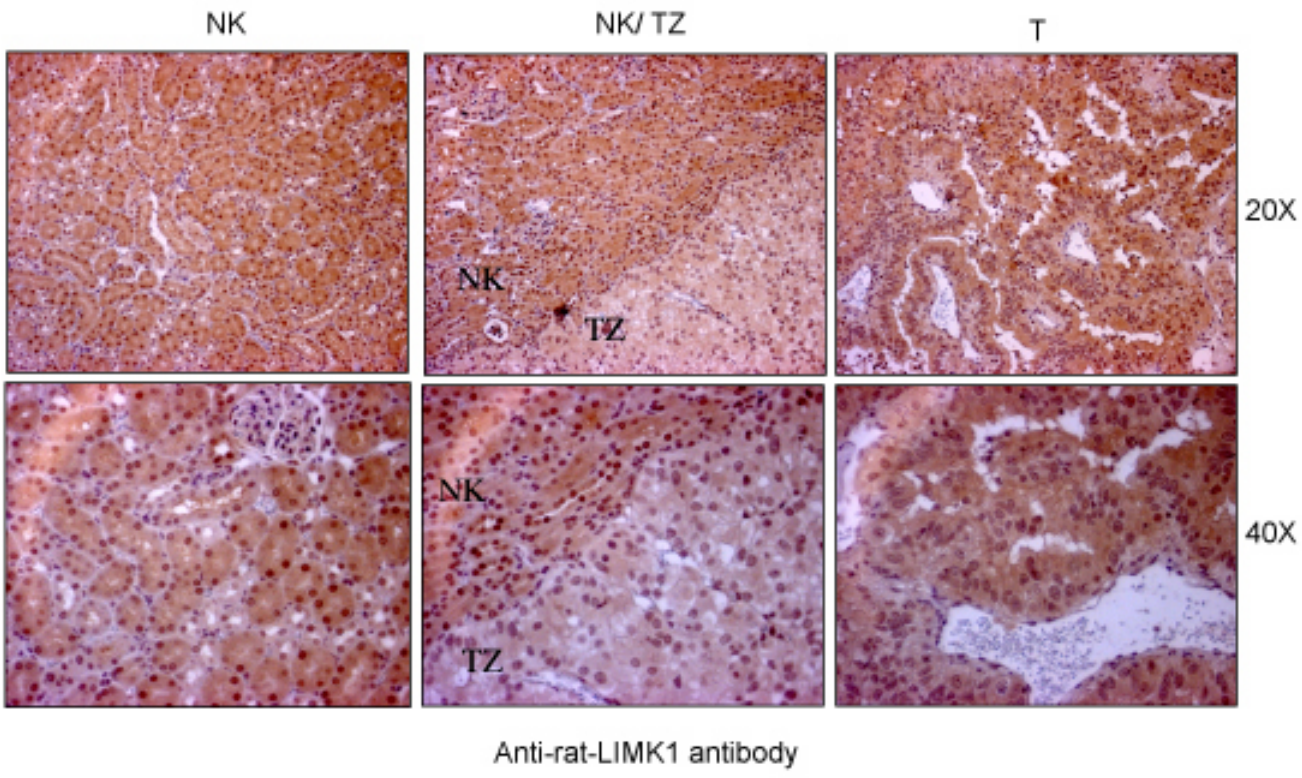

Fig. 3.16: **Differential localization of LIMK1 in kidney and tumor cells** Formalin fixed and paraffin-embedded mouse kidney was sectioned, stained with anti-rat LIMK1 antibody and photographed in 20X and 40X magnifications. Abbreviations: NZ: normal mouse kidney, TZ: transition zone, T: tumor

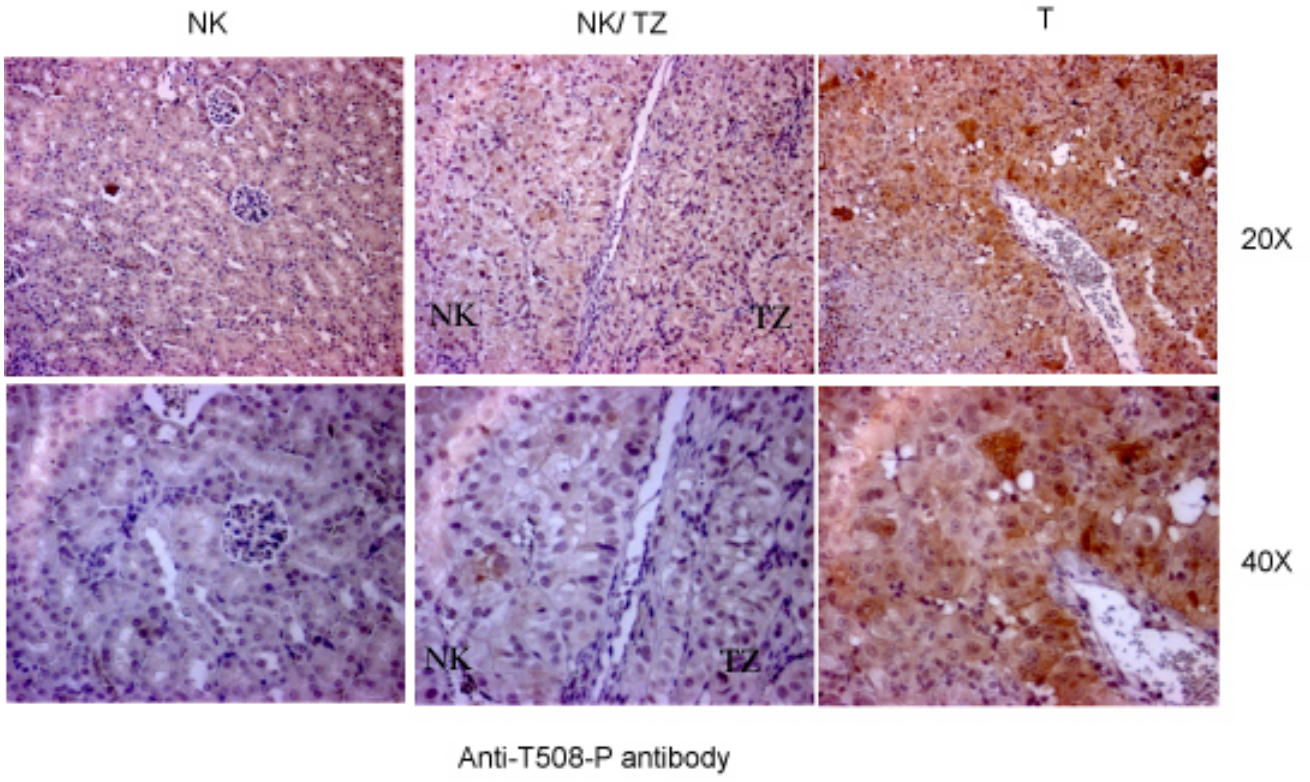

Fig. 3.17: **High activity of LIMKs in tumor cells** Formalin fixed and paraffin-embedded mouse kidney was sectioned, stained with anti-T508-P antibody and photographed in 20X and 40X magnifications. Abbreviations: NZ: normal mouse kidney, TZ: transition zone, T: tumor

and G2 checkpoint [Winters et al., 1998, Dulic et al., 1998]. Recent evidence including subcellular localization suggested that p21 could localize to cytoplasm in cancer tissues and cell lines, where it inhibits apoptosis by binding and inhibiting the apoptosis signal regulating kinase- 1 [Orend et al., 1998, Barboule et al., 1998, Asada et al., 1999]. Also, cytoplasmic p21 was associated with poor prognosis of breast cancer [Winters et al., 2001]. Finally, p21 was reported to be increased early after mitogen stimulation, and it has been found that overexpression of p21 was an early event in the development of some neoplasms such as pancreatic intra-epithelial neoplasia [Biankin et al., 2001]. Even though there was no staining of p21 in mouse kidney, some cells in TZ were stained by p21 antibody and the localization of p21 in that cells were nuclear (figure 3.18). Interestingly, in the tumor most of tumor cells were stained with p21 antibody and there was mainly cytoplasmic staining. These results suggested that, the checkpoints may be active in TZ cells since p21 localized to the nucleus, but in tumor cells, it was not active any more since p21 localized to the cytoplasm. Additionally, the cytoplasmic localization of p21 in tumor cells confirmed the development of neoplasm.

Altogether, these data suggest that tumor progression is correlated with a change in localization of LIMK1. Indeed, from both nuclear/cytoplasmic staining seen in normal kidney tissue, tumor tissue is characterized by the loss of nuclear immunoreactivity. Moreover, a significant increase in cytoplasmic activity is suggested as we observed an higher staining with the anti- T508-P antibody.

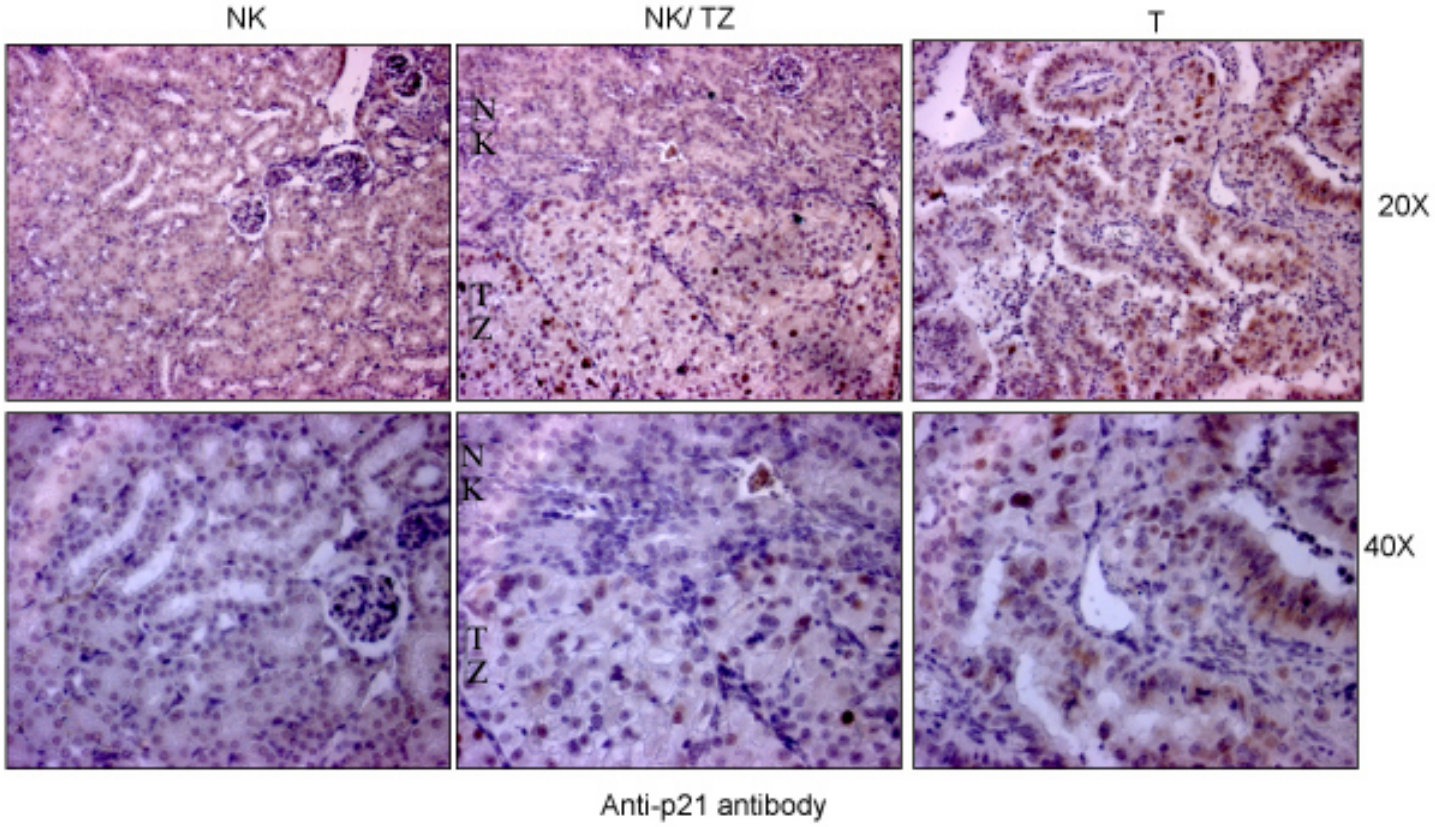

Fig. 3.18: **Nuclear and cytoplasmic localization of p21 in TZ and tumor cells, respectively** Formalin fixed and paraffin-embedded mouse kidney was sectioned, stained with anti- p21 antibody and photographed in 20X and 40X magnifications. Abbreviations: NZ: normal mouse kidney, TZ: transition zone, T: tumor

3.1.2.3 Immunohistochemical analysis of LIMK1 in prostate tissue and conditional PTEN prostate cancer model

The localization of LIMK1 in another tissue, namely prostate was examined using IHC in collaboration with Melanie Sticker and an analysis of normal mouse prostate and prostate cancer model was performed. As a prostate cancer model, conditional PTEN knockout mice, which was available in the laboratory, was used. Indeed, loss of function of PTEN is significantly correlated to progression of prostate cancer, and mouse model for prostate cancer have been commonly used by knocking out PTEN specifically in prostate tissue. Briefly, PTEN floxed/floxed mice and mice with PB-Cre4 (probasin promoter controlled Cre recombinase) were outsourced from Mouse Repository consortium and after crossing these two strains, conditional PTEN knockout mice (PTEN fl/fl) specific to prostate tissue was created.

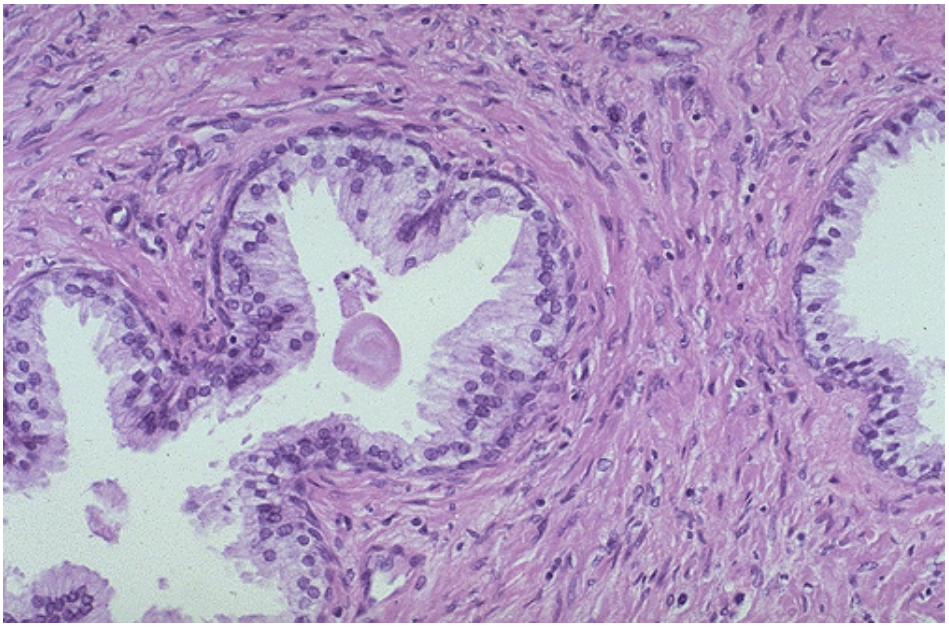

Fig. 3.19: **Normal histological appearance of prostate glands and surrounding fibromuscular stroma**

The prostate is the part of male reproductive system, and consists of irregular glands embedded in an extensive fibromuscular stroma (figure 3.19). The staining of LIMK1 by anti-rat LIMK1

antibody in prostate of 4 and 12 weeks old mice indicated that LIMK1 localized both to cytoplasm and nucleus of prostate glands confirming the dual cytoplasmic/nuclear localization of LIMK1 in differentiated tissues (figure 3.20).

Previous studies reported LIMK1 overexpression in prostate cells and tissues [Davila et al., 2003]. To investigate whether there was a difference in expression of LIMK1 in prostate tumor, immunohistochemical analyses were performed using anti-rat LIMK1 antibody. The staining of LIMK1 was performed in 4 and 12 weeks old PTEN fl/fl mice and its wild-type counterparts. Even though, nuclear and cytoplasmic staining was observed in prostate of 4 and 12 weeks old wild type mice as mentioned above, the cytoplasmic relocalization started in the 4 weeks old PTEN fl/fl mice's prostate tissue. In prostate tissue of 12 weeks old mice, there was only cytoplasmic staining which was slightly higher than its wild type counterpart. Altogether, this observation suggests that also in prostate cancer there is relocalization of LIMK1 from nucleus to cytoplasm.

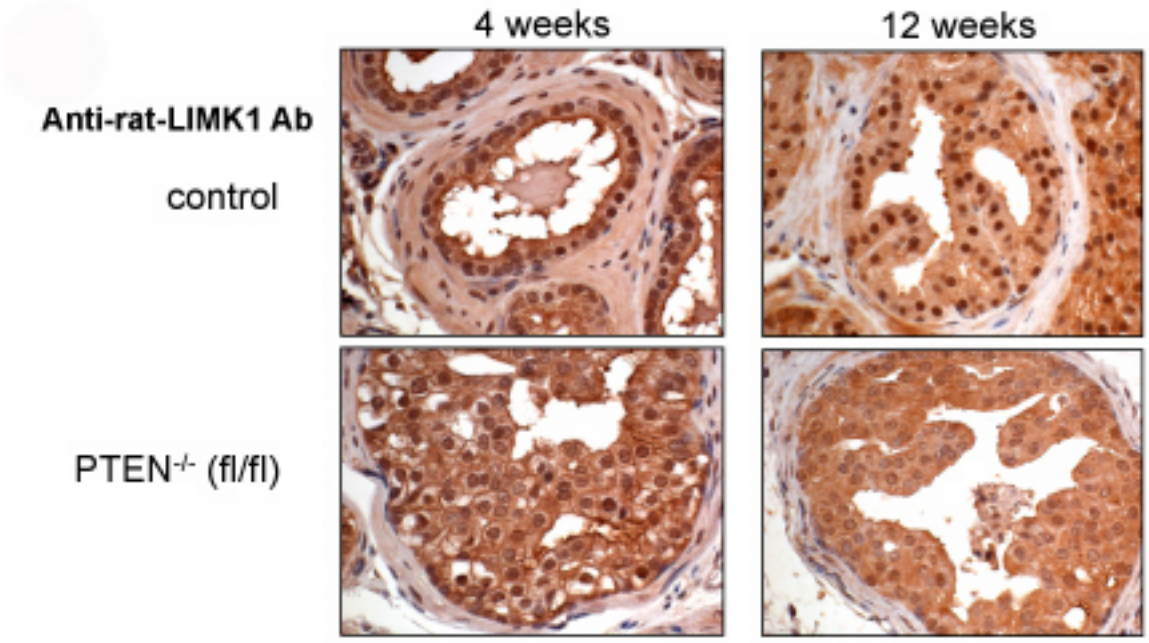

Fig. 3.20: **Cytoplasmic relocalization of LIMK1 in prostate cancer cells A.**Prostate glands from 4 and 12 weeks old wild type or PTEN fl/fl mice, were sectioned, and stained with anti- rat LIMK1 antibody, and photographed using 40 X magnification

3.1.3 Conclusion Remarks

This section summarizes the subcellular localization studies of LIMK. Firstly, in cultured cells we could identify cytoplasmic localization of LIMK1 and LIMK2 with lamellipodial staining in the direction of cell migration, consistent with the role of LIMKs in regulation of actin cytoskeleton. Moreover, we could observed a specific nuclear localization of active LIMK2, suggesting a potential role of LIMK2 in the nucleus. Interestingly, specific localization of LIMK1 to the mitochondria was also demonstrated, which could provide a novel mechanism of LIMK1 regulation.

Secondly, LIMK1 localization to nucleus and cytoplasm was observed in normal kidney and prostate tissues. Therefore, one can assume that differentiated cells display a different distribution of LIMK1 compared to exponentially growing cells. Remarkably, we could show that, when these cells progresses to the tumor phenotype, they loose their nuclear localization. Altogether, these raised the hypothesis that cytoplasmic LIMK1 localization participates in tumor progression.

3.2 Functional inactivation of LIMK1

3.2.1 LIMK1 knockout mice

3.2.1.1 Introduction

ÒGene targetingÓ is a technique using pluripotent embryonic stem cells to generate a mouse line deficient in a specific target gene. Mice deficient in the target protein may then undergo changes in phenotype, which can be identified through comparative studies against wild-type mice and correlated with possible functions of the target gene. The first step in a gene targeting procedure is the construction of a targeting vector that contains a drug resistance gene flanked by homologous DNA of the target gene (figure 3.21). The insertion of a drug resistance gene into the crucial genomic region of the target gene by homologous recombination allows for drug selection and also results in the disruption of the target gene. The targeting vector is then used to transfect embryonic stem cells (ES cells), which is followed by selection with drugs based on drug resistance and susceptibility cassettes contained within the plasmid, and screening the drug-resistant colonies for proper homologous recombination by the Southern blot analysis. The correctly targeted ES cells are injected into mouse blastocysts where they divide and ultimately differentiate into random parts of the body, including the germ cells, dur-

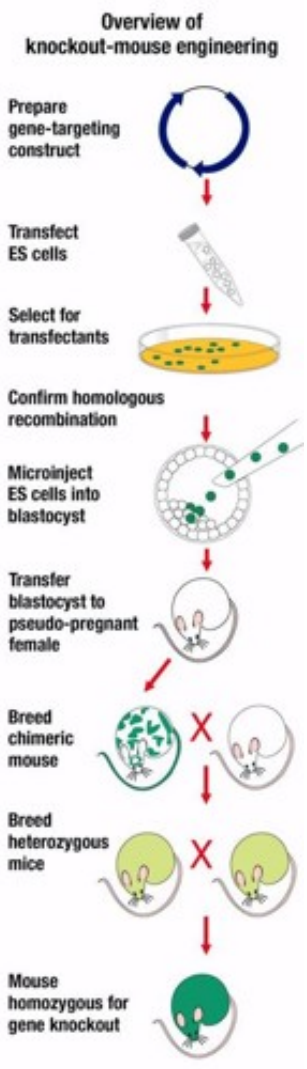

Fig. 3.21: **The overview of generation of knockout mice**

ing development. The resulting ÒchimericÓ mice are then screened for germ line differentiation of the targeted ES cells by appropriate mating crosses to produce heterozygous, and then homozygous ÒknockoutÓ progeny (figure 3.21) [Capecchi, 1989].

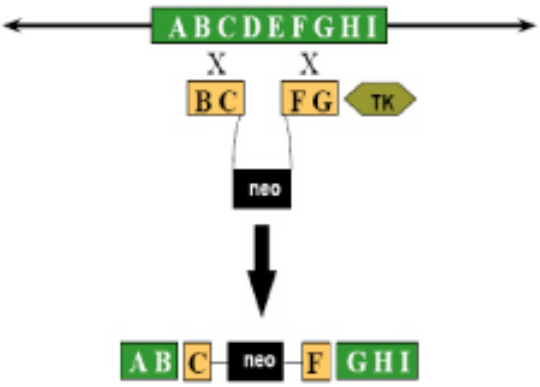

Fig. 3.22: **The schematic representation of homologous recombination of drug resistance gene (neo)**

Recently, newer technologies have been developed which allow for conditional knockouts or tissue-specific gene targeting. Whereas conventional knockout technology leads to loss of both alleles of a target gene in all cells, the purpose of conditional knockouts is to delete a gene in a particular organ, cell type, or stage of development. Conditional knockout is used to overcome lethality or strong phenotype due to total knockout. The most widely used method to create conditional knockout is the Cre-loxP recombinase system (figure 3.23). Cre (causes recombination) recombinase is an enzyme that works like scissors to cut out a gene that is in between two target sequences called loxP. The Cre recombinase used here fore is an enzyme which catalyzes the site-specific recombination between 34 bp sequences referred to as a loxP (locus of crossover (x)in P1) leading to the excision of the target sequence situated in between.

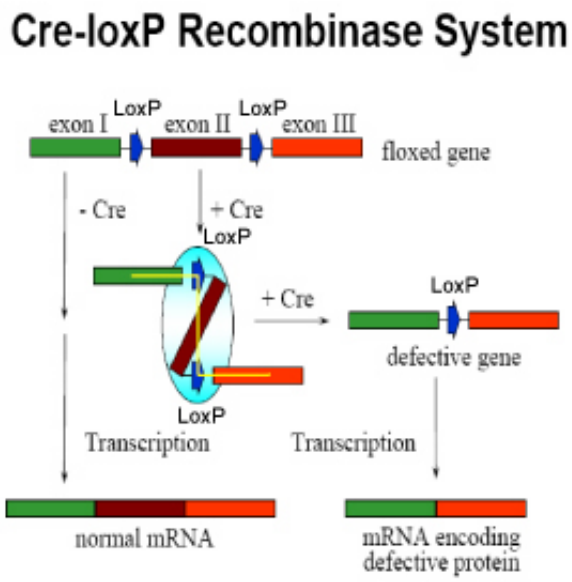

Fig. 3.23: **The schematic representation of Cre-loxP recombinase system**

3.2.1.2 Generation of LIMK1 knockout mice

LIMK1 knockout mice deficient in the expression of LIMK1 had already been generated. These knockout mice with a deletion of exon 5 and 6 showed alterations in cofilin phosphorylation and actin cytoskeleton. Additionally, perturbed synaptic structure and function related to actin network and consistently behavioral response abnormalities were detected [Meng et al., 2002].

These already generated LIMK1 knockout mice represented through a complete knockout and did not give the possibility to specifically target tissues. Therefore, the aim of our project was to create conditional LIMK1 floxed/floxed (fl/fl). These mice could then be crossed to prostate-specific Cre- mice in order to obtain conditional prostate specific LIMK1 knockout mice. After crossing conditional LIMK1 knockout mice to prostate specific- PTEN (fl/fl) mice, it would have been possible to monitor whether LIMK1 depletion prevents prostate cancer metastasis since the expression and activity of LIMK1 is increased in invasive prostate cancer cell lines [Davila et al., 2003]. As our findings showed a difference in LIMK1 localization in prostate-

specific PTEN (fl/fl) cancer model, it was of high interest to investigate the role of LIMK1 in prostate cancer metastasis.

The LIMK1 knockout project was initated by a former postdoc, Dr. Francois Lehembre in a collaboration with Transgenic mouse production unit, FMI (the cloning of 5' and 3' constructs as targeting vectors was performed).

LIMK1 gene comprises 16 exons and the functional domains are shown in figure 3.24 upper panel. In summary the cloning strategy was as follows: two targeting vectors were generated as 5'- and 3'- constructs (figure 3.24. 5' construct was generated by insertion of a neo cassette (loxP-neo-LoxP) into a genomic clone containing first exon of LIMK1, positioning the cassette before exon 1. The 3' construct was generated by insertion of a neo cassette (loxP-neo-LoxP) into a genomic clone containing exon 15 and 16, positioning it after exon 16. After transfection of 5' construct to ES cells, subsequent screening of the clones allowed to find clones where homologous recombination had placed the neo cassette 5' of LIMK1 exon 1. Subsequent Cre electroporation of these positive clones made it then possible to have a single loxP site at the 5' end of the LIMK1 gene.

At this stage the project was taken over by me and a collaborative study for ES cell handling and blastocyte injection with Dr. Birgit Ledermann from the Institute of Labortierkunde, University of Zurich, was initiated. The transfection of 3' construct to the ES cells that had already the 5' loxP was performed . Following electroporation of one (clone number 106) out of five positive clones with Cre , 50 clones were picked and subjected to Southern Blot analysis though revealed that the transfection of the 3' construct had not targeted the same allele as the 5' construct (figure 3.25). The Cre electroporation though could lead to 3 possible excisions of DNA sequences in between loxP target sequences which are depicted schematically in figure 3.26. The sizes of the wild type allele and recombinant allele after Southern blot analysis of ES cells cut with XbaI and

probed with either external KO 2.5' or KO 2.3' are also indicated in figure 3.26. As 3' construct didn't target the same allele as the 5'construct , a second positive clone for 3'- construct (clone 123) was electropolated with Cre. Subsequently, Southern blot analysis of 35 clones indicated that 5'- and 3'- constructs were integrated on the same allele.

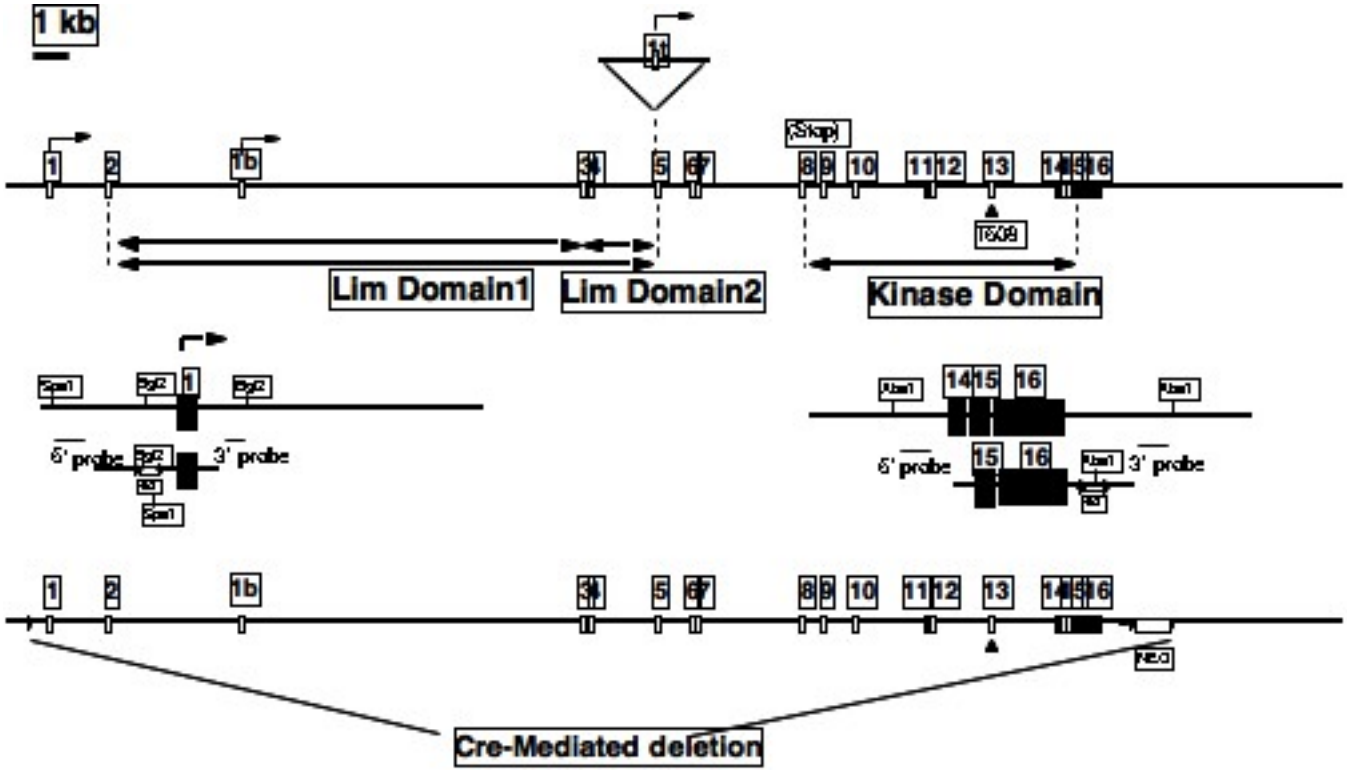

Fig. 3.24: **Schematic representation of cloning strategy of LIMK1 knock-out mice**

As it was not possible to distinguish between floxed (1), or totally deleted (3) LIMK1 in ES clones by using KO 2.5' probe in Southern blot analysis, KO 2.3' probe was used after digestion of ES cell genomic DNA with XbaI. This probe allowed identification of 5 clones with completely deleted LIMK1 (figure 3.26). Total deletion of LIMK1in these clones was additionally confirmed by PCR analysis (figure 3.27). As the forward primer (gLK 1.27) designed for this PCR analysis localized at the 5'-end of exon 1 and the reverse primer (gLK 1.26) at the 3'-end of exon 16, the amplification of DNA was only possible upon total deletion of the LIMK1 gene yielding a

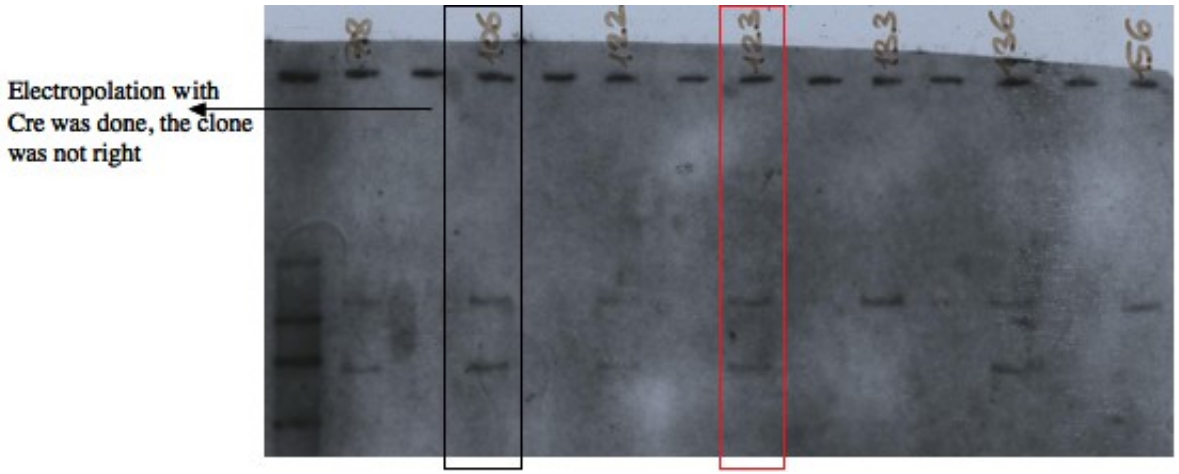

Fig. 3.25: **The clones with 5' loxP and 3' loxP-neo-loxP cassette** The clones 106, 122,123,136 and 178 are positive clones with 5'loxP and 3' loxP-neo-loxP cassette.

PCR product of 1 kb. In order to detect clones with a LIMK1 floxed allele, further investigation by PCR analysis was performed (figure3.27). PCR amplification was performed using forward (gLK1.28) and reverse (gLK 1.26) primer which localized before and after the 3' construct. Since the distance between two primers was too big to be ampified in case of an inserted loxP-neo-loxP cassette, the DNA amplification was only possible for a wild type allele giving rise to 800 bp band or, in case of floxed allele, 900 bp band due to the addition of a loxP site. 3 clones with floxed LIMK1 allele could be found.

With these analysis, the correctly targeted ES cells, 5 clones with total deleted LIMK1 allele and 3 clones with floxed LIMK1 allele were detected. The floxed clones were then injected into mouse blastocysts. Unfortunately, after injecting 3 positive clones into blastocysts, the embryos were always resorbed and it was not possible to get any living offspring.

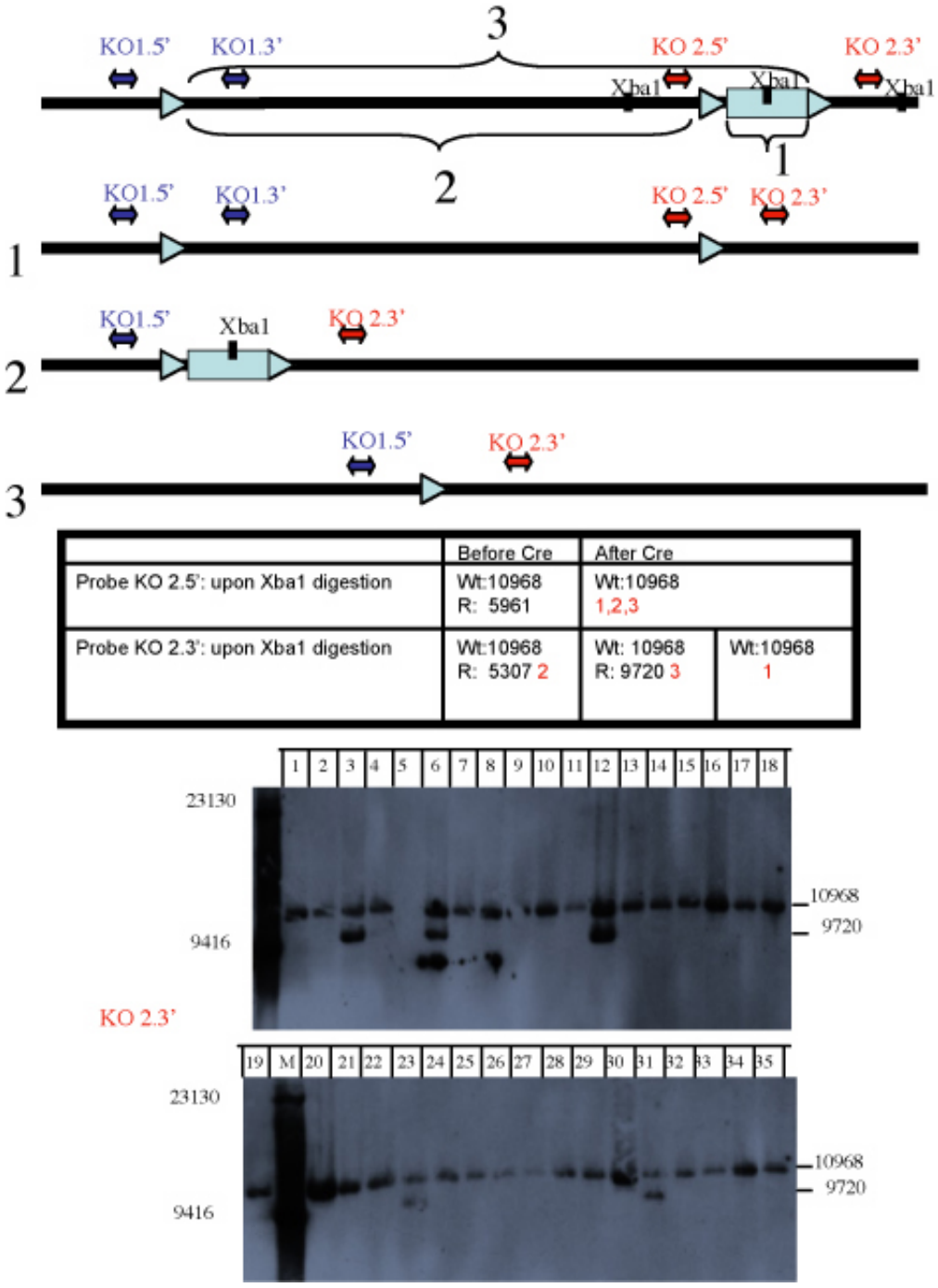

Fig. 3.26: **The schematic representation of 3 possible clones after Cre electroporation, their expected sizes in Southern blot analysis after XbaI digestion and probing either with KO 2.5' or KO 2.3' and Southern Blot analysis of 35 clones after Cre electroporation with KO 2.3' probe**

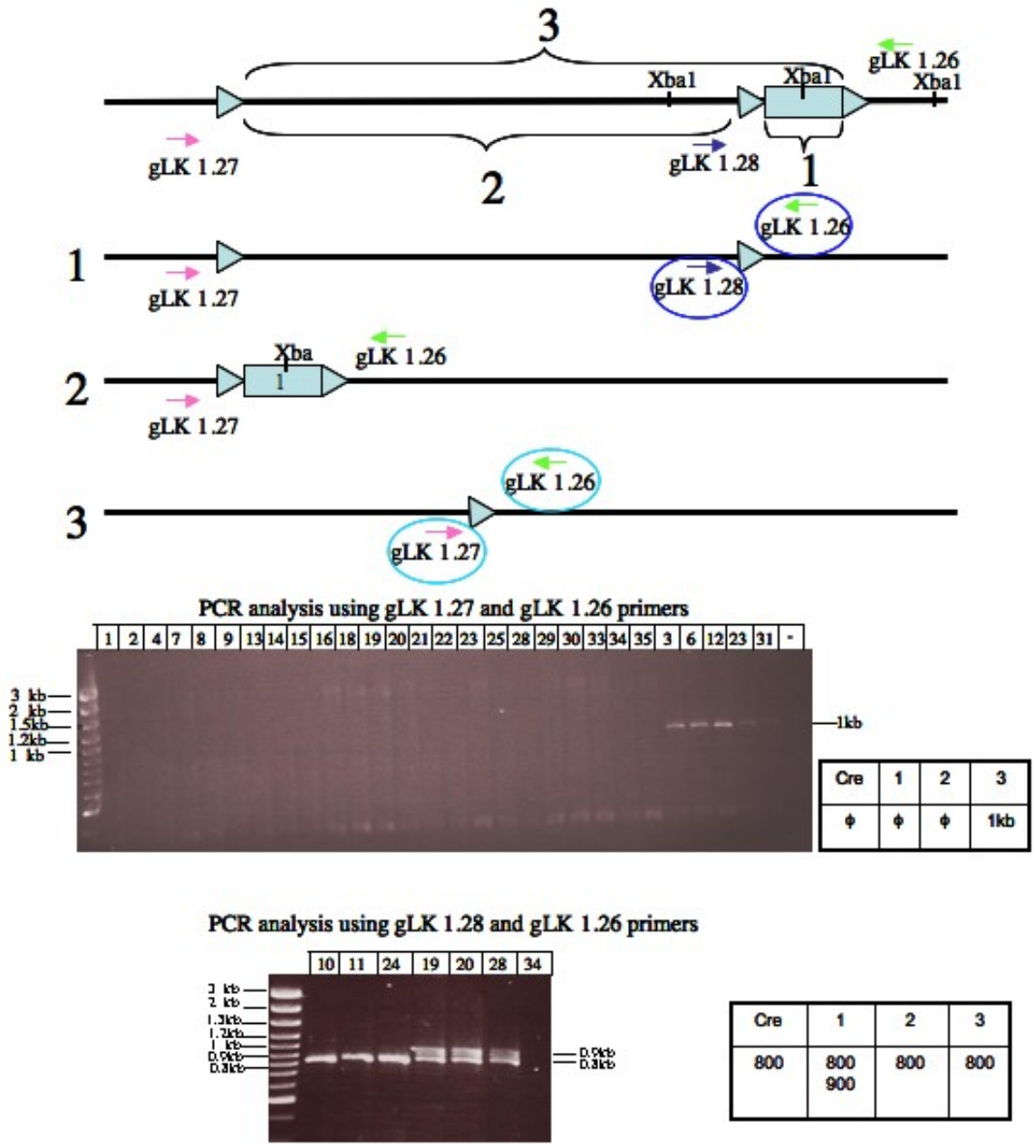

Fig. 3.27: **The schematic representation of 3 possible clones after Cre electroporation, their expected sizes in Southern blot analysis after XbaI digestion and probing either with KO 2.5' or KO 2.3' and Southern Blot analysis of 35 clones after Cre electroporation with KO 2.3' probe**

3.2.1.3 Perspectives

This section has outlined the detection of correctly targeted ES cells with a floxed or deleted LIMK1 allele. Unfortunately, the project was suspended since blastocyst injections of these ES cells didn't give any offspring. There would now though be a couple of ways to continue: One possibility could be to subclone one of the positive clones and after analysis to detecting the correctly targeted ES cells repeat the blastocyst injection. Alternatively, Cre electroporation could be performed to another parental ES clone with 5' loxP site and 3' neo cassette.

In addition, there is a new technology to generate transgenic mice using lentivirus-mediated expression of shRNA (small hairpin RNA) that targets the RNA of interest for degradation. Retroviral vectors are efficient, stable gene delivery tools in mammalian cells and recently it was suggested that they can stably express shRNAs in transformed and primary cells. A lentivirus-based vector that expresses RNAi-inducing shRNAs was developed. This vector was engineered to co-express enhanced green fluorescent protein (GFP) as a reporter gene, permitting infected cells to be tracked by flow cytometry. In addition to the use of lentiviral RNAi in mammalian cells it was recently shown that it could be used to generate knockout mice since transgenes expressed from lentiviruses are not silenced during development. The advantages of using lentiviral RNAi to generate transgenic mice are as follows: Lentiviruses that express RNAi-inducing shRNA can be infected into ES cells or directly to single-cell embryo. Infecting the single-cell embryo make it possible to bypass the use of ES cells. Furthermore, the co-expression of GFP permits to track the cells with depletion of the protein of interest. This system needs though still additional modifications as inclusion of tissue-specific promoters to create conditional knockout mice [Rubinson et al., 2003].

3.2.2 Investigating LIMK1 RNA interference

3.2.2.1 Introduction

As said before, one of the most effective ways to determine the biological function of a protein is to knock down the gene of interest, using directed manner, homologous recombination, and to create a knockout mice, which has either a nonfunctional or nonexisting protein product. However, this method is time-consuming, expensive and cannot be applied to human tissues. Alternative methods for silencing specific genes are antisense strategy using either DNA or RNA. Although these methods are straightforward, there are artefacts because of questionable specificity and incomplete efficacy. Recently, a new strategy has emerged called RNA interference (RNAi). RNAi is the process of sequence-specific post-transcriptional gene silencing in a wide range of organisms, initiated by double-stranded RNA (dsRNA) that is homologous in sequence to the targeted gene. The mediators of sequence-specific messenger RNA degradation are 21- and 22-nucleotide small interfering RNAs (siRNAs) generated by a RNase III family of dsRNA-specific endonuclease called dicer, which cleaves longer dsRNAs to siRNAs. These siRNAs are characterized by 2-nt-long 3' overhangs. SiRNAs are then incorparated into a protein complex, called RNA-induced silencing complex (RISC), which degrades homologous mRNA. Accordingly expression of the targeted gene is inhibited at the post-transcriptional level resulting in inhibition of the corresponding protein. Because of that, RNAi is usually described as post-transcriptional gene-silencing (PTGS) (figure 3.28) [Mello and Conte, 2004]. RNAi phenomenon was first elucidated in *C.elegans*, when probing gene function by using antisense approaches [Fire et al., 1998]. Afterwards, it was reported that chemically synthesized siRNAs, designed to mimic the product of the Dicer enzyme, could induce gene silencing in a wide range of human and mouse cell lines. Another type of noncoding small RNA is the microRNA (miRNA). miRNAs are processed from conserved endogenous hairpin transcripts that a single miRNA is produced from one arm of each hairpin molecule, and are single stranded and paired with target mRNAs containing homology

to specific regions (target sequences) of the 3'-untranslated regions (UTRs) complementary to miRNA and unlike siRNAs repressing mRNA translation without alteration of mRNA stability (figure 3.28). Since it was realized that endogenously encoded hairpin RNAs, could regulate gene expression via elements of RNAi machinery, exogenously synthesized hairpins, called short hairpin RNAs (shRNAs), which are structurally related to miRNAs were used to provoke silencing of targeted gene (figure 3.28) [Paddison et al., 2002].

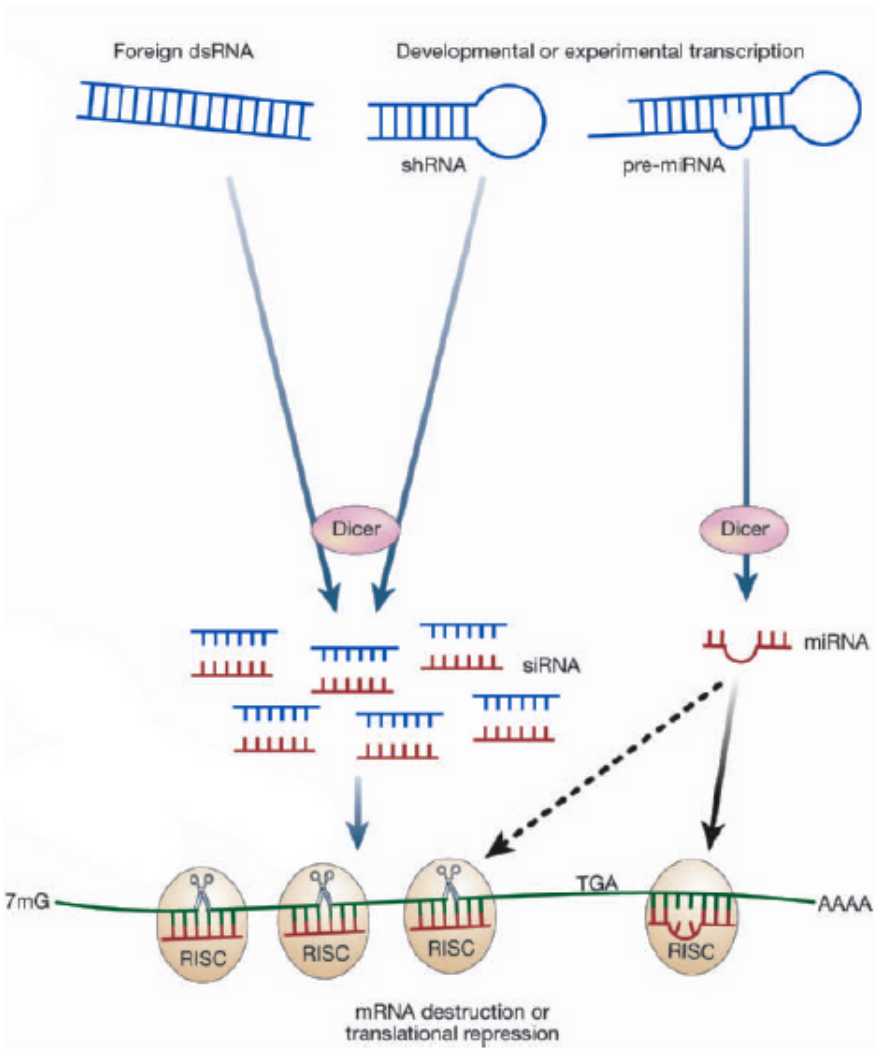

Fig. 3.28: **How does RNA interference work?**

LIMK1 inactivation studies at the time of commencing this project had relied only on overexpression of dominant negative mutants of LIMK1. For that reason, siRNA oligonucleotides were used as an alternative approach as it could be used effectively and specifically to deplete target proteins. Additional to LIMK1 siRNAs, drug- inducible lentiviral-mediated LIMK1 shRNA were generated to investigate the effects of depletion of LIMK1 in human origin cell lines.

3.2.2.2 LIMK1 small interfering RNAs (siRNAs)

RNA nucleotides corresponding to 19 base pair stretch of the human LIMK1 coding regions (521-541) referred as LIMK1(521) siRNA, and (662-680) referred as LIMK1(662) siRNA) were ordered and prepared as described in Materials and Methods. Figure 3.29 shows the sequences in open reading frame (ORF) that LIMK1 siRNAs were targeted.

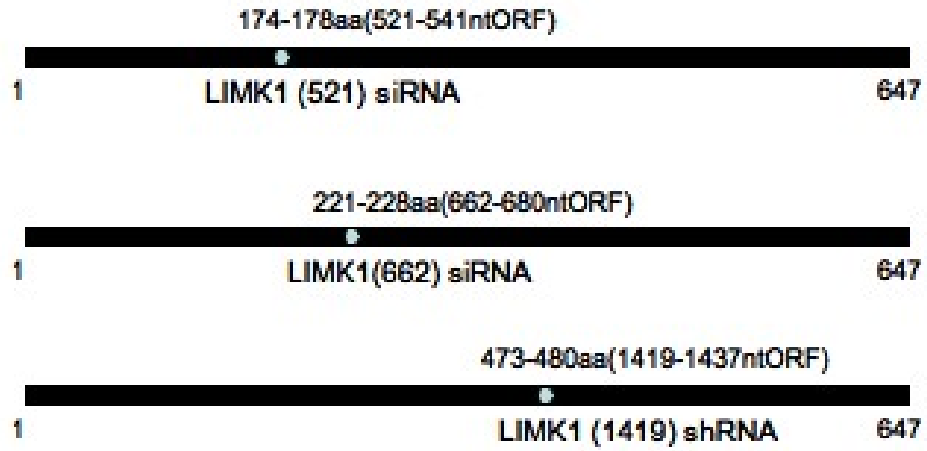

Fig. 3.29: **Target sequences of the location of LIMK1 siRNAs and shRNA**

Characterization of LIMK1 siRNAs

To define the efficiency of LIMK1 (521) siRNA on LIMK1 knockdown, transfection with LIMK1 siRNA to HeLa cells was performed over a 24-72 hour period, and subsequently samples were analyzed by Western blotting. Figure 3.29 shows that maximal knockdown is reached after 48 hours, and that this level of knockdown is maintained up to 72 hours, and presumably beyond. Additionally, it was indicated that depletion of LIMK1 by LIMK1 (521) siRNA, resulted in dephosphorylation of cofilin, which suggested that LIMK1 is the main kinase that phosphorylates cofilin in HeLa cells. LIMK1(512) siRNA was shown to downregulate LIMK1 also in U20S cells with a lesser extent (unpublished data from Dr. J. Listzwan).

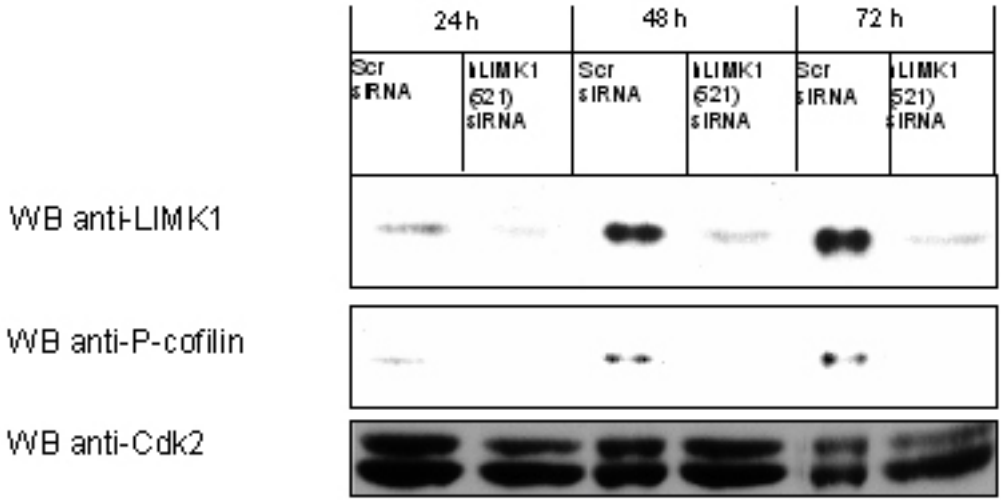

Fig. 3.30: **Time dependent knockdown of LIMK1 by LIMK1 (521) siRNA**. HeLa cells were treated with 150nM of nonsilencing Scramble siRNA (Scr), and LIMK1(521) siRNA for 24, 48 and 72 hours, then lyzed and processed for Western Blotting using anti-LIMK1, anti-P-cofilin and anti-Cdk2 antibodies (as loading control). 100 μg of total protein was loaded. The WB shown is representative of 5 independent experiments.

HeLa cells were also analyzed for adverse affects, which might be either LIMK1 (512) siRNA specific or technique related. Indeed, after 48 hours of LIMK1 (521) siRNA treatment of HeLa cells, cell death was observed as shown in phase contrast images (figure 3.31).

In order to analyze the form of cell death, anti-PARP antibody was used in Western blotting of lysates from LIMK1 (521) siRNA, nonsilencing siRNA treated or untreated HeLa cells. Poly (ADP-ribose) polymerase -1 (PARP-1) is a nuclear enzyme activated by DNA breaks and its degradation occurs in cells that undergo apoptotic versus nonapoptotic forms of cell death. The results indicated that, even though there was no PARP cleavage after 24 hours of LIMK1 (521) siRNA treatment, the cleavage of 113kDa PARP-1 to 89kDa and 24kDa after 48 hours was observed, suggesting that LIMK1 (521) siRNA treated cells undergo apoptosis after 48 hours of treatment (figure 3.31). The size of cleavage products suggested that PARP cleavage was through caspase 3. Indeed, caspase 3 inhibitors inhibited apoptosis and cleavage of PARP upon 48 h of LIMK1 (512) siRNA treatment, confirming caspase 3-mediated cleavage (data not shown). Although there was apoptosis upon 48 hours of LIMK1 (512) siRNA treatment of HeLa cells, very little apoptosis was observed at 48 hours of siRNA treatment in U2OS cells. Since there was different phenotype in HeLa and U2OS cells, after siRNA treatment, it may be a cell type specific effect. As HeLa cells have a faster cell cycle rate, one possibility can be that the effects in U2OS may be monitored only at later time points of siRNA treatment. To validate whether the apoptosis observed was an falsely identified phenotype resulting from potential off-target effect or not, another siRNA was designed and ordered for usage (LIMK1 (662) siRNA).

To investigate the efficiency of LIMK1 (662) and whether it causes apoptosis, HeLa cells were treated either with LIMK1 (521) or LIMK1 (662) siRNAs for 48 hours, and after taking their phase-contrast pictures, cells were lyzed and processed for Western blotting . Although, both LIMK1 (521) and LIMK1 (662) siRNAs showed similar knockdown of LIMK1 in Western blot analysis in HeLa cells, only LIMK1 (521) siRNA caused PARP cleavage, and apoptotic phenotype indicated in phase-contrast images (figure3.32, A). Furthermore, morphological changes were monitored upon treatment with both siRNAs such as more flattened and rounded cell shape which may be indications of the loss of cell migration. Also when phase contrast images of LIMK1 (662) siRNA treated cells and nonsilencing (Scr) siRNA treated cells were compared,

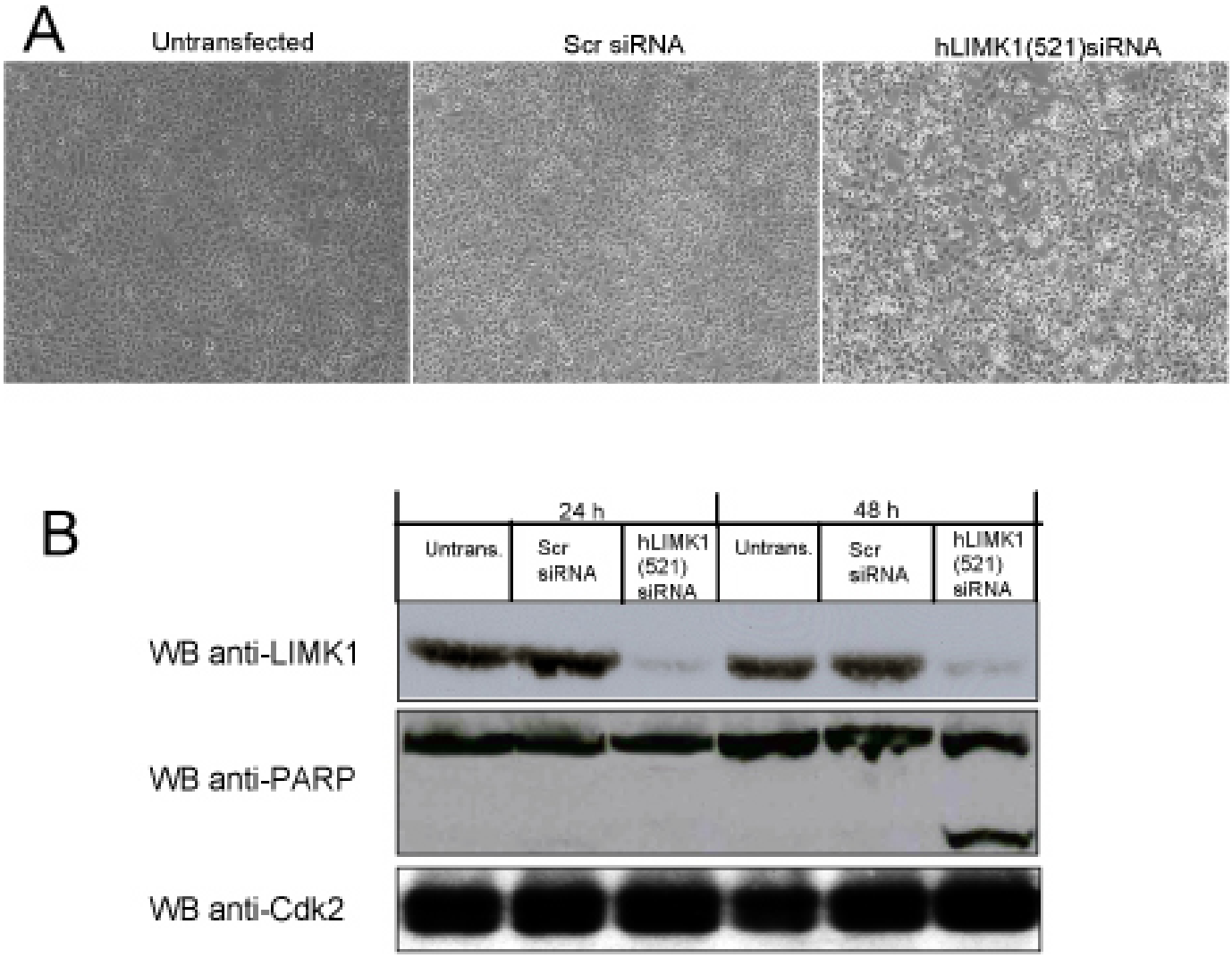

Fig. 3.31: **RNAi treatment of LIMK1 by LIMK1 (512) siRNA caused apoptosis after 48 hours of treatment A.** HeLa cells were treated with 150nM of nonsilencing siRNA (Scr) or LIMK1(521) siRNA or kept untreated for 24 and 48 hours, and following lysis of cells, it was processed for Western Blotting using anti-LIMK1, anti-PARP and anti-Cdk2 antibodies (as loading control). 150 μg of total protein was loaded. **B.** The phase-contrast images of untransfected, Scr or LIMK1 (521) siRNA treated cells were taken by Zeiss Axiovert microscope, 48 hours after siRNA treatment. The WB and phase contrast images shown are representative of 3 independent experiments

conformational changes and migration rate decrease were monitored as cells were creating clusters in LIMK1 (662) siRNA treated cells (figure 3.33). Additionally, treatment of U2OS and HCT116 cells with LIMK1 (662) siRNA showed a high knockdown efficiency of this siRNA. These results indicated that LIMK1 (662) siRNA caused the depletion of LIMK1 to same extent as LIMK1 (521) siRNA in HeLa cells, and didn't caused apoptosis. This suggested that in addition to specific effect of LIMK1 (521) siRNA as depletion of LIMK1, it may cause an additional apoptotic effect. Additional analysis using siRNA rescue plasmids to reexpress LIMK1, with a mutation resulting in resistance to siRNA treatment, should be performed to clarify if apoptosis monitored was a off- target effect of siRNA in HeLa cells.

To further characterize the siRNAs for LIMK1, HeLa and U2OS cells were treated either with LIMK1 (521) or LIMK1 (662) siRNAs for 48 hours, and following fixation with PFA/triton, cells were stained with anti- LIMK1 (J) antibody. It was monitored that, there was total depletion of LIMK1 staining in HeLa cells treated with LIMK1 (521) siRNA. However, even though, there was a high reduction of LIMK1 staining with LIMK1 (662) siRNA treatment, the depletion was not complete in HeLa cells (figure 3.34). In U2OS cells, both siRNAs showed similar knockdown of LIMK1 levels, despite a slightly higher efficiency of LIMK1 (521) siRNA. The staining of LIMK1 in siRNA treated cells indicated that the staining of LIMK1 in cell membrane, especially in the direction of movement was abrogated and as a consequence cells created clusters and their migration rate was lower, as it was monitored in phase-contrast images of HeLa cells treated with LIMK1 (662) siRNA (figure 3.33, 3.35). The differential depletion efficiency shown in immunostaining, may question the effect of LIMK1 (521) regarding apoptosis to be a dose-dependent effect of siRNA or a off-target effect. Furher studies are warranted to answer this question.

Altogether, these data allowed to identify one siRNA, namely LIMK1(662) siRNA as an potent tool to specifically downregulate LIMK1, and to study the consequences of functional inactiva-

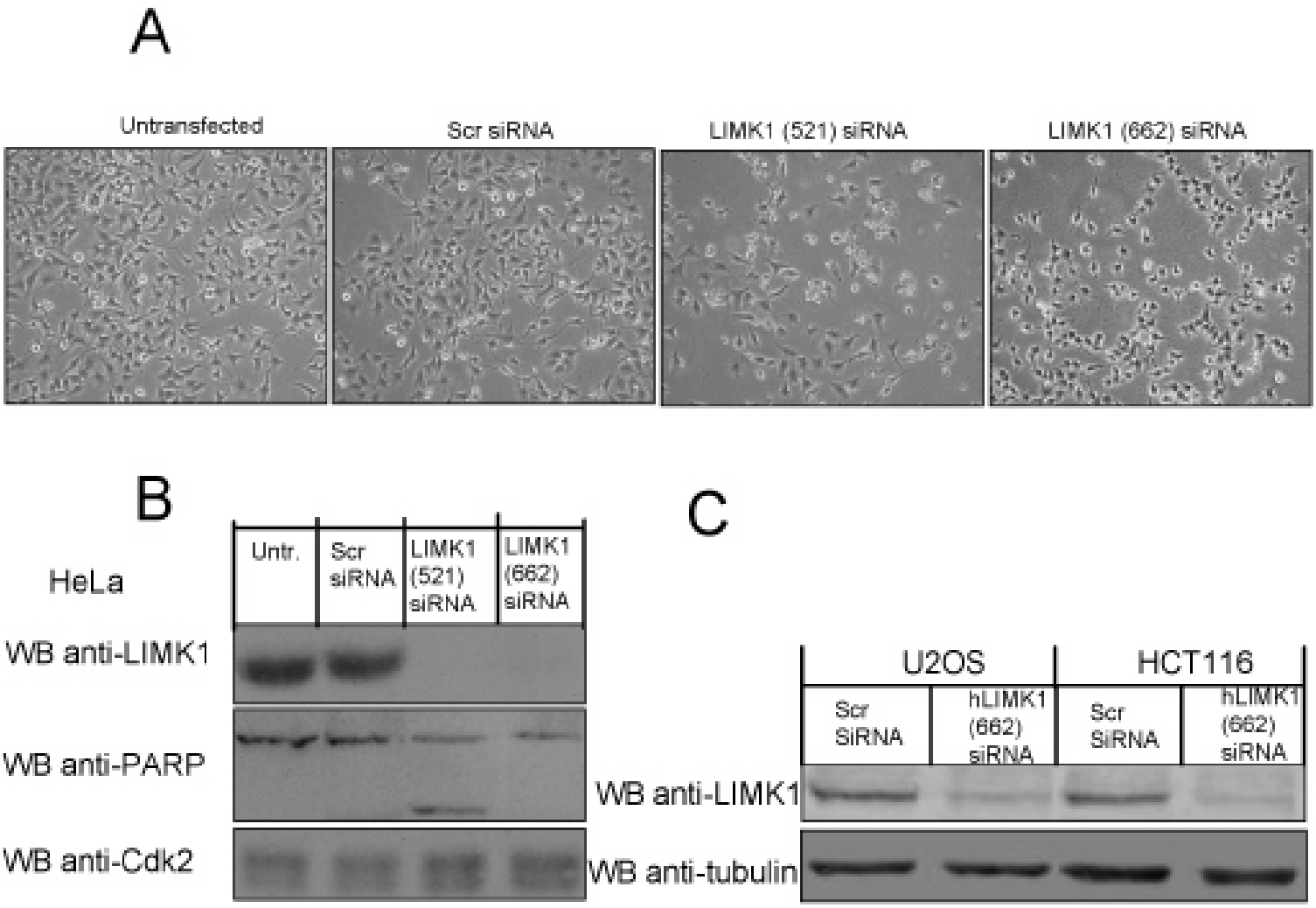

Fig. 3.32: **RNAi treatment of LIMK1 by LIMK1 (662) siRNA didn't caused apoptosis after 48 hours of treatment, opposite to LIMK1 (521) siRNA A.** The phase-contrast images of untransfected, Scr, LIMK1 (521) or LIMK1 (662) siRNA treated cells were taken by Axiovert microscope, 48 hours after siRNA treatment. **B.** HeLa cells were treated with 150nM of non-silencing siRNA (Scr) or LIMK1(521) siRNA or LIMK1(662) siRNA or kept untreated for 48 hours, and following lysis of cells, it was processed for Western Blotting using anti-LIMK1, anti-PARP and anti-Cdk2 antibodies (as loading control). 100 μg of total protein was loaded. **C.** U2OS and HCT116 cells were treated with 150nM of nonsilencing siRNA (Scr) or LIMK1(662) siRNA for 48 hours, and following lysis of cells, it was processed for Western Blotting using anti-LIMK1 and anti-tubulin antibodies (as loading control). The WB and phase contrast images shown are representative of 3 independent experiments.

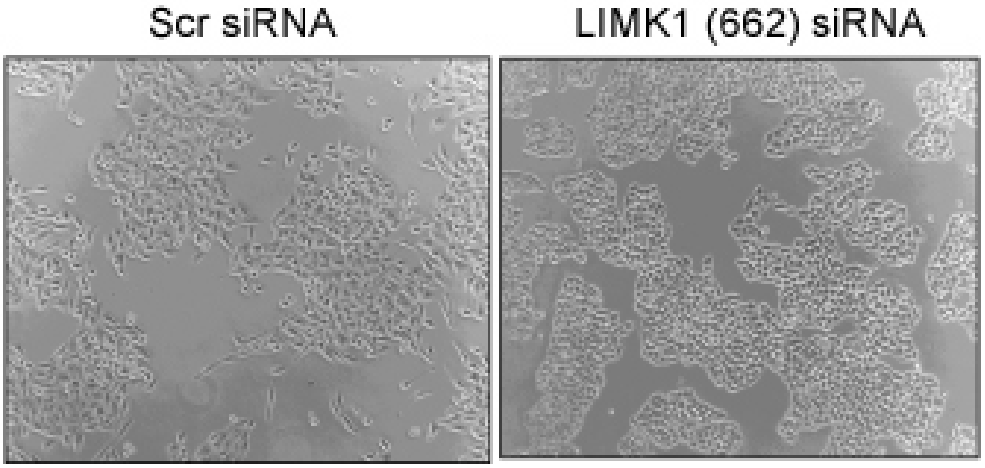

Fig. 3.33: **LIMK1 (662) siRNA treated cells created clusters**. HeLa cells were treated with either nonsilencing (Scr) siRNA or with LIMK1 (662) siRNA. 48 hours after transfection of SiRNA, cells were photographed by Zeiss Axiovent Microscope. The phase contrast images shown are representative of 3 independent experiments.

tion of LIMK1. This will be developed in section 3.4, regarding the role of LIMK1 in cell cycle regulation.

3.2.2.3 The lentivirus vector-mediated LIMK1 RNA interference

Introduction

Since the downregulation of gene expression mediated by siRNA varies by transfection efficiency in different cell lines, the alternative method is to do stable expression of RNAi effector molecules from plasmids or viral vectors. The advantage of using vector-based RNAi is that it permits co-expression of reporter genes such as GFP or luciferase, which facilitates tracking and/or selection/enrichment of transfected/transduced cells. The most commonly used approach of vector-based RNAi, involves RNA polymerase III (U6)-mediated transcription of shRNA structures with a stem of 19-29 bp and a short loop of 4-10nt. The generation of shRNA structures are performed by annealing of two complementary oligonucleotides, generating a double-stranded

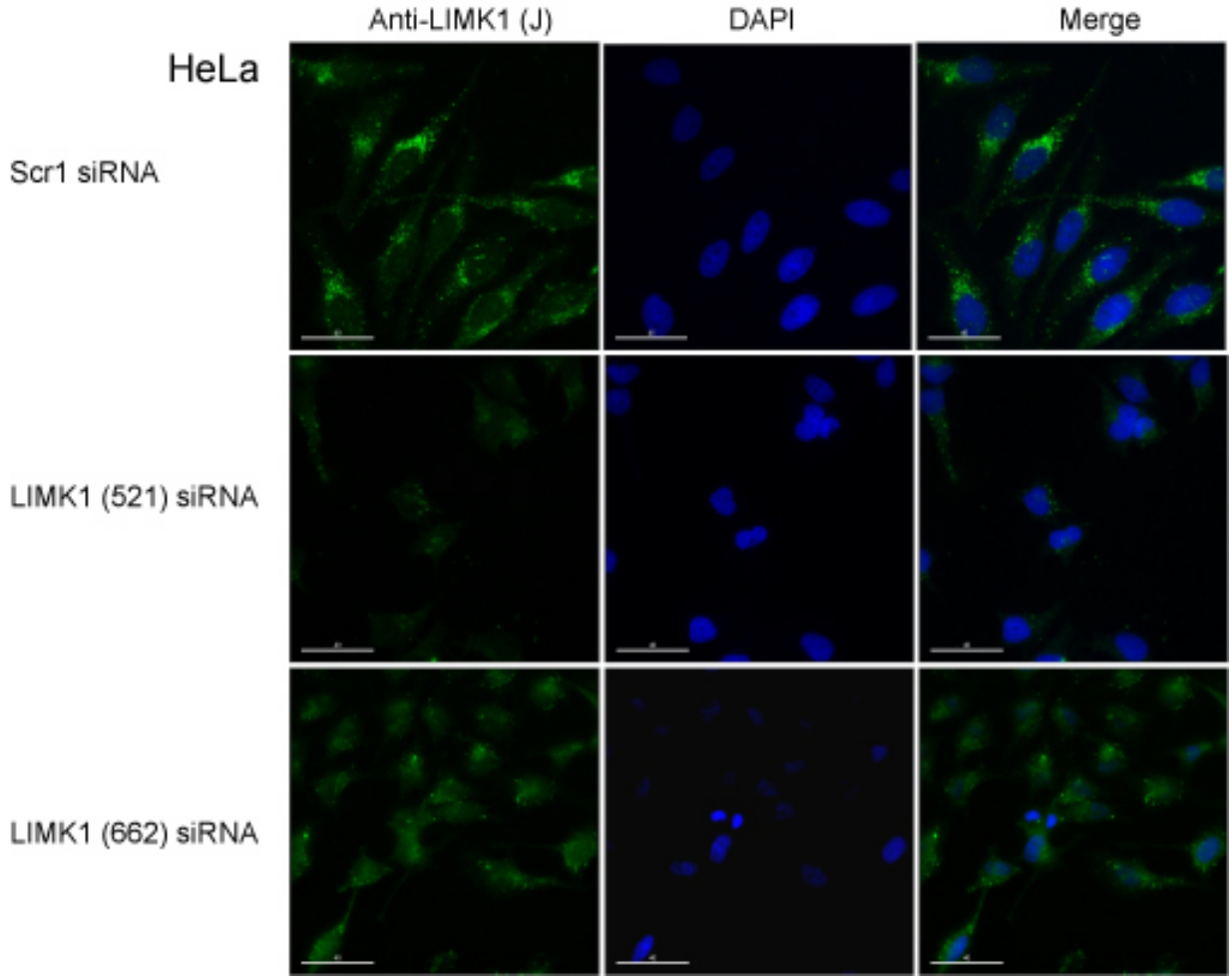

Fig. 3.34: **Depletion of LIMK1 in HeLa cells by LIMK1 (521) and LIMK1 (662) siRNA** HeLa cells were treated with LIMK1 (521) and LIMK1 (662) siRNAs or kept untreated for 48 hours, fixed with PFA/triton and immunostained by anti-LIMK1 (J) antibody. DAPI was used as a nuclear marker. The images were taken by DeltaVision Microscope. Images shown are representative of 3 independent experiments

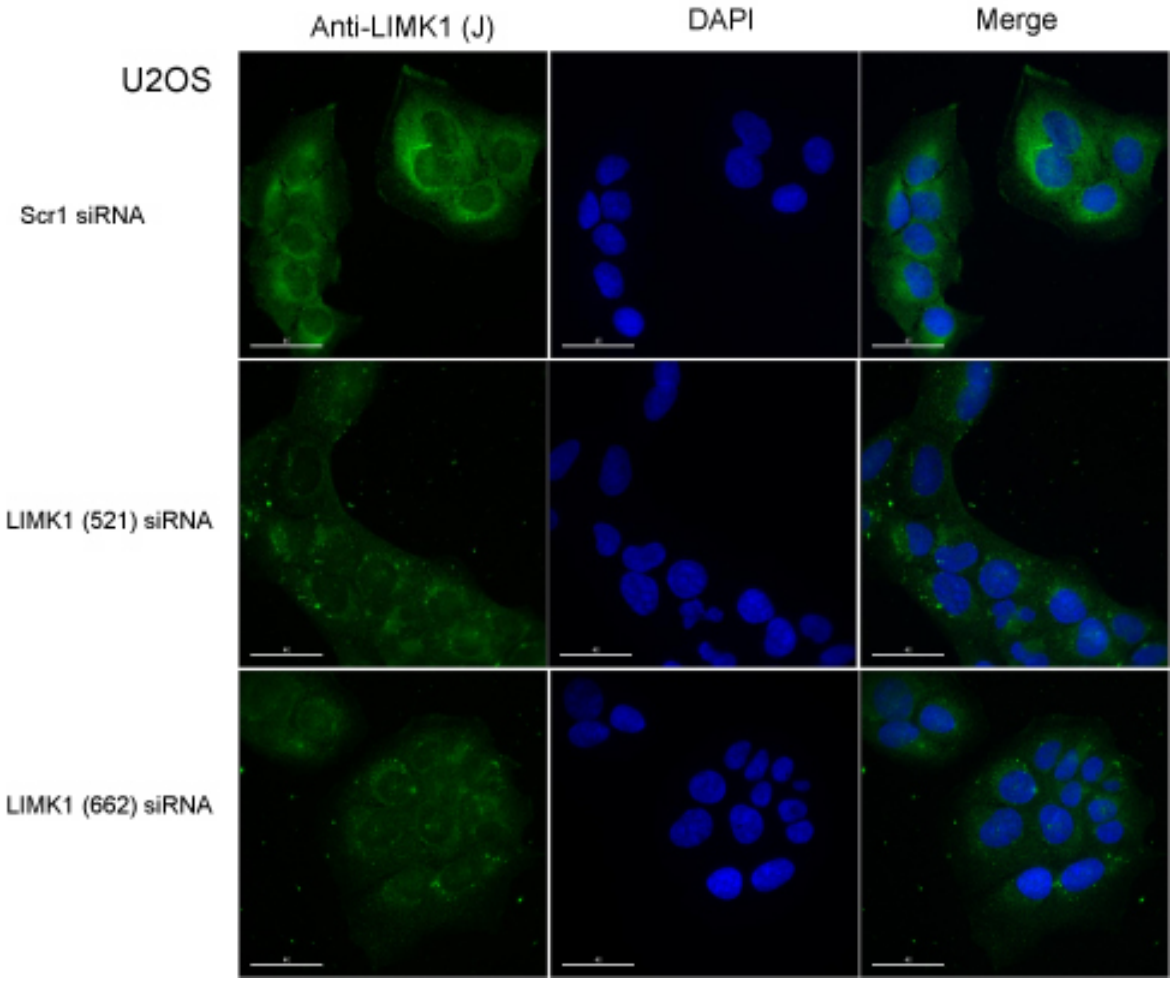

Fig. 3.35: **Knockdown of LIMK1 in U2OS cells by LIMK1 (521) and LIMK1 (662) siRNA** U20S cells were treated with LIMK1 (521) and LIMK1 (662) siRNAs or kept untreated for 48 hours, fixed with PFA/triton and immunostained by anti-LIMK1 (J) antibody. DAPI was used as a nuclear marker. The images were taken by DeltaVision Microscope. Images shown are representative of 3 independent experiments

oligonucleotide cassette which is called shRNA expression cassette with appropriate overhangs for directional cloning downstream of the polymerase III promoter.

One of the stable expression of RNAi molecules can be achieved by viral vectors such as lentiviruses and adenoviruses. The use of viruses allows easy generation of transgenics of transformed and primary cells. Lentiviruses have two key advantages over other gene delivery systems. First, they can infect non-cycling and post-mitotic cells. Second, transgenes expressed from lentiviruses are not silenced during development and can be used to generate transgenic animals through infection of ES cells and embryos as mentioned in the perspectives of previous section.

The lentivector expression system consist of three main components: the lentiviral expression vector, the lentiviral packaging vectors and producer cell line. The lentiviral expression vectors contain the genetic elements responsible for packaging, transduction, stable integration of viral expression construct into genomic DNA, and expression of the target gene sequence. On the other hand, lentiviral packaging vectors provide all the proteins essential for transcription and packaging of an RNA copy of the expression construct into recombinant viral particles. To produce a high titer of viral particles, expression and packaging vectors are transiently co-transfected into producer mammalian cells (e.g. 293 cells). After viral particles are produced, they are used to infect target cells (e.g. HeLa cells) (figure 3.36, B).

Recently, the conditional expression of siRNAs have been performed by the development of lentivector-facilitating drug-controllable RNAi. One approach, from Prof. D Trono's laboratory, represents the doxycline controllable gene silencing. In that setting, the lentiviral vector contains a marker gene (GFP) under the promoter of EF1a and the small hairpin RNA expression cassette (H1-shRNA) is inserted downstream of TET-operator (*tetO*) sequence (LV-THsi). On the other hand, the KRAB (Krueppel-associated box) domain of transcriptional repressor protein, which can suppress both polymerase II and polymerase III-mediated transcription within a distance

of up to 3kb from its DNA binding site, was fused to the TET DNA binding domain in LV-tTR-KRAB-Red vector, which also contains a dsRed marker gene (figure 3.36, A). Therefore, cotransduction of these two vectors lead to KRAB-mediated repression of both GFP gene and shRNA transcription, which is also TET-inducible.

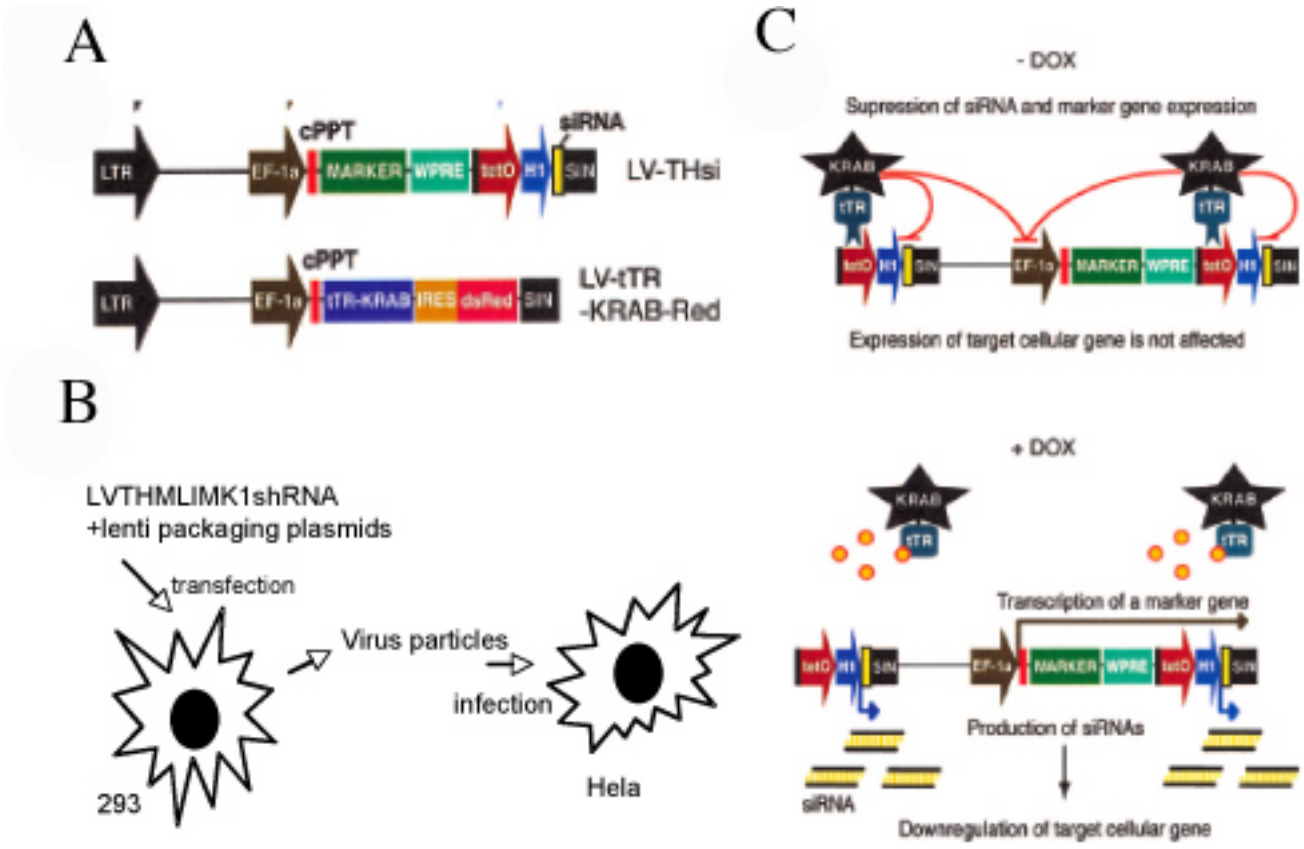

Fig. 3.36: **A lentivirus vector-based system for conditional gene suppression with DOX-inducible siRNAs**. **A.** Scematic drawing of Lentivirus vector plasmids LV-THsi and LV-tTR-KRAB-Red. **B.** A diagram showing how viral particles are produced and subsequently transduce the target cell line. **C.** Mode of action of the DOX-controllable transrepressor. In the absence of DOX, tTR-KRAB binds to (*tetO*) and suppresses H1-mediated siRNA transcription, thus allowing normal expression of the target gene (on). In the presence of DOX, tTR-KRAB cannot bind to (*tetO*) and hence siRNAs are produced, leading to downregulation of their target (off) adapted from Wiznerowicz et al. 2003

Indeed, in the absence of doxycycline, the resulting tTR-KRAB protein binds specifically to

tetO sequences and suppresses the activity of the nearby H1 promoter in LV-THsi construct, therefore inhibiting the expression of shRNA and GFP marker gene. Conversely, in the presense of doxycycline, tTR-KRAB is sequestered away from *tetO*, thereby permitting expression of both shRNA and GFP marker genes, resulting in downregulation of target cellular gene (figure 3.36, C).

Production and characterization of lentivector-mediated LIMK1 shRNA

The production of lentiviral vector-mediated LIMK1 shRNA gave an additional advantage to LIMK1 siRNAs, as it has a GFP reporter gene which allows tracking and/or selection of LIMK1 depleted cells. The lentiviral expression and packaging vectors were received from Prof. D. Trono, University of Lausanne, Switzerland.

In order to deplete LIMK1 by lentivirus-mediated RNAi, shRNA was designed using the identical target sequence as LIMK1 (662) siRNA. HeLa cells were transduced with viral particles with LIMK1 (662)shRNA for acute infection and the infection efficiency was monitored by tracking GFP signal in HeLa cells by fluorescent microscopy as an indicator of shRNA expression. At 4 days post infection, nearly all cells highly expressed GFP. Cells were harvested, lyzed and processed for Western Blotting. However despite high GFP expression, no LIMK1 downregulation was observed (data not shown). The results indicated that the target sequence that was used previously to deplete LIMK1 by siRNA approach didn't cause any down regulation when used for shRNA. The data suggested that the target sequence of LIMK1 (662) was not suitable for lentiviral-mediated RNAi system.

After unfortunate results from the first LIMK1 shRNA, another target sequence was designed for lentiviral-mediated RNAi system (LIMK1 (1419) shRNA). Cloning of LIMK1 (1419) into LV-THsi (LV-THsi/LIMK1(1419)) was followed by viral particle production by cotransfection of LV-THsi/LIMK1 expression vector or LV-THsi empty vector and packaging vectors to 293T

cells. HeLa cells were transduced with these particles for acute infection. In addition to that, LV-tr-KRAB-Red viral particles were also produced. The cotransduction of HeLa cells with LV-THsi/LIMK1 or LV-THsi empty vector and LV-tr-KRAB-Red was performed to make the drug-inducible RNAi. In order to be able to compare doxycyline treated and untreated cells, the coinfection experiments were performed in duplicate.

Efficiency of acute infection was monitored by tracking GFP green fluorescent protein expression in HeLa cells by fluorescent microscope which is indicator of shRNA expression. 2 days after infection, GFP signal was started to be detected in both LV-THsi empty vector or LV-THsi/LIMK1 infected HeLa cells (figure 3.37). Conversely, HeLa cells, which were coinfected with LV-tr-KRAB-Red and LV-THsi/LIMK1 or LV-THsi empty vector, started to express *Discosoma sp. reef coral* Red (dsRed), a red florescent protein which serves as a marker of KRAB. In that setting, cells loose the indicating an efficient repression of shRNA and GFP marker expression by KRAB (figure 3.37). Remarkably, treatment with doxycyline released this repression giving rise to expression of GFP.

To evaluate the efficiency of infection, infected cells were processed for FACS analysis to monitor GFP expression. As shown in figure 3.37, while almost all of cells infected with LV-THsi or LV-THsi/LIMK1, were GFP positive, coexpression of KRAB repressed GFP expression at 95 and 92 % respectively. Furthermore, fluorescence-activated cell sorting (FACS) analysis of these cells showed GFP-silencing effect of KRAB and the release of inhibition upon doxycycline treatment (figure 3.38).

Next, we addressed whether this LIMK1 (1419) shRNA can induce an efficient downregulation of LIMK1 expression. The WB results from acute infection of LV-THsi/LIMK1 showed striking depletion of LIMK1 protein (figure 3.39, upper blot lane 4). The cells which were coinfected with LV-tr-KRAB-Red produced normal levels of LIMK1, demonstrating an efficient repres-

sion of shRNA by KRAB (figure 3.39, first lanes 2 and 5). Furthermore, doxycycline treatment resulted in complete depletion of LIMK1 protein (figure 3.39,upper blot lane 6) whereas doxycycline treatment to HeLa cells with LV-tr-KRAB-Red and LV-THsi empty vector didn't affect the endogenous levels of LIMK1(figure 3.39,first blot lane 3). Altogether, these results showed that shRNA mediated downregulation of LIMK1 could be efficiently induced by doxycycline treatment. Western blotting using anti-LIMK2 antibody showed that this shRNA is specific to LIMK1 (figure 3.39, second blot). Interestingly, the depletion of LIMK1 caused a decrease in phospho-cofilin, although it was not affecting the total cofilin (figure 3.39,third and fourth blots, lanes 4 and 6).

To complete the characterization of this system, we defined the expression levels of LIMK1 in HeLa cells where acute infection was performed by immunoflorescence (after 5 days of infection, cells were fixed by PFA/triton and processed for immunoflorescence using anti-pMAL-LIMK1 antibody). The cells that were infected by LV-THsi empty vector containing viral particles didn't show any difference in endogenous expression of LIMK1, regardless of the level of GFP expression. On the contrary, in LV-THsi/LIMK1infected cells, the protein level of LIMK1 was correlated directly with GFP expression levels. Indeed, the cells with high GFP expression, had knockdown of LIMK1 by shRNA expression.

With these results we could characterize an shRNA against LIMK1, which potently inhibits LIMK1 expression. These findings, showed that usage of lentivirus-mediated shRNA, made it possible to track the LIMK1 depleted cells in Western blotting, FACS and immunofluorescence.

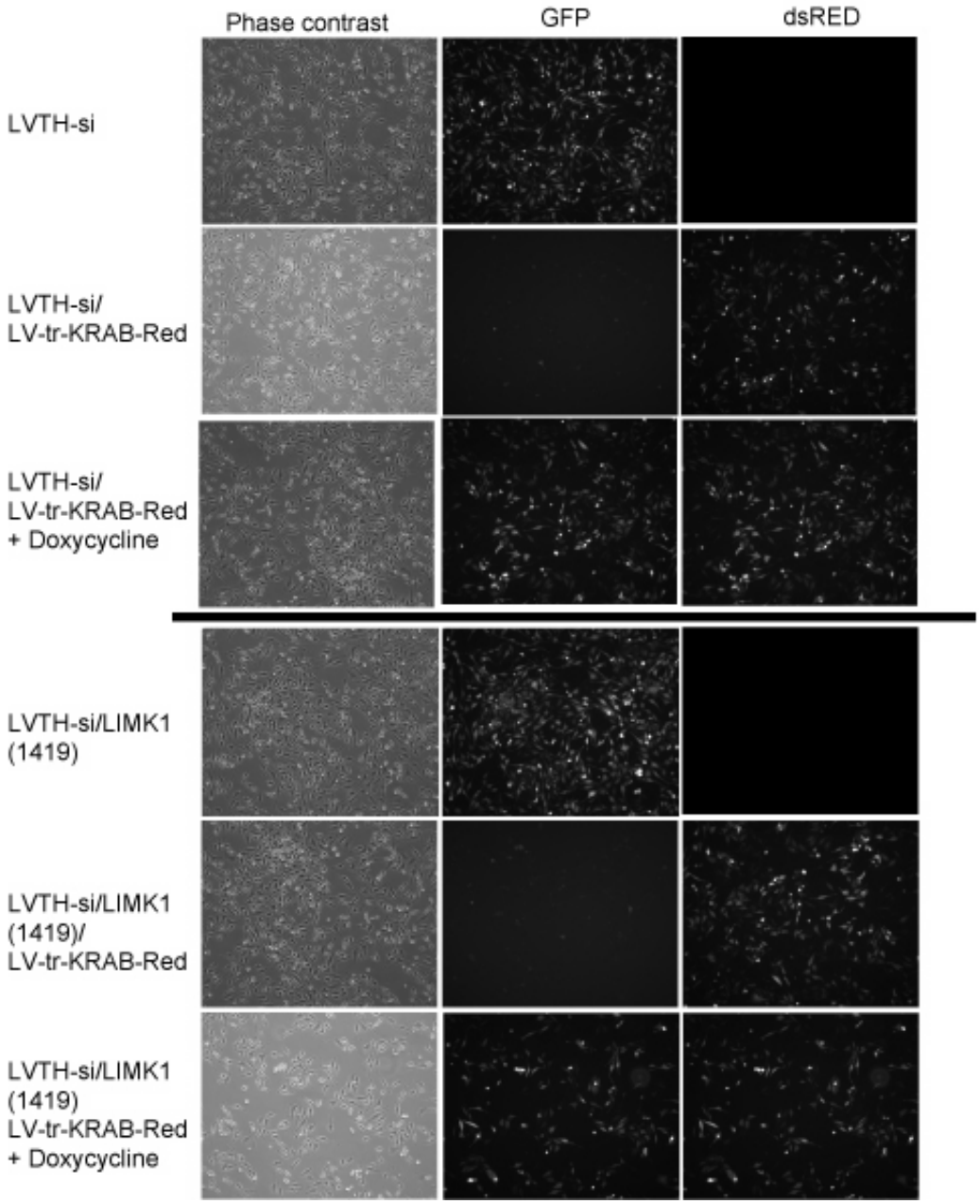

Fig. 3.37: **Images of HeLa cells transduced with LVTH-si empty vector (A) or LVTH-si/LIMK1 (B) or cotransduced with LV-tr-KRAB-Red and LVTH-si empty vector or LVTH-si/LIMK1 +/- Doxycyclline**. **A.** Cells were transduced with LV-THsi with or without LV-tR-KRAB-Red vector. After 5 days of infection images were taken, and at this stage, 5 μg/ml doxyycline (DOX) was added to cells cotransduced with LV-THsi and LV-tR-KRAB-Red. Following 3 days of treatment, the images was taken. **B.** Cells were transduced with LV-THsi/LIMK1 with or without LV-tR-KRAB-Red vector. After 5 days of infection images were taken, and at this stage, 5 μg/ml doxyycline (DOX) was added to cells cotransduced with LV-THsi/LIMK1 and LV-tR-KRAB-Red. Following 3 days of treatment, the images were taken by Zeiss Axiovert microscope. Images are representative of 3 independent experiments

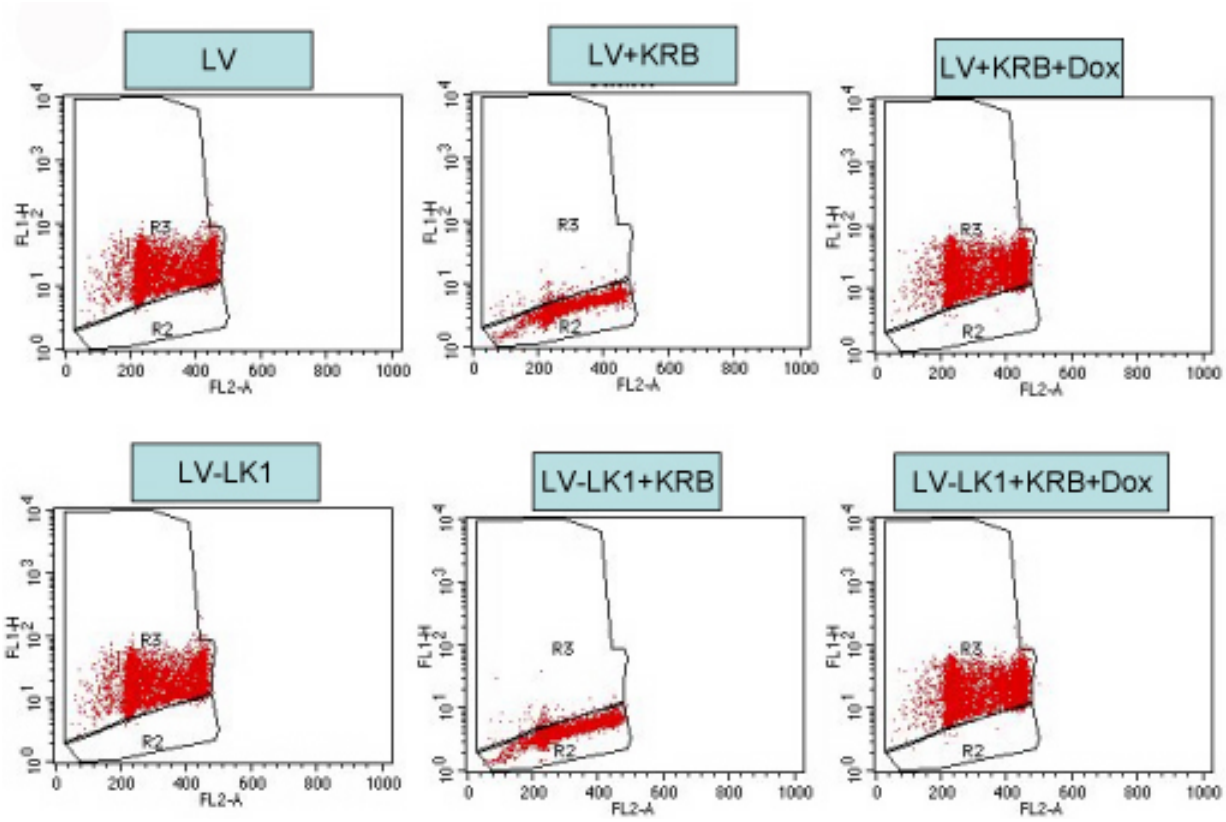

Fig. 3.38: **The GFP silencing effect of KRAB protein and releasing by DOX** HeLa cells which were infected with LV-THsi (LV), LVTH-si/LIMK1(LV-LK1) alone or with LV-tR-KRAB-Red(LV+KRB, LVLK+KRB) +/- DOX (LV+KRB+DOX, LVLK+KRB+DOX), were harvested, and processed for FACS analysis using FACSCalibur. The FACS results are representative of 3 independent experiments.

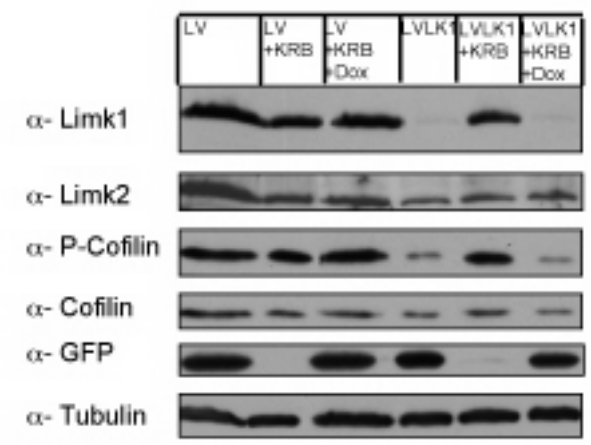

Fig. 3.39: **Lentivirus-mediated LIMK1 shRNA caused efficient depletion of LIMK1 protein**. **A.** HeLa cells, infected with LVTH-si or LVTH-si/LIMK1 +/- KRAB, kept 5 days and harvested or LVTH-si or LVTH-si/LIMK1 +KRAB cells were treated with Doxycycline (Dox) for additional 3 days and harvested. All cells were lyzed and processed by Western blotting using anti-pMAL-LIMK1, anti-LIMK2, anti-P-cofilin, anti-cofilin, anti-GFP and anti-tubulin (loading control). 100 μg of protein was loaded to 15 % of SDS-PAGE. **B.** HeLa cells after harvesting were processed for FACS analysis using FACSCalibur. The WB results are representative of 3 independent experiments.

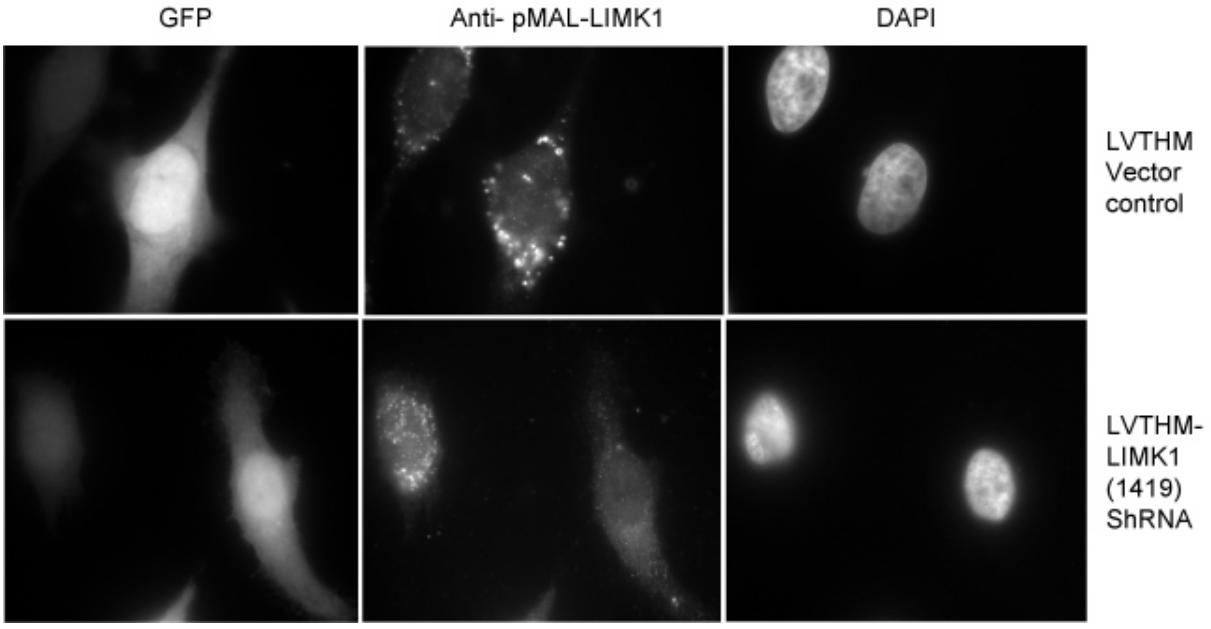

Fig. 3.40: **The depletion of LIMK1 protein level was monitored using immunofluorescence** Acute infection of LV-THsi empty vector or LV-THsi/LIMK1 vector was performed. 5 days after infection, cells were fixed using PFA/triton and processed for immunofluorescence using anti-pMAL-LIMK1 antibody. Images were taken using Deltavision Microscope. Images are representative of 3 independent experiments.

3.2.2.4 Conclusion Remarks and Perspectives

The data from siRNA studies, identified that LIMK1 (662) siRNA, can efficiently downregulate LIMK1 expression. This will be used in section 3.4, to elucidate the functional consequences of LIMK1 depletion regarding its role in cell cycle regulation.

Moreover, the shRNA that has been characterized during this study will certainly make it possible to answer open questions regarding LIMK1 that cannot be addressed with siRNA. i) By investigating the effect of dose- dependent depletion of LIMK1, ii) By bypassing the toxicity effect of oligonucleotides transfection, iii) To downregulate LIMK1 efficiently in non-dividing or primary cells, and finally iv) To create transgenic mice.

3.3 The regulation of LIMK1 by VHL

3.3.1 Introduction

VHL (von Hippel Lindau) is a tumor suppressor protein which germline mutations cause an autosomal-dominant inherited familial cancer syndrome called von Hippel-Lindau (VHL) disease. VHL disease is characterized by a diverse array of tumors such as CNS haemangioblastomas, renal cell carcinomas and pheochromocytomas [Barry and Krek, 2004]. At the molecular level, VHL tumor suppressor protein forms a complex with elongin C, elongin B, Cul2 and RING-H2 protein Rbx1(collectively referred as VCB- Cul2 complex) and targets Hif α for ubiquitin- mediated degradation in normal oxygen conditions [Krek, 2000]. This leads to inhibition of Hif target genes such as VEGF (vascular endothelial growth factor) that is a key factor in new blood vessel formation. Furthermore, recently it has been discovered by our group that the chemokine receptor CXCR4 is a novel HIF target [Staller et al., 2003]. CXCR4 had high expression in invasive breast tumors, and its ligand (SDF-1) was shown to exhibit a peak levels of expression in organs where breast cancer cells metastasize. Moreover, in breast cancer cells, signaling through CXCR4 has been shown to mediate actin polymerization, and this induces chemotactic and invasive responses [Muller et al., 2001]. All these findings suggest that VHL may affect actin cytoskeleton directly or indirectly. Interestingly, it has been shown that SDF1 stimulation of A498 cells, which are deficient for VHL, led to rapid activation of LIMK1 and the effect was abrogated upon VHL reintroduction [Staller et al., 2003] suggesting that LIMK1 might be a downstream effector of VHL.

3.3.2 LIMK1 expression and activity levels are regulated by VHL

Collaborative work between J.Listzwan, a former postdoctoral fellow in the laboratory, and the proteomics centre Novartis, Basel, had demonstrated differential expression of several proteins in the VHL null 786O cells compared to their isogenic counterparts expressing HA-pVHL30. One

of the differentially expressed protein was cofilin. Interestingly, cofilin was shown to be 2.5 fold higher in 7860 cells when compared to their isogenic counterpart expressing HA-VHL30. Afterwards, it was also confirmed by 2D gel electrophoresis the higher levels of phospho-cofilin in 7860 than in the isogenic counterparts with HA-VHL30 (Lisztwan and Krek, unpublished). Furthermore the increase of phospho-cofilin was shown in HeLa cell where VHL was depleted (Dr. Robert Barry, unpublished). Since VHL loss is in different tumors and the increase of LIMK1 expression levels as well as activity in some of these tumors, it was intriguing to investigate if the increase of phospho-cofilin levels observed in VHL null cells was as a result of increase of LIMK1 level/activity. To elucidate this question, HeLa cells were treated with VHL siRNA and after 24, 48 and 72 hours cells were analyzed by WB for LIMK1, VHL and phospho-cofilin levels (figure 3.41). Remarkably, VHL depletion was correlated with increased levels of LIMK1. Moreover, consistent with previous findings, phospho-cofilin level was higher in VHL siRNA treated cells which was a clue of a high kinase activity of LIMK1. To find out if increase in phosphorylation of cofilin upon VHL depletion was via LIMK1 activation increase, HeLa cells were treated with LIMK1, VHL and both LIMK1 and VHL siRNAs. The phosphorylation of cofilin was lost both with LIMK1 and LIMK1/VHL siRNA treatments, demonstrating that LIMK1 activity increase was the reason for phospho-cofilin level increase observed in VHL- depleted cells (figure 3.42). Additionally, both experiments pointed out that there was an increase in total LIMK1 protein levels upon VHL depletion, which could be due to inhibition of LIMK1 degradation or activation of a transcriptional factor that caused an increase in LIMK1 expression.

3.3.3 LIMK1 protein level increase upon VHL depletion is not due to its inhibition of degradation

The proteolysis of cellular proteins is a complex, temporally controlled and tightly regulated process which is carried out by a complex cascade of enzymes and displays a high degree of specificity towards its numereous substrates. Degradation by ubiquitin-proteasome pathway involves

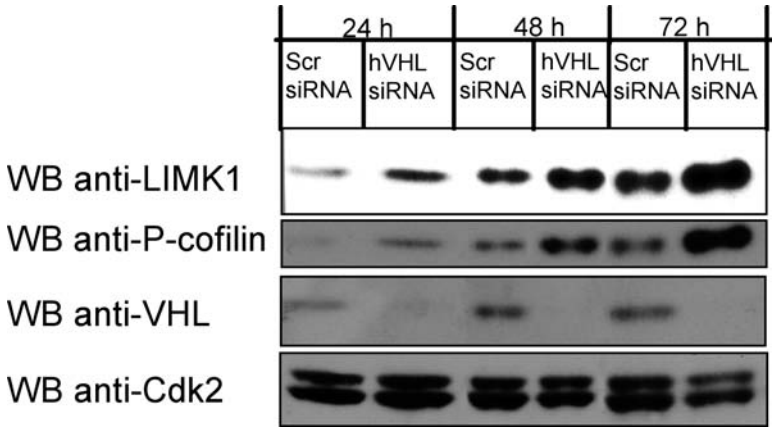

Fig. 3.41: **VHL depletion causes increase in both activity and protein levels of LIMK1**. Lysates from nonsilencing siRNA (Scr siRNA) or VHL siRNA treated HeLa cells were immunoblotted using anti-pMAL-LIMK1 (f.l), anti-phospho-cofilin, anti-VHL (CT) and anti-Cdk2 (as a loading control) antibodies. 100 μg of whole cell extracts were loaded to 12%PAGE. The WB shown are representative of 3 independent experiments.

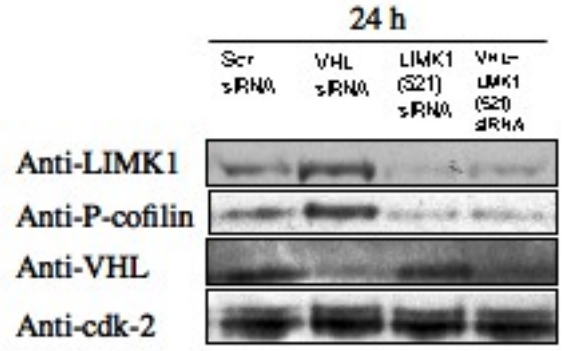

Fig. 3.42: **The increase in phospho-cofilin level upon VHL depletion is via LIMK1** Lysates from 24 h nonsilencing siRNA (Scr siRNA), LIMK1 (521), VHL siRNA or both LIMK1 (521) and VHL siRNA treated HeLa cells were immunoblotted using anti-pMAL-LIMK1 (f.l), anti-phospho-cofilin, anti-VHL (CT) and anti-Cdk2 (loading control) antibodies. 100 μg of whole cell extracts were loaded to 12%PAGE gel. The WB shown are representative of 4 independent experiments.

two steps: first is the covalent attachment of multiple ubiquitin molecules to the target protein and second is the degradation of tagged protein by the 26S proteasome. Conjugation of ubiquitin to the substrate proceeds by three step mechanism including binding of ubiquitin-activating enzyme, E1, following activation of E2 enzymes which are ubiquitin-conjugating enzymes that transfers ubiquitin from E1 to E3. E3 is a ubiquitin-protein ligase that binds specifically to the substrate protein [Ciechanover, 1998].

VHL is reported as a component of E3 ubiquitin-protein ligase complex with elongin C and Cul-2. In conjuction with universally required components E1, E2 and ubiquitin, the complex including VHL displays ubiquitin promoting activity [Lisztwan et al., 1999]. Because of the role of VHL in a ubiquitin promoting complex, it was intriguing to investigate if VHL regulates the stability of LIMK1 as it does to HIF. To elucidate whether LIMK1 is degradated via ubiquitin- proteasome pathway, two approaches were followed. As a first approach, HeLa cells were treated with a proteasome inhibitor MG132 for 4 hours and subsequently the protein levels were analyzed by Western blotting. As shown in figure 3.43, there was no difference in total protein levels with or without MG132, suggesting that LIMK1 is not degraded through ubiquitin/proteosome pathway. p53 used as a positive control to demonstrate the inhibition of proteasome pathway (figure 3.43 A). As a second approach ts20 mouse fibroblasts which are temperature-sensitive (ts) mutants of BALB/c 3T3 was used. Ts20 cell lines have a functional E1 enzyme at 33 $^{\circ}$ C, but when temperature increased to 39 $^{\circ}$ C E1 enzyme is deficient [Chowdary et al., 1994]. Even though, there was accumulation of p53 at 39 $^{\circ}$ C implying that the ubiquitin-proteasome pathway was shut down because of deficient E1, no change was detected in protein level of LIMK1. Additionally, there was no activity difference of LIMK1 since phospho-cofilin levels stayed same at 39 $^{\circ}$ C (figure 3.43 B). These results suggested that the protein level increase of LIMK1 was not due to inhibition of degradation.

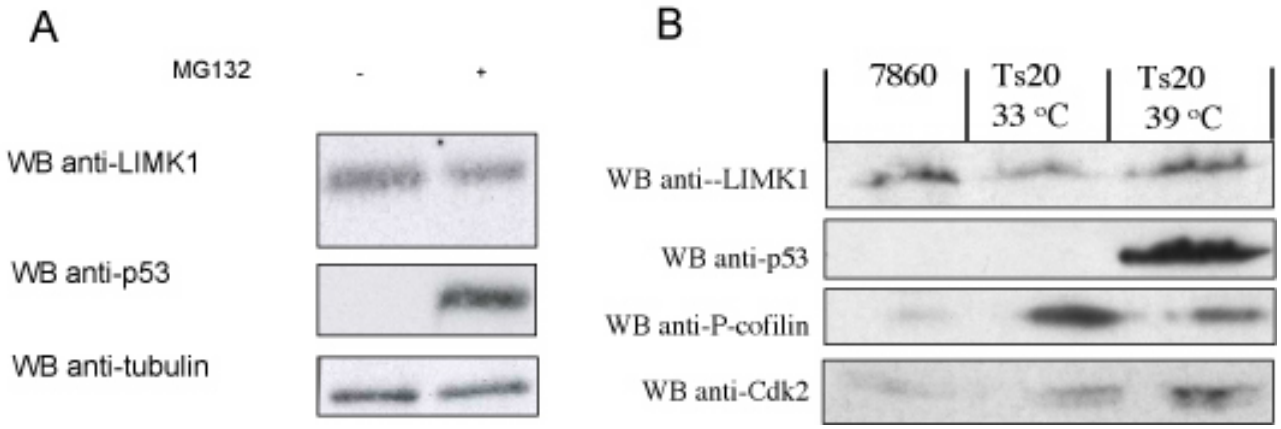

Fig. 3.43: **LIMK1 protein levels didn't change either with MG132 treatment or with E1 deficiency A.** Lysates from MG132 treated or untreated HeLa cells were immunoblotted using anti-pMAL-LIMK1 (f.l), anti-p53 and anti-tubulin (loading control) antibodies. 100 μg of whole cell extracts were loaded to 10%PAGE. **B.** Lysates from 7860, ts20 (33 °) and ts20 (39 °) were immunoblotted using anti-pMAL-LIMK1 (f.l), anti-phospho-cofilin, anti-p53 and anti-Cdk2 (loading control) antibodies. 100 μg of whole cell extracts were loaded to 10% SDS PAGE gel. The WB shown are representative of 3 independent experiments.

3.3.4 LIMK1 protein level increase upon VHL depletion is due to a transcriptional activation

After finding that VHL didn't regulate LIMK1 at the protein level, we investigated if regulation of LIMK1 was at the transcriptional level. In order to elucidate transcriptional level of LIMK1, real time quantitative PCR (RQ-PCR) assay was performed. RQ-PCR is based on the continuous measurement of the accumulation or reduction of fluorescence signals during the amplification reaction. One of the important features of RQ-PCR is the ability to monitor the increasing amount of product at early time points during the PCR reaction. This facilitates quantification of the target in the exponential phase

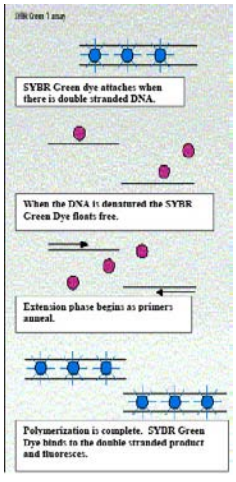

Fig. 3.44: **SYBR Green Dye Assay**

of PCR, when the amplification product first becomes detectable. Therefore, the quantification by RQ-PCR is not affected by limiting concentrations of reagents or by cycling conditions [Watzinger et al., 2006]. For RQ-PCR analysis, we used SYBR Green I, a fluorescent DNA-binding dye, which binds the minor groove of double stranded DNA leading to increase of intensity of the fluorescent emissions. During the annealing and extension steps, an increasing amount of dye binds to the newly synthesized DNA strands leading to maximum fluorescence emission at the end of elongation phase. As soon as the DNA is denatured again during PCR cycling, intercalated dye molecules released into the solution resulting in a drop of fluorescence. The fluorescence is recorded after each cycle at the end of elongation phase, and reflects the number of PCR products generated during the amplification process (figure 3.44) [Morrison et al., 1998].

HeLa cells were treated with nonsilencing (Scr) siRNA and VHL siRNA for 24 and 48 hours and following RNA isolation from these cells, cDNA was synthesized, and the transcriptional expression levels were investigated using RQ-PCR. Two different sets of experiments were performed: (1) HeLa cells treated with Scr siRNA or VHL siRNA for 24 and 48 hours were assessed for LIMK1 RNA level. The expression level of LIMK1 in VHL depleted cells were compared to Scr siRNA treated HeLa cells for 24 and 48 hours, (2) HeLa cells kept untreated or treated with Scr siRNA or VHL siRNA for 48 hours were assessed for LIMK1 RNA levels. The expression level of LIMK1 in Scr siRNA treated or VHL depleted cells were compared to untreated cells. Expression of LIMK1 was normalized to 18S rRNA levels. LIMK1 expression level was shown to be 2.65 and 5.7 fold higher after 24 hours and 48 hours of VHL siRNA treatment, respectively when compared to Scr siRNA treated cells. Additionally, the second experiment pointed out that, there was a 5.45 fold increase in LIMK1 expression level when compared to untreated cells.

These results, suggested that LIMK1 protein level increase upon VHL depletion is due to an increase rate of transcription. These findings are consistent with previous reports from studies of prostate and breast cancer which suggested an increase in LIMK1 transcription, expression level,

and activity in tumors and during metastasis [Davila et al., 2003].

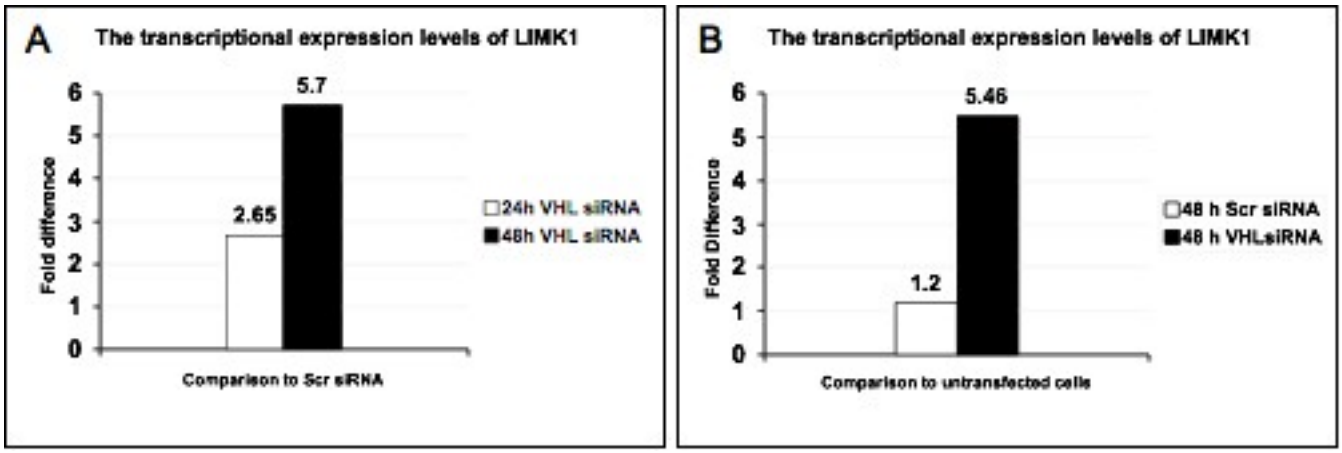

Fig. 3.45: $\sim$ **5 fold increase in LIMK1 expression level upon VHL depletion A.**HeLa cells were treated with Scr and VHL siRNAs, and following RNA isolation, and cDNA synthesis, samples were processed for RQ-PCR. The expression levels of LIMK1 upon VHL depletion were compared to cells treated with Scr siRNA after 24 hour and 48 hour of siRNA treatment. **B.**HeLa cells were kept untreated or treated with Scr or VHL siRNAs, and following RNA isolation, and cDNA synthesis, samples were processed for RQ-PCR. The expression levels of LIMK1 upon VHL or Scr siRNA treatment were compared to untreated cells (48 hour siRNA treatment). Expression of LIMK1 was normalized to 18S rRNA levels.

3.3.5 LIMK1 expression levels didn't increase upon hypoxia treatment

Hypoxia is a state of oxygen deficiency in the body which is caused by the reduction in partial pressure of oxygen, inadequate oxygen transport, or inability of the tissue to use oxygen. Microenvironmental hypoxia occurs in development of solid tumor and acts to promote tumor growth. Hypoxia induces the expression of numerous gene products involved in processes such as angiogenesis, apoptosis, glycolysis and cell cycle control, which are central to the survival and expansion of a malignant cell population in an O_2 deficient environment [Knowles and Harris, 2001].

Hypoxia-inducible factor 1 (HIF-1) is a transcriptional factor that controls the expression of more than 40 gene products which play a role in hypoxia response. HIF-1 is a heterodimer composed of HIF-1α and HIF-1 β subunits. HIF-1 β is constitutively expressed , whereas the expression

of HIF-1α is maintained at low levels in most cells in normoxic conditions. Oxygen-dependent prolyl hydroxylases (PHD) negatively regulates HIF-1α by causing modification in residues 564 and 402 that results in the binding of VHL and targeting HIF-1α for proteosomal degradation in normoxic conditions (figure3.46). Under hypoxic conditions, because oxygen levels are a limiting factor for prolyl hydroxylases, the enzymatic modification of HIF-1α doesn't occur and HIF-1α is not ubiquitinated and degraded [Krek, 2000]. Additionally, the ability of HIF-1α to induce transcription is also oxygen-regulated as a result of cooperative binding of VHL and the co-repressor FIH-1 (factor binding HIF-1), which recruit histone deacetylases (HDAC) to HIF-1α under normoxic conditions. Furthermore, oxygen-dependent hydroxylation of Asn803 inhibits the interaction of HIF-1α with co-activator p300 (figure3.46). Increased steady-state levels of HIF-1α from intratumoral hypoxia or genetic alterations(or both) lead to increased transcription of target genes whose protein products play key roles in tumor progression [Semenza, 2002].

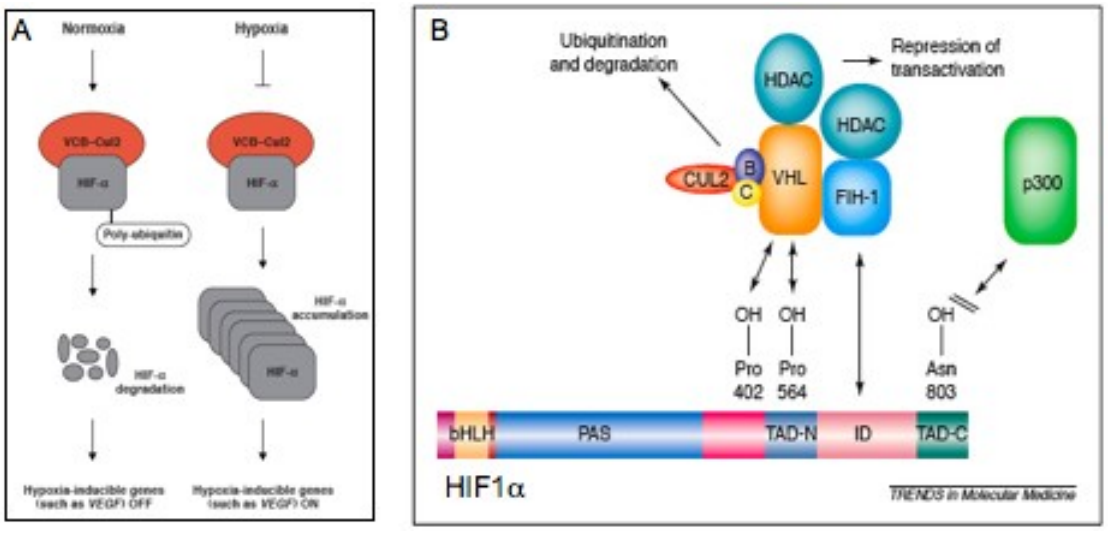

Fig. 3.46: **Regulation of HIF-1α protein expression and transcriptional activity by oxygen-dependent post-translational modifications.** Under normoxic conditions, VHL binds to HIF-1α, recruits an E3 ubiquitin-protein ligase, and target it for ubiquitin-mediated degradation, thereby inhibits activation of hypoxia-induible genes such as VEGF (A,B). Additionally, VHL and FIH-1recruits HDAC that repress transactivation function of HIF-1α. Furthermore, hydroxylation of HIF-1 in Asn803 inhibits its interaction with co-activator p300 in normoxic conditions (B)adapted from Krek, 2000 and Semenza, 2002

As our results showed that there was an increase in expression level of LIMK1 in VHL depleted HeLa cells, we investigated whether upregulation of LIMK1 upon VHL depletion was through HIF-1α dependent transcriptional activation. To assess this question, the transcriptional expression and protein levels of LIMK1 were compared in normoxic and hypoxic conditions, when HIF-1α was degraded and transcriptionally inactive or stabilized, respectively.

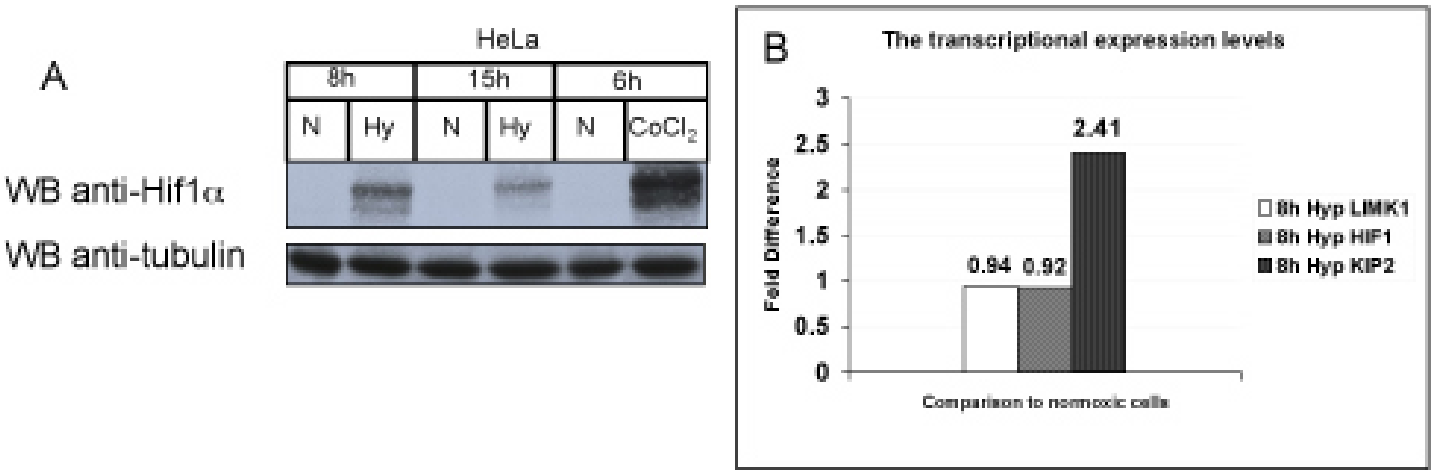

Fig. 3.47: **No change in expression level of LIMK1 upon hypoxia treatment**. **A.**HeLa cells were kept in normoxic condition or treated with hypoxia for 8 and 15 hours, or with $CoCl_2$ for 6 hours, harvested, lyzed and processed for immunoblotting using anti- Hif1α and anti-tubulin antibodies (as loading control). 100 μg protein was loaded to 10% SDS PAGE gel. **B.** From HeLa cells, which were kept in hypoxic (1% oxygen) or normoxic conditions for 8 hours, RNA was isolated, then after cDNA synthesis, processed for RQ-PCR. The expression levels of LIMK1, HIF-1α, and p57(KIP2) in cells which were hypoxia treated, was compared to cells kept in normoxic condition. Expression levels were normalized to 18s rRNA levels.

Initially, in order to select the hypoxic condition when there was high HIF-1α accumulation, HeLa cells were kept in hypoxia incubator with 1% O_2 for 8 hours (8h) or 15 hours (15h), and HIF-1α accumulation was assessed by Western blotting. Treatment with cobalt chloride ($CoCl_2$), an hypoxia mimicking reagent which stabilize HIF1 by inhibiting PHDs, was used as a positive control. When compared to normoxic (N) conditions, HIF-1α was shown to accumulate upon hypoxia (Hy) treatment. Additionally, HIF-1α protein levels were higher at 8h than 15h of hypoxia treatment (figure 3.47 A). Therefore, subsequent hypoxia experiments to assess the

LIMK1 expression levels were performed after 8 h of hypoxia treatment.

To investigate the transcriptional expression level of LIMK1 in hypoxic condition, HeLa cells were kept in normoxic condition (100% O_2) or hypoxic condition (1% O_2) for 8 h. Total RNA was prepared immediately from normoxic and hypoxia treated HeLa cells, and following cDNA synthesis, samples were processed for RQ-PCR analysis. The analysis was performed for LIMK1, HIF-1α and p57(KIP2) (figure3.47 B), and normalized to 18S rRNA levels. We could not detect any difference in LIMK1 transcriptional expression level between cells in normoxic or hypoxic conditions. The HIF-1α expression values were used as negative control for expression increase in this experiment since HIF-1α accumulates in hypoxic conditions is due to protein stabilization. Additionally, we used as a positive control cyclin-dependent kinase (CDK) inhibitor p57 (KIP2), which was previously shown to be a HIF- target gene, whose transcription increased upon HIF activation [Schipani et al., 2001]. There was 2.41 fold increase of p57(KIP2) expression upon hypoxia treatment, demonstrating that the transactivation role of HIF-1α is functional.

Overall, these findings suggested that there was no increase of expression of LIMK1 upon HIF-1α transactivation, directing the underlying hypothesis that the transcriptional regulation of LIMK1 by VHL might be HIF-1α independent.

3.3.6 Conclusion Remarks and Perspectives

This section pointed out that, VHL loss, which is a feature of many tumors, results in LIMK1 accumulation. At the molecular level, we could demonstrate that this increase in LIMK1 expression is due to transcriptional activation. Interestingly, preliminary data suggest that this might be a HIF- independent mechanism, opening perspectives to identify new targets of VHL that can regulate LIMK1 gene transcription. In that setting, LIMK1 appears to be a novel effector of VHL, directly or indirectly, which might participate when dysregulated to tumor progression. Indeed, as LIMK1 hyperactivation is correlated to invasion of different cancers, one might assume that LIMK1 upregulation can secondarly affect tumorigenesis and metastasis resulting from VHL loss.

3.4 Role of LIMK1 through cell cycle

In addition to the function of LIMK1 in cell migration in physiological and pathological conditions, it has been reported that LIMK1 functions in cell cycle progression. Indeed, during G1 progression, LIMK1 prevents the premature activation of cyclin D1 by causing inhibition of Rac and sustained ERK activity [Welsh et al., 2001] (see introduction chapter 'LIMK1 in cell cycle regulation' part for detailed information). Additional to that, overexpression of LIMK1 causes defect in cytokinesis and forms multinucleated cells, which indicated that LIMK1 needs to be highly regulated during cytokinesis. Finally, LIMK1 shows a mitosis-specific hyperphosphorylation and activation during early stages of mitosis that leads to cofilin phosphorylation [Sumi et al., 2002, Amano et al., 2002]. Since, cell cycle studies to identify the role of LIMK1 were based mainly on overexpression of LIMK1 protein we decided to use the siRNA approach, to elucidate the cell cycle function of LIMK1 more in detail. To that aim, LIMK1 was depleted by using LIMK1 (662) siRNA in HeLa cells. The reason behind selecting this siRNA instead of LIMK1(521) being due to the apoptotic phenotype that was observed with LIMK1 (521) siRNA treatment.

To elucidate the effect of LIMK1 in cell cycle progression, after treatment with LIMK1 (662) siRNA, HeLa cells were synchronized at the G1/S boundary or at M phase by double thymidine or nocodazole treatment, respectively. After that, cells were released, and processed for flow cytometry using FACS Calibur and immunoblotting at indicated time points.

As illustrated in figure 3.48, 8-10 hours after thymidine release, most of the Scr and LIMK1 (662) siRNA treated cells were in G2/M phase. Moreover, following thymidine release, the percentages of cells in G1, S, and G2/M were similar in both Scr and LIMK1 (662) siRNA treated cells until 12 hour time point after release (figure 3.48, Histograms which are shown under each FACS graphs). Interestingly, at 12 h time point, when cells were entering G1 phase, the cells which were

LIMK1 depleted, were quicker than Scr siRNA treated cells on exiting G2/M phase and entering G1 phase. As a control, immunoblotting of these samples were performed using anti-pMAL-LIMK1 antibody to confirm the downregulation of LIMK1 in LIMK1 (662) siRNA treated cells in different time points. These results (in the lower panel) indicated that there was an premature enter to G1 phase when LIMK1 was depleted in these cells.

To investigate whether the premature entering to G1 phase was due to improper exit from mitosis, or because of quicker G2 to M phase transition, HeLa cells were treated with Scr siRNA or LIMK1 (662) siRNA for 33 hours and then synchronized in M phase by treated with nocodazole for 15 hours. Such a treatment induces an enrichment in mitotic cells since nocodazole specifically blocks cells at metaphase by destabilizing microtubule structure. Indeed, 90 % of cells were mitotic cells (figure 3.49). Then the mitotic cells were collected by shaking the cell culture plate, (mitotic shake-off), transferred to another plate, and subsequently released at different time points as indicated in figure 3.49. It was found that, 4 hours after nocodazole release, 31% of LIMK1 depleted cells entered G1 phase when, only %20 of Scr siRNA treated cells entered that phase. The difference in cell population treated with LIMK1(662) siRNA and Scr siRNA that entered G1 phase, suggested a premature exit of LIMK1 (662) siRNA treated cells (figure 3.49, FACS histograms and graphs of % of cell). Later on, the nocodazole release experiments were performed after shorter time points, 1,2 and 3 hours and it was found that the difference of exit from mitosis started as early as 2 hours (data not shown). After the entrance to G1 phase, no difference was monitored in progression through G1 phase up to 13 hours release from nocodazole arrest.

Immunoblotting of these samples using anti-pMAL-LIMK1 antibody, confirmed the downregulation of LIMK1 in LIMK1 (662) siRNA treated cells in different time points (figure 3.49, WB). Additionally, WB results pointed out the mitotic shift of LIMK1 upon hyperphosphorylation which was reported before by Amano et al. [Amano et al., 2002].

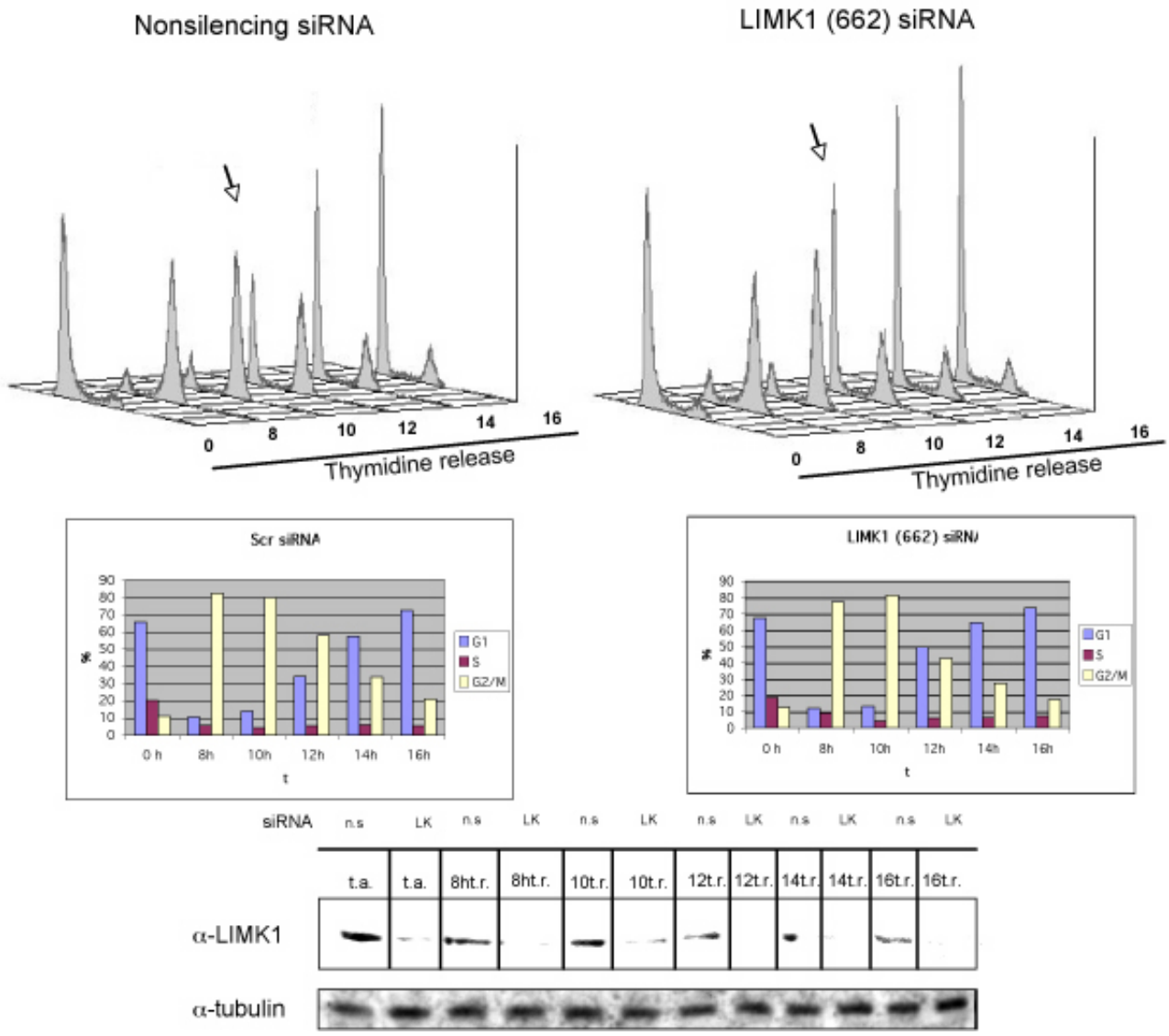

Fig. 3.48: **LIMK1-deficient cells enter prematurely to G1 phase**. HeLa cells, were synchronized at G1/S by treatment with thymidine (double thymidine), 24 hours after treatment with nonsilencing (Scr) or LIMK1(662) siRNAs. At the indicated time points after release from double thymidine block, cells were harvested and analyzed by FACS(fluorescence activated cell sorter) (FACS histograms showed at the top). The % of cells in G1, S and G2/M for this experiment was shown in the graphs below the FACS histograms, which is representative of three independent experiment. HeLa cells harvested in the experiment described above were analyzed by immunoblotting with anti-pMAL-LIMK1antibody. The corresponding tubulin levels are shown as a loading control. 100 μg of protein was loaded to 12 % SDS-PAGE. WB results are representative of 3 independent experiments.Abbreviations: %: % of cells, t: time, n.s: nonsilencing siRNA treatment, LK: LIMK1 (662) siRNA treatment, t.a: thymidine arrest, t.r: thymidine release

Moreover, it was monitored that, in nocodazole treated cells, in addition to the mitotic shift, the LIMK1 protein levels were also lower than the cells which were exponentially growing (figure 3.49, WB, compare lane1 and lane 2), a finding that has been previously described [Sumi et al., 2002]. When Sumi et al. showed that mitotic shift of LIMK1 was due to phosphorylation, they treated HeLa cells with λ-phosphatase. Interestingly even though λ-phosphatase treatment diminished the mobility shift of LIMK1 in mitotic cells, the protein levels of LIMK1 stayed low [Sumi et al., 2002], demonstrating that phosphorylation of LIMK1 did not alter the affinity of the antibody and that there was indeed a decreased expression of LIMK1 in mitotic cells.

Altogether, these data suggest that LIMK1 is regulated during mitosis by both phosphorylation and expression level modulation. Importantly, we could demonstrate that loss of expression of LIMK1 induces a premature exit from mitosis, suggesting that LIMK1 might negatively regulate M to G1 transition, or might be required for proper, controlled progression through mitosis.

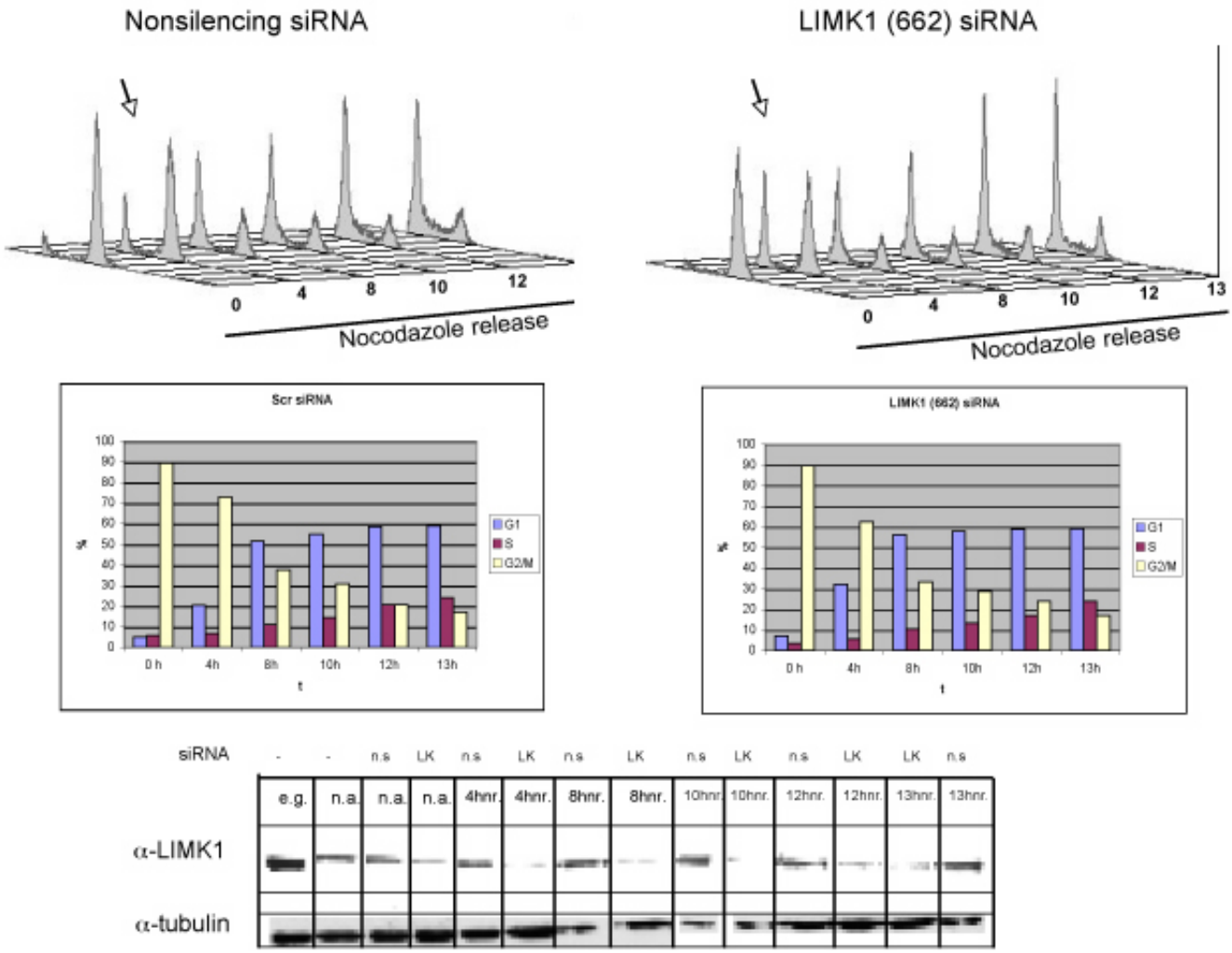

Fig. 3.49: **LIMK1-deficient cells have premature exit form mitosis**. HeLa cells as indicated, were synchronized at prometaphase by treatment with nocodazole for 15 hours. At the indicated time points after release from nocodazole block, cells were harvested and analyzed by FACS. The % of cells in G1, S and G2/M are shown for this experiment in the graphs located under the FACS histograms, which is a representative of 3 independent experiments. HeLa cells harvested in the experiment described above were analyzed by immunoblotting with anti-pMAL-LIMK1antibody. The corresponding tubulin levels are shown as a loading control. 100 μg of protein was loaded to 12 % SDS-PAGE. WB results are representative of 3 independent experiments.Abbreviations: %: % of cells, t: time, n.s: nonsilencing siRNA treatment, LK: LIMK1 (662) siRNA treatment, e.g.: exponentially growing cells, n.a: nocodazole arrest, nr: nocodazole release

3.4.1 Phosphorylation status of LIMK1 is high in mitotic cells

The hyperphosphorylation of LIMK1 in mitotic cells were previously shown by λ-phosphatase treatment which diminished the mitotic shift of LIMK1 as discussed above. To elucidate more in detail the phosphorylation status of LIMK1 in exponentially growing and mitotic cells, HeLa cells were either kept untreated or treated with nocodazole, harvested and processed by immunoprecipitation (IP) with anti-pMAL-LIMK1 antibody followed by Western blotting with anti-pMAL-LIMK1 antibody or anti-T508-P antibody. Immunoprecipitation was performed to detect only the phosphorylated-LIMK1 as anti-T508-P antibody recognizes both LIMK1 and LIMK2. As shown in figure 3.50, LIMK1 could be efficiently immunoprecipitated. Additionally, no immunoreactivity was detected with anti-rabbit IgG which was used as negative control. WB with anti-T508-P antibody revealed that very little amount of LIMK1 was in its phosphorylated state in exponentially growing HeLa cells, however in mitotic cells it was highly phosphorylated. Thus, these results suggested that LIMK1 is highly phosphorylated during early M phase, highlighting a specific activation of LIMK1 during mitosis.

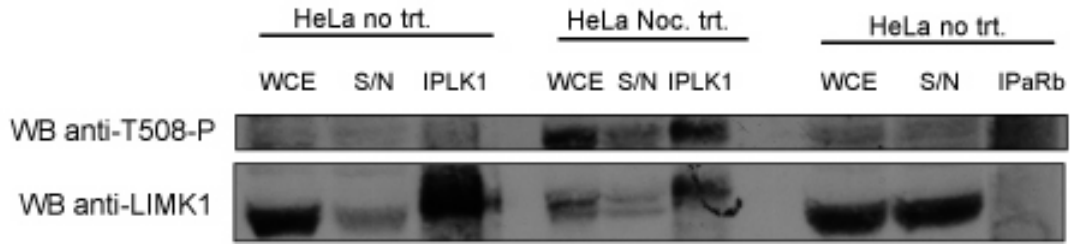

Fig. 3.50: **LIMK1 phosphorylation status in exponentially growing and mitotic cells** Lysates from exponentially growing and mitotic HeLa cells were immonuprecipitated using anti-pMAL-LIMK1 (f.l) antibody and the immunoprecipitates were probed with anti- pMAL-LIMK1 or anti-T508-P antibodies. WCE: whole cell extract, S/N: supernatant after immunoprecipitation, IPLK1: immunoprecipitation using anti-pMAL-LIMK1 antibody, IPaRb: IP using rabbit IgG as negative control, no trt: no treatment, Noc. trt.: nocodazole treatment.

3.4.2 Localization of phosphorylated LIMKs during mitosis

After showing high phosphorylation status of LIMK1 in mitosis by IP using anti-T508-P antibody, we then used this antibody in immunofluorescence. In the first section of results chapter, it was shown that anti-T508P antibody staining was diffuse in the cytoplasm, and in addition, that it accumulates at the cell edges or membrane ruffles. Additionally, the nuclear signal that was observed by anti-T508P antibody was interpreted as from LIMK2 protein as only LIMK2 localized to the nucleus in exponentially growing cells. When mitotic HeLa cells were analyzed using this antibody, centrosomes of early phase mitotic cells (prometaphase and metaphase) and spindle midzones of telophase cells and postmitotic bridges were stained. Localization to centrosomes was confirmed by colocalization with γ tubulin (figure 3.51) .

After receiving a LIMK1 antibody (anti-LIMK1(J)) from T. Nakamura, we examined the localization of LIMK1 in mitotic U2OS cells. The staining of LIMK1 by anti-LIMK1 (J) antibody showed localization to centrosomes of U2OS cells in early mitotic phases (prometaphase and metaphase) and midbody in late phases of mitosis as it was recently reported by the same group [Sumi et al., 2006] (figure 3.52). Localization of LIMK1 to centrosomes was confirmed by colocalization with γ tubulin (figure 3.53). Additionally an antibody against LIMK2, which was received from the same group (anti-LIMK2 (J)), was used for staining of U20S cells. The staining of LIMK2 indicated that it localized to mitotic spindles and to midbody in late mitotic phase (figure 3.54). The immunofluorescence studies with α-tubulin showed the co-localization as it was also reported in this recent article for HeLa cells (figure 3.55) [Sumi et al., 2006].

As LIMK1 localized to centrosomes and LIMK2 to mitotic spindles, it can be suggested that the staining of anti-T508-P in centrosomes corresponds to phospho-LIMK1, which is consistent with the hyperphosphorylation of LIMK1 in prometaphase and metaphase. Another finding that support this observation was from Sumi et al. as they reported that LIMK2 got phosphorylated in prometaphase and metaphase only upon spindle assembly checkpoint activation. Therefore,

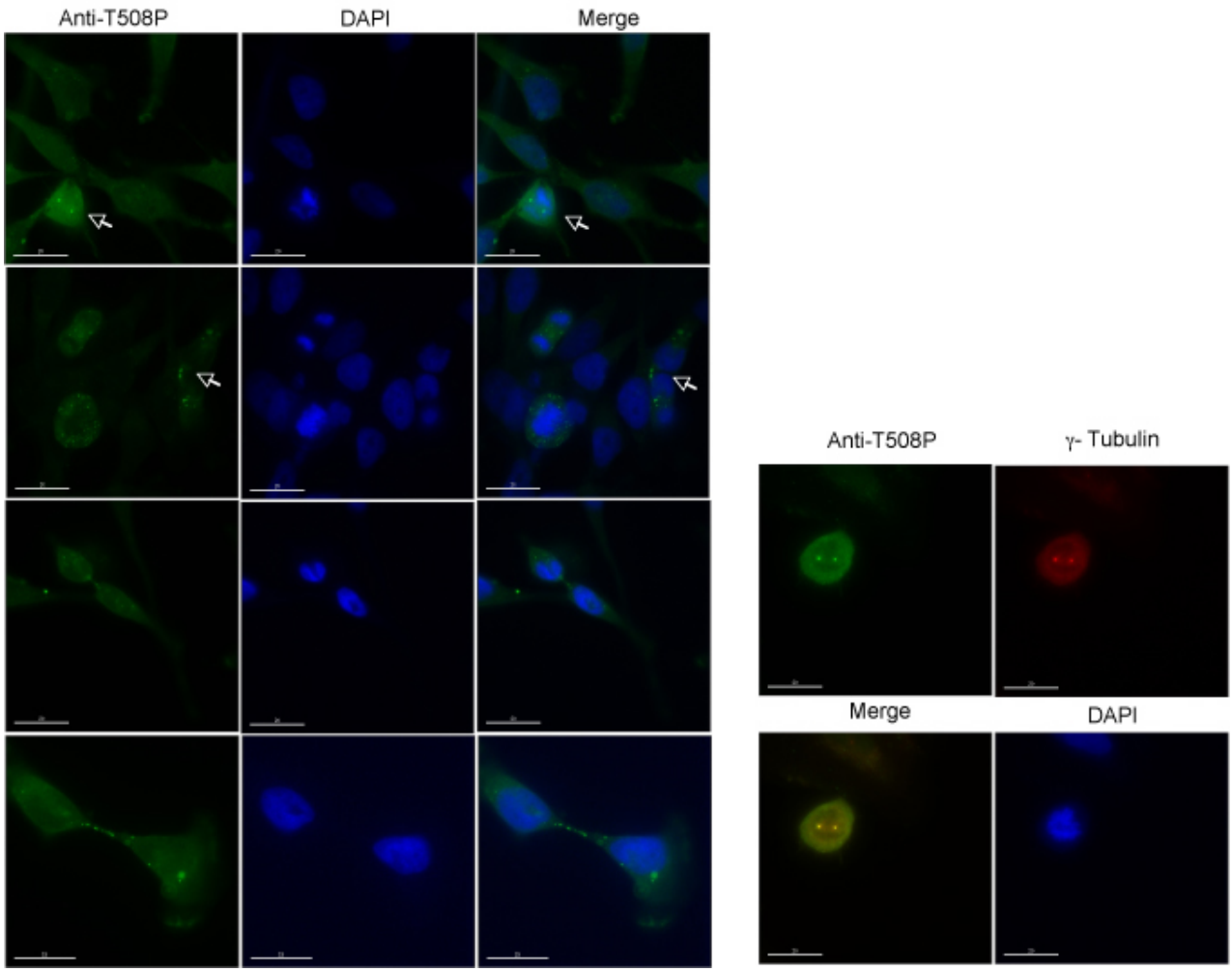

Fig. 3.51: **Centrosomes of early phase mitotic cells (prometaphase and metaphase) and spindle midzones of telophase cells and postmitotic bridges were stained by anti-T508-P antibody**. HeLa cells were fixed by PFA/triton and processed for immunofluorescence using anti-T508-P antibody. In the right panel, colocalization of centrosome staining of anti-T508-P with γ- tubulin is shown. Slides were processed using DeltaVision microscope. DAPI was used as a nuclear marker. Green: anti-T508-P, Blue: DAPI, Red: anti- γ- tubulin. Images are representative of 2 independent experiments. Scale bar 15 μm.

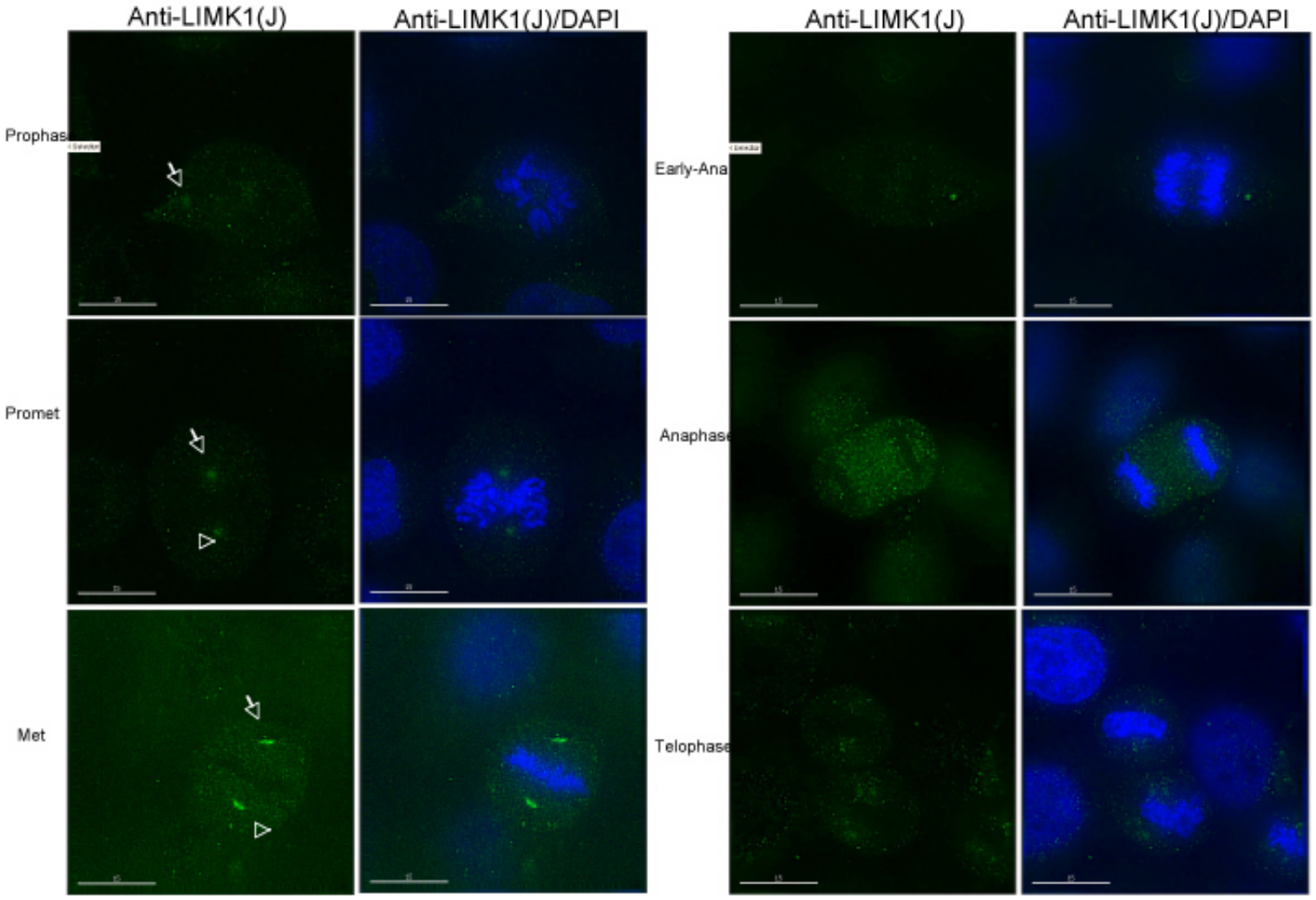

Fig. 3.52: **Subcellular localization of LIMK1 in U2OS cells during cell cycle transition.** At various stages, HeLa cells were immunostained with anti-LIMK1 (J)antibody (green), and DAPI(DNA)(blue). The cell cycle stages of U2OS cells are shown at the site. Images are representative of 3 independent experiments. Scale bar, 15μm.

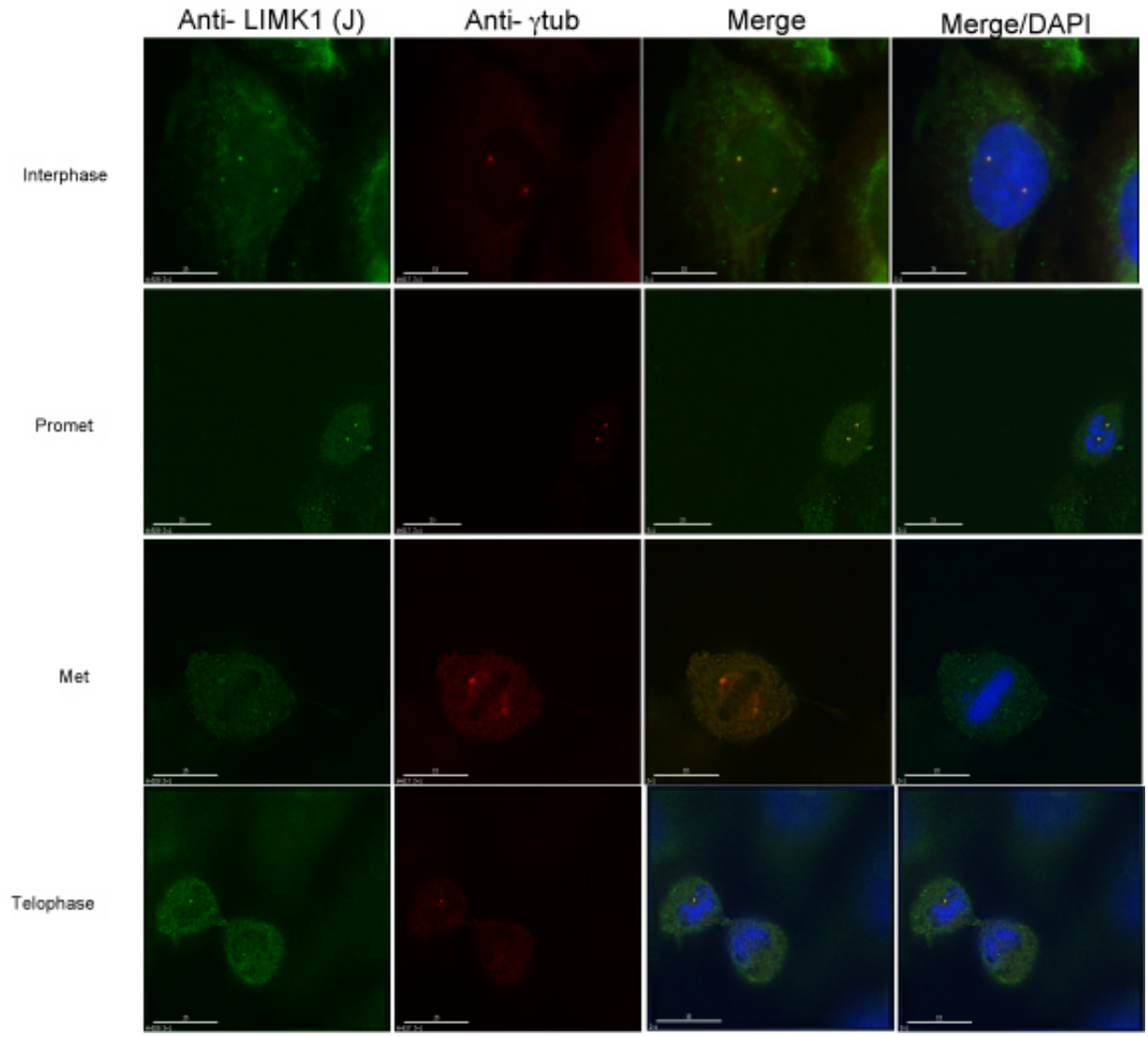

Fig. 3.53: **Colocalization of LIMK1 with γ- tubulin in U2OS cells during cell cycle transition.** At various stages, U2OS cells were immunostained with anti-LIMK1(J) antibody(green), and DAPI(DNA)(blue). The cell cycle stages of U2OS cells are shown at the site. Images are representative of 2 independent experiments. Scale bar, 15μm.

one can assume that, only phospho-LIMK1, but not LIMK2, is active in pro/metaphase cells. In addition to that, the staining of spindle midzone in late phase of mitosis by anti-T508-P antibody would propose that LIMK2 could be active in late phases of mitosis since it localized to spindle midzone during these phases. Further biochemical analysis would be warranted to clarify these findings.

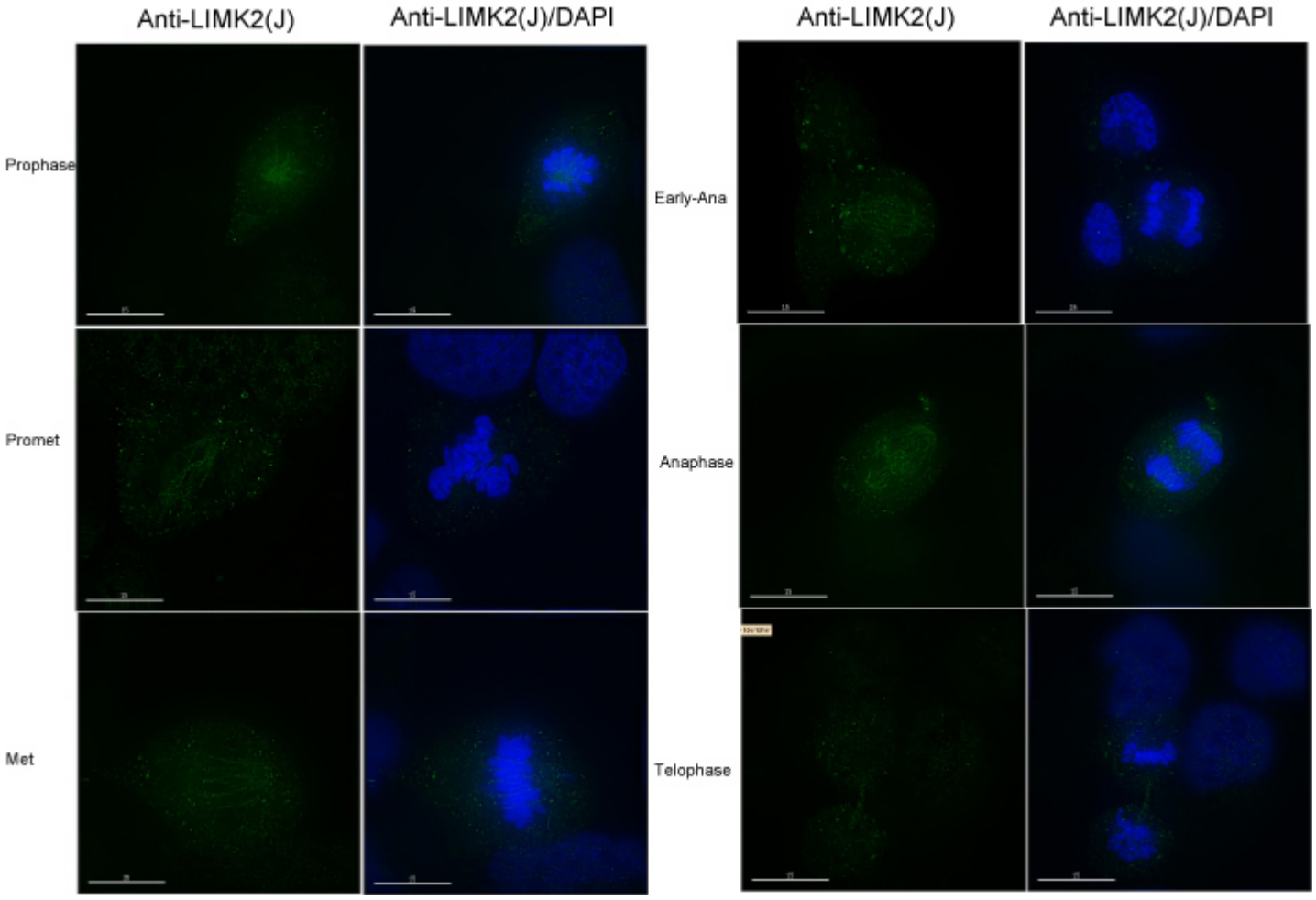

Fig. 3.54: **Subcellular localisation of LIMK2 in U2OS cells during cell cycle transition.** At various stages, U2OS cells were immunostained with LIMK2 (J)antibody (green) and DAPI(DNA)(blue). The cell cycle stages of U2OS cells are shown at the site. Images are representative of 3 independent experiments. Scale bar, 15μm.

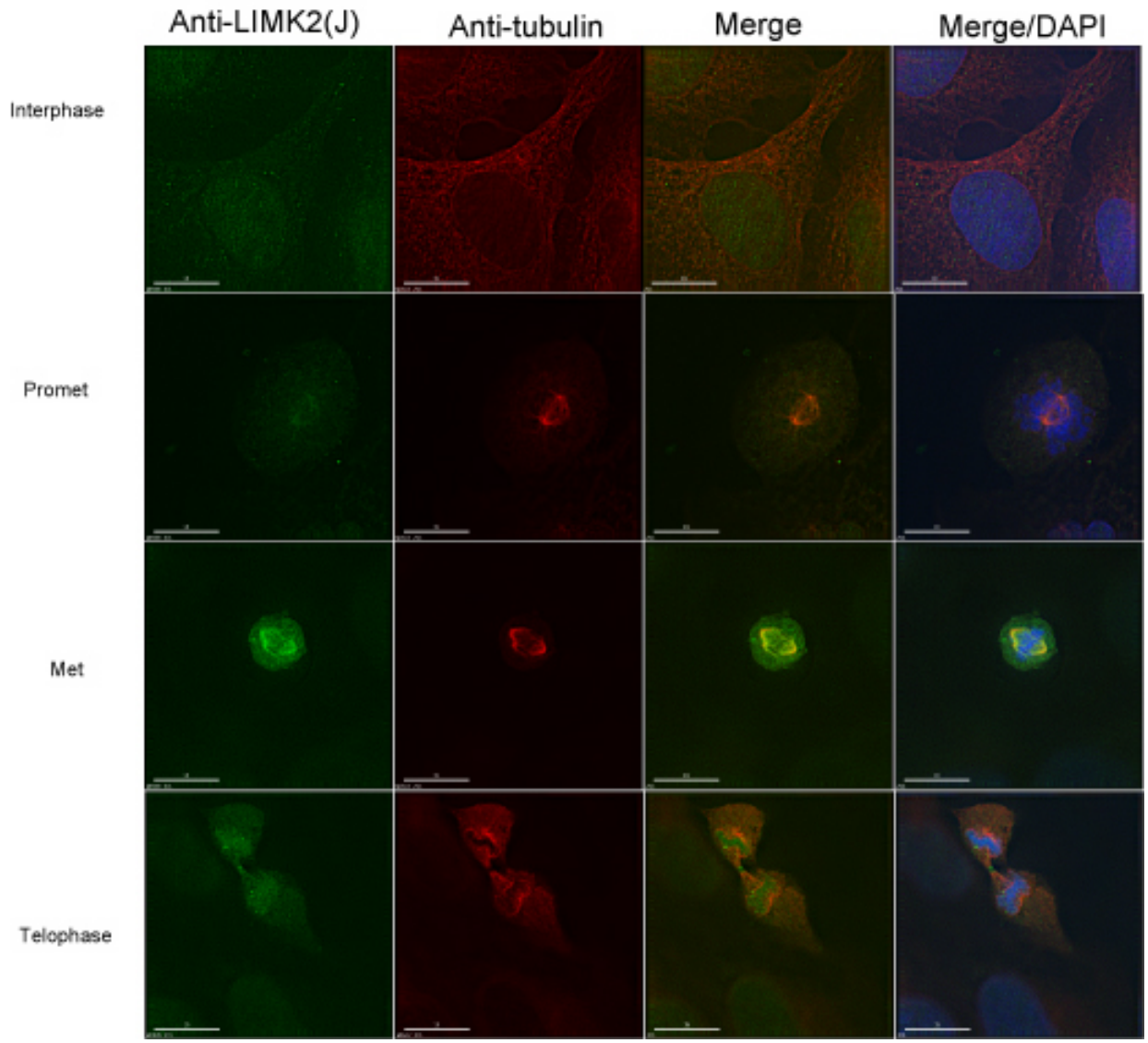

Fig. 3.55: **Colocalization of LIMK2 with α- tubulin in U2OS cells during cell cycle transition.** At various stages, U2OS cells were immunostained with anti-LIMK2(J) antibody(green), and DAPI(DNA)(blue). The cell cycle stages of U2OS cells are shown at the site. Images are representative of 2 independent experiments. Scale bar, 15μm.

3.4.3 Cofilin also localizes to mitotic spindles and spindle midzones

To investigate where cofilin localized during mitosis, we performed an immunostaining using anti-cofilin antibody, which was raised against full length cofilin fused to GST (Dr.J.Listzwan). In previous sections, this antibody was used for immunohistochemical analysis and for western blotting. Here, the antibody was used for immunostaining in HeLa and U2OS cells. As described in previous reports, staining with anti-cofilin antibody in interphase cells showed that cofilin was diffuse in the cytoplasm, and in addition, that it accumulates at the cell edges or membrane ruffles (figure 3.56) [Nagaoka et al., 1995, Dawe et al., 2003].

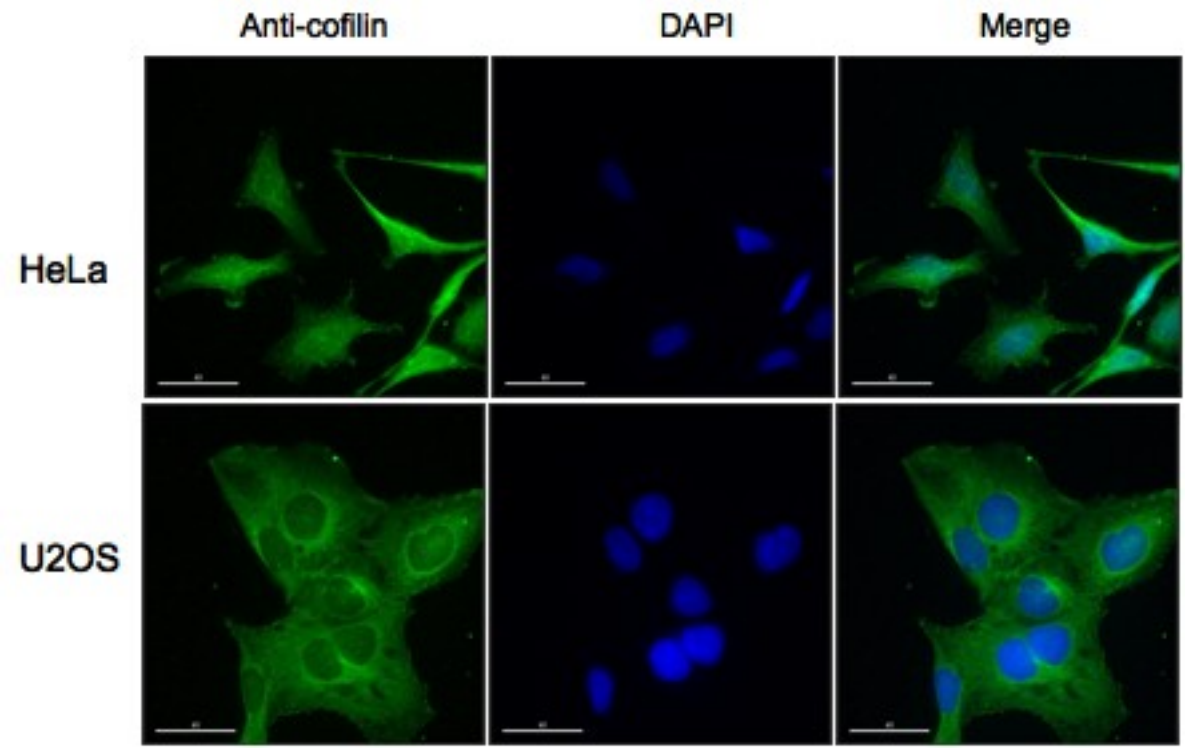

Fig. 3.56: **Subcellular localization of cofilin using anti-cofilin antibody in HeLa and U2OS cells**. Both of the cell lines were fixed with methanol and labeled using anti-cofilin antibody. Slides were processed using DeltaVision microscope. Green: anti-cofilin, Blue: DAPI. Images are representative of 2 independent experiments. Scale bar 15 μm.

In addition to that, as shown in figure 3.57, cofilin appeared to localize to mitotic spindles in

metaphase and anaphase and to spindle midzone during late telophase and during cytokinesis in U2OS cells. Similar results were obtained from HeLa cell immunostaining (data not shown). These findings can be connected to previous data, showing in *Drosophila* that mutations of cofilin homolog *twinstar* resulted in defects in centrosome migration and cytokinesis and raise the intriguing hypothesis that cofilin might have a direct role in spindle function and/or cytokinesis in mammalian cells [Nagaoka et al., 1995]. Moreover, the localization of both cofilin and LIMK2 to mitotic spindles showed a possibility that cofilin could be regulated by LIMK2 during mitosis. Further studies are warranted to elucidate this hypothesis.

3.4.4 Time lapse imaging of LIMK1- depleted HeLa-H2B-GFP cells

To investigate further the phenotype of premature exit from M phase upon LIMK1 depletion observed by FACS analysis, we combined siRNA-based LIMK1 gene silencing and time-lapse fluorescence imaging of HeLA-H2B-GFP cells (received from Dr. Patrick Meraldi, ETH Zurich). The cell lines were created by the fusion of human histone H2B gene to the gene encoding GFP and transfected into human HeLa cells to generate a stable cell line constitutively expressing H2B-GFP.

Following confirmation of efficient depletion of LIMK1 by LIMK1 (662) siRNA in HeLa-H2B-GFP cells (figure 3.58, B), cells were filmed for 10 hours. For the analysis of mitotic timing, nuclear envelope breakdown (NEBD) in each mitotic cell was set as T = 0, and the relative time of the onset of chromosome- to- pole movement (anaphase A time) was determined (figure 3.58, A). Phototoxicity asssociated with fluorescence microscopy limited the time interval of these movies to one frame every 3 min.

Anaphase A times of T = 20 to 55 min were obtained in a set of 300 nonsilencing (Scr) and LIMK1- depleted cells. When the total number of Scr and LIMK1 (662) siRNA treated cells starting anaphase A, after 20, 25, 30, 35, 40, 45, 50, and 55 minutes were compared, no difference

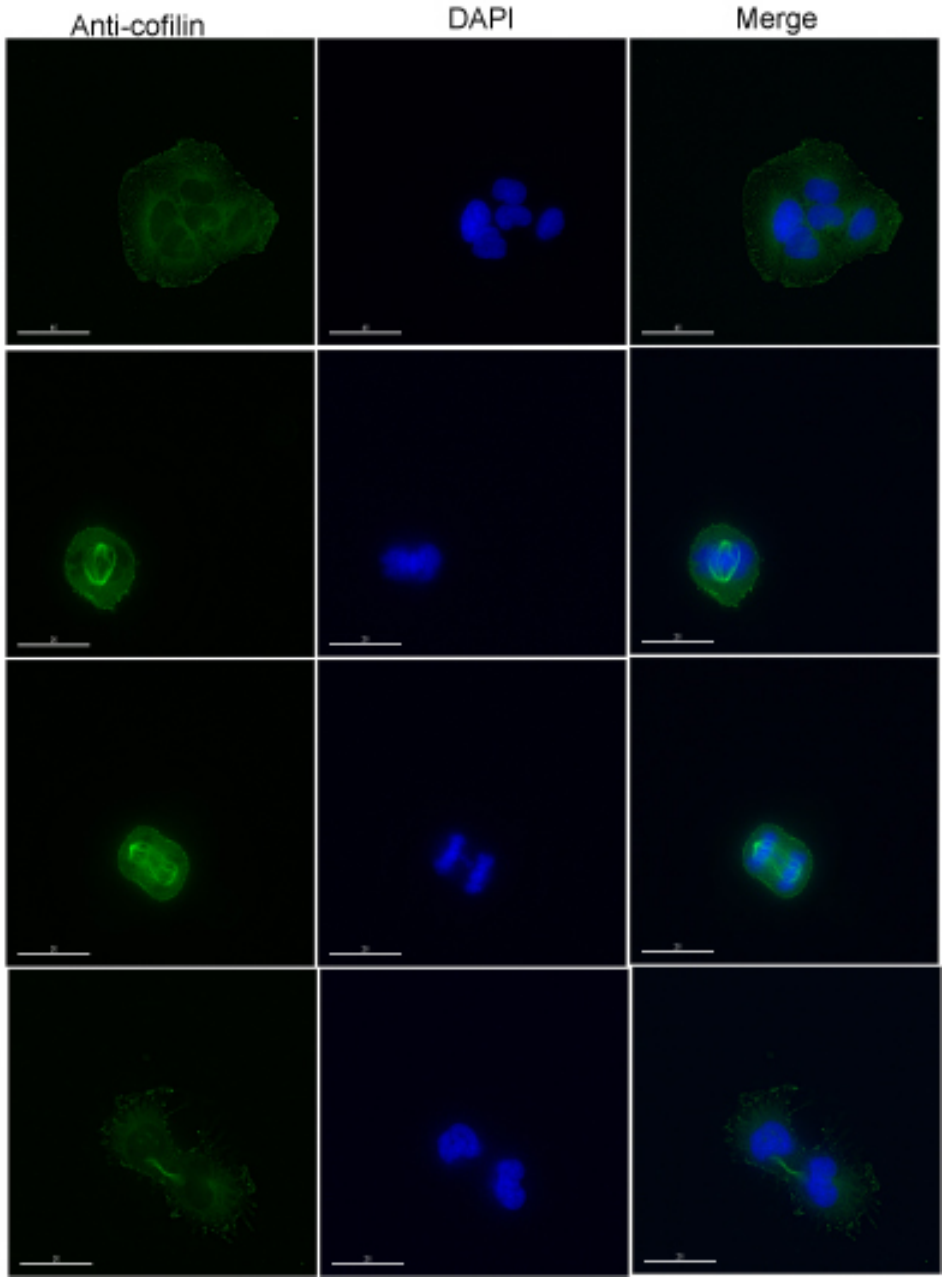

Fig. 3.57: **Cofilin localizes to mitotic spindles and spindle midzones**. U2OS cells were fixed with methanol and labeled using anti-cofilin antibody. Slides were processed using DeltaVision microscope. Green: anti-cofilin, Blue: DAPI. Images are representative of 2 independent experiments. Scale bar 15 μm.

between these two set of cells were found. The cumulative frequency graph in figure 3.58, D also indicated that the distribution of anaphase A times are not different between these two sets. These results suggested that there is not a time difference between Scr and LIMK1 (662) siRNA treated cells in early phases of mitosis. Further experiments to analyze the late phases of mitosis should be done. Because of the limitations of HeLa-H2B-GFP cells to monitor the late phase of mitosis, additional markers such as tubulin or actin in addition to H2B can be added to these cell lines.

During the analysis, even though there was no apparent timing difference between Scr siRNA and LIMK1(662) siRNA, an increase in spindle misorientation was monitored (figure 3.59, A). Following the quantitative analysis, it was shown that there was 20% increase in spindle misorientation in LIMK1 depleted cells. These finding is intriguing as it was reported in fission yeast that, the disturbance of actin cytoskeleton by actin depolymerizing drug latrunculin B (lat B), was correlated to misorientation of spindle axis, suggesting that, the disorganization of the actin cytoskeleton might perturb proper spindle orientation [Gachet et al., 2001]. This opens new perspectives of a possible role of LIMK1 in proper spindle orientation via regulating actin cytoskeleton. Additionally, as it localizes to the centrosomes, this function may be centrosomal-related effect of LIMK1. Further analysis should be performed to clarify these findings.

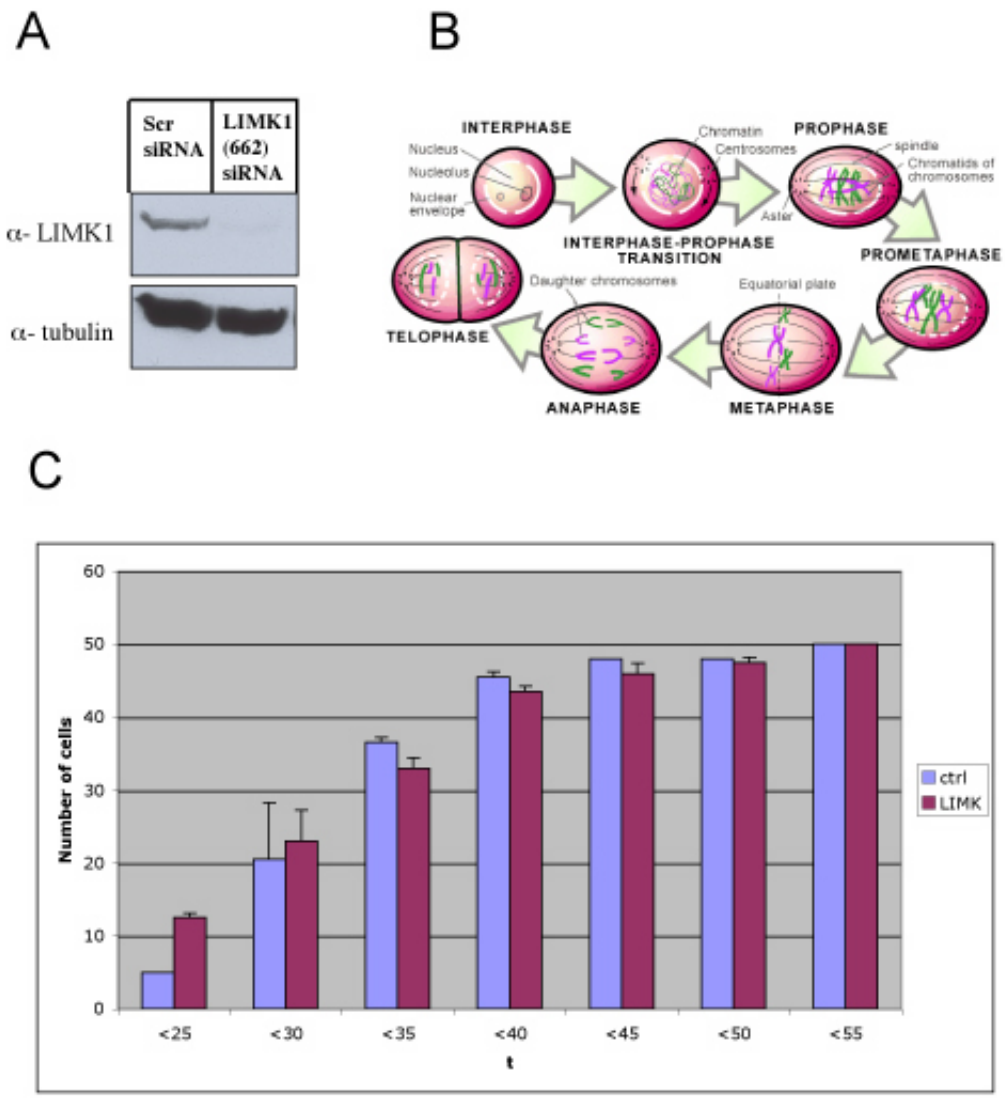

Fig. 3.58: **No difference in timing from NEBD to Anaphase A onset**. **A.** Hela-H2B-GFP cells were treated ether with Scr siRNA or LIMK1 (662) siRNA for 48 hours, harvested, lyzed and processed for immunoblotting using anti-pMAL-LIMK1 and anti-tubulin (as a loading control) antibodies. 100 μg of protein was loaded to 10 % SDS PAGE gel. **B.** Schematic representation of phases of mitosis. **C.** Cells were treated with Scr or LIMK1 (662) siRNA for 48 hours and processed for time-lapse imaging. The graph represents the quantification from 2 independent experiments(mean $\pm$ S.D.) of cumulative values of cells entering Anaphase A at the indicated times.

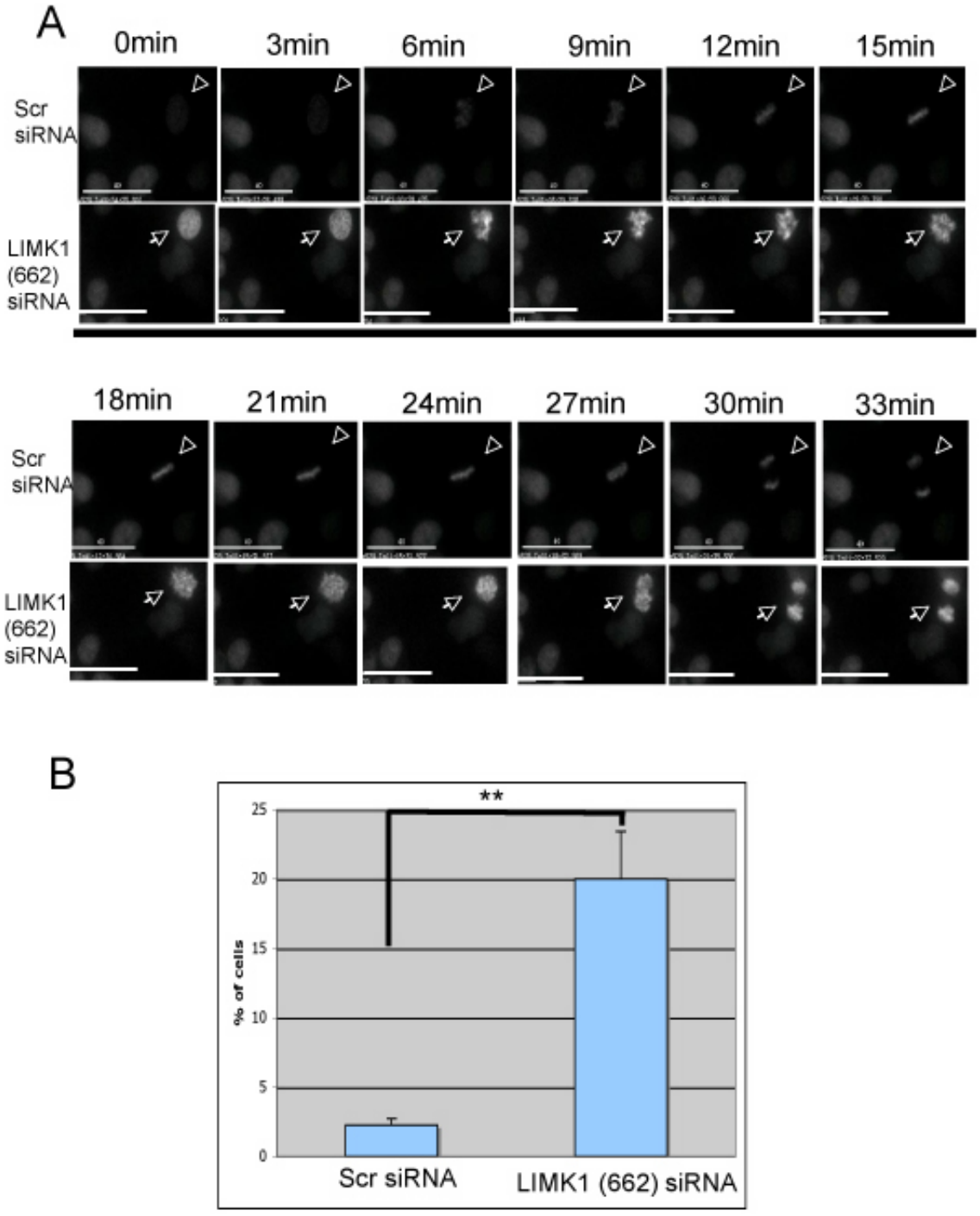

Fig. 3.59: **LIMK1 depletion causes 20% increase in spindle misorientation**. **A.** HeLa-H2B-GFP cells were treated with Scr siRNA or LIMK1 (662) siRNA for 48 hours, and then processed for time-lapse imaging using DeltaVision microscope. Using nuclear envelope breakdown (NEBD) as T = 0, the times of chromosome congression, and Anaphase onset were monitored. Scale bar 40 μm. **B.** The graph represents the quantification of percentage of cells which has a misorientated spindle, from three independent experiments (mean$\pm$). more than control, p $\langle$ 0.01, paired t test.

3.4.4.1 Conclusion and Perspectives

With this set of experiments, we could demonstrate that LIMK1 depletion results in premature M phase exit, suggesting that LIMK1 might control proper progression of mitosis. It has been shown that, activation of LIMK1 is upregulated during early phases of mitosis, supporting role of LIMK1 in early stages of M phase. However, we have not identified the timing difference in early phases in LIMK1 depleted cells. Interestingly, we have identified by immunofluorescence active LIMK in early phases of mitotic cells , but also in late phases, i.e. cytokinesis. Despite this apparent discrepancies, one can envision that the misregulation of LIMK1 in early mitosis may affect the latest stages of mitosis. To address this question, the molecular targets of LIMK1 during mitosis need to be identified. Interestingly, we have identified that an important effect of LIMK1 depletion was the inproper spindle orientation. Therefore, one might hypothesize that LIMK1 can act on centrosome function, and that its depletion leads to spindle misorientation, and its consequences on the last stages of mitosis. Whether this is the cause of premature exit from M phase needs to be established. Additionally from a pathophysiological point of view, one would expect that LIMK1 overexpression, and not LIMK1 depletion could cause centrosomal misfunction given the role of LIMK1 upregulation in cancer progression. However, given the observation of LIMK1 mislocalization in cancer cells, one can speculate that, this misregulation specifically affects the function of LIMK1 during mitosis by some mechanisms which need to be elucidated.

Chapter 4

Discussion and Perspectives

During this PhD work, differents results were obtained regarding on one hand LIMK localization in cultured cells versus normal or cancer tissues, and on the other hand concerning LIMK function in cancer progression. These participate in a better understanding of LIMK physiological and pathological functions, but also raise several questions.

Firstly, as, the subcellular localization of a protein can give hints about its function, we identified the subcellular localization of endogenous LIMK. A cytoplasmic localization with an enrichment in perinuclear area, and in membrane, mainly in lamellipodia is demonstrated in cultured cells for LIMK1 protein, consistent with a role of LIMK1 in actin cytoskeleton remodeling. Although, LIMK2 also localizes to lamellipodia, an additional specific nuclear localization is detected, as also reported recently in [K et al., 2006]. Further experiments using phospho- LIMK antibody, suggest that the LIMK2 that localizes to the nucleus is the active form, which opens new perspectives about a potential role of LIMK2 in the nucleus.

Moreover, in contrast to cell lines, we have shown that LIMK1 localizes both to nucleus and cytoplasm in kidney and prostate tissues, demonstrating a differential localization of LIMK in exponentially growing cells and in differentiated cells. Moreover, this might reflect discrepancies

in LIMK1 functions between proliferating versus non dividing cells. Especially, the possible nuclear function of LIMK1 in differentiated cells needs to be elucidated. In that setting, how LIMK localization is modulated during differentiation is certainly an interesting field of investigation, as it could be an important event for the cells to differentiate. In order to investigate that hypothesis, PC12 chromaffin cell lines which differentiates into cells with neuronal behavior upon induction with nerve growth factor (NGF) can be used.

Additionally, we observed, the relocalization of LIMK1 only to cytoplasm in orthotopic kidney cancer model, and PTEN (fl/fl) prostate cancer model, implying that transition from differentiated to proliferating cells during cancer progression is correlated with LIMK1 cytoplasmic relocalization. Whether loss of nuclear localization (and function, which needs to be analyzed) of LIMK1 is a cause or a consequence of tumor progression is still an open question. Nevertheless, these data raise the possibility that LIMK cytoplasmic staining could be a molecular marker of prostate and kidney cancer.

Interestingly, a specific localization of LIMK1 to the mitochondria has been detected by both immunostaining and fractionation assays, suggesting that LIMK1 can play a role in that particular compartment. However, as, SSH-1L, the phosphatase of LIMK1, has also been detected in the same fraction, one might propose that LIMK1 is inactivated by SSH-1L at mitochondria. Although additional biochemical experiments are certainly required, this observation raises the interesting hypothesis that LIMK1 can be specifically sequestered and inactivated at mitochondria, therefore providing a new mechanism to selectively modulate LIMK1 activation.

The depletion of LIMK1 protein in a cell, can help us to understand the physiological role of the protein. In part 2 of results chapter, the generation and characterization of powerful tools, siRNAs and shRNAs, have been described. Both siRNA and lentivector-based shRNA strategies result in an efficient depletion of LIMK1. Interestingly, these cause total inhibition of the phos-

phorylation of its substrate, cofilin in HeLa cells, demonstrating that LIMK1 is the main kinase that phosphorylates cofilin in that cell line.

Moreover, this efficient depletion by LIMK1 siRNA has been used to elucidate the role of LIMK1 in cell cycle progression. Upon LIMK1 depletion, a premature exit from mitosis has been detected. Although, there are some knowledge about LIMK1 in M phase, such as the localization to centrosomes, hyperactivation in prometaphase, metaphase, and overexpression being the cause of multinucleated cells, the function of LIMK1 during M phase was not known. The premature exit from mitosis opens a new perspective about understanding the role of LIMK1 during M phase. Although, further analysis with time-lapse imaging, does not indicate any timing difference in the first part of mitosis (nuclear envelope breakdown to anaphase onset), additional analysis of the late phase timing need to be performed, since a misregulation of the protein in early phases can affect the late phases which might result in a premature exit.

These perspectives should certainly take advantage of the development of the drug-inducible lentivector-based shRNA against LIMK1, notably to downregulate LIMK1 at specific stages of mitosis. Interestingly, even though no timing difference in early phases of mitosis has been observed, LIMK1 depleted cells displayed a 20 % increase in spindle disorientation. Interestingly, this finding can be connected to a report in fission yeast, demonstrating a role of actin cytoskeleton in spindle [Gachet et al., 2001]. Additional biochemical experiments are required to understand the function of LIMK1 and actin cytoskeleton in proper spindle orientation in mammalian cells.

Intriguingly, these results also raise new questions about the effect of overexpressed LIMK1 in cancer cells regarding their capability to complete mitosis. Indeed, since LIMK1 depletion results in quicker exit from mitosis, one should expect that overexpression of LIMK1 might dampen mitosis progression, which does not fit to the common features of cancer cells. However, we also

observed improper localization of LIMK1 in cancer cells, raising the possibility that specifically in cancer cells, mislocalization of LIMK1 might impair its function during mitosis. Alternatively, one might consider that upon LIMK1 depletion, LIMK2 can overcompensate LIMK1 loss, or that the remaining LIMK1 is hyperactivated. These hypotheses will certainly be addressed by studying the activity of LIMK1 and LIMK2 during the different phases of mitosis, , by investigating the consequences of dose dependent downregulation of LIMK1 using the inducible lentivector based system, and finally by analyzing the effect of double LIMK1/LIMK2 knock down.

Additional to the localization of LIMK1 and to its role in cell cycle, we could provide a interesting regulation mechanism for LIMK1. Indeed, we could show that LIMK1 is upregulated at the transcriptional level upon VHL loss, a mechanism that seems to be HIF independent. This open new perspectives to identify novel targets of VHL that can regulate LIMK1 gene transcription. Moreover, as VHL loss is a feature of many tumors, this suggests that VHL-associated tumors might display increased activation of LIMK1, which might participate to tumor progression. Indeed, as LIMK1 hyperactivation is correlated to invasion of different cancers, one might assume that LIMK1 upregulation can secondarly affect tumorigenesis and metastasis resulting from VHL loss. As a perspective to these observations, a particularly interesting experiment would be to address whether shRNA-mediated LIMK1 downregulation would inhibit the development of tumors normally driven by VHL loss. Moreover, one can investigate whether VHL-associated tumors display increased levels of LIMK1. In the affirmative, LIMK1 itself, or its downstream effectors, might represent interesting pharmacological targets against tumor growth and metastasis that are associated with VHL loss.

References

[Abe et al., 1996] Abe, H., Obinata, T., Minamide, L. S., and Bamburg, J. R. (1996). Xenopus laevis actin-depolymerizing factor/cofilin: a phosphorylation-regulated protein essential for development. *J Cell Biol*, 132:871–85.

[Aizawa et al., 2001] Aizawa, H., Wakatsuki, S., Ishii, A., Moriyama, K., Sasaki, Y., Ohashi, K., Sekine-Aizawa, Y., Sehara-Fujisawa, A., Mizuno, K., Goshima, Y., and Yahara, I. (2001). Phosphorylation of cofilin by lim-kinase is necessary for semaphorin 3a-induced growth cone collapse. *Nat Neurosci*, 4:367–73.

[Amano et al., 2002] Amano, T., Kaji, N., Ohashi, K., and Mizuno, K. (2002). Mitosis-specific activation of lim motif-containing protein kinase and roles of cofilin phosphorylation and dephosphorylation in mitosis. *J Biol Chem*, 277:22093–102.

[Ang et al., 2006] Ang, L.-H., Chen, W., Yao, Y., Ozawa, R., Tao, E., Yonekura, J., Uemura, T., Keshishian, H., and Hing, H. (2006). Lim kinase regulates the development of olfactory and neuromuscular synapses. *Dev Biol*, 293:178–90.

[Arber et al., 1998] Arber, S., Barbayannis, F. A., Hanser, H., Schneider, C., Stanyon, C. A., Bernard, O., and Caroni, P. (1998). Regulation of actin dynamics through phosphorylation of cofilin by lim-kinase. *Nature*, 393:805–9.

[Asada et al., 1999] Asada, M., Yamada, T., Ichijo, H., Delia, D., Miyazono, K., Fukumuro, K., and Mizutani, S. (1999). Apoptosis inhibitory activity of cytoplasmic p21(cip1/waf1) in monocytic differentiation. *EMBO J*, 18:1223–34.

[Ashworth et al., 2001] Ashworth, S. L., Sandoval, R. M., Hosford, M., Bamburg, J. R., and Molitoris, B. A. (2001). Ischemic injury induces adf relocalization to the apical domain of rat proximal tubule cells. *Am J Physiol Renal Physiol*, 280:F886–94.

[Aspenstrom, 1999] Aspenstrom, P. (1999). Effectors for the rho gtpases. *Curr Opin Cell Biol*, 11:95–102.

[Bagheri-Yarmand et al., 2006] Bagheri-Yarmand, R., Mazumdar, A., Sahin, A. A., and Kumar, R. (2006). Lim kinase 1 increases tumor metastasis of human breast cancer cells via regulation of the urokinase-type plasminogen activator system. *Int J Cancer*, 118:2703–10.

[Bamburg, 1999] Bamburg, J. R. (1999). Proteins of the adf/cofilin family: essential regulators of actin dynamics. *Annu Rev Cell Dev Biol*, 15:185–230.

[Bamburg and Bray, 1987] Bamburg, J. R. and Bray, D. (1987). Distribution and cellular localization of actin depolymerizing factor. *J Cell Biol*, 105:2817–25.

[Bamburg and Wiggan, 2002] Bamburg, J. R. and Wiggan, O. P. (2002). Adf/cofilin and actin dynamics in disease. *Trends Cell Biol*, 12:598–605.

[Barboule et al., 1998] Barboule, N., Baldin, V., JOzan, S., Vidal, S., and Valette, A. (1998). Increased level of p21 in human ovarian tumors is associated with increased expression of cdk2, cyclin a and pcna. *Int J Cancer*, 76:891–6.

[Barry and Krek, 2004] Barry, R. E. and Krek, W. (2004). The von hippel-lindau tumour suppressor: a multi-faceted inhibitor of tumourigenesis. *Trends Mol Med*, 10:466–72.

[Bernard et al., 1996] Bernard, O., Burkitt, V., Webb, G. C., Bottema, C. D., Nicholl, J., Sutherland, G. R., and Matthew, P. (1996). Structure and chromosomal localization of the genomic locus encoding the kiz1 lim-kinase gene. *Genomics*, 35:593–6.

[Bernard et al., 1994] Bernard, O., Ganiatsas, S., Kannourakis, G., and Dringen, R. (1994). Kiz-1, a protein with lim zinc finger and kinase domains, is expressed mainly in neurons. *Cell Growth Differ*, 5:1159–71.

[Bernstein et al., 2000] Bernstein, B. W., Painter, W. B., Chen, H., Minamide, L. S., Abe, H., and Bamburg, J. R. (2000). Intracellular ph modulation of adf/cofilin proteins. *Cell Motil Cytoskeleton*, 47:319–36.

[Bertling et al., 2004] Bertling, E., Hotulainen, P., Mattila, P. K., Matilainen, T., Salminen, M., and Lappalainen, P. (2004). Cyclase-associated protein 1 (cap1) promotes cofilin-induced actin dynamics in mammalian nonmuscle cells. *Mol Biol Cell*, 15:2324–34.

[Bharadwaj and Yu, 2004] Bharadwaj, R. and Yu, H. (2004). The spindle checkpoint, aneuploidy, and cancer. *Oncogene*, 23:2016–27.

[Biankin et al., 2001] Biankin, A. V., Kench, J. G., Morey, A. L., Lee, C. S., Biankin, S. A., Head, D. R., Hugh, T. B., Henshall, S. M., and Sutherland, R. L. (2001). Overexpression of p21(waf1/cip1) is an early event in the development of pancreatic intraepithelial neoplasia. *Cancer Res*, 61:8830–7.

[Bierne et al., 2001] Bierne, H., Gouin, E., Roux, P., Caroni, P., Yin, H. L., and Cossart, P. (2001). A role for cofilin and lim kinase in listeria-induced phagocytosis. *J Cell Biol*, 155:101–12.

[Birkenfeld et al., 2001] Birkenfeld, J., Betz, H., and Roth, D. (2001). Inhibition of neurite extension by overexpression of individual domains of lim kinase 1. *J Neurochem*, 78:924–7.

[Birkenfeld et al., 2003] Birkenfeld, J., Betz, H., and Roth, D. (2003). Identification of cofilin and lim-domain-containing protein kinase 1 as novel interaction partners of 14-3-3 zeta. *Biochem J*, 369:45–54.

[Blasi and Carmeliet, 2002] Blasi, F. and Carmeliet, P. (2002). upar: a versatile signalling orchestrator. *Nat Rev Mol Cell Biol*, 3:932–43.

[Bryan and Wilson, 1971] Bryan, J. and Wilson, L. (1971). Are cytoplasmic microtubules heteropolymers? *Proc Natl Acad Sci U S A*, 68:1762–6.

[Burridge and Wennerberg, 2004] Burridge, K. and Wennerberg, K. (2004). Rho and rac take center stage. *Cell*, 116:167–79.

[Capecchi, 1989] Capecchi, M. R. (1989). The new mouse genetics: altering the genome by gene targeting. *Trends Genet*, 5:70–6.

[Carmeliet and Jain, 2000] Carmeliet, P. and Jain, R. K. (2000). Angiogenesis in cancer and other diseases. *Nature*, 407:249–57.

[Cassimeris, 2002] Cassimeris, L. (2002). The oncoprotein 18/stathmin family of microtubule destabilizers. *Curr Opin Cell Biol*, 14:18–24.

[Cerutti and Simanis, 2000] Cerutti, L. and Simanis, V. (2000). Controlling the end of the cell cycle. *Curr Opin Genet Dev*, 10:65–9.

[Chambers et al., 2002] Chambers, A. F., Groom, A. C., and MacDonald, I. C. (2002). Dissemination and growth of cancer cells in metastatic sites. *Nat Rev Cancer*, 2:563–72.

[Chen et al., 2001] Chen, J., Godt, D., Gunsalus, K., Kiss, I., Goldberg, M., and Laski, F. A. (2001). Cofilin/adf is required for cell motility during drosophila ovary development and oogenesis. *Nat Cell Biol*, 3:204–9.

[Chowdary et al., 1994] Chowdary, D. R., Dermody, J. J., Jha, K. K., and Ozer, H. L. (1994). Accumulation of p53 in a mutant cell line defective in the ubiquitin pathway. *Mol Cell Biol*, 14:1997–2003.

[Chua et al., 2003] Chua, B. T., Volbracht, C., Tan, K. O., Li, R., Yu, V. C., and Li, P. (2003). Mitochondrial translocation of cofilin is an early step in apoptosis induction. *Nat Cell Biol*, 5:1083–9.

[Ciechanover, 1998] Ciechanover, A. (1998). The ubiquitin-proteasome pathway: on protein death and cell life. *EMBO J*, 17:7151–60.

[Clark et al., 2000] Clark, E. A., Golub, T. R., Lander, E. S., and Hynes, R. O. (2000). Genomic analysis of metastasis reveals an essential role for rhoc. *Nature*, 406:532–5.

[Condeelis, 2001] Condeelis, J. (2001). How is actin polymerization nucleated in vivo? *Trends Cell Biol*, 11:288–93.

[Dai et al., 2004] Dai, S., Sarmiere, P. D., Wiggan, O., Bamburg, J. R., and Zhou, D. (2004). Efficient salmonella entry requires activity cycles of host adf and cofilin. *Cell Microbiol*, 6:459–71.

[Dan et al., 2001] Dan, C., Kelly, A., Bernard, O., and Minden, A. (2001). Cytoskeletal changes regulated by the pak4 serine/threonine kinase are mediated by lim kinase 1 and cofilin. *J Biol Chem*, 276:32115–21.

[Danen and Yamada, 2001] Danen, E. H. and Yamada, K. M. (2001). Fibronectin, integrins, and growth control. *J Cell Physiol*, 189(0021-9541 (Print)):1–13.

[Davidson and Haslam, 1994] Davidson, M. M. and Haslam, R. J. (1994). Dephosphorylation of cofilin in stimulated platelets: roles for a gtp-binding protein and ca2+. *Biochem J*, 301 (Pt 1):41–7.

[Davila et al., 2003] Davila, M., Frost, A. R., Grizzle, W. E., and Chakrabarti, R. (2003). Lim kinase 1 is essential for the invasive growth of prostate epithelial cells: implications in prostate cancer. *J Biol Chem*, 278:36868–75.

[Dawe et al., 2003] Dawe, H. R., Minamide, L. S., Bamburg, J. R., and Cramer, L. P. (2003). Adf/cofilin controls cell polarity during fibroblast migration. *Curr Biol*, 13:252–7.

[de Gramont and Cohen-Fix, 2005] de Gramont, A. and Cohen-Fix, O. (2005). The many phases of anaphase. *Trends Biochem Sci*, 30:559–68.

[DeGregori et al., 1995] DeGregori, J., Kowalik, T., and Nevins, J. R. (1995). Cellular targets for activation by the e2f1 transcription factor include dna synthesis- and g1/s-regulatory genes. *Mol Cell Biol*, 15:4215–24.

[Denicourt and Dowdy, 2004] Denicourt, C. and Dowdy, S. F. (2004). Cip/kip proteins: more than just cdks inhibitors. *Genes Dev*, 18:851–5.

[DesMarais et al., 2005] DesMarais, V., Ghosh, M., Eddy, R., and Condeelis, J. (2005). Cofilin takes the lead. *J Cell Sci*, 118:19–26.

[Dulic et al., 1998] Dulic, V., Stein, G. H., Far, D. F., and Reed, S. I. (1998). Nuclear accumulation of p21cip1 at the onset of mitosis: a role at the g2/m-phase transition. *Mol Cell Biol*, 18:546–57.

[Eaton and Davis, 2005] Eaton, B. A. and Davis, G. W. (2005). Lim kinase1 controls synaptic stability downstream of the type ii bmp receptor. *Neuron*, 47:695–708.

[Eden et al., 2002] Eden, S., Rohatgi, R., Podtelejnikov, A. V., Mann, M., and Kirschner, M. W. (2002). Mechanism of regulation of wave1-induced actin nucleation by rac1 and nck. *Nature*, 418:790–3.

[Edwards et al., 1999] Edwards, D. C., Sanders, L. C., Bokoch, G. M., and Gill, G. N. (1999). Activation of lim-kinase by pak1 couples rac/cdc42 gtpase signalling to actin cytoskeletal dynamics. *Nat Cell Biol*, 1(1465-7392 (Print)):253–9.

[Endo et al., 2003] Endo, M., Ohashi, K., Sasaki, Y., Goshima, Y., Niwa, R., Uemura, T., and Mizuno, K. (2003). Control of growth cone motility and morphology by lim kinase and slingshot via phosphorylation and dephosphorylation of cofilin. *J Neurosci*, 23:2527–37.

[Etienne-Manneville and Hall, 2002] Etienne-Manneville, S. and Hall, A. (2002). Rho gtpases in cell biology. *Nature*, 420:629–35.

[Fire et al., 1998] Fire, A., Xu, S., Montgomery, M. K., Kostas, S. A., Driver, S. E., and Mello, C. C. (1998). Potent and specific genetic interference by double-stranded rna in caenorhabditis elegans. *Nature*, 391:806–11.

[Foletta et al., 2003] Foletta, V. C., Lim, M. A., Soosairajah, J., Kelly, A. P., Stanley, E. G., Shannon, M., He, W., Das, S., Massague, J., and Bernard, O. (2003). Direct signaling by the bmp type ii receptor via the cytoskeletal regulator limk1. *J Cell Biol*, 162:1089–98.

[Foletta et al., 2004] Foletta, V. C., Moussi, N., Sarmiere, P. D., Bamburg, J. R., and Bernard, O. (2004). Lim kinase 1, a key regulator of actin dynamics, is widely expressed in embryonic and adult tissues. *Exp Cell Res*, 294:392–405.

[Folkman and Shing, 1992] Folkman, J. and Shing, Y. (1992). Angiogenesis. *J Biol Chem*, 267:10931–4.

[Fritz et al., 1999] Fritz, G., Just, I., and Kaina, B. (1999). Rho gtpases are over-expressed in human tumors. *Int J Cancer*, 81:682–7.

[Gachet et al., 2001] Gachet, Y., Tournier, S., Millar, J. B., and Hyams, J. S. (2001). A map kinase-dependent actin checkpoint ensures proper spindle orientation in fission yeast. *Nature*, 412:352–5.

[Galkin et al., 2001] Galkin, V. E., Orlova, A., Lukoyanova, N., Wriggers, W., and Egelman, E. H. (2001). Actin depolymerizing factor stabilizes an existing state of f-actin and can change the tilt of f-actin subunits. *J Cell Biol*, 153:75–86.

[Ghosh et al., 2004] Ghosh, M., Song, X., Mouneimne, G., Sidani, M., Lawrence, D. S., and Condeelis, J. S. (2004). Cofilin promotes actin polymerization and defines the direction of cell motility. *Science*, 304:743–6.

[Giodini et al., 2002] Giodini, A., Kallio, M. J., Wall, N. R., Gorbsky, G. J., Tognin, S., Marchisio, P. C., Symons, M., and Altieri, D. C. (2002). Regulation of microtubule stability and mitotic progression by survivin. *Cancer Res*, 62:2462–7.

[Glotzer, 2001] Glotzer, M. (2001). Animal cell cytokinesis. *Annu Rev Cell Dev Biol*, 17:351–86.

[Gohla et al., 2005] Gohla, A., Birkenfeld, J., and Bokoch, G. M. (2005). Chronophin, a novel had-type serine protein phosphatase, regulates cofilin-dependent actin dynamics. *Nat Cell Biol*, 7:21–9.

[Gohla and Bokoch, 2002a] Gohla, A. and Bokoch, G. M. (2002a). 14-3-3 regulates actin dynamics by stabilizing phosphorylated cofilin. *Curr Biol*, 12:1704–10.

[Gohla and Bokoch, 2002b] Gohla, A. and Bokoch, G. M. (2002b). 14-3-3 regulates actin dynamics by stabilizing phosphorylated cofilin. *Curr Biol*, 12:1704–10.

[Gong et al., 2004] Gong, C., Stoletov, K. V., and Terman, B. I. (2004). Vegf treatment induces signaling pathways that regulate both actin polymerization and depolymerization. *Angiogenesis*, 7:313–21.

[Gorovoy et al., 2005] Gorovoy, M., Niu, J., Bernard, O., Profirovic, J., Minshall, R., Neamu, R., and Voyno-Yasenetskaya, T. (2005). Lim kinase 1 coordinates microtubule stability and actin polymerization in human endothelial cells. *J Biol Chem*, 280:26533–42.

[Gray et al., 2006] Gray, V., Karmiloff-Smith, A., Funnell, E., and Tassabehji, M. (2006). In-depth analysis of spatial cognition in williams syndrome: A critical assessment of the role of the limk1 gene. *Neuropsychologia*, 44:679–85.

[Gungabissoon and Bamburg, 2003] Gungabissoon, R. A. and Bamburg, J. R. (2003). Regulation of growth cone actin dynamics by adf/cofilin. *J Histochem Cytochem*, 51:411–20.

[Gunsalus et al., 1995] Gunsalus, K. C., Bonaccorsi, S., Williams, E., Verni, F., Gatti, M., and Goldberg, M. L. (1995). Mutations in twinstar, a drosophila gene encoding a cofilin/adf homologue, result in defects in centrosome migration and cytokinesis. *J Cell Biol*, 131:1243–59.

[Hagting et al., 1999] Hagting, A., Jackman, M., Simpson, K., and Pines, J. (1999). Translocation of cyclin b1 to the nucleus at prophase requires a phosphorylation-dependent nuclear import signal. *Curr Biol*, 9:680–9.

[Hall, 1998] Hall, A. (1998). Rho gtpases and the actin cytoskeleton. *Science*, 279:509–14.

[Harbour et al., 1999] Harbour, J. W., Luo, R. X., Dei Santi, A., Postigo, A. A., and Dean, D. C. (1999). Cdk phosphorylation triggers sequential intramolecular interactions that progressively block rb functions as cells move through g1. *Cell*, 98:859–69.

[Harris and Lim, 2001] Harris, B. Z. and Lim, W. A. (2001). Mechanism and role of pdz domains in signaling complex assembly. *J Cell Sci*, 114:3219–31.

[Hisaoka et al., 2002] Hisaoka, M., Tanaka, A., and Hashimoto, H. (2002). Molecular alterations of h-warts/lats1 tumor suppressor in human soft tissue sarcoma. *Lab Invest*, 82:1427–35.

[Hoenger and Milligan, 1996] Hoenger, A. and Milligan, R. A. (1996). Polarity of 2-d and 3-d maps of tubulin sheets and motor-decorated sheets. *J Mol Biol*, 263:114–9.

[Hotulainen et al., 2005] Hotulainen, P., Paunola, E., Vartiainen, M. K., and Lappalainen, P. (2005). Actin-depolymerizing factor and cofilin-1 play overlapping roles in promoting rapid f-actin depolymerization in mammalian nonmuscle cells. *Mol Biol Cell*, 16:649–64.

[Huang et al., 2006] Huang, T. Y., DerMardirossian, C., and Bokoch, G. M. (2006). Cofilin phosphatases and regulation of actin dynamics. *Curr Opin Cell Biol*, 18:26–31.

[Ichetovkin et al., 2002] Ichetovkin, I., Grant, W., and Condeelis, J. (2002). Cofilin produces newly polymerized actin filaments that are preferred for dendritic nucleation by the arp2/3 complex. *Curr Biol*, 12:79–84.

[Iida et al., 1992] Iida, K., Matsumoto, S., and Yahara, I. (1992). The kkrkk sequence is involved in heat shock-induced nuclear translocation of the 18-kda actin-binding protein, cofilin. *Cell Struct Funct*, 17:39–46.

[Ikebe et al., 1998] Ikebe, C., Ohashi, K., and Mizuno, K. (1998). Identification of testis-specific (limk2t) and brain-specific (limk2c) isoforms of mouse lim-kinase 2 gene transcripts. *Biochem Biophys Res Commun*, 246:307–12.

[Itoh et al., 1999] Itoh, K., Yoshioka, K., Akedo, H., Uehata, M., Ishizaki, T., and Narumiya, S. (1999). An essential part for rho-associated kinase in the transcellular invasion of tumor cells. *Nat Med*, 5:221–5.

[Jaffe and Hall, 2005] Jaffe, A. B. and Hall, A. (2005). Rho gtpases: biochemistry and biology. *Annu Rev Cell Dev Biol*, 21:247–69.

[J.Lisztwan, 2001] J.Lisztwan (2001). *The Pleomorphic Character of the von Hippel-Lindau Tumor Suppressor Protein*. PhD thesis, University of Basel.

[Jordan and Wilson, 2004] Jordan, M. A. and Wilson, L. (2004). Microtubules as a target for anticancer drugs. *Nat Rev Cancer*, 4:253–65.

[Joyce et al., 1999] Joyce, D., Bouzahzah, B., Fu, M., Albanese, C., D'Amico, M., Steer, J., Klein, J. U., Lee, R. J., Segall, J. E., Westwick, J. K., Der, C. J., and Pestell, R. G. (1999). Integration of rac-dependent regulation of cyclin d1 transcription through a nuclear factor-kappab-dependent pathway. *J Biol Chem*, 274:25245–9.

[Justice et al., 1995] Justice, R. W., Zilian, O., Woods, D. F., Noll, M., and Bryant, P. J. (1995). The drosophila tumor suppressor gene warts encodes a homolog of human myotonic dystrophy kinase and is required for the control of cell shape and proliferation. *Genes Dev*, 9:534–46.

[K et al., 2006] K, A., N, M., R, L., P, S., and O, B. (2006). Lim kinase 2 is widely expressed in all tissues. *J Histochem Cytochem*, 54(5):487–501.

[Kaji et al., 2003] Kaji, N., Ohashi, K., Shuin, M., Niwa, R., Uemura, T., and Mizuno, K. (2003). Cell cycle-associated changes in slingshot phosphatase activity and roles in cytokinesis in animal cells. *J Biol Chem*, 278:33450–5.

[Kalil and Dent, 2005] Kalil, K. and Dent, E. W. (2005). Touch and go: guidance cues signal to the growth cone cytoskeleton. *Curr Opin Neurobiol*, 15:521–6.

[Khurana et al., 2002] Khurana, T., Khurana, B., and Noegel, A. A. (2002). Lim proteins: association with the actin cytoskeleton. *Protoplasma*, 219:1–12.

[Knowles and Harris, 2001] Knowles, H. J. and Harris, A. L. (2001). Hypoxia and oxidative stress in breast cancer. hypoxia and tumourigenesis. *Breast Cancer Res*, 3:318–22.

[Kobayashi et al., 2006] Kobayashi, M., Nishita, M., Mishima, T., Ohashi, K., and Mizuno, K. (2006). Mapkapk-2-mediated lim-kinase activation is critical for vegf-induced actin remodeling and cell migration. *EMBO J*, 25:713–26.

[Koshimizu et al., 1997] Koshimizu, U., Takahashi, H., Yoshida, M. C., and Nakamura, T. (1997). cdna cloning, genomic organization, and chromosomal localization of the mouse lim motif-containing kinase gene, limk2. *Biochem Biophys Res Commun*, 241:243–50.

[Kozma et al., 1995] Kozma, R., Ahmed, S., Best, A., and Lim, L. (1995). The ras-related protein cdc42hs and bradykinin promote formation of peripheral actin microspikes and filopodia in swiss 3t3 fibroblasts. *Mol Cell Biol*, 15:1942–52.

[Krek, 2000] Krek, W. (2000). Vhl takes hif's breath away. *Nat Cell Biol*, 2:E121–3.

[Kuroda et al., 1996] Kuroda, S., Tokunaga, C., Kiyohara, Y., Higuchi, O., Konishi, H., Mizuno, K., Gill, G. N., and Kikkawa, U. (1996). Protein-protein interaction of zinc finger lim domains with protein kinase c. *J Biol Chem*, 271:31029–32.

[Lee-Hoeflich et al., 2004] Lee-Hoeflich, S. T., Causing, C. G., Podkowa, M., Zhao, X., Wrana, J. L., and Attisano, L. (2004). Activation of limk1 by binding to the bmp receptor, bmprii, regulates bmp-dependent dendritogenesis. *EMBO J*, 23:4792–801.

[Ligon et al., 2003] Ligon, L. A., Shelly, S. S., Tokito, M., and Holzbaur, E. L. F. (2003). The microtubule plus-end proteins eb1 and dynactin have differential effects on microtubule polymerization. *Mol Biol Cell*, 14:1405–17.

[Lisztwan et al., 1999] Lisztwan, J., Imbert, G., Wirbelauer, C., Gstaiger, M., and Krek, W. (1999). The von hippel-lindau tumor suppressor protein is a component of an e3 ubiquitin-protein ligase activity. *Genes Dev*, 13:1822–33.

[Lisztwan et al., 1998] Lisztwan, J., Marti, A., Sutterluty, H., Gstaiger, M., Wirbelauer, C., and Krek, W. (1998). Association of human cul-1 and ubiquitin-conjugating enzyme cdc34 with the f-box protein p45(skp2): evidence for evolutionary conservation in the subunit composition of the cdc34-scf pathway. *EMBO J*, 17:368–83.

[Maciver and Hussey, 2002] Maciver, S. K. and Hussey, P. J. (2002). The adf/cofilin family: actin-remodeling proteins. *Genome Biol*, 3:reviews3007.

[Mackay and Hall, 1998] Mackay, D. J. and Hall, A. (1998). Rho gtpases. *J Biol Chem*, 273:20685–20688.

[Malliri et al., 1998] Malliri, A., Symons, M., Hennigan, R. F., Hurlstone, A. F., Lamb, R. F., Wheeler, T., and Ozanne, B. W. (1998). The transcription factor ap-1 is required for egf-induced activation of rho-like gtpases, cytoskeletal rearrangements, motility, and in vitro invasion of a431 cells. *J Cell Biol*, 143:1087–99.

[Margolis and Wilson, 1998] Margolis, R. L. and Wilson, L. (1998). Microtubule treadmilling: what goes around comes around. *Bioessays*, 20:830–6.

[McGough et al., 1997] McGough, A., Pope, B., Chiu, W., and Weeds, A. (1997). Cofilin changes the twist of f-actin: implications for actin filament dynamics and cellular function. *J Cell Biol*, 138:771–81.

[Meberg et al., 1998] Meberg, P. J., Ono, S., Minamide, L. S., Takahashi, M., and Bamburg, J. R. (1998). Actin depolymerizing factor and cofilin phosphorylation dynamics: response to signals that regulate neurite extension. *Cell Motil Cytoskeleton*, 39:172–90.

[Mello and Conte, 2004] Mello, C. C. and Conte, D. J. (2004). Revealing the world of rna interference. *Nature*, 431:338–42.

[Meng et al., 2004] Meng, Y., Takahashi, H., Meng, J., Zhang, Y., Lu, G., Asrar, S., Nakamura, T., and Jia, Z. (2004). Regulation of adf/cofilin phosphorylation and synaptic function by lim-kinase. *Neuropharmacology*, 47:746–54.

[Meng et al., 2002] Meng, Y., Zhang, Y., Tregoubov, V., Janus, C., Cruz, L., Jackson, M., Lu, W. Y., MacDonald, J. F., Wang, J. Y., Falls, D. L., and Jia, Z. (2002). Abnormal spine morphology and enhanced ltp in limk-1 knockout mice. *Neuron*, 35:121–33.

[Minamide et al., 1997] Minamide, L. S., Painter, W. B., Schevzov, G., Gunning, P., and Bamburg, J. R. (1997). Differential regulation of actin depolymerizing factor and cofilin in response to alterations in the actin monomer pool. *J Biol Chem*, 272:8303–9.

[Miralles et al., 2003] Miralles, F., Posern, G., Zaromytidou, A.-I., and Treisman, R. (2003). Actin dynamics control srf activity by regulation of its coactivator mal. *Cell*, 113:329–42.

[Mitchison and Kirschner, 1984] Mitchison, T. and Kirschner, M. (1984). Dynamic instability of microtubule growth. *Nature*, 312:237–42.

[Mizuno et al., 1994] Mizuno, K., Okano, I., Ohashi, K., Nunoue, K., Kuma, K., Miyata, T., and Nakamura, T. (1994). Identification of a human cdna encoding a novel protein kinase with two repeats of the lim/double zinc finger motif. *Oncogene*, 9:1605–12.

[Moon and Drubin, 1995] Moon, A. and Drubin, D. G. (1995). The adf/cofilin proteins: stimulus-responsive modulators of actin dynamics. *Mol Biol Cell*, 6:1423–31.

[Morrison et al., 1998] Morrison, T. B., Weis, J. J., and Wittwer, C. T. (1998). Quantification of low-copy transcripts by continuous sybr green i monitoring during amplification. *Biotechniques*, 24:954–8, 960, 962.

[Muller et al., 2001] Muller, A., Homey, B., Soto, H., Ge, N., Catron, D., Buchanan, M. E., McClanahan, T., Murphy, E., Yuan, W., Wagner, S. N., Barrera, J. L., Mohar, A., Verastegui, E., and Zlotnik, A. (2001). Involvement of chemokine receptors in breast cancer metastasis. *Nature*, 410:50–6.

[Nagaoka et al., 1995] Nagaoka, R., Abe, H., Kusano, K., and Obinata, T. (1995). Concentration of cofilin, a small actin-binding protein, at the cleavage furrow during cytokinesis. *Cell Motil Cytoskeleton*, 30:1–7.

[Nagata et al., 1999] Nagata, K., Ohashi, K., Yang, N., and Mizuno, K. (1999). The n-terminal lim domain negatively regulates the kinase activity of lim-kinase 1. *Biochem J*, 343 Pt 1:99–105.

[Nagata-Ohashi et al., 2004] Nagata-Ohashi, K., Ohta, Y., Goto, K., Chiba, S., Mori, R., Nishita, M., Ohashi, K., Kousaka, K., Iwamatsu, A., Niwa, R., Uemura, T., and Mizuno, K. (2004). A pathway of neuregulin-induced activation of cofilin-phosphatase slingshot and cofilin in lamellipodia. *J Cell Biol*, 165:465–71.

[Nakano et al., 2003] Nakano, K., Kanai-Azuma, M., Kanai, Y., Moriyama, K., Yazaki, K., Hayashi, Y., and Kitamura, N. (2003). Cofilin phosphorylation and actin polymerization by nrk/nesk, a member of the germinal center kinase family. *Exp Cell Res*, 287:219–27.

[Narumiya et al., 2004] Narumiya, S., Oceguera-Yanez, F., and Yasuda, S. (2004). A new look at rho gtpases in cell cycle: role in kinetochore-microtubule attachment. *Cell Cycle*, 3:855–7.

[Narumiya and Yasuda, 2006] Narumiya, S. and Yasuda, S. (2006). Rho gtpases in animal cell mitosis. *Curr Opin Cell Biol*, 18(0955-0674 (Print)):199–205.

[Nebl et al., 2004] Nebl, G., Fischer, S., Penzel, R., and Samstag, Y. (2004). Dephosphorylation of cofilin is regulated through ras and requires the combined activities of the ras-effectors mek and pi3k. *Cell Signal*, 16:235–43.

[Nigg, 2001] Nigg, E. A. (2001). Mitotic kinases as regulators of cell division and its checkpoints. *Nat Rev Mol Cell Biol*, 2:21–32.

[Nishida et al., 1987] Nishida, E., Iida, K., Yonezawa, N., Koyasu, S., Yahara, I., and Sakai, H. (1987). Cofilin is a component of intranuclear and cytoplasmic actin rods induced in cultured cells. *Proc Natl Acad Sci U S A*, 84:5262–6.

[Nishida et al., 1984] Nishida, E., Maekawa, S., and Sakai, H. (1984). Cofilin, a protein in porcine brain that binds to actin filaments and inhibits their interactions with myosin and tropomyosin. *Biochemistry*, 23:5307–13.

[Nishimura et al., 2004] Nishimura, Y., Yoshioka, K., Bernard, O., Himeno, M., and Itoh, K. (2004). Lim kinase 1: evidence for a role in the regulation of intracellular vesicle trafficking of lysosomes and endosomes in human breast cancer cells. *Eur J Cell Biol*, 83:369–80.

[Nishita et al., 2002] Nishita, M., Aizawa, H., and Mizuno, K. (2002). Stromal cell-derived factor 1alpha activates lim kinase 1 and induces cofilin phosphorylation for t-cell chemotaxis. *Mol Cell Biol*, 22:774–83.

[Nishita et al., 2005] Nishita, M., Tomizawa, C., Yamamoto, M., Horita, Y., Ohashi, K., and Mizuno, K. (2005). Spatial and temporal regulation of cofilin activity by lim kinase and slingshot is critical for directional cell migration. *J Cell Biol*, 171:349–59.

[Nishita et al., 2004] Nishita, M., Wang, Y., Tomizawa, C., Suzuki, A., Niwa, R., Uemura, T., and Mizuno, K. (2004). Phosphoinositide 3-kinase-mediated activation of cofilin phosphatase slingshot and its role for insulin-induced membrane protrusion. *J Biol Chem*, 279:7193–8.

[Niwa et al., 2002] Niwa, R., Nagata-Ohashi, K., Takeichi, M., Mizuno, K., and Uemura, T. (2002). Control of actin reorganization by slingshot, a family of phosphatases that dephosphorylate adf/cofilin. *Cell*, 108:233–46.

[Nobes and Hall, 1995] Nobes, C. D. and Hall, A. (1995). Rho, rac, and cdc42 gtpases regulate the assembly of multimolecular focal complexes associated with actin stress fibers, lamellipodia, and filopodia. *Cell*, 81:53–62.

[Nomoto et al., 1999] Nomoto, S., Tatematsu, Y., Takahashi, T., and Osada, H. (1999). Cloning and characterization of the alternative promoter regions of the human limk2 gene responsible for alternative transcripts with tissue-specific expression. *Gene*, 236:259–71.

[Oceguera-Yanez et al., 2005] Oceguera-Yanez, F., Kimura, K., Yasuda, S., Higashida, C., Kitamura, T., Hiraoka, Y., Haraguchi, T., and Narumiya, S. (2005). Ect2 and mgcracgap regulate the activation and function of cdc42 in mitosis. *J Cell Biol*, 168:221–32.

[Oft et al., 1998] Oft, M., Heider, K. H., and Beug, H. (1998). Tgfbeta signaling is necessary for carcinoma cell invasiveness and metastasis. *Curr Biol*, 8:1243–52.

[Ohashi et al., 2000a] Ohashi, K., Hosoya, T., Takahashi, K., Hing, H., and Mizuno, K. (2000a). A drosophila homolog of lim-kinase phosphorylates cofilin and induces actin cytoskeletal reorganization. *Biochem Biophys Res Commun*, 276:1178–85.

[Ohashi et al., 2000b] Ohashi, K., Nagata, K., Maekawa, M., Ishizaki, T., Narumiya, S., and Mizuno, K. (2000b). Rho-associated kinase rock activates lim-kinase 1 by phosphorylation at threonine 508 within the activation loop. *J Biol Chem*, 275:3577–82.

[Ohashi et al., 1994] Ohashi, K., Toshima, J., Tajinda, K., Nakamura, T., and Mizuno, K. (1994). Molecular cloning of a chicken lung cdna encoding a novel protein kinase with n-terminal two lim/double zinc finger motifs. *J Biochem (Tokyo)*, 116:636–42.

[Ohta et al., 2003] Ohta, Y., Kousaka, K., Nagata-Ohashi, K., Ohashi, K., Muramoto, A., Shima, Y., Niwa, R., Uemura, T., and Mizuno, K. (2003). Differential activities, subcellular distribution and tissue expression patterns of three members of slingshot family phosphatases that dephosphorylate cofilin. *Genes Cells*, 8:811–24.

[Okano et al., 1995] Okano, I., Hiraoka, J., Otera, H., Nunoue, K., Ohashi, K., Iwashita, S., Hirai, M., and Mizuno, K. (1995). Identification and characterization of a novel family of serine/threonine kinases containing two n-terminal lim motifs. *J Biol Chem*, 270:31321–30.

[Olson et al., 1998] Olson, M. F., Paterson, H. F., and Marshall, C. J. (1998). Signals from ras and rho gtpases interact to regulate expression of p21waf1/cip1. *Nature*, 394:295–9.

[Ono, 2003] Ono, S. (2003). Regulation of actin filament dynamics by actin depolymerizing factor/cofilin and actin-interacting protein 1: new blades for twisted filaments. *Biochemistry*, 42:13363–70.

[Ono et al., 1994] Ono, S., Minami, N., Abe, H., and Obinata, T. (1994). Characterization of a novel cofilin isoform that is predominantly expressed in mammalian skeletal muscle. *J Biol Chem*, 269:15280–6.

[Orend et al., 1998] Orend, G., Hunter, T., and Ruoslahti, E. (1998). Cytoplasmic displacement of cyclin e-cdk2 inhibitors p21cip1 and p27kip1 in anchorage-independent cells. *Oncogene*, 16:2575–83.

[Osada et al., 1996] Osada, H., Hasada, K., Inazawa, J., Uchida, K., Ueda, R., and Takahashi, T. (1996). Subcellular localization and protein interaction of the human limk2 gene expressing alternative transcripts with tissue-specific regulation. *Biochem Biophys Res Commun*, 229:582–9.

[Ossowski and Aguirre-Ghiso, 2000] Ossowski, L. and Aguirre-Ghiso, J. A. (2000). Urokinase receptor and integrin partnership: coordination of signaling for cell adhesion, migration and growth. *Curr Opin Cell Biol*, 12:613–20.

[Paavilainen et al., 2004] Paavilainen, V. O., Bertling, E., Falck, S., and Lappalainen, P. (2004). Regulation of cytoskeletal dynamics by actin-monomer-binding proteins. *Trends Cell Biol*, 14:386–94.

[Paddison et al., 2002] Paddison, P. J., Caudy, A. A., Bernstein, E., Hannon, G. J., and Conklin, D. S. (2002). Short hairpin rnas (shrnas) induce sequence-specific silencing in mammalian cells. *Genes Dev*, 16:948–58.

[Pantaloni et al., 2001] Pantaloni, D., Le Clainche, C., and Carlier, M. F. (2001). Mechanism of actin-based motility. *Science*, 292:1502–6.

[Pendleton et al., 2003] Pendleton, A., Pope, B., Weeds, A., and Koffer, A. (2003). Latrunculin b or atp depletion induces cofilin-dependent translocation of actin into nuclei of mast cells. *J Biol Chem*, 278:14394–400.

[Peters, 2002] Peters, J.-M. (2002). The anaphase-promoting complex: proteolysis in mitosis and beyond. *Mol Cell*, 9:931–43.

[Piekny et al., 2005] Piekny, A., Werner, M., and Glotzer, M. (2005). Cytokinesis: welcome to the rho zone. *Trends Cell Biol*, 15:651–8.

[Raftopoulou and Hall, 2004] Raftopoulou, M. and Hall, A. (2004). Cell migration: Rho gtpases lead the way. *Dev Biol*, 265:23–32.

[Rando et al., 2000] Rando, O. J., Zhao, K., and Crabtree, G. R. (2000). Searching for a function for nuclear actin. *Trends Cell Biol*, 10:92–7.

[Ridley, 2001] Ridley, A. J. (2001). Rho gtpases and cell migration. *J Cell Sci*, 114:2713–22.

[Ridley and Hall, 1992] Ridley, A. J. and Hall, A. (1992). The small gtp-binding protein rho regulates the assembly of focal adhesions and actin stress fibers in response to growth factors. *Cell*, 70:389–99.

[Ridley et al., 1992] Ridley, A. J., Paterson, H. F., Johnston, C. L., Diekmann, D., and Hall, A. (1992). The small gtp-binding protein rac regulates growth factor-induced membrane ruffling. *Cell*, 70:401–10.

[Robinson and Spudich, 2000] Robinson, D. N. and Spudich, J. A. (2000). Towards a molecular understanding of cytokinesis. *Trends Cell Biol*, 10:228–37.

[Rodionov and Borisy, 1997] Rodionov, V. I. and Borisy, G. G. (1997). Microtubule treadmilling in vivo. *Science*, 275:215–8.

[Rohatgi et al., 1999] Rohatgi, R., Ma, L., Miki, H., Lopez, M., Kirchhausen, T., Takenawa, T., and Kirschner, M. W. (1999). The interaction between n-wasp and the arp2/3 complex links cdc42-dependent signals to actin assembly. *Cell*, 97:221–31.

[Roovers and Assoian, 2003] Roovers, K. and Assoian, R. K. (2003). Effects of rho kinase and actin stress fibers on sustained extracellular signal-regulated kinase activity and activation of g(1) phase cyclin-dependent kinases. *Mol Cell Biol*, 23:4283–94.

[Roovers et al., 1999] Roovers, K., Davey, G., Zhu, X., Bottazzi, M. E., and Assoian, R. K. (1999). Alpha5beta1 integrin controls cyclin d1 expression by sustaining mitogen-activated protein kinase activity in growth factor-treated cells. *Mol Biol Cell*, 10:3197–204.

[Rosenblatt et al., 2004] Rosenblatt, J., Cramer, L. P., Baum, B., and McGee, K. M. (2004). Myosin ii-dependent cortical movement is required for centrosome separation and positioning during mitotic spindle assembly. *Cell*, 117:361–72.

[Rosok et al., 1999] Rosok, O., Pedeutour, F., Ree, A. H., and Aasheim, H. C. (1999). Identification and characterization of tesk2, a novel member of the limk/tesk family of protein kinases, predominantly expressed in testis. *Genomics*, 61:44–54.

[Rosso et al., 2004] Rosso, S., Bollati, F., Bisbal, M., Peretti, D., Sumi, T., Nakamura, T., Quiroga, S., Ferreira, A., and Caceres, A. (2004). Limk1 regulates golgi dynamics, traffic of golgi-derived vesicles, and process extension in primary cultured neurons. *Mol Biol Cell*, 15:3433–49.

[Rubinson et al., 2003] Rubinson, D. A., Dillon, C. P., Kwiatkowski, A. V., Sievers, C., Yang, L., Kopinja, J., Rooney, D. L., Ihrig, M. M., McManus, M. T., Gertler, F. B., Scott, M. L., and Van Parijs, L. (2003). A lentivirus-based system to functionally silence genes in primary mammalian cells, stem cells and transgenic mice by rna interference. *Nat Genet*, 33:401–6.

[S, 2006] S, F. (2006). Protein kinases controlling the onset of mitosis. *Cell Mol Life Sci*.

[Saito et al., 1994] Saito, T., Lamy, F., Roger, P. P., Lecocq, R., and Dumont, J. E. (1994). Characterization and identification as cofilin and destrin of two thyrotropin- and phorbol ester-regulated phosphoproteins in thyroid cells. *Exp Cell Res*, 212:49–61.

[Sarmiere and Bamburg, 2002] Sarmiere, P. D. and Bamburg, J. R. (2002). Head, neck, and spines: a role for limk-1 in the hippocampus. *Neuron*, 35:3–5.

[Sarmiere and Bamburg, 2004] Sarmiere, P. D. and Bamburg, J. R. (2004). Regulation of the neuronal actin cytoskeleton by adf/cofilin. *J Neurobiol*, 58:103–17.

[Schipani et al., 2001] Schipani, E., Ryan, H. E., Didrickson, S., Kobayashi, T., Knight, M., and Johnson, R. S. (2001). Hypoxia in cartilage: Hif-1alpha is essential for chondrocyte growth arrest and survival. *Genes Dev*, 15:2865–76.

[Schwartz et al., 1999] Schwartz, N., Hosford, M., Sandoval, R. M., Wagner, M. C., Atkinson, S. J., Bamburg, J., and Molitoris, B. A. (1999). Ischemia activates actin depolymerizing factor: role in proximal tubule microvillar actin alterations. *Am J Physiol*, 276:F544–51.

[Seasholtz et al., 1999] Seasholtz, T. M., Majumdar, M., and Brown, J. H. (1999). Rho as a mediator of g protein-coupled receptor signaling. *Mol Pharmacol*, 55:949–56.

[Semenza, 2002] Semenza, G. L. (2002). Hif-1 and tumor progression: pathophysiology and therapeutics. *Trends Mol Med*, 8:S62–7.

[Settleman, 2003] Settleman, J. (2003). A nuclear mal-function links rho to srf. *Mol Cell*, 11:1121–3.

[Sherr and Roberts, 1999] Sherr, C. J. and Roberts, J. M. (1999). Cdk inhibitors: positive and negative regulators of g1-phase progression. *Genes Dev*, 13:1501–12.

[Smolich et al., 1997] Smolich, B., Vo, M., Buckley, S., Plowman, G., and Papkoff, J. (1997). Cloning and biochemical characterization of limk-2, a protein kinase containing two lim domains. *J Biochem (Tokyo)*, 121:382–8.

[Somlyo et al., 2000] Somlyo, A. V., Bradshaw, D., Ramos, S., Murphy, C., Myers, C. E., and Somlyo, A. P. (2000). Rho-kinase inhibitor retards migration and in vivo dissemination of human prostate cancer cells. *Biochem Biophys Res Commun*, 269:652–9.

[Song and Mandelkow, 1995] Song, Y. H. and Mandelkow, E. (1995). The anatomy of flagellar microtubules: polarity, seam, junctions, and lattice. *J Cell Biol*, 128:81–94.

[Soosairajah et al., 2005] Soosairajah, J., Maiti, S., Wiggan, O., Sarmiere, P., Moussi, N., Sarcevic, B., Sampath, R., Bamburg, J. R., and Bernard, O. (2005). Interplay between components of a novel lim kinase-slingshot phosphatase complex regulates cofilin. *EMBO J*, 24:473–86.

[Sotiropoulos et al., 1999] Sotiropoulos, A., Gineitis, D., Copeland, J., and Treisman, R. (1999). Signal-regulated activation of serum response factor is mediated by changes in actin dynamics. *Cell*, 98:159–69.

[Spittle et al., 2000] Spittle, C., Charrasse, S., Larroque, C., and Cassimeris, L. (2000). The interaction of togp with microtubules and tubulin. *J Biol Chem*, 275:20748–53.

[St John et al., 1999] St John, M. A., Tao, W., Fei, X., Fukumoto, R., Carcangiu, M. L., Brownstein, D. G., Parlow, A. F., McGrath, J., and Xu, T. (1999). Mice deficient of lats1 develop soft-tissue sarcomas, ovarian tumours and pituitary dysfunction. *Nat Genet*, 21:182–6.

[Staller et al., 2003] Staller, P., Sulitkova, J., Lisztwan, J., Moch, H., Oakeley, E. J., and Krek, W. (2003). Chemokine receptor cxcr4 downregulated by von hippel-lindau tumour suppressor pvhl. *Nature*, 425:307–11.

[Stanyon and Bernard, 1999] Stanyon, C. A. and Bernard, O. (1999). Lim-kinase1. *Int J Biochem Cell Biol*, 31:389–94.

[Stephens et al., 1999] Stephens, R. W., Nielsen, H. J., Christensen, I. J., Thorlacius-Ussing, O., Sorensen, S., Dano, K., and Brunner, N. (1999). Plasma urokinase receptor levels in patients with colorectal cancer: relationship to prognosis. *J Natl Cancer Inst*, 91:869–74.

[Straight and Field, 2000] Straight, A. F. and Field, C. M. (2000). Microtubules, membranes and cytokinesis. *Curr Biol*, 10:R760–70.

[Sumi et al., 2006] Sumi, T., Hashigasako, A., Matsumoto, K., and Nakamura, T. (2006). Different activity regulation and subcellular localization of limk1 and limk2 during cell cycle transition. *Exp Cell Res*, 312:1021–30.

[Sumi et al., 2002] Sumi, T., Matsumoto, K., and Nakamura, T. (2002). Mitosis-dependent phosphorylation and activation of lim-kinase 1. *Biochem Biophys Res Commun*, 290:1315–20.

[Sumi et al., 2001] Sumi, T., Matsumoto, K., Shibuya, A., and Nakamura, T. (2001). Activation of lim kinases by myotonic dystrophy kinase-related cdc42-binding kinase alpha. *J Biol Chem*, 276:23092–6.

[Sumi et al., 1999] Sumi, T., Matsumoto, K., Takai, Y., and Nakamura, T. (1999). Cofilin phosphorylation and actin cytoskeletal dynamics regulated by rho- and cdc42-activated lim-kinase 2. *J Cell Biol*, 147:1519–32.

[Swedlow and Hirano, 2003] Swedlow, J. R. and Hirano, T. (2003). The making of the mitotic chromosome: modern insights into classical questions. *Mol Cell*, 11:557–69.

[Takahashi et al., 2003] Takahashi, H., Funakoshi, H., and Nakamura, T. (2003). Lim-kinase as a regulator of actin dynamics in spermatogenesis. *Cytogenet Genome Res*, 103:290–8.

[Takahashi et al., 2002] Takahashi, H., Koshimizu, U., Miyazaki, J.-i., and Nakamura, T. (2002). Impaired spermatogenic ability of testicular germ cells in mice deficient in the lim-kinase 2 gene. *Dev Biol*, 241:259–72.

[Takahashi et al., 1998] Takahashi, H., Koshimizu, U., and Nakamura, T. (1998). A novel transcript encoding truncated lim kinase 2 is specifically expressed in male germ cells undergoing meiosis. *Biochem Biophys Res Commun*, 249:138–45.

[Takahashi et al., 1997] Takahashi, T., Aoki, S., Nakamura, T., Koshimizu, U., and Matsumoto, K. (1997). Xenopus lim motif-containing protein kinase, xlimk1, is expressed in the developing head structure of the embryo. *Dev Dyn*, 209(1058-8388 (Print)):196–205.

[Takahashi et al., 2001] Takahashi, T., Koshimizu, U., Abe, H., Obinata, T., and Nakamura, T. (2001). Functional involvement of xenopus lim kinases in progression of oocyte maturation. *Dev Biol*, 229:554–67.

[Tao et al., 1999] Tao, W., Zhang, S., Turenchalk, G. S., Stewart, R. A., St John, M. A., Chen, W., and Xu, T. (1999). Human homologue of the drosophila melanogaster lats tumour suppressor modulates cdc2 activity. *Nat Genet*, 21:177–81.

[Tatsumoto et al., 2003] Tatsumoto, T., Sakata, H., Dasso, M., and Miki, T. (2003). Potential roles of the nucleotide exchange factor ect2 and cdc42 gtpase in spindle assembly in xenopus egg cell-free extracts. *J Cell Biochem*, 90:892–900.

[Taylor and Stark, 2001] Taylor, W. R. and Stark, G. R. (2001). Regulation of the g2/m transition by p53. *Oncogene*, 20:1803–15.

[Terada et al., 1998] Terada, Y., Tatsuka, M., Suzuki, F., Yasuda, Y., Fujita, S., and Otsu, M. (1998). Aim-1: a mammalian midbody-associated protein required for cytokinesis. *EMBO J*, 17:667–76.

[Tilney et al., 1973] Tilney, L. G., Bryan, J., Bush, D. J., Fujiwara, K., Mooseker, M. S., Murphy, D. B., and Snyder, D. H. (1973). Microtubules: evidence for 13 protofilaments. *J Cell Biol*, 59:267–75.

[Tojima and Ito, 2004] Tojima, T. and Ito, E. (2004). Signal transduction cascades underlying de novo protein synthesis required for neuronal morphogenesis in differentiating neurons. *Prog Neurobiol*, 72:183–93.

[Tomiyoshi et al., 2004] Tomiyoshi, G., Horita, Y., Nishita, M., Ohashi, K., and Mizuno, K. (2004). Caspase-mediated cleavage and activation of lim-kinase 1 and its role in apoptotic membrane blebbing. *Genes Cells*, 9:591–600.

[Toshima et al., 1998] Toshima, J., Koji, T., and Mizuno, K. (1998). Stage-specific expression of testis-specific protein kinase 1 (tesk1) in rat spermatogenic cells. *Biochem Biophys Res Commun*, 249:107–12.

[Toshima et al., 1995] Toshima, J., Ohashi, K., Okano, I., Nunoue, K., Kishioka, M., Kuma, K., Miyata, T., Hirai, M., Baba, T., and Mizuno, K. (1995). Identification and characterization of a novel protein kinase, tesk1, specifically expressed in testicular germ cells. *J Biol Chem*, 270:31331–7.

[Toshima et al., 1999] Toshima, J., Tanaka, T., and Mizuno, K. (1999). Dual specificity protein kinase activity of testis-specific protein kinase 1 and its regulation by autophosphorylation of serine-215 within the activation loop. *J Biol Chem*, 274:12171–6.

[Toshima et al., 2001] Toshima, J., Toshima, J. Y., Takeuchi, K., Mori, R., and Mizuno, K. (2001). Cofilin phosphorylation and actin reorganization activities of testicular protein kinase 2 and its predominant expression in testicular sertoli cells. *J Biol Chem*, 276:31449–58.

[Toyoshima-Morimoto et al., 2001] Toyoshima-Morimoto, F., Taniguchi, E., Shinya, N., Iwamatsu, A., and Nishida, E. (2001). Polo-like kinase 1 phosphorylates cyclin b1 and targets it to the nucleus during prophase. *Nature*, 410:215–20.

[Tursun et al., 2005] Tursun, B., Schluter, A., Peters, M. A., Viehweger, B., Ostendorff, H. P., Soosairajah, J., Drung, A., Bossenz, M., Johnsen, S. A., Schweizer, M., Bernard, O., and Bach, I. (2005). The ubiquitin ligase rnf6 regulates local lim kinase 1 levels in axonal growth cones. *Genes Dev*, 19:2307–19.

[Vartiainen et al., 2002] Vartiainen, M. K., Mustonen, T., Mattila, P. K., Ojala, P. J., Thesleff, I., Partanen, J., and Lappalainen, P. (2002). The three mouse actin-depolymerizing factor/cofilins evolved to fulfill cell-type-specific requirements for actin dynamics. *Mol Biol Cell*, 13:183–94.

[Vivanco and Sawyers, 2002] Vivanco, I. and Sawyers, C. L. (2002). The phosphatidylinositol 3-kinase akt pathway in human cancer. *Nat Rev Cancer*, 2:489–501.

[Wang et al., 2000] Wang, J. Y., Wigston, D. J., Rees, H. D., Levey, A. I., and Falls, D. L. (2000). Lim kinase 1 accumulates in presynaptic terminals during synapse maturation. *J Comp Neurol*, 416:319–34.

[Wang, 2001] Wang, X. (2001). The expanding role of mitochondria in apoptosis. *Genes Dev*, 15:2922–33.

[Wang et al., 2005] Wang, Y., Shibasaki, F., and Mizuno, K. (2005). Calcium signal-induced cofilin dephosphorylation is mediated by slingshot via calcineurin. *J Biol Chem*, 280:12683–9.

[Watanabe et al., 2005] Watanabe, T., Noritake, J., and Kaibuchi, K. (2005). Regulation of microtubules in cell migration. *Trends Cell Biol*, 15:76–83.

[Watzinger et al., 2006] Watzinger, F., Ebner, K., and Lion, T. (2006). Detection and monitoring of virus infections by real-time pcr. *Mol Aspects Med*, 27:254–98.

[Weaver et al., 2003] Weaver, A. M., Young, M. E., Lee, W.-L., and Cooper, J. A. (2003). Integration of signals to the arp2/3 complex. *Curr Opin Cell Biol*, 15:23–30.

[Weber et al., 1997] Weber, J. D., Hu, W., Jefcoat, S. C. J., Raben, D. M., and Baldassare, J. J. (1997). Ras-stimulated extracellular signal-related kinase 1 and rhoa activities coordinate platelet-derived growth factor-induced g1 progression through the independent regulation of cyclin d1 and p27. *J Biol Chem*, 272:32966–71.

[Welch and Mullins, 2002] Welch, M. D. and Mullins, R. D. (2002). Cellular control of actin nucleation. *Annu Rev Cell Dev Biol*, 18:247–88.

[Welsh et al., 2001] Welsh, C. F., Roovers, K., Villanueva, J., Liu, Y., Schwartz, M. A., and Assoian, R. K. (2001). Timing of cyclin d1 expression within g1 phase is controlled by rho. *Nat Cell Biol*, 3:950–7.

[Westwick et al., 1997] Westwick, J. K., Lambert, Q. T., Clark, G. J., Symons, M., Van Aelst, L., Pestell, R. G., and Der, C. J. (1997). Rac regulation of transformation, gene expression, and actin organization by multiple, pak-independent pathways. *Mol Cell Biol*, 17:1324–35.

[Wiggan et al., 2005] Wiggan, O., Bernstein, B. W., and Bamburg, J. R. (2005). A phosphatase for cofilin to be had. *Nat Cell Biol*, 7:8–9.

[Winters et al., 2001] Winters, Z. E., Hunt, N. C., Bradburn, M. J., Royds, J. A., Turley, H., Harris, A. L., and Norbury, C. J. (2001). Subcellular localisation of cyclin b, cdc2 and p21(waf1/cip1) in breast cancer. association with prognosis. *Eur J Cancer*, 37:2405–12.

[Winters et al., 1998] Winters, Z. E., Ongkeko, W. M., Harris, A. L., and Norbury, C. J. (1998). p53 regulates cdc2 independently of inhibitory phosphorylation to reinforce radiation-induced g2 arrest in human cells. *Oncogene*, 17:673–84.

[Wittmann et al., 2001] Wittmann, T., Hyman, A., and Desai, A. (2001). The spindle: a dynamic assembly of microtubules and motors. *Nat Cell Biol*, 3:E28–34.

[Wiznerowicz and Trono, 2003] Wiznerowicz, M. and Trono, D. (2003). Conditional suppression of cellular genes: lentivirus vector-mediated drug-inducible rna interference. *J Virol*, 77:8957–61.

[Xia et al., 2002] Xia, H., Qi, H., Li, Y., Pei, J., Barton, J., Blackstad, M., Xu, T., and Tao, W. (2002). Lats1 tumor suppressor regulates g2/m transition and apoptosis. *Oncogene*, 21:1233–41.

[Xu et al., 1995] Xu, T., Wang, W., Zhang, S., Stewart, R. A., and Yu, W. (1995). Identifying tumor suppressors in genetic mosaics: the drosophila lats gene encodes a putative protein kinase. *Development*, 121:1053–63.

[Yabuta et al., 2000] Yabuta, N., Fujii, T., Copeland, N. G., Gilbert, D. J., Jenkins, N. A., Nishiguchi, H., Endo, Y., Toji, S., Tanaka, H., Nishimune, Y., and Nojima, H. (2000). Structure, expression, and chromosome mapping of lats2, a mammalian homologue of the drosophila tumor suppressor gene lats/warts. *Genomics*, 63:263–70.

[Yamazaki et al., 2005] Yamazaki, D., Kurisu, S., and Takenawa, T. (2005). Regulation of cancer cell motility through actin reorganization. *Cancer Sci*, 96:379–86.

[Yang et al., 2004a] Yang, E. J., Yoon, J.-H., Min, D. S., and Chung, K. C. (2004a). Lim kinase 1 activates camp-responsive element-binding protein during the neuronal differentiation of immortalized hippocampal progenitor cells. *J Biol Chem*, 279:8903–10.

[Yang et al., 1998a] Yang, N., Higuchi, O., and Mizuno, K. (1998a). Cytoplasmic localization of lim-kinase 1 is directed by a short sequence within the pdz domain. *Exp Cell Res*, 241:242–52.

[Yang et al., 1998b] Yang, N., Higuchi, O., Ohashi, K., Nagata, K., Wada, A., Kangawa, K., Nishida, E., and Mizuno, K. (1998b). Cofilin phosphorylation by lim-kinase 1 and its role in rac-mediated actin reorganization. *Nature*, 393:809–12.

[Yang and Mizuno, 1999] Yang, N. and Mizuno, K. (1999). Nuclear export of lim-kinase 1, mediated by two leucine-rich nuclear-export signals within the pdz domain. *Biochem J*, 338 (Pt 3):793–8.

[Yang et al., 2001] Yang, X., Li, D. M., Chen, W., and Xu, T. (2001). Human homologue of drosophila lats, lats1, negatively regulate growth by inducing g(2)/m arrest or apoptosis. *Oncogene*, 20:6516–23.

[Yang et al., 2004b] Yang, X., Yu, K., Hao, Y., Li, D.-m., Stewart, R., Insogna, K. L., and Xu, T. (2004b). Lats1 tumour suppressor affects cytokinesis by inhibiting limk1. *Nat Cell Biol*, 6:609–17.

[Yasuda et al., 2004] Yasuda, S., Oceguera-Yanez, F., Kato, T., Okamoto, M., Yonemura, S., Terada, Y., Ishizaki, T., and Narumiya, S. (2004). Cdc42 and mdia3 regulate microtubule attachment to kinetochores. *Nature*, 428:767–71.

[Yeoh et al., 2002] Yeoh, S., Pope, B., Mannherz, H. G., and Weeds, A. (2002). Determining the differences in actin binding by human adf and cofilin. *J Mol Biol*, 315:911–25.

[Yokoo et al., 2003] Yokoo, T., Toyoshima, H., Miura, M., Wang, Y., Iida, K. T., Suzuki, H., Sone, H., Shimano, H., Gotoda, T., Nishimori, S., Tanaka, K., and Yamada, N. (2003). p57kip2 regulates actin dynamics by binding and translocating lim-kinase 1 to the nucleus. *J Biol Chem*, 278:52919–23.

[Yonezawa et al., 1987] Yonezawa, N., Nishida, E., Koyasu, S., Maekawa, S., Ohta, Y., Yahara, I., and Sakai, H. (1987). Distribution among tissues and intracellular localization of cofilin, a 21kda actin-binding protein. *Cell Struct Funct*, 12:443–52.

[Yoshioka et al., 2003] Yoshioka, K., Foletta, V., Bernard, O., and Itoh, K. (2003). A role for lim kinase in cancer invasion. *Proc Natl Acad Sci U S A*, 100:7247–52.

[Yoshioka et al., 1999] Yoshioka, K., Nakamori, S., and Itoh, K. (1999). Overexpression of small gtp-binding protein rhoa promotes invasion of tumor cells. *Cancer Res*, 59:2004–10.

[Zhan et al., 2003] Zhan, Q., Bamburg, J. R., and Badwey, J. A. (2003). Products of phosphoinositide specific phospholipase c can trigger dephosphorylation of cofilin in chemoattractant stimulated neutrophils. *Cell Motil Cytoskeleton*, 54:1–15.